CANADIAN THESES ON MICROFICHE

THÈSES CANADIENNES SUR MICROFICHE

Canadä

67357

PERMISSION TO MICROFILM — AUTORISATION DE MICROFILMER

• Please print or type — Écrire en lettres moulées ou dactylographier

Full Name of Author — Nom complet de l'auteur

TERESINHA DO MENINO JESUS ALVES

Date of Birth — Date de naissance	Country of Birth — Lieu de naissance
14/08/48	BRAZIL

Permanent Address — Résidence fixe

RUA MIGUEL LEMOS 99/303
COPACABANA
20 000 RIO DE JANEIRO — BRASIL

Title of Thesis — Titre de la thèse

PRESTRESSED CONCRETE BEAMS WITH LARGE RECTANGULAR
WEB OPENINGS

University — Université

UNIVERSITY OF ALBERTA

Degree for which thesis was presented — Grade pour lequel cette thèse fut présentée

Ph. D.

Year this degree conferred — Année d'obtention de ce grade	Name of Supervisor — Nom du directeur de thèse
1984	ANDREW SCANLON

Date	Signature
September 7, 1984	Teresinha do M.J. Alves

THE UNIVERSITY OF ALBERTA

Prestressed Concrete Beams With

Large Rectangular Web Openings

by

Teresinha do Menino Jesus Alves

A THESIS

SUBMITTED TO THE FACULTY OF GRADUATE STUDIES AND RESEARCH

IN PARTIAL FULFILMENT OF THE REQUIREMENTS FOR THE DEGREE

OF DOCTOR OF PHILOSOPHY
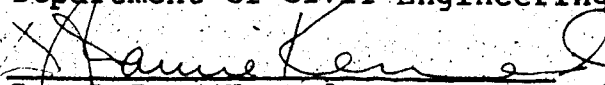
DEPARTMENT OF CIVIL ENGINEERING
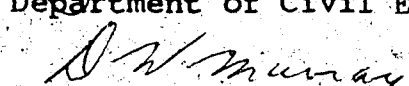
EDMONTON, ALBERTA
FALL, 1984

THE UNIVERSITY OF ALBERTA

RELEASE FORM

NAME OF AUTHOR   Teresinha do Menino Jesus Alves

TITLE OF THESIS   Prestressed Concrete Beams With Large

Rectangular Web Openings

DEGREE FOR WHICH THESIS WAS PRESENTED   Ph.D.

YEAR THIS DEGREE GRANTED   1984

Permission is hereby granted to THE UNIVERSITY OF
ALBERTA LIBRARY to reproduce single copies of this thesis
and to lend or sell such copies for private, scholarly or
scientific research purposes only.

The author reserves other publication rights, and
neither the thesis nor extensive extracts from it may be
printed or otherwise reproduced without the author's
written permission.

Teresinha da B. J. Alves

Teresinha do Menino Jesus Alves

PERMANENT ADDRESS:

Rua Miguel Lemos 99/303

Copacabana

20000 Rio de Janeiro, Brasil

Dated..Aug.,.31,..1984

THE UNIVERSITY OF ALBERTA

FACULTY OF GRADUATE STUDIES AND RESEARCH

The undersigned certify that they have read, and recommend to the Faculty of Graduate Studies and Research, for acceptance, a thesis entitled "Prestressed Concrete Beams With Large Rectangular Web Openings" submitted by Teresinha do Menino Jesus Alves in partial fulfilment of the requirements for the degree of Doctor of Philosophy in Civil Engineering.

Dr. A. Scanlon (Supervisor)
Department of Civil Engineering

Dr. D.J.L. Kennedy
Department of Civil Engineering

Dr. D.W. Murray
Department of Civil Engineering

Prof. E. Fowler
Department of Civil Engineering

Dr. J.S. Kennedy
Department of Mech. Engineering

Dr. M.S. Mirza (External Examiner) McGill University at Montreal, Quebec

Date. Aug. 31, 1984

A meus pais

ABSTRACT

The aim of this research was to investigate behavior of prestressed concrete beams with large rectangular web openings and to provide recommendations for design. The study included tests on laboratory beams and development of an analytical model based on a truss analogy.

The experimental program consisted of tests to failure of eleven full-size simply supported prestressed concrete T-beams. The variables considered in the study were the length of the opening, the depth of the top strut and the shear reinforcement of the opening.

Failure modes observed in this test program were:

1. full hinging mechanism, involving two hinges in the bottom strut and two hinges in the top strut.
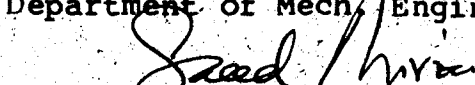
2. development of a partial hinging mechanism consisting of two hinges in the bottom strut and one hinge in the top strut, followed by a shear failure away from the opening.

3. shear failure at solid shear span followed by strand debonding.

4. flexural failure at midspan.

Proper detailing of reinforcement around the opening was found essential to prevent brittle failure and widening of cracks at the corners of openings.

Recommendations are provided for shear design in the vicinity of openings.

A computer-based analytical model was developed to determine the load-deflection response, up to yielding of reinforcement, of prestressed concrete beams with large rectangular web openings. The analysis was based on a truss model that includes the effects of progressive cracking. Post-cracking response is based on application of the effective moment of inertia concept. In addition, a simplified method is presented for calculation of deflections by hand.

ACKNOWLEDGEMENTS

TABLE OF CONTENTS

x

LIST OF TABLES

LIST OF FIGURES

A cross-sectional area

A_b cross-sectional area of truss top chord

A_d cross-sectional area of diagonal web truss member

A_p area of prestressing strand

A_s area of shear reinforcement

A_t cross-sectional area of truss bottom chord

A_v cross-sectional area of vertical web truss member

C^n average axial compressive force in the top strut at load step n

C_i^n axial compressive force in the top strut in section i at load step n

b_w web width

c_1 distance of top fiber from centroid

c_2 distance of bottom fiber from centroid

C axial compressive force in the top strut

C_t compressive force in the truss top chord

d distance from extreme compression fiber to centroid of longitudinal tension reinforcement

d_p distance between centroid of prestressing strand and bottom strut centroid

d_{st} distance between centroids of top and bottom struts

e eccentricity of prestress force

E_c modulus of elasticity of concrete

f'_c concrete compressive strength

f_{ci} compressive strength of concrete at the time of initial prestress

f_{pu} tensile strength of prestressing strand

f_r modulus of rupture of concrete

f'_{sp} splitting tensile strength

f_y yield strength of shear reinforcement

h vertical distance between top and bottom chords of truss

h_1 distance from centroid of bottom chord to centroid of beam section

h_2 distance from centroid of top chord to centroid of beam section

I_1 gross moment of inertia of beam section

I_2 gross moment of inertia of a section through the opening

I_b gross moment of inertia of bottom strut

I_{cr} moment of inertia of cracked section transformed to concrete

I_e effective moment of inertia

I_g moment of inertia of gross section

I_t gross moment of inertia of top strut

L span length

ℓ opening length

m	number of cross sections considered
M_1, M_2	moments at the ends of top strut
M_3, M_4	moments at the ends of bottom strut
M_a	moment due to applied loads
M_{cr}	cracking moment
M_i^n, M_k^n	moments at sections i and k, respectively, at load step n
M_o	decomposition moment
M_p	moment due to prestress
M_n	difference between applied load moment and the sum of the decompression and prestress moments $(M_o + M_p)$
M_u	ultimate moment at the center of the opening
$P_{cal.}$	calculated ultimate load
P_e	effective prestress force
P_b, P_t	horizontal forces applied to the ends of truss, statically equivalent to prestress force
P_{test}	maximum load carried by the specimen
r	radius of gyration of cross-section
s	spacing of shear reinforcement
$(s_b)_{i,j}^n, (s_t)_{i,j}^n$	bottom and top fiber strains, respectively, in section i at point j of the top strut at load step n
s_1, s_2	lengths of adjacent truss panels
$x_{i,k}$	distance between sections i and k

$(S_b)_i^n, (S_t)_i^n$ average bottom and top fiber strains, respectively, in section i of the top strut at load step n

S_2 section modulus relative to tension fibre

T axial tensile force in the bottom strut

T_i force acting at the tension corner of the opening causing inclined crack to be formed

T_t tensile force in the truss bottom chord

V shear due to applied load

V^n average shear force in the top strut at load step n

V_b shear carried by bottom strut

V_c nominal shear strength provided by concrete

$V_{i,k}^n$ shear force in the top strut acting at sections i and k at load step n

V_s nominal shear strength provided by shear reinforcement

V_t shear carried by top strut

W_h horizontal component of force in the diagonal truss member

α angle formed by inclined crack at the tension corner of the opening and beam longitudinal axis

Δ_ℓ deflection of the beam as a whole caused by live load

Δ_m total deflection at midspan caused by live load

Δ_p deflection due to prestress

Δ_s deflection due to localized bending moment of the struts caused by live load

θ angle between diagonal and bottom chord truss members

ϕ curvature

xxx

1. INTRODUCTION

1.1 General Remarks

In modern building construction, the mechanical and electrical services are usually carried in the space within the floor-ceiling sandwich. Passing utility services through openings in the floor beam webs minimizes the required storey height, reducing the cost of the structure. Thus, the ceiling may be attached directly to the underside of the floor beams. Unless proper provisions are made by the designer for these web openings, the effect of web openings on the strength and serviceability of the floor beams may be critical.

Limited research has been carried out on the effect of web openings on the behavior and strength of prestressed concrete beams. However, there is still a need for further investigation since some issues have not been completely resolved. The aims of this investigation were:

1. to investigate behavior at the ultimate load level and provide recommendations concerning design for the ultimate limit state.

2. to develop an analytical model able to simulate the behavior in the serviceability range of

1

prestressed concrete beams with large rectangular web openings.

The experimental program consisted of tests to failure of eleven full-size simply supported prestressed concrete T-beams. The variables selected were the length of the openings, the depth of the top strut, and the shear reinforcement of the opening. An analytical model based on a truss analogy was developed to simulate behavior in the post-cracking range. The truss model permits evaluation of variations in flexural stiffness in the struts above and below openings, as well as at solid sections of the beam. Experimental results were compared with results obtained from the analytical model. Based on the results of this investigation, design recommendations are presented for both the serviceability and ultimate limit states.

1.2 Literature Review

1.2.1 Introduction

This section reviews the results of previous research on concrete beams with web openings. The effect of the selected parameters on the behavior of such beams as well as the suggested design recommendations are examined. Existing codes provisions are also discussed.

A number of papers were found to deal specifically with reinforced concrete beams containing multiple or isolated web openings. However, only a few major investigations dealing with prestressed concrete beams with multiple large web openings or isolated large web openings were found.

1.2.2 Reinforced Concrete Beams

Lorentsen[13] conducted an experimental investigation on reinforced concrete T-beams containing a single rectangular opening. The objective of his work was to present a design method for reinforced concrete beams with web openings. Lorentsen tested four beams under different loading conditions. The modes of failure observed were yielding of main reinforcement, bond failure at the edge of the opening and secondary stress concrete crushing. Two beams that failed by yielding of main reinforcement were not weakened by the presence of the opening and the capacity of the main tensile reinforcement was fully developed. In the beams presenting bond failure at the edge of the opening or secondary stress concrete crushing, the sections at the edge of the opening were deciding factors in the magnitude of the failure loads. The crack formed at the end of the reinforcing bars in the upper framing flange opened and extended at an angle toward the

edge of the opening so that bond between steel and concrete was destroyed. From the tests it was concluded that additional stirrups should be placed near the edges of the openings to avoid bond cracks.

An elastic analysis for determining the forces in the struts was proposed by Lorentsen. The capacity of the top strut to resist these forces was determined according to the German Concrete Code DIN 4227[9]. The main assumption in the analysis was that the bottom strut where the tensile reinforcement was placed would be considered as a tension member, unable to resist moment, as shown in Fig. 1.2.2.1. Therefore the total shear force would be carried by the top strut. Lorentsen's main assumption resulted in a very conservative estimate of beam strength.

Nasser, Acavalos and Daniel[16] provided a theoretical approach for reinforced concrete beams with large web openings. The assumptions made in the analysis and design of such beams were that the top and bottom struts would behave like the chords of a Vierendeel panel, would have contraflexure points at their midspan, and when adequately reinforced would carry the external shear in proportion to their areas. It was also assumed that the shear in the struts would induce a diagonal force concentration at the corner of the opening and its value would be twice the shear force.

To verify the validity of the assumptions made, ten simply supported reinforced concrete beams with rectangular cross- sections were tested. The selected parameters were the size and location of rectangular openings and the amount of shear reinforcement in the struts. The test results corroborated most of the assumptions. It was verified that the top and bottom struts behave in a manner similar to the chords of a Vierendeel panel, as proposed earlier by Segner[23]. At ultimate, the shear force at the opening was found to be carried by the struts in proportion to their cross-sectional areas. Readings taken at the top strut showed that the position of the contraflexure point was not necessarily at its midlength, but its range of variation was relatively small. Inclined reinforcement placed at the corners of the opening to avoid severe and extensive diagonal cracking was found to be effective. The reinforcement details of a test specimen are shown in Fig. 1.2.2.2. A method to determine a safe value for the shear concentration factor at the corners of the opening was proposed. Adequately- reinforced large openings in rectangular beams did not reduce the ultimate capacity of the beam but reduced its stiffness.

A study of square web openings in continuous lightweight-aggregate concrete joists was made by Hanson[10]. The principal variables considered were

horizontal and vertical positions of the opening, size of the opening and the effect of the stirrup reinforcement along the sides of the opening.

The test data indicated that, near the midlength of the compressive strut, the compressive force could be considered to be concentrated at the centroid of the strut. The magnitude of the axial compressive force could be calculated from the external bending moment. It was found that until cracking, the distribution of shear between the struts was approximately in proportion to the cross-sectional areas of the struts. After cracking, the compressive strut tended to carry all of the shear. It was observed that the stirrup reinforcement along the sides of the opening was of great benefit. Failure occurred either by crushing of the concrete in flexure at the stub, not being influenced by the presence of the opening, or by shear at a location between the opening and the center stub, resulting in a 12 percent increase in the specimen capacity.

A conservative prediction of the strength of beams with square openings in unreinforced webs could be obtained by calculating the load causing tensile cracking at the opening. Hanson's work was extended by considering other shapes of openings, multiple openings and openings near noncontinuous supports.

1.2.3 Prestressed Concrete Beams

The effect of web openings in prestressed concrete beams was first reported by Ragan and Warwaruk[19]. Four model beams were tested to provide experimental information to permit the design of prestressed concrete T-beams with large web openings. To confirm the validity of the suggested design method two full size T-beams were tested to failure. Both sets of beams were provided with multiple openings. Figure 1.2.3.1 and Fig. 1.2.3.2 respectively show the details of a typical model beam and a full size beam.

[...]c information derived from the model beam tests [...] the load-deflection relationship. The mode of failure [...] all the model beams with web openings was through [...] formation of a mechanism in the struts. In two of the beams the mechanism developed over two openings.

Based on the test results of the model beams, full size beams were designed and tested. The main assumption was that the shear at a critical section containing a web opening would be resisted by the bottom and top struts in proportion to their areas. Since the model beams exhibited severe cracking at the connection of the vertical posts to the flange No. 5 stirrups were provided at the posts close

to the short faces. To avoid failure by inclined cracking in the bottom strut No. 3 stirrups were provided in the bottom strut. The full-size beams also failed through formation of a mechanism, but it was not as clearly shown as in the test model beams. The authors concluded that failure occurred when the flange above a web opening failed by shear-compression resulting in a sudden release of energy with a stress wave traveling along the beam and failing each post in turn.

It was concluded that long span single-tee members with large web openings could be built to meet code requirements in every manner. No design procedure was suggested.

Linder[12] conducted tests on thirty simply supported prestressed concrete beams with multiple large web openings. His test program was based on the results of the tests of Sauve[21] and Le Blanc[11] on prestressed concrete T-beams containing large multiple rectangular and parallellogram shaped openings. The investigation was concerned with the behavior and the development of design procedures for prestressed concrete T-beams with large web openings. The prime variable in the test program was the reinforcing requirements in the region around the openings. Other parameters such as loading conditions and flexural capacity were varied to place different demands on

the reinforcement. Figure 1.2.3.3 shows details of a typical test specimen.

The failure modes observed in this test program were flexural, post shear, strut shear and strut flexure. Ten of the beams failed in flexure under three of five different loadings. The failure was caused by rupture of one or more of the prestressing strands. The beams failing in post shear presented a failure indicated by the failure of a post in the shear span which resulted in the lateral displacement of the top and bottom portions of the post. The strut flexural reinforcement failed and a mechanism formed over two openings. It was found that for the beams failing in post shear the reinforcement in the post closer to the support had the greatest influence on the ability of the post to resist the applied forces. It was also observed that load carrying capacity of the beams increased by increasing the area of vertical stirrups in the post closer to the support and by providing inclined post reinforcement. The addition of the horizontal stirrups in the posts increased the shear capacity of the post. The size and shape of the posts also affected the post behavior. Larger posts had their flexural capacity increased. The author stated that increasing the horizontal dimension of vertical posts increases the post's ability to resist horizontal shear and reduces the strain

in the post reinforcement. The beams failing in strut
shear presented a shear compression failure of the top
strut and/or a shear and tension failure of the bottom
strut. The addition of shear reinforcement in the top and
bottom struts usually eliminated this type of failure.
Beams failing in strut flexure presented a failure in which
both ends of the top and bottom strut failed in flexure
developing a mechanism over one opening with hinges at both
ends of the struts. Based on the test results Linder
suggested that the strut flexural capacity could be
reasonably well predicted by calculating the load at which
the first hinge would be formed. This prediction was based
on the following assumptions:

-the shear at the opening is distributed to the top and
bottom struts according to the cross-sectional area of
the struts.

-the inflection points are located at the strut
midlength.

-the axial force in the top strut acts through its
centroid and in the bottom strut through the centroid
of the tension reinforcement. The axial force in the
strut is equal to the beam moment at the strut
centerline divided by the distance between the forces.

-the axial load-bending moment interaction diagrams are
considered for checking the strut flexural capacity.

This procedure was found to lead to a conservative prediction of the strut flexural capacity. Linder also proposed that the solid shear span should be designed in the usual manner using ACI Building Code (318-71) provisions, and extra stirrups carrying the total shear on the section should be placed adjacent to the opening closer to the support. The posts should be designed to resist the horizontal shear due to the change in the struts axial forces. The determination of a relationship for the distribution of shear to the top and bottom struts required further investigation.

A study of large rectangular web openings in simply supported prestressed concrete beams was conducted by Barney[4]. Thirteen full size simply supported prestressed concrete T-beams were tested. Figure 1.2.3.4 shows the details of a typical specimen. The variables investigated were the size of the rectangular web opening, the location of the opening along the span and the amount of main flexural and web shear reinforcement.

An analytical model was developed for calculating forces in the struts. The model consisted of two members corresponding to the top and bottom struts which were assumed to frame into rigid abutments as shown in Fig. 1.2.3.5. Since it was observed by Hanson that cracking affected the distribution of forces in the struts, the

determination of the stiffness of cracked members was taken into account in the analytical procedure. The application of the analytical procedure is limited to beams with struts not penetrated by a full depth crack. Although the analytical procedure was based on the assumption of linear elastic materials properties it was used to predict the distribution of forces in the inelastic range of response.

The test results established that the strength of prestressed concrete beams with large web openings was drastically reduced when cracking at an opening was allowed to extend into the required strand embedment length. It was emphasized that web openings must be located outside the required embedment length and additional vertical stirrups must be provided adjacent to the openings to carry the full design ultimate shear force. It was also observed that cracking had a significant effect on the shear distribution in the struts. Before cracking, shear was distributed to the struts in proportion to their gross moment of inertia.

To take into account the redistribution of forces in the struts after cracking had occurred, Barney proposed a design procedure that depends on the extent of cracking in the tensile strut. Before a crack extends the full depth of the tensile strut, the tensile strut is designed to carry some of the shear. The recommended design forces are:

$$V_t = V \frac{I_t}{I_t + I_{b(cr)}} \qquad (1.1)$$

$$V_b = V \frac{I_b}{I_t + I_b} \qquad (1.2)$$

When a crack had extended the full depth of the tensile strut, the compressive strut should be designed to carry the total shear. The recommended design forces are:

$$V_t = V \qquad (1.3)$$
$$V_b = 0 \qquad (1.4)$$

The use of this procedure for determining the shear forces in the struts at ultimate load leads to a conservative design since Barney's test results showed that at ultimate the shear carried by the compressive strut varied from 43% to 59% of the total shear.

1.2.4 Existing Code Provisions

Most codes of practice make little or no recommendation about web openings in prestressed or reinforced concrete beams. The ACI Building Code (318-77)[1] makes general recommendations concerning the size of openings created by pipes embedded in concrete

beams. The size of the opening is restricted to one third of the beam thickness and the space between openings is restricted to three diameters or widths on center. However the Code makes no reference to requirements for reinforced or prestressed concrete beams provided with web openings.

The British Standard Code of Practice (CP110-72)[6] and the Canadian Standard (CAN-A23.3-M77)[17], although they refer to openings in floor slabs, do not specifically deal with beams containing web openings.

The New Zealand Standard (DZ3101-80)[18] does give some recommendations which have been largely restricted to the restatement of general principles in "good engineering practice". The Code states that adjacent web openings placed in flexural members shall be arranged so that potential failure planes across such openings cannot occur.

Small square or circular web openings may be placed in the mid-depth of the web provided that cover requirements for longitudinal and transverse reinforcement are satisfied. The clear distance between such openings shall not be less than 150 mm. The size of a small opening shall not exceed 1000 mm^2 for flexural members with an effective depth less than or equal to 500 mm or 0.004 d^2 when the effective depth is more than 500 mm.

A web opening is considered large whenever its largest dimension exceeds one quarter of the effective depth of the

A web opening is considered large whenever its largest dimension exceeds one quarter of the effective depth of the member. Large web openings shall not be placed where they could affect the flexural or shear capacity of the member nor where the total shear stress exceeds $0.4 \sqrt{f_c'}$ or in potential plastic hinge zones. In no case shall the height of the opening exceed 0.4 d nor shall its edge be closer than 0.33 d to the compression face of the member.

The Code also makes some recommendations concerning the longitudinal and transverse reinforcement at large openings. The longitudinal and transverse reinforcement shall be placed in the compression side of the web to resist one and one half times the shear and moment generated by the shear across the opening. The transverse web reinforcement extending over the full depth of the web shall be placed adjacent to both sides of a large opening over a distance not exceeding one half of the effective depth of the member to resist the entire design shear across the opening. Typical details of reinforcement around a large web opening according to the New Zealand Standard (DZ3101-80) are presented in Fig. 1.2.4.1.

1.2.5 Summary and Conclusions

Some literature is available on aspects of the problems 'encountered in dealing with prestressed and reinforced concrete beams with large web openings. Existing papers were briefly reviewed in the previous sections. From these references it can be concluded that the most common failure mode observed in both prestressed and reinforced concrete beams with web openings is the formation of a hinging mechanism in the struts. Frequently, the capacity of the specimen was reached when the bottom strut had failed in shear followed by a hinging mechanism in the top strut. Test results show that the top and bottom struts behave in a manner similar to the chords of a Vierendeel panel.

The most important parameters affecting specimen behavior are location and length of the opening and shear reinforcement at the opening region. When the opening is located inside the strand embedment length, cracking extends toward the support propagating along the prestressing strand and initiating failure by causing the strand to slip. As the opening length is increased, the load causing cracking at the opening decreases and consequently a reduction in the specimen strength occurs. The shear reinforcement at the opening region has the

greatest effect on specimen behavior and strength since it is able to restrict crack propagation if properly designed.

The only analytical model available in the literature is the one presented by Barney[4]. The model system proposed behavior as an elastic frame with the predominant property of each strut being its flexural stiffness. The model is intended to provide a method for calculating forces in the struts. Although the method is based on the assumption of linear elastic material properties it is applied to the distribution of forces in both the elastic and inelastic ranges of response.

The design procedures recommended basically involve the determination of shear distribution between struts at ultimate, reinforcement detailing at the opening region to avoid premature failures and calculations of shear and flexural capacities of the struts. Most researchers[11,12,16,21] propose a shear distribution between struts at ultimate in proportion to their cross sectional areas. Barney proposes a shear distribution dependent on the extent of cracking in the bottom strut. If the bottom strut is fully cracked the top strut is designed to carry the total shear. The reinforcement detailing at the opening region is restricted to the lateral reinforcement placed adjacent to the opening to avoid severe cracking extension. Acavalos suggests a

reinforcement at the corners of the opening able to resist two times the simple shear force and placed around the opening. Barney recommends an additional vertical stirrup reinforcement at each side of the opening to resist the total shear force.

Based on the review of literature presented in this chapter it is concluded that some aspects of behavior and design of prestressed concrete beams with web openings are not yet totally resolved. There is a need for analytical models able to treat the geometric discontinuity present in such beams and to simulate the post-cracking behavior. It is felt that the proposed distributions of shear to the top and bottom struts may be quite conservative and in many cases are not compatible with test results. Although proposals for additional reinforcement at the corners of the opening are beneficial in restricting crack propagation, more rational bases for designing and detailing that reinforcement are required.

In view of the above limitations an analytical model including the effects of progressive cracking was developed and an experimental test series was conducted to provide data for establishing criteria for strength design of prestressed concrete beams with large rectangular web openings.

Tension Member
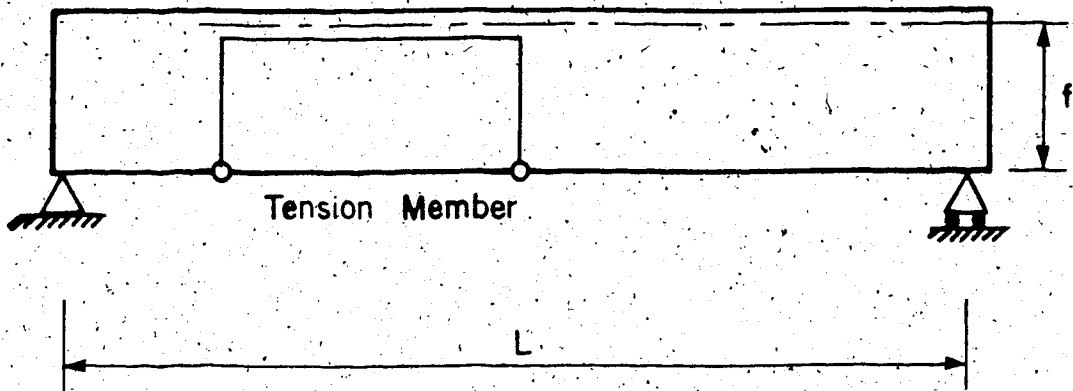
Figure 1.2.2.1 Lorentsen's Idealized Beam with Web Opening.

6'-0"

A

B

6"

A

B

6"

7'-6"

2'-6"

2'-0"

6"

12'-0"

A'

B'

#4

A'

B'

7" o.c.

1 1/4" o.c.

7" o.c.

5"

8"

5"

18"

9"

9"

Section
A-A

Section
B-B

#6

#6

#2

#6

#6

Section
A'-A'

Section
B'-B'
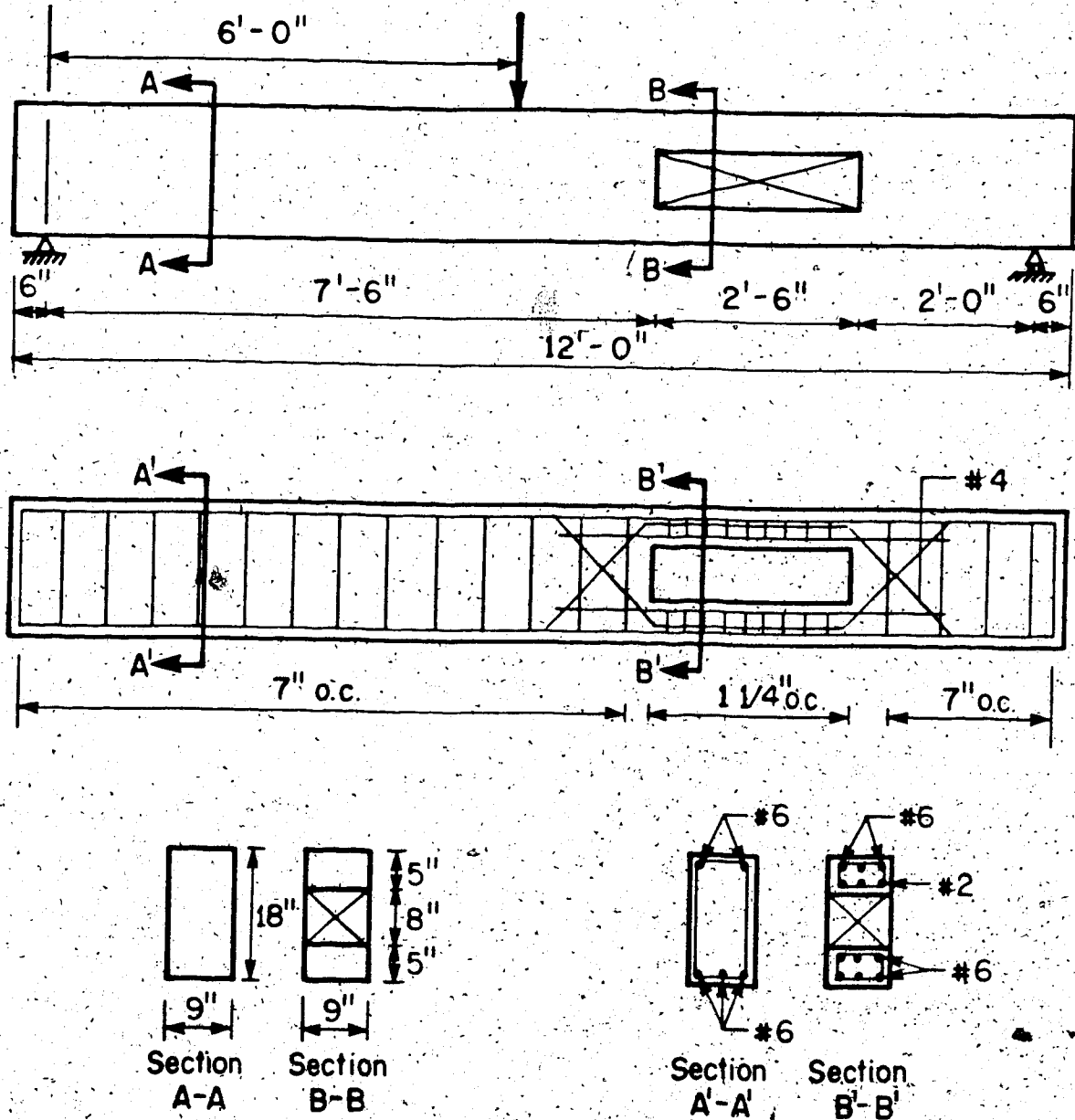
Figure 1.2.2.2   Details of Nasser, Acavalos and Daniel's

Specimen.
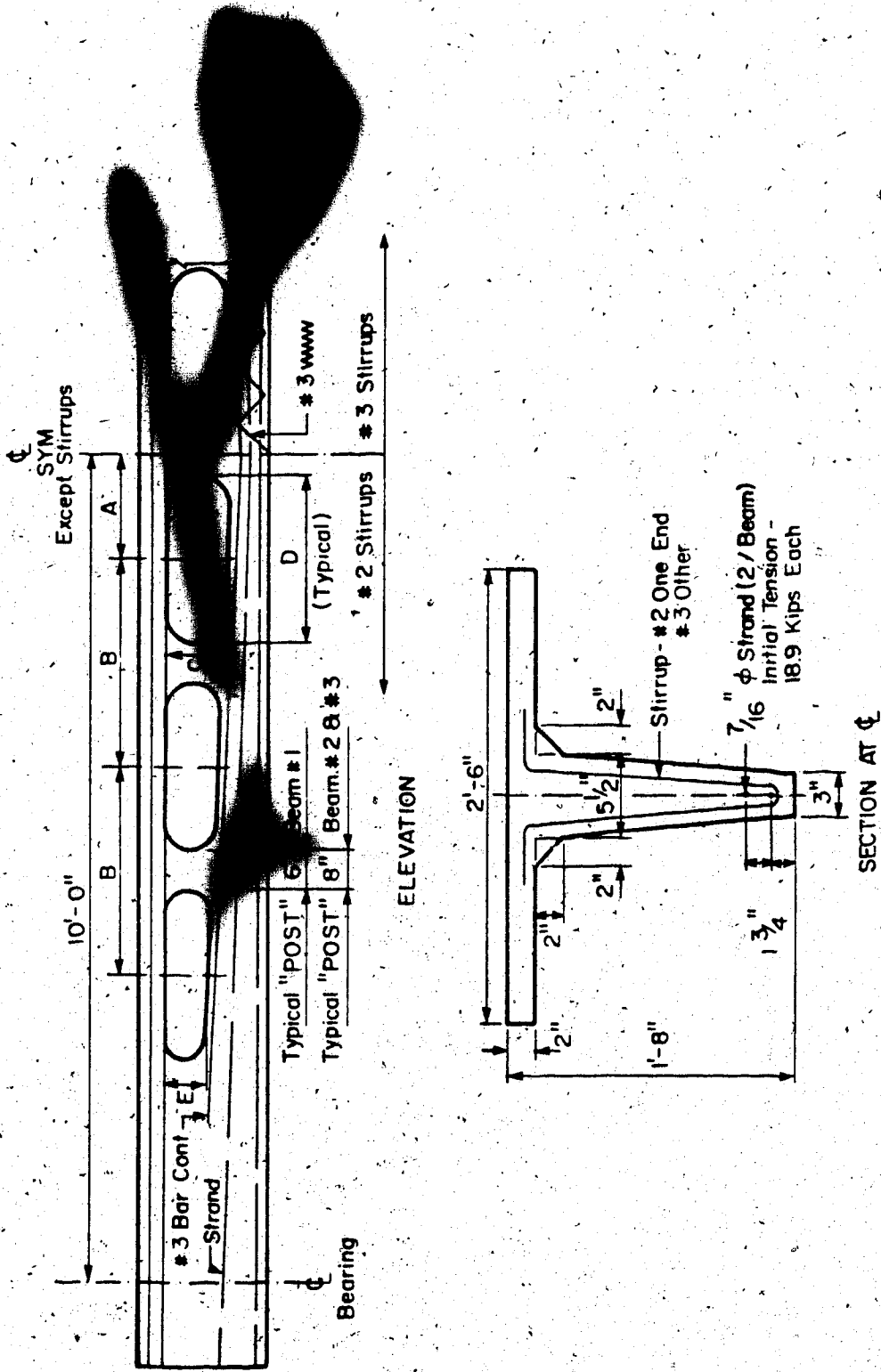
Figure 1.2.3.1   Details of Model Beam Tested by Ragan and Warwaruk.
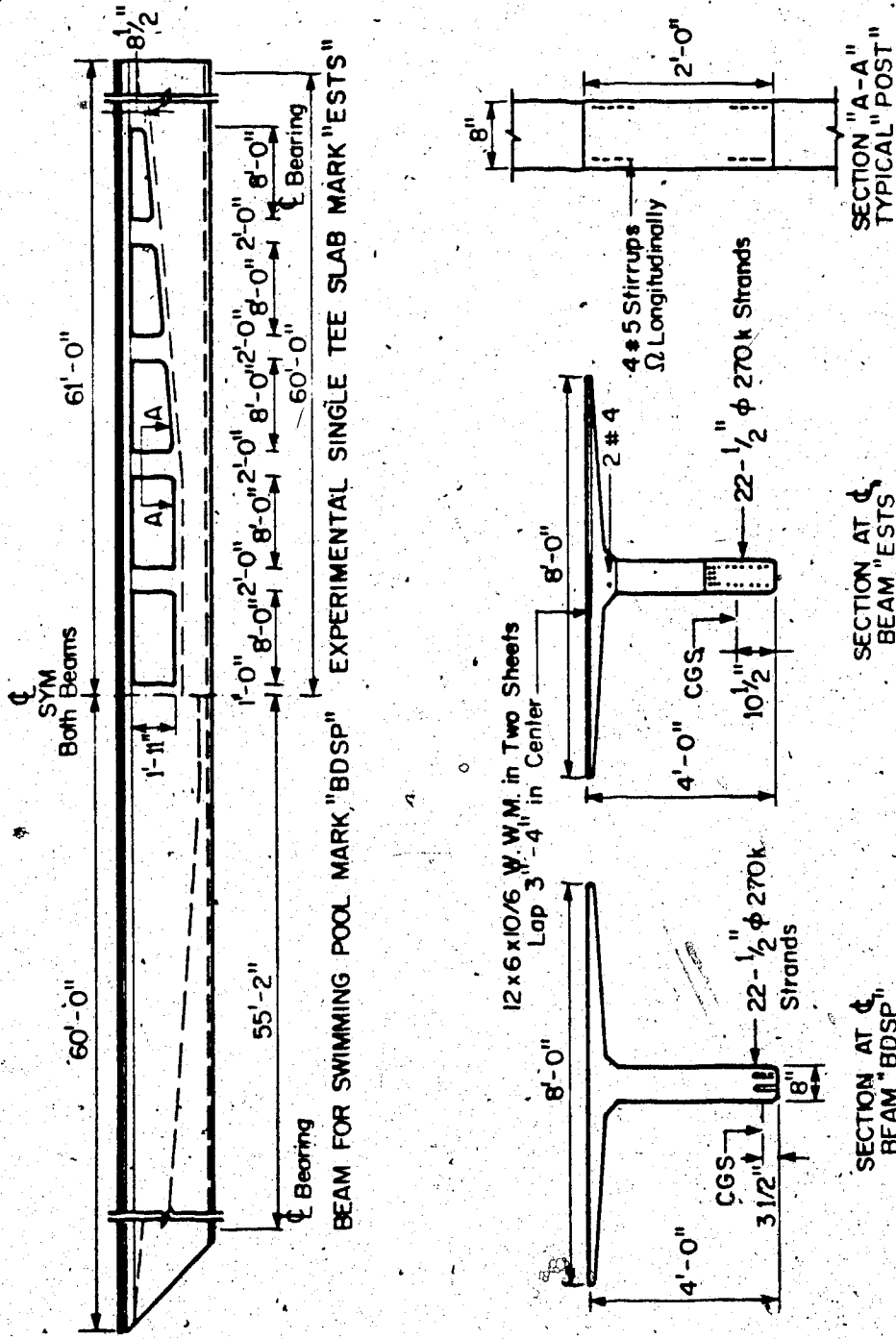
Figure 1.2.3.2   Details of Full Size Beam Tested by Ragan and Warwaruk.
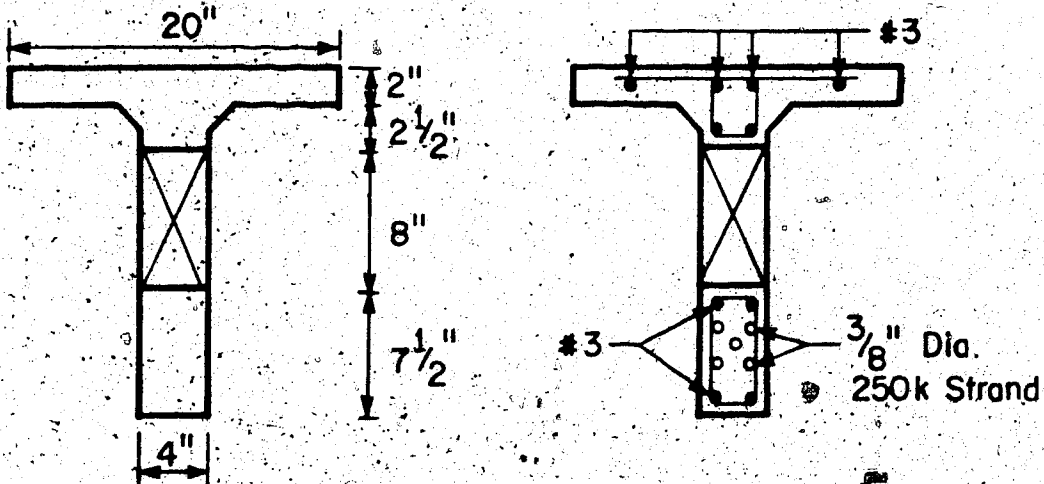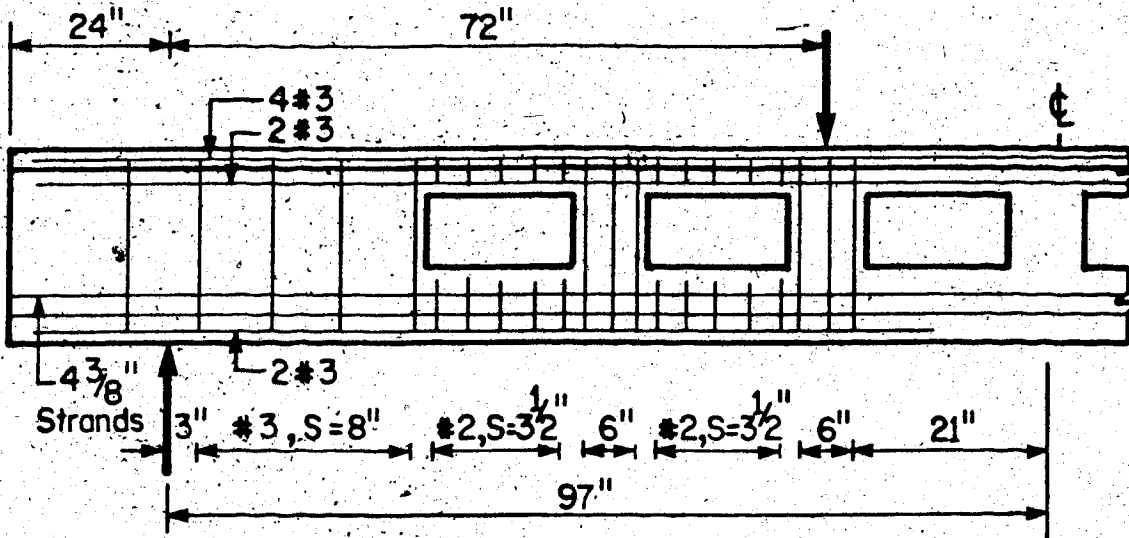
Figure 1.2.3.3 Details of Typical Specimen Tested by Linder.
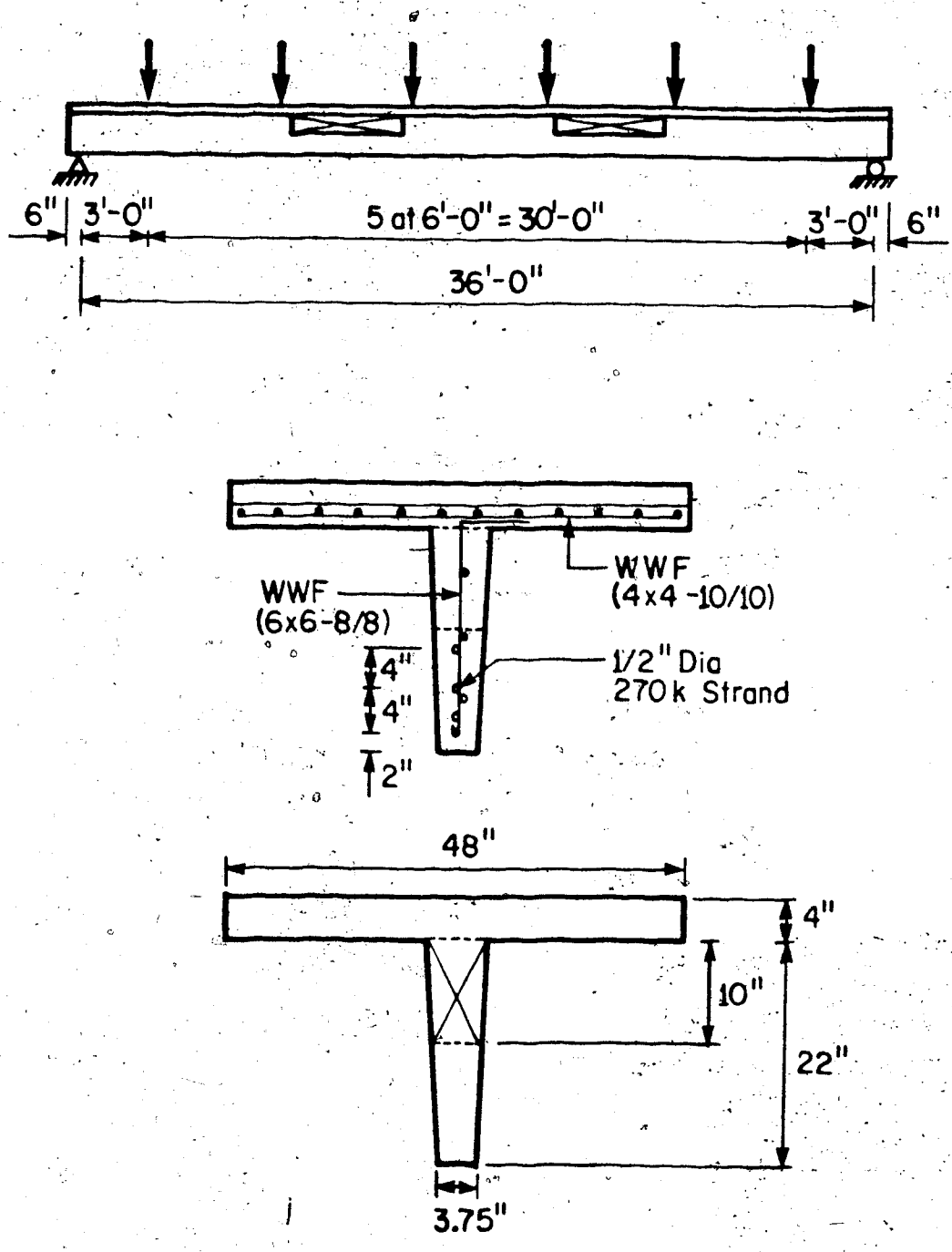
Figure 1.2.3.4   Typical Beam Tested by Barney.

* Point of Contraflexure
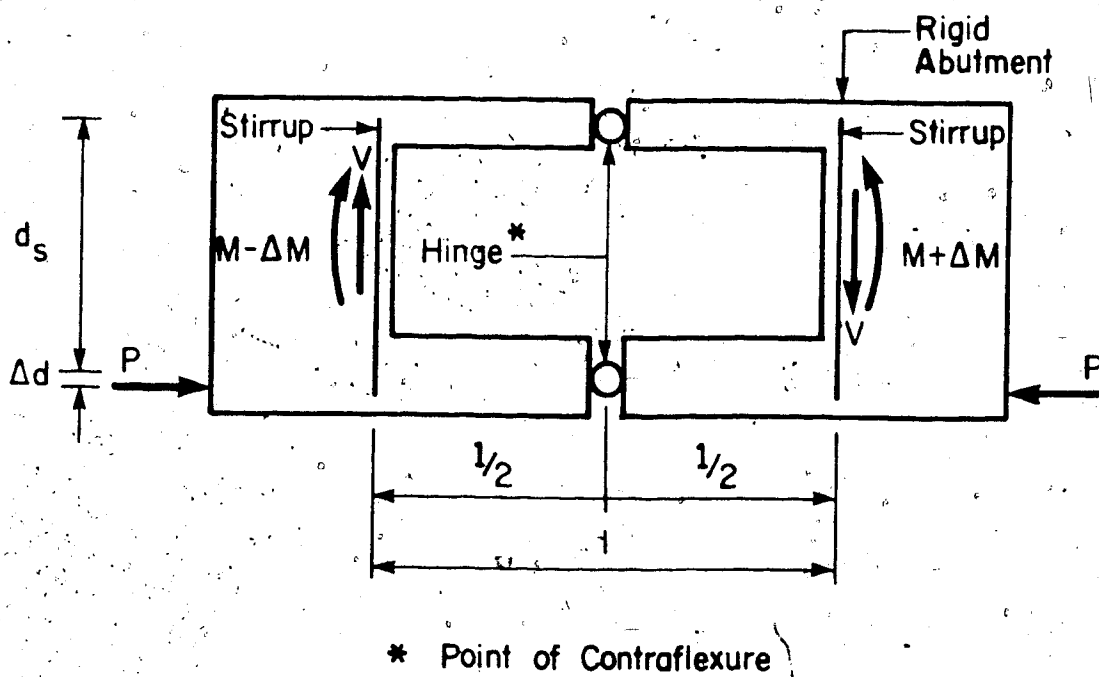
Figure 1.2.3.5   Idealized Model Proposed by Barney.
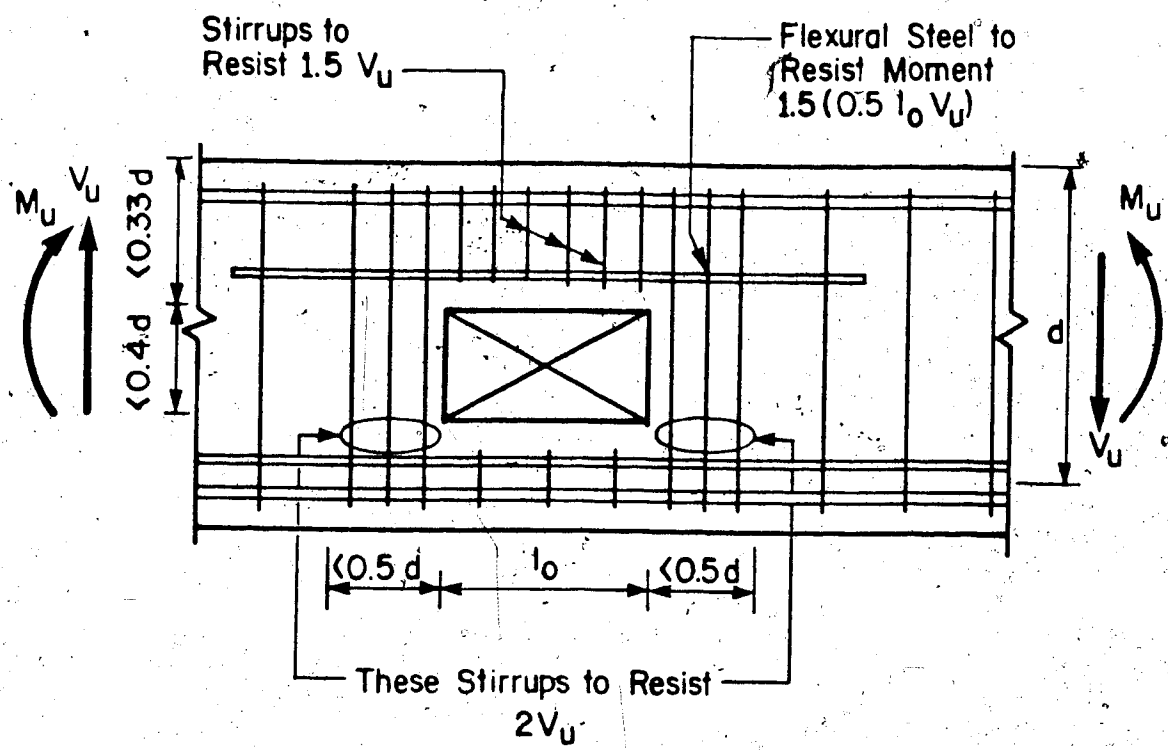
Figure 1.2.4.1 Details of Requirments of a Large Web
Opening According to New Zealand Standard
(DZ 3101-80).

2. EXPERIMENTAL PROGRAM

2.1 Introduction

The prime concern of this program was to study the overall behavior of prestressed concrete beams with large web openings. Eleven simply supported specimens containing rectangular openings were tested. The external dimensions of all specimens were the same.

Measurements taken during each test included applied loads, deflections, and concrete and steel strains. Strains were measured either mechanically over 2 in. or 5 in. gage lengths, or using electrical resistance strain gages.

The selected parameters were:

- the length of the opening
- the depth of the top strut
- the amount and type of shear reinforcement

2.2 Specimens

The eleven specimens tested were simply supported on a span of 29 ft. with four point loads located as shown in Fig. 2.2.1. The loading system is described in Section

2.6. Overall cross-section dimensions were kept constant for all specimens with the size and location of web openings varying as indicated in Fig. 2.2.2 to 2.2.6.

The specimens were designed according to the ACI Building Code (318-77)[1] for an ultimate midspan moment of 2040 kip. in. (P = 8.8 kips) and service load moment at midspan of 1090 kip. in. (P = 5.17 kips). The maximum shear force at ultimate load was 19.6 kips. Minimum shear reinforcement as required by ACI Building Code (318-77) provided a shear capacity of 28.0 kips and was used for all beams except A2 and Series D where the stirrup spacing in the end shear span was decreased by half resulting in a calculated shear capacity of 32.0 kips. All openings were located outside the strand embedment length calculated according to provisions of the ACI Building Code (318-77) as 56.5 in.

Longitudinal reinforcement consisted of a combination of prestressing strand and mild reinforcement. Prestressing was provided by four 3/8 in. diameter, 250K Grade, seven-wire straight strands for all specimens. The bottom mild reinforcement consisted of four 0.44 in. diameter reinforcing bars. The position of these bars varied according to the vertical location of the openings. The top longitudinal reinforcement was also provided by four 0.44 in. diameter reinforcing bars. In

the specimens corresponding to Series C, two additional longitudinal W2.9 wires were located along the length of the opening to hold the stirrups in place.

Web shear reinforcement was provided by double-legged stirrups set vertically and bent from W2.9 wires. Additional 0.44 in. diameter inclined reinforcing bars were placed adjacent to the tension corners of the openings in the specimens corresponding to Series D. Figures 2.2.4, 2.2.5 and 2.2.6 show the reinforcement details of specimens B1, C1 and D2. Appendix A contains the reinforcement details for all other specimens.

To study the effect of parameters listed in Section 2.1, the specimens were divided into four series. Series A consisted of two beams without openings. Series B, C and D consisted of beams, each with two openings placed symmetrically about the midspan with the distance from the support to the center of the opening constant at 8.7 ft.

Specimens in Series A were control beams, tested to provide a standard with which to compare the results from beams with openings. BEAM A1 contained double the minimum shear reinforcement in the end shear span.

Series B, C and D each consisted of three beams with opening lengths of 56 in., 40 in., and 24 in. In Series B and D the openings were located immediately below the flange. In Series C the openings were located 4 in. below the flange so that the top strut consisted of a T-section.

Specimens in Series D were provided with diagonal web reinforcing bars adjacent to the openings as well as double the minimum shear reinforcement required in the end shear span.

Details of the specimens tested are summarized in Table 2.2.1.

2.3 Materials

The concrete mix was designed to produce a 15 day cylinder strength of about 6.0 ksi. High Early Strength Type 30 Portland Cement and normal weight river washed aggregate were used. The maximum coarse aggregate size was 3/8 in. and the fineness modulus of the sand was 2.75. The water-cement ratio was 0.4. Superplasticizer Pozzolith 400-N was used to provide adequate workability of the concrete mix. The proportions used were as follows:

Cement	280 lb
Sand	322 lb
Coarse aggregate	329 lb
Water	112 lb
Superplasticizer	796 mL

For each specimen, four batches of concrete were required. Two 6 in. by 12 in. cylinders were cast for each batch and subjected to the same curing as the specimens.

The properties of concrete were determined from compressive and splitting tensile tests on those cylinders. The modulus of elasticity for each specimen was the secant modulus of elasticity at 0.4 f_c' found from the the load-deformation curve. All measured concrete properties are presented in Table 2.3.1.

The prestressing reinforcement used in all specimens was four 3/8 in., 250 K Grade, seven-wire prestressing strands which were continuous throughout the beam. Three physical tests in the strand indicated an average strength of 276.0 ksi and a modulus of elasticity of 28,900 ksi. The stress-strain diagram reduced from load-strain curve obtained directly from test machine is presented in Fig. 2.3.1.

The longitudinal reinforcement in all specimens and the inclined reinforcing bars, when provided at the tension corners of the openings, were 0.44 in. in diameter. The average yield stress determined for three specimens was 70.7 ksi and the modulus of elasticity was 31,000 ksi. The stress-strain diagram for a 0.44 in. diameter reinforcing bar is shown in Fig. 2.3.2.

Minimum web shear reinforcement as specified by the ACI Building Code was provided by double-legged stirrups bent from W2.9 wires. The average yield stress determined for three specimens was 81.0 ksi and the modulus of

elasticity was 30,000 ksi. The stress-strain diagram for W2.9 wire is shown in Fig. 2.3.3.

2.4 .Construction

Fabrication of the test specimens was carried out in the I.F. Morrison Structural Engineering Laboratory of the University of Alberta.

Once the stirrups had been set in place on the prestressing bed, the prestressing strands were threaded and prestressed to 186 ksi. The force in each strand was monitored by load cells at the fixed end. Next, the reinforcement cage was completed.

The openings were formed by styrofoam blocks cut to the shape of web openings and attached to the form at the required location. To avoid flaws in the concrete in the vicinity of the openings, holes were made vertically in the styrofoam blocks to allow the air to escape. High early strength concrete mixed in the laboratory batch plant was used. Twenty-four hours after casting, the form was removed and the cylinder moulds were stripped. All the specimens and cylinders were cured the same way. A moist burlap was wrapped around the specimens and the cylinders. Large pieces of waterproof plastic sheets were used to cover the specimens to keep the atmosphere inside

the plastic cover moist. Regular wetting was needed to prevent the burlap from drying.

The prestressing strands were cut after five days of moist curing. Prior to cutting, demec gage points were attached to the concrete web and flange at midspan. Data recorded at these points were used to determine prestress losses, ranging from 10.45 ksi to 10.52 ksi with a mean value of 10.5 ksi.

2.5 Instrumentation

The specimens were instrumented to obtain data throughout the complete range of loading. A 20 kips capacity load cell was used to monitor loads applied through four 15 kips capacity hydraulic jacks.

Electrical resistance strain gages were mounted and waterproofed on the mild longitudinal reinforcement at the bottom and top struts and also at the midspan. In all specimens containing openings, one of the openings was instrumented with electrical resistance strain gages at locations shown in Fig. 2.5.1.

The web shear reinforcement and concrete strains were measured using 5 in. and 2 in. demec gages (demountable mechanical extensometers). Before the specimens were cast, 0.25 in. rods were brazed 5 in. or 2 in. apart along the

stirrups in the region of the opening. Rubber hoses were then sleeved onto those rods. After the specimen was cast and the concrete hardened, the rubber hoses were removed. Demec points were then attached to the tip of each rod. Figure 2.5.2 shows the demec point locations on the stirrups for a typical specimen.

To determine the distribution of forces in the top strut, demec points were also attached to its upper and lower surfaces. The number of demec points at the top strut depended on the length of the opening. Figure 2.5.3 shows the demec point locations at the top strut for BEAM D2.

Data to determine the prestress losses were obtained from demec points attached to the web and flange at midspan. Deflections were measured using LVDT (linear variable-differential transformers) placed beneath the openings and at midspan of the specimen. Figure 2.5.4 shows the LVDT locations for BEAM D3.

The data acquisition Nova 2 mini computer was used to record data for all specimens. Appendix B contains the strain-gage locations and locations of demec points in stirrups and top strut for all specimens.

2.6 Test Setup and Test Procedure

The specimens were tested in the load frame shown in Fig. 2.6.1. Lateral braces were provided to prevent the specimens from deflecting laterally during loading. The specimen supports were hinged to permit rotation. One of the supports was fixed longitudinally and the other was mounted on rollers to permit simple beam action. The simple support roller system rested on concrete pedestals. Prior to loading, level readings were taken at the supports and at mid-span to determine the camber due to prestress.

A four-point loading system was used for all specimens. The loads were applied by hydraulic jacks positioned at intervals of 69.6 in. along the span. Load was applied to the specimens in increments, with approximately 24 load steps until failure, to facilitate data recording and accurate observation of the behavior of the specimen. During each increment, the load was kept constant while cracks were marked, and loads, displacements and strains were measured and recorded. The L.V.D.T. at midspan and a load-cell monitoring the load were connected to the H.P. 2FA X-Y plotter to provide a continuous load-deflection curve. Each specimen was tested to failure. Photogr████████████en after failure.

Table 2.2.1. Test Program

Specimen Number	Opening Size	Depth of Top Strut	Web Reinforcement
A1	None	–	W2.9 Stirrups
A2	None	–	W2.9 Stirrups
B1	56x8 in.	4 in.	W2.9 Stirrups
B2	40x8 in.	4 in.	W2.9 Stirrups
B3	24x8 in.	4 in.	W2.9 Stirrups
C1	56x8 in.	8 in.	W2.9 Stirrups
C2	40x8 in.	8 in.	W2.9 Stirrups
C3	24x8 in.	8 in.	W2.9 Stirrups
D1	56x8 in.	4 in.	W2.9 Stirrups and 0.44 in. diameter Inclined Bars
D2	40x8 in.	4 in.	
D3	24x8 in.	4 in.	

Table 2.3.1 Measured Concrete Properties.

Specimen	f'_{ci}(ksi)[1]	f'_c(ksi)[2]	f'_{sp}(ksi)[2]	E_c(ksi)[2]
A1	5.66	6.27	0.447	3354
A2	5.80	7.03	0.402	3660
B1	6.18	6.90	0.456	3672
B2	5.95	6.57	0.457	3425
B3	5.89	6.15	0.432	3287
C1	5.23	6.45	0.402	3186
C2	5.20	6.65	0.450	3447
C3	5.48	6.60	0.451	3459
D1	5.50	6.78	0.432	3441
D2	5.30	6.10	0.410	3412
D3	5.81	7.22	0.420	3551
Mean Value	5.64	6.61	0.43	3495
Standard Deviation	0.32	0.36	0.02	154
Coefficient of Variation	6%	5%	5%	4%

Note: (1) Reported values represent the average of 2 tests.

(2) Reported values represent the average of 3 tests.
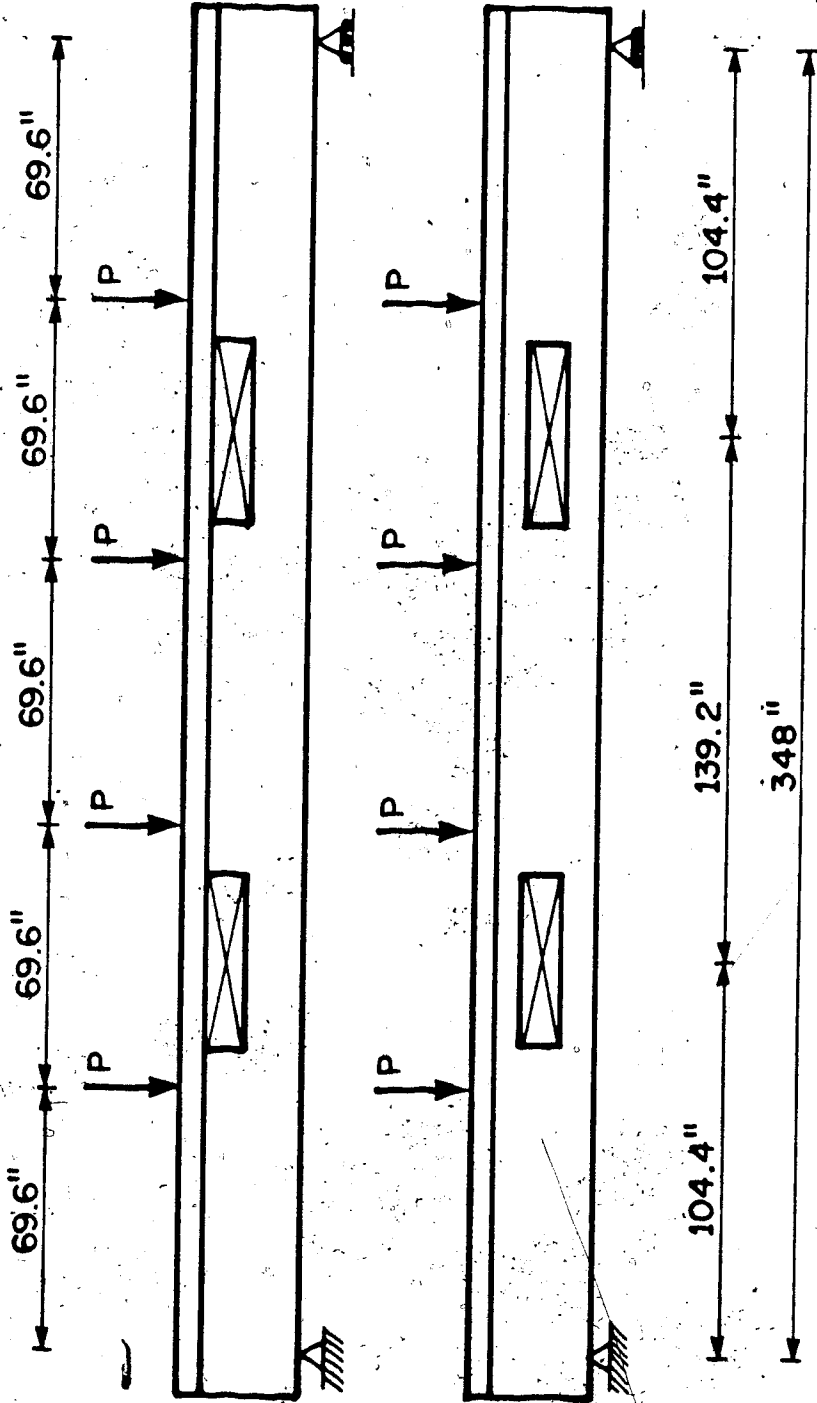
Figure 2.2.1 Typical Specimens Tested
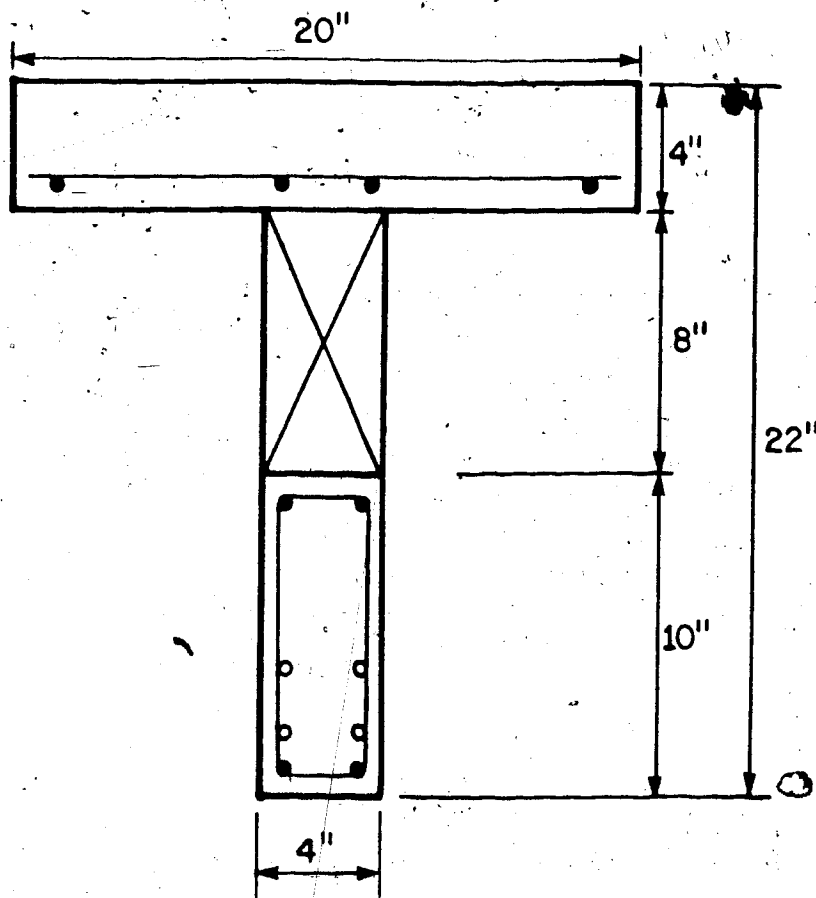
Figure 2.2.2   Typical Concrete Cross-Section - Series B
and Series D.
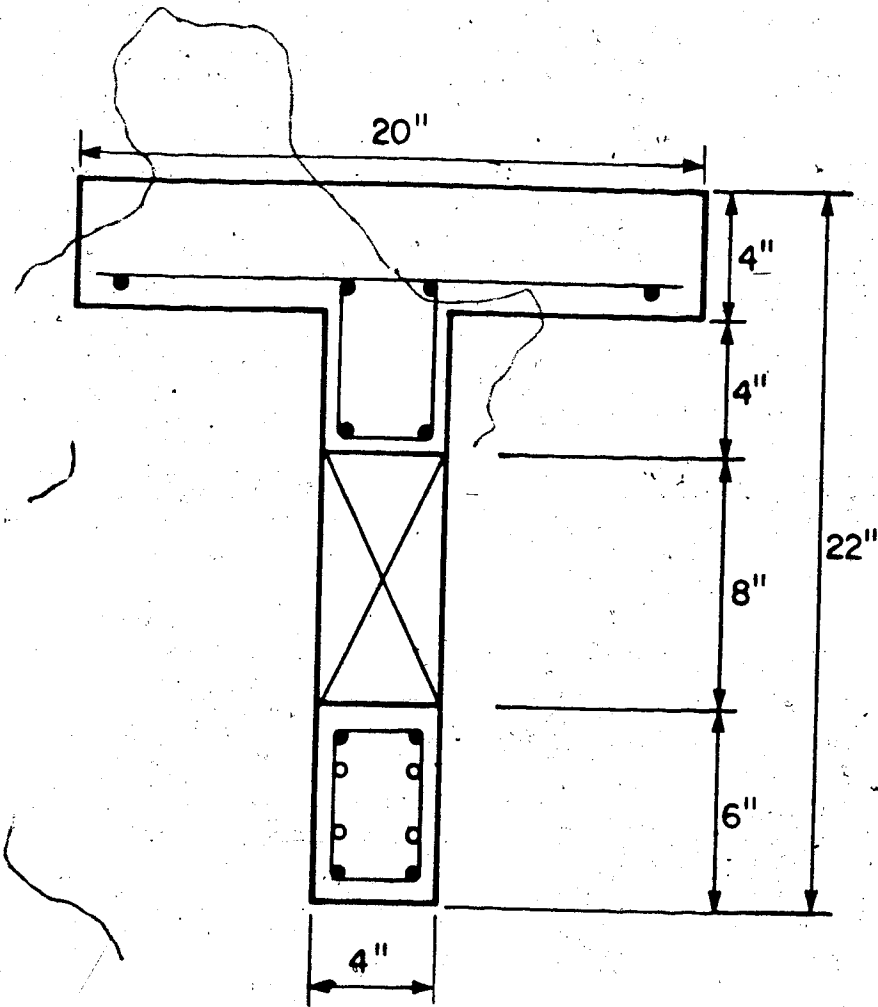
Figure 2.2.3   Typical Concrete Cross-Section – Series C.
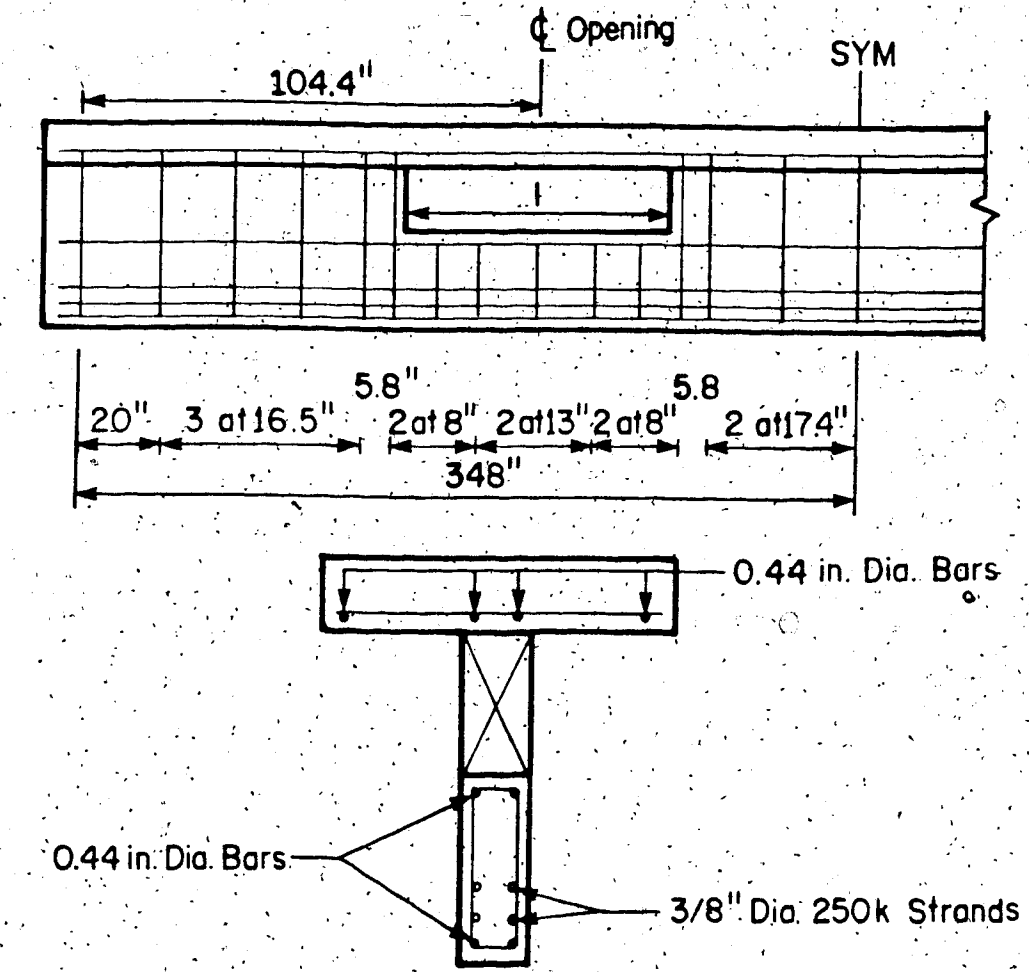
Specimen	I (in.)
Beam B1	56
Beam B2	40
Beam B3	24

Figure 2.2.4   Reinforcement Details — BEAM B1.
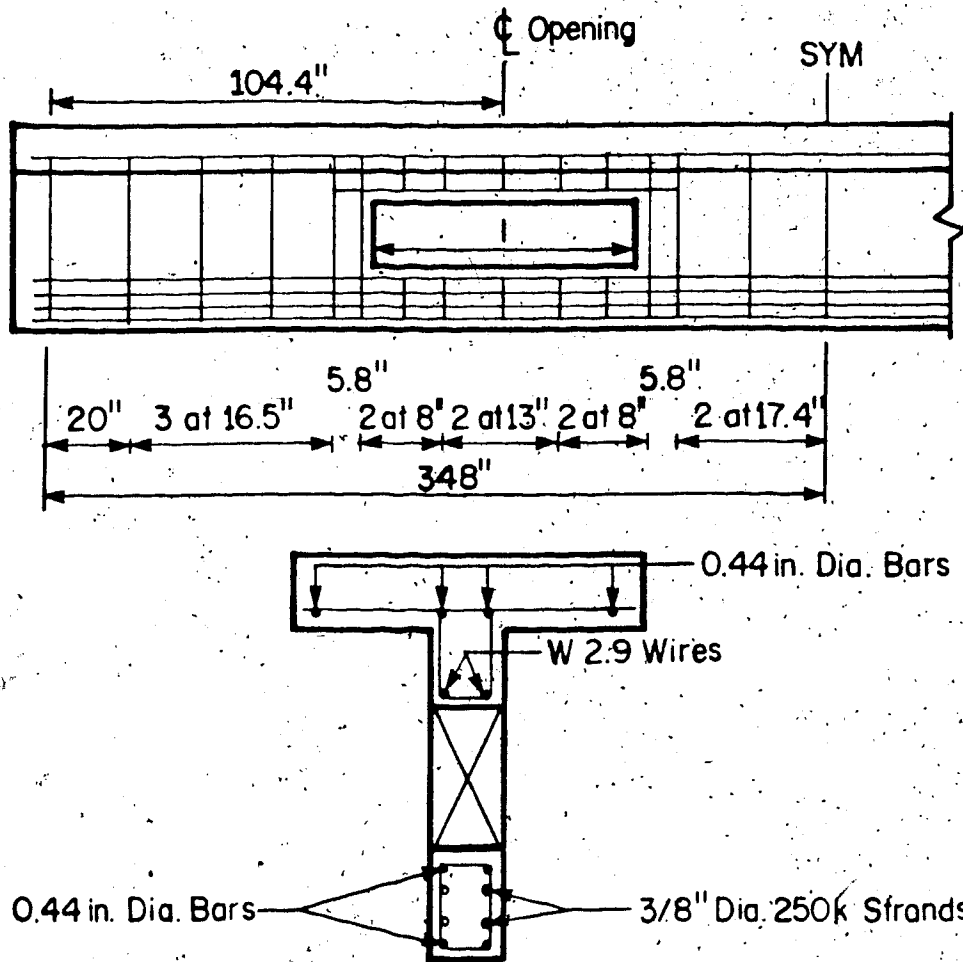
Specimen	l(in.)
Beam C1	56
Beam C2	40
Beam C3	24

Figure 2.2.5 Reinforcement Details - BEAM C1.

Figure 2.2.6   Reinforcement Details – BEAM D2.
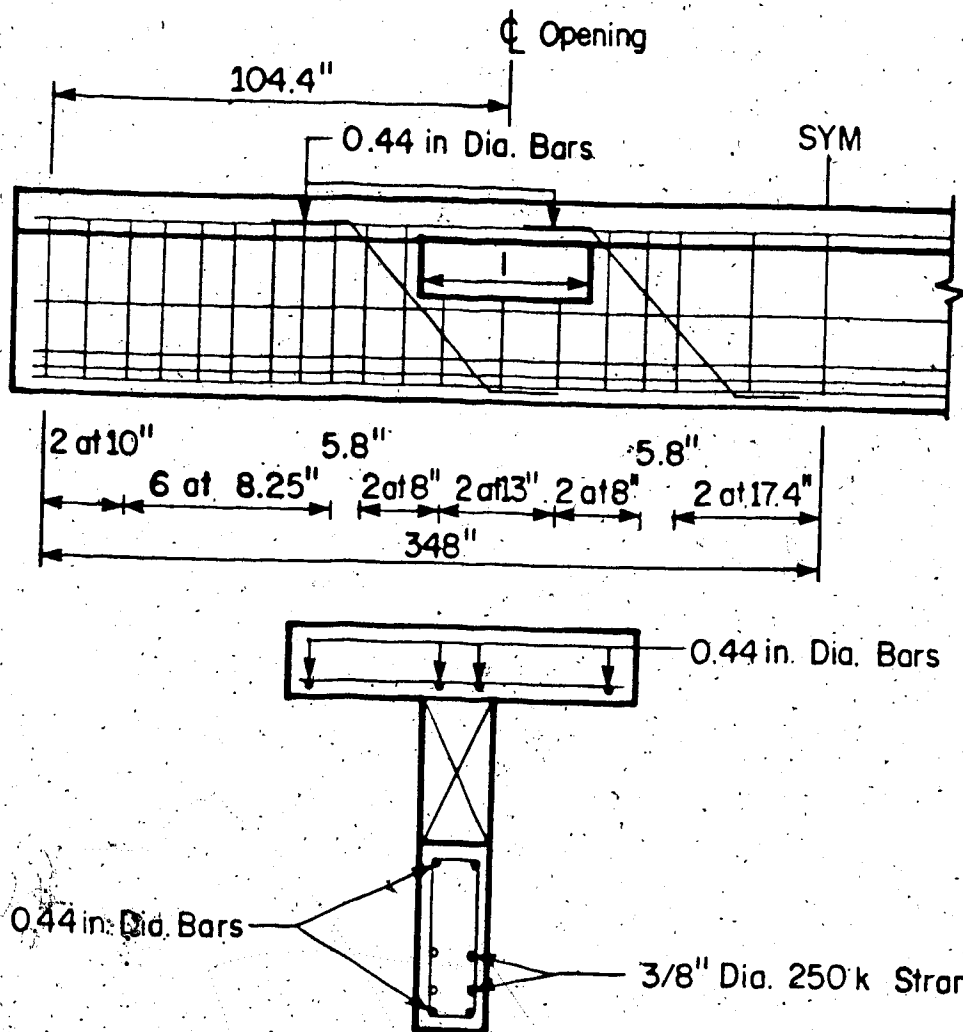
Specimen	I(in.)
Beam D1	56
Beam D2	40
Beam D3	24

STRESS (ksi)

STRAIN (in/in)

Strand Size	3/8 in.
Grade	250 k
Area	0.08 in.^{2}
Ultimate Stress	276 ksi
Modulus of Elasticity	28,900 ksi
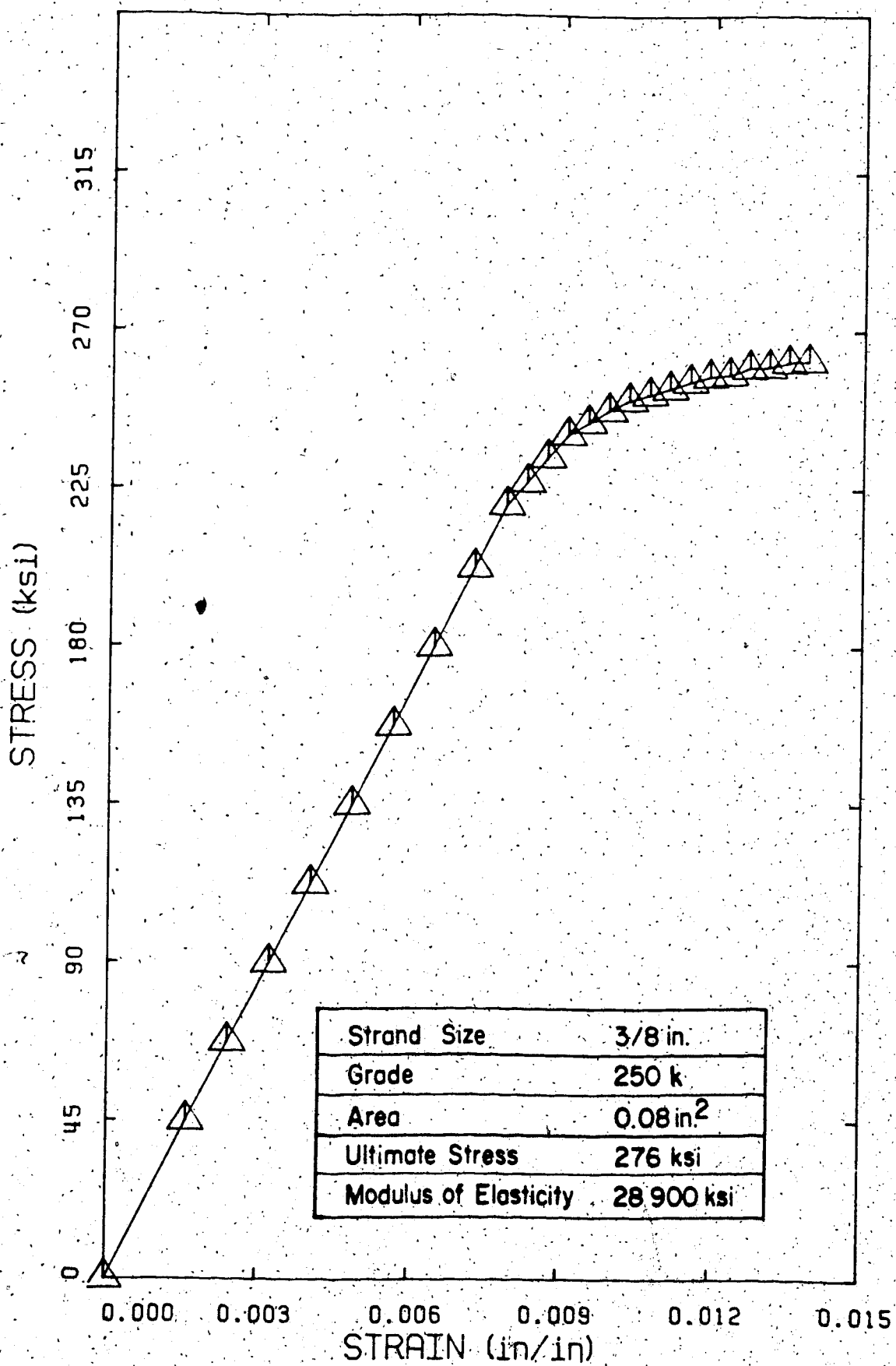
Figure 2.3.1   Stress-Strain Curve for Prestressing

Reinforcement.

Bar Size	No. 10
Area	0.15 in^2
Yield Stress	70.7 ksi
Modulus of Elasticity	31 000 ksi
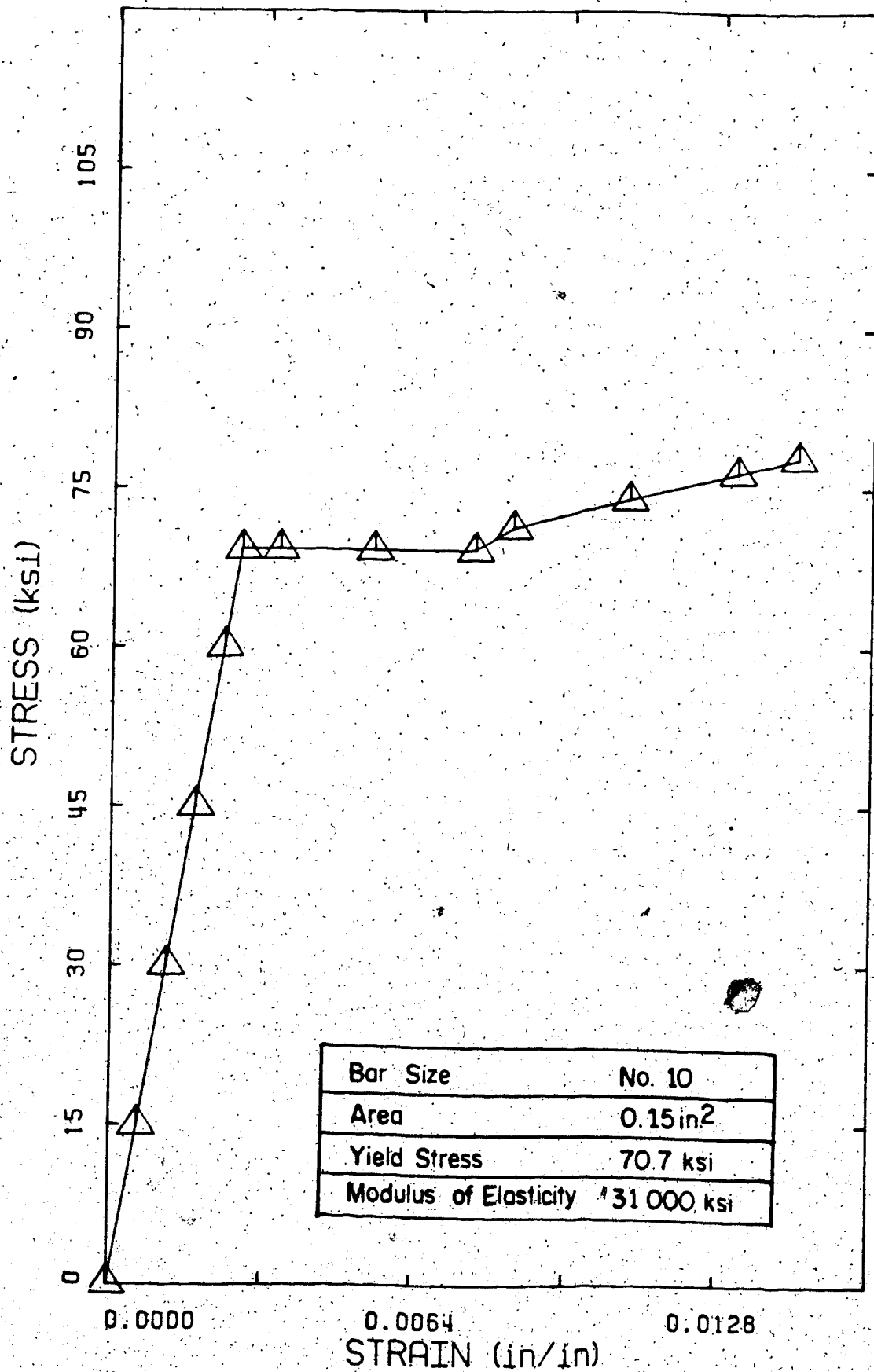
Figure 2.3.2 Stress-Strain Curve for Longitudinal

Reinforcement

Wire Size	W 2.9
Area	0.0289 in^2
Yield Stress	81 ksi
Modulus of Elasticity	30000 ksi
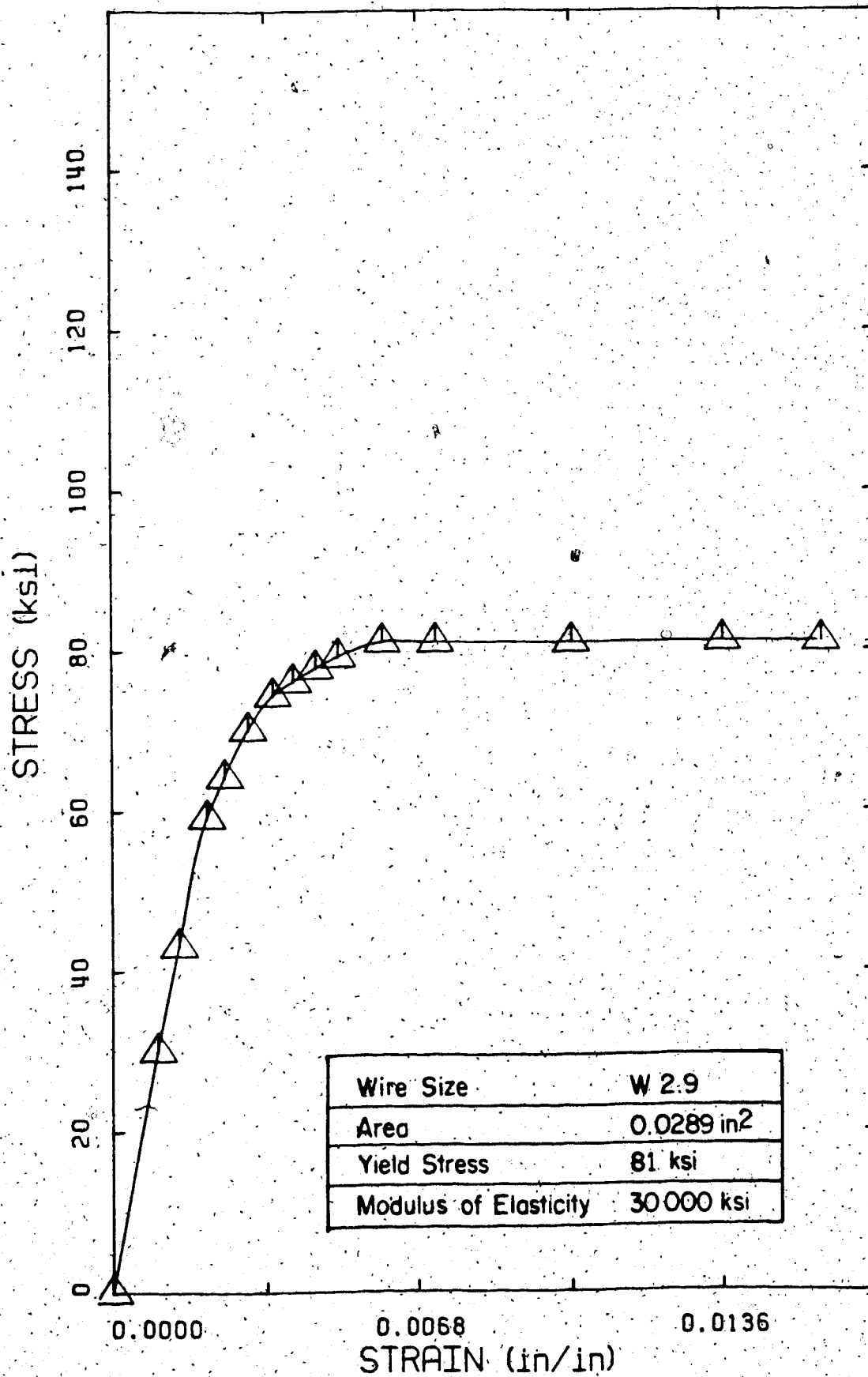
Figure 2.3.3 Stress-Strain Curve for Shear Reinforcement
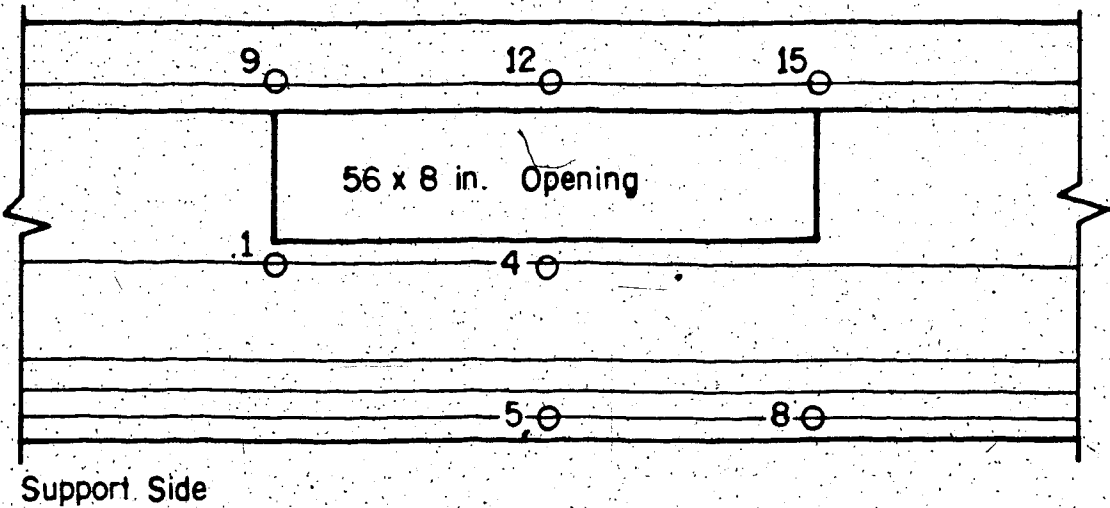
Figure 2.5.1   Strain-Gage Locations – BEAM B1.

Support Side
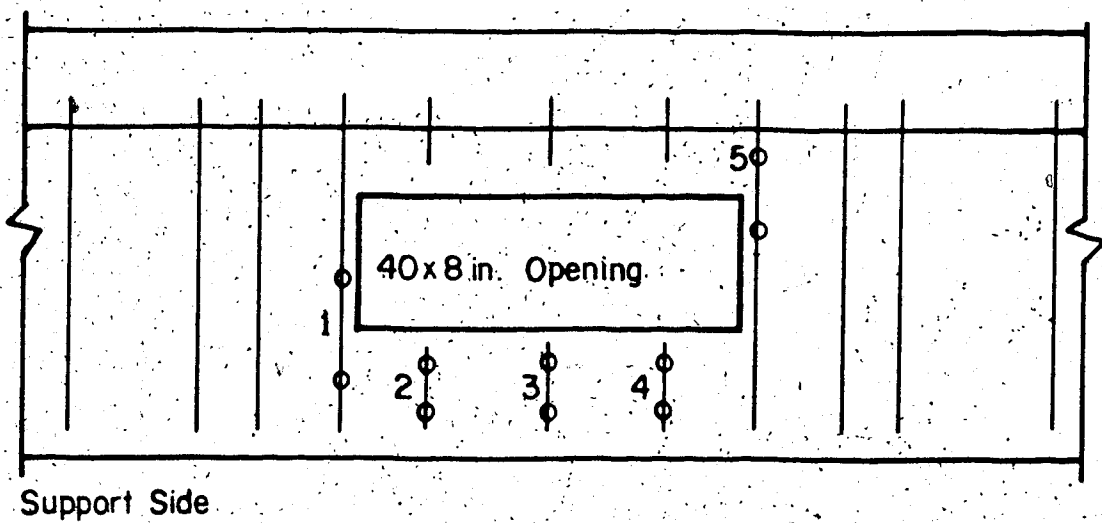
Figure 2.5.2   Demec Points on Stirrups - BEAM C2.

4"

4"

5" 12 1/2" 5" 12 1/2" 5"

Plan view

40 x 8 in. Opening
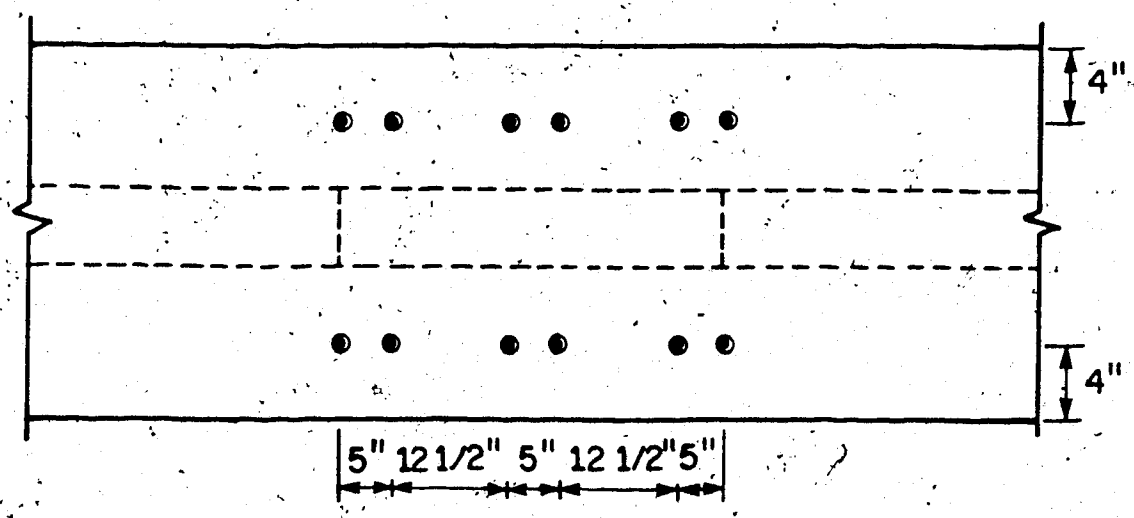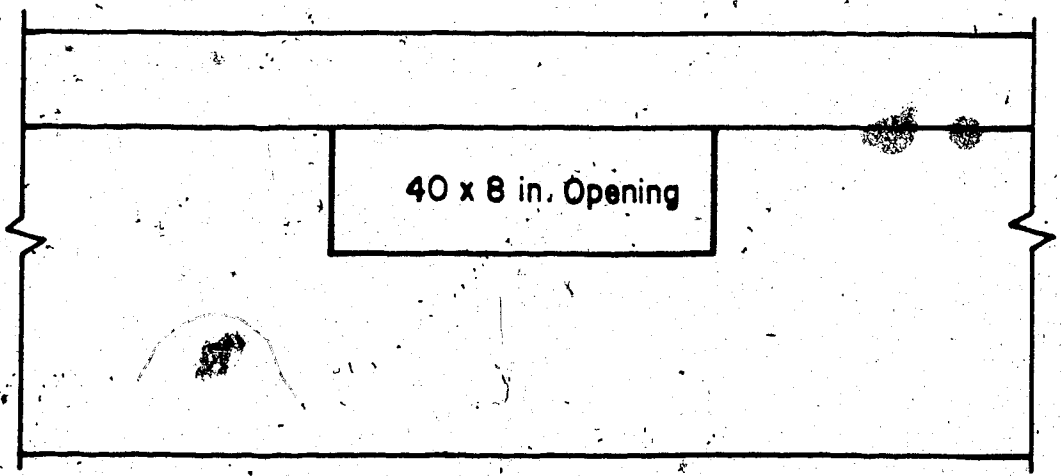
Beam elevation

Figure 2.5.3   Demec Points on Top Strut - BEAM B2 and

BEAM D2.

SYM

24 x 8 in.
Opening

1   2   3   4   5   6   7

Midspan

8"   8"   24"   8"   8"
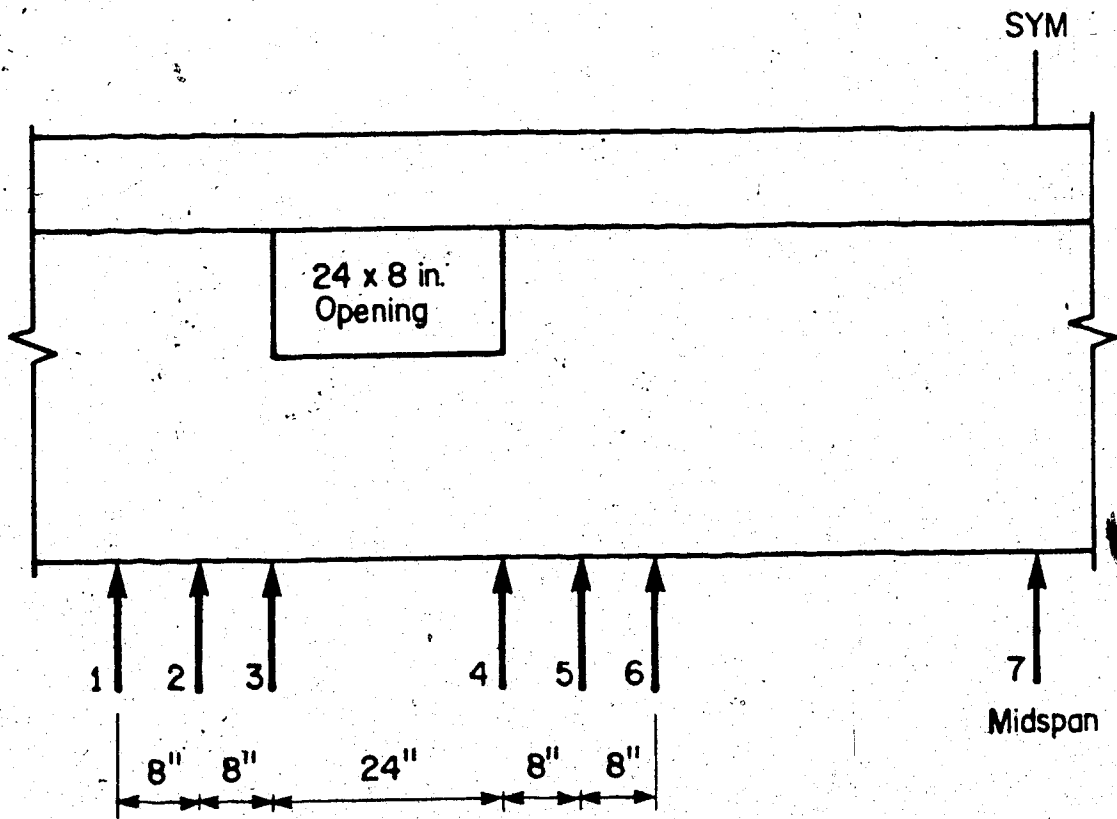
Figure 2.5.4   L.V.D.T. Locations – BEAM B3 and BEAM D3.
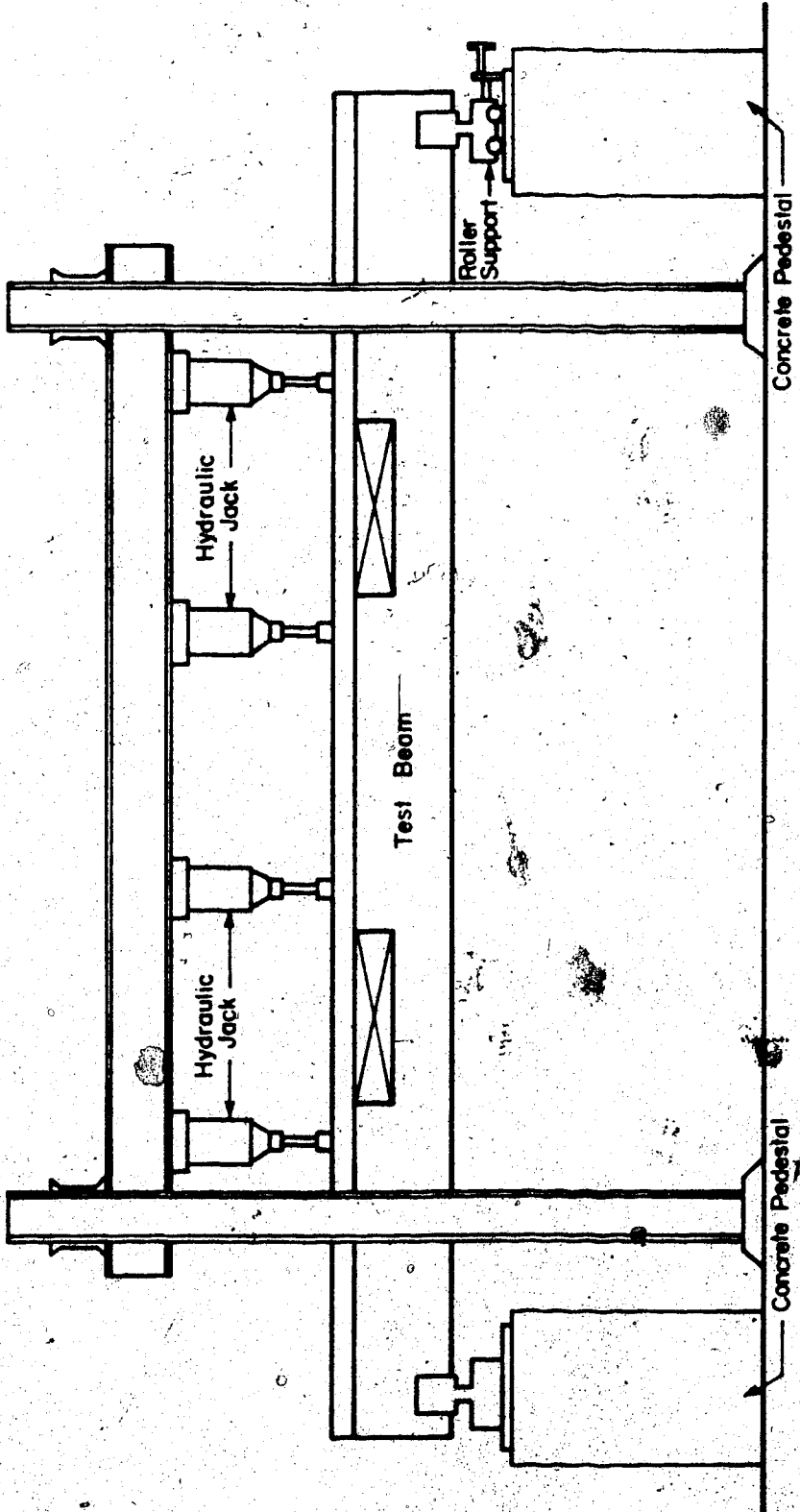
Figure 2.6.1   Test Load Frame.

3. TEST RESULTS

3.1 Principal Test Results

Principal test results presented in Table 3.1.1 consist of loads at first cracking, locations of first cracking, ratios of maximum load carried by the specimen to calculated ultimate load, failure loads, and types of failure.

The cracking load was the load under which cracks became visible to the naked eye or began to elongate from cracks due to concrete shrinkage. Locations of the most common observed cracks at the opening in tested specimens are shown in Fig. 3.1.1. The failure load was the maximum load per jack carried by the specimen. Failure was reached when the specimen was not able to carry any additional load. Failure modes observed in this test program were flexural, shear, and strut hinging mechanism.

The following sections, present for each beam series, the most significant test results to illustrate the behavior of the specimens. These results consist of crack pattern of the specimen, photographs of the specimen at failure and the load-deflection curve at midspan. Complete additional data for each specimen are present in Appendix

52

C.   These data involve load vs. forces in the stirrups at the opening, load vs. strains in the mild longitudinal reinforcement and load-deflection curves at the corners of the opening. The analysis of measured strains in the top strut for determination of axial force and portion of shear carried by the top strut is presented in Section 3.3.

3.2   Specimen Behavior

3.2.1. Series A

Series A consisted of two beams A1 and A2. These beams were control beams, without openings, tested to provide a standard with which to compare the results of beams with openings. The only difference between the two beams was that stirrup spacing for BEAM A2 was one half of that for BEAM A1 in the region between the support and first load position.

Figure 3.2.1.1 shows the crack pattern of BEAM A1 at failure. The first crack was observed at midspan region under 3.6 kips which corresponded to 30% of the failure load. At 6.0 kips flexural cracks that had formed in the shear span between the support and first loading position, developed into inclined cracks. As load increased, new inclined cracks extended into the flange. Near failure these cracks penetrated into the flange, causing web-flange

separation. The cracks also extended toward the support causing loss of bond between longitudinal reinforcement and concrete. As the load increased to 10.93 kips the specimen failed by loss of shear capacity. Figure 3.2.1.2 shows a photograph of BEAM A1 after unloading.

The load-deflection curve at midspan is shown in Fig. 3.2.1.3. The curve is essentially a straight line up to 3.25 kips which corresponds to the start of cracking. The cracking load observed during test is indicated on the load-deflection curve. Beyond cracking, as the tension is lost by the concrete a rapid change of slope in the load-deflection curve is observed. A maximum midspan deflection of 8.30 in. was recorded at failure. The load-deflection curves for all specimens were determined by connecting experimental points. For clarity of the plots, those points are explicitly shown only on the load-deflection curve for BEAM A1.

BEAM A2 was designed to reach its flexural capacity before failing in shear. The web shear reinforcement was double the amount provided in BEAM A1 in the shear span between the support and first loading position.

Figure 3.2.1.4 shows the crack pattern of BEAM A2. Flexural cracks were first observed at midspan at a load of 4.0 kips corresponding to 28% of the failure load. Within the shear span between the support and second loading

position the flexural cracks developed into inclined cracks at 6.8 kips.

At the end of the test, flexural cracks were wide and had penetrated into the flange. The longitudinal reinforcement at midspan yielded. At 11.22 kips the beam reached its flexural capacity at midspan.

Figure 3.2.1.5 shows a photograph of BEAM A2 after unloading. The load-deflection curve at midspan is shown in Fig. 3.2.1.6. The initial behavior of the beam was linear up to 3.8 kips. The loads under which first cracking and yielding of mild longitudinal reinforcement were detected during testing are indicated on the load-deflection curve. A maximum midspan deflection of 9.53 in. was observed at failure.

3.2.2 Series B

Test Series B included BEAMS B1, B2 and B3. These beams contained openings below the flange and placed symmetrically about midspan with the distance from the supports to the center of the openings being 104.4 in. The only difference between the three beams was the length of the openings. Lengths of 56 in., 40 in. and 24 in. were provided in BEAMS B1, B2 and B3 respectively. The web shear reinforcement was similar to BEAM A1 and the longitudinal reinforcement was similar to BEAM A2.

BEAM Bl was tested with 56 x 8 in. openings. The presence of the openings considerably affected the behavior of the specimen.

The crack pattern of BEAM Bl at failure is shown in Fig. 3.2.2.1. The first crack occurred at the lower tension corner of the opening as an elongation from a shrinkage crack. The cracking load was 3.2 kips corresponding to 29% of the failure load. At this same load, flexural cracks formed at the bottom strut and at the midspan region. With a small increase of loading, cracking occurred at the web-flange junction in the upper tension corner of the opening.

Prior to reaching 5.54 kips corresponding to the service load level this crack extended and flexural cracks formed at the flange in the same region. At 5.2 kips inclined cracks formed close to the edge of the opening at the support side. As load increased new inclined cracks occurred at the shear span between the support and first loading position. However they did not penetrate into the flange nor did they extend toward the support.

Beyond the service load level the stirrup adjacent to the lower tension corner of the opening yielded. The mild longitudinal reinforcement below the opening and at midspan yielded. Yielding was detected from strain gage readings. As the load increased beyond 9.0 kips the cracks

at the lower and upper tension corner of the opening widened significantly. Near failure the longitudinal reinforcement at the top strut yielded. Failure occurred at 11.03 kips when a hinging mechanism formed in the top strut and the specimen was not able to carry any additional load. Figure 3.2.2.2 shows a photograph of BEAM B1 after unloading.

The load-deflection curve at midspan is shown in Fig. 3.2.2.3. As can be observed BEAM B1 behaved elastically up to 3.0 kips. The change of slope in the load-deflection curve reflects the formation of a crack at the lower tension corner of the opening at 3.2 kips. The loads under which the mild longitudinal reinforcement and the stirrup adjacent to the opening yielded are indicated on the load-deflection curve. At failure a maximum midspan deflection of 9.95 in. was recorded.

Figure 3.2.2.4 shows the axial force in the top strut determined from strain measurements on the top strut. Figure 3.2.2.5 shows the shear force carried by the top strut versus the total shear force at the opening. Near failure, the top strut carried 58% of the total shear. The procedure for calculating axial force and shear in the strut from strain readings is described in Section 3.

BEAM B2 was provided with 40 x 8 in. openings. The crack pattern of BEAM B2 is shown in Fig. 3.2.2.6. The

first cracks to be formed were the inclined crack at the lower tension corner of the opening and a flexural crack at the bottom strut. They formed simultaneously at 2.8 kips corresponding to 24% of the failure load. At 3.6 kips flexural cracks were detected at the midspan region. At 4.4 kips cracking occurred at the web-flange junction in the upper tension corner of the opening. Simultaneously an inclined crack formed near the edge of the opening at the support side.

Below 5.78 kips corresponding to the service load level, flexural cracks that had formed at the bottom strut developed into inclined cracks. With increments of loading, inclined cracks occurred at the shear span between the support and first loading position.

Beyond the service load level the crack at the web-flange junction at the upper tension corner of the opening widened considerably. Flexural cracks formed at the flange in that region. At 59% of failure load, all stirrups in the bottom strut and adjacent to the opening yielded, except the stirrup at the lower tension corner of the opening. Near failure the mild longitudinal reinforcement below the lower tension corner of the opening and at midspan yielded. An inclined crack at the shear span between the support and first loading position widened significantly, penetrating into the flange. Failure was

initiated by loss of shear capacity in that shear span. The failure load was 11.4 kips. Figure 3.2.2.7 shows a photograph of BEAM B2 after unloading.

The load-deflection curve at midspan is shown in Fig. 3.2.2.8. Formation of first cracking in BEAM B2 is shown on the load-deflection curve by the change of slope at 2.81 kips. First cracking detected during testing is indicated on the load-deflection curve. The loads under which the stirrup adjacent to the opening and the mild reinforcement below the tension corner of the opening yielded are shown on the load-deflection diagram. At failure a midspan deflection of 10.25 in. was recorded.

The relationship between the axial force in the top strut and the applied load is presented in Fig. 3.2.2.9. Figure 3.2.2.10 shows the relationship of shear force carried by the top strut to the total shear at the opening. Near failure, the top strut carried 58% of the total shear.

BEAM B3 contained 24 x 8 in. openings. Figure 3.2.2.11 shows the crack pattern of BEAM B3 at failure. An inclined crack at the lower tension corner of the opening and flexural cracks at the bottom strut were the first to be formed. The cracking load was 3.2 kips corresponding to 28% of the failure load. As load increased to 3.6 kips the flexural cracks that had formed at the middle of the bottom

strut extended through its full depth. At 4.0 kips the inclined crack formed at the lower tension corner of the opening elongated substantially toward the bottom of the specimen. Flexural cracks occurred in the midspan region. As load increased to 5.6 kips inclined cracks occurred simultaneously close to the edges of the opening.

Prior to reaching 5.79 kips corresponding to the service load, the inclined cracks extended and penetrated into the flange. The flexural cracks at the shear span between the support and the opening developed into inclined cracks. Cracking occurred at the web-flange junction in the upper tension corner of the opening.

Beyond the service load level inclined cracks formed at the shear span between the support and first loading position penetrated into the flange. As the load increased beyond 9.5 kips the crack at the upper tension corner of the opening widened significantly and propagated into the flange. The crack at the lower tension corner of the opening and flexural cracks at midspan were wide. The stirrup adjacent to the lower tension corner of the opening and the mild longitudinal reinforcement below the opening yielded. Prior to failure some inclined cracks that had formed in the shear span between the support and first loading position widened considerably and elongated toward the support causing loss of shear capacity at 11.45 kips.

Figure 3.2.2.12 shows a photograph of BEAM B3 after unloading.

Figure 3.2.2.13 shows the load-deflection curve at midspan. Up to 3.10 kips the curve is linear indicating elastic behavior of the specimen. The cracking load recorded during testing is indicated on the load-deflection curve corresponding approximately to the change of slope in the curve. The loads corresponding to yielding of the stirrup adjacent to the opening and yielding of mild longitudinal reinforcement below the opening are shown on the load deflection curve. A maximum midspan deflection of 10.33 in. was observed at failure.

Figure 3.2.2.14 shows the experimentally determined values of the axial force acting in the top strut. The shear force carried by the top strut compared with the total shear force at the opening is presented in Fig. 3.2.2.15. The top strut carried 65% of the total shear, near failure.

3.2.3. Series C.

Test Series C consisted of BEAMS C1, C2 and C3. These beams were similar to Series B, except that they were provided with openings located 4 in. below the flange. The web shear reinforcement and longitudinal reinforcement were

similar to BEAM A1. Since the openings were placed 4 in. below the flange, shear reinforcement was provided in the top strut.

BEAM C1 contained 56 x 8 in. openings. The crack pattern of BEAM C1 is shown in Fig. 3.2.3.1. The first cracks formed simultaneously at the lower tension corner and at the upper tension corner of the opening. The cracking load was 1.6 kips corresponding to 16% of the failure load. Beyond 1.6 kips both cracks elongated, particularly the one at the upper tension corner of the opening that extended along the web-flange junction. At 2.4 kips flexural cracks formed at the bottom strut. At 4.0 kips flexural cracks occurred at the midspan region but did not elongate significantly.

Below 4.93 kips corresponding to the service load level the crack at the lower tension corner of the opening widened considerably. New flexural cracks formed at the bottom strut and extended to its full depth. At 4.8 kips an inclined crack occurred close to the edge of the opening at the support side. As load increased, inclined cracks formed at the shear span between the support and first cracking position, but did not extend into the flange.

Beyond the service load level the crack at the upper tension corner of the opening penetrated into the flange causing web-flange separation. Many flexural cracks

occurred at the flange in that region. At 9.2 kips inclined cracks that had formed at the shear span between the support and first loading position, extended toward the support. Near failure the mild longitudinal reinforcement below the opening and at the midspan, and the stirrup adjacent to the lower tension corner of the opening yielded. The inclined crack that had elongated toward the upper compression corner of the opening opened up appreciably. Failure took place at 10.0 kips caused by loss of shear capacity in that region. A photograph of BEAM C1 after unloading is shown in Fig. 3.2.3.2.

Figure 3.2.3.3 shows the load-deflection curve at right corner of the opening. Cracking is evident at 2.50 kips as shown by the linear portion of the load-deflection curve. The loads under which the mild longitudinal reinforcement below the opening and the stirrup adjacent to the opening yielded are specified on the load-deflection curve. A maximum midspan deflection of 5.88 in. was detected at failure.

Axial force in the top strut, determined from test data is presented in Fig. 3.2.3.4. Figure 3.2.3.5 shows the shear force carried by the top strut as determined from test data versus total shear at the opening. Near failure, the top strut carried 83% of the total shear.

BEAM C2 was tested with 40 x 8 in. openings. The crack pattern of BEAM C2 is shown in Fig. 3.2.3.6. At 2.0 kips corresponding to 19% of the failure load first cracking was observed at the lower and upper tension corners of the opening and at the bottom strut. As load increased to 3.2 kips new flexural cracks formed at the bottom strut and extended through its full depth. At 3.6 kips the crack at the upper tension corner of the opening elongated toward the flange and extended along the web-flange junction. At 4.0 kips various flexural cracks occurred at the midspan region. Inclined cracks formed close to the edge of the opening at the support side.

Below 5.27 kips corresponding to the service load level inclined cracks occurred at the shear span between the support and first loading position, but only a few elongated toward the flange.

Beyond the service load level the crack at the upper tension corner of the opening penetrated into the flange and web-flange separation was initiated. The stirrup adjacent to the opening and located at the upper tension corner region yielded. The mild longitudinal reinforcement at the bottom strut and at midspan yielded. Near failure the inclined cracks at the shear span between the support and first loading position, that had extended toward the upper compression corner of the opening, widened

considerably. Concrete crushing was observed near the upper compression corner of the opening. Failure was precipitated when the inclined cracks extended to the support causing loss of bond between concrete and longitudinal reinforcement. The failure load was 10.57 kips. Figure 3.2.3.7 shows a photograph of BEAM C2 after unloading.

The load-deflection curve at the right corner of the opening is shown in Fig. 3.2.3.8. As shown by the load-deflection curve, cracking occurred at 1.75 kips although during testing it was detected at 2.0 kips. The loads corresponding to yielding of the stirrup adjacent to the opening and yielding of mild longitudinal reinforcement below the opening are indicated on the load-deflection curve. The maximum midspan deflection observed at failure was 6.48 in.

Figure 3.2.3.9 shows the axial force in the top strut determined from strain measurements on the top strut. The shear force carried by the top strut ver▮▮▮▮e total shear at the opening is presented in Fig. 3.▮▮10. Eighty-one percent of the total shear force was carried by the top strut, near failure.

BEAM C3 contained 24 x 8 in. openings. Figure 3.2.3.11 shows the crack pattern of BEAM C3 at failure. The first crack formed at the upper tension corner of the

opening at 1.6 kips corresponding to 15% of the failure load. At 2.4 kips this crack elongated vertically and a crack occurred at the lower tension corner of the opening. As load increased to 3.2 kips a flexural crack formed at the middle section of the bottom strut and extended into its full depth. At 4.0 kips corresponding to 38% of the failure load several flexural cracks formed at the midspan region. The crack at the upper tension corner of the opening elongated toward the flange and extended along the web-flange junction. As load increased, flexural cracks were detected at the bottom strut and at the midspan region. At 5.6 kips an inclined crack occurred close to the edge of the opening at the support side. Flexural cracks formed at the shear span between the support and first loading position.

Beyond the service load level, a few inclined cracks that had formed at the shear span between the support and first loading position extended into the flange. The mild reinforcement at the midspan and below the opening yielded. Near failure these inclined cracks were noticeably widened. As the shear capacity of that region was reached failure occurred. The failure load was 10.5 kips. Figure 3.2.3.12 shows a photograph of BEAM C3 after unloading.

The load-deflection curve at the right corner of the opening is shown in Fig. 3.2.3.13. Cracking occurred at 2.25 kips as indicated by the change of slope of the curve. Cracking was first observed during the test at 2.4 kips. Yielding of the mild longitudinal reinforcement at midspan took place at 8.8 kips as shown on the load-deflection curve. At failure a maximum midspan deflection of 5.56 in. was recorded.

The axial force in the top strut versus the applied load is shown in Fig. 3.2.3.14. The values of the experimentally determined shear force carried by the top strut versus the total shear force at the opening is presented in Fig. 3.2.3.15. The top strut carried 82% of the total shear, near failure.

3.2.4 Series D

Test Series D included BEAMS D1, D2 ,and D3. These beams were provided with openings having the same dimensions and location of Series B. The web shear reinforcement at the shear span between the support and first loading position was similar to BEAM A2. As discussed in Chapter 2 additional inclined bars were placed close to the tension corners of the openings to minimize crack propagation and web-flange separation.

BEAM D1 was provided with 56 x 8 in. openings. Figure 3.2.4.1 shows the crack pattern of BEAM D1 at failure. The first crack occurred at the lower tension corner of the opening as an elongation from a shrinkage crack. The cracking load was 3.2 kips corresponding to 31% of the failure load. As load increased to 4.0 kips flexural cracks were observed at the bottom strut and at the midspan region. At 4.8 kips cracking occurred at the web-flange junction in the upper tension corner of the opening but did not elongate.

Prior to reaching 5.18 kips corresponding to the service load level, flexural cracks were observed at the flange close to the upper tension corner of the opening. An inclined crack occurred near both edges of the opening. Flexural cracks that had formed at the shear span between the support and first loading position developed into inclined cracks.

Beyond the service load level, inclined cracks were observed at the bottom strut. The cracks at the lower and upper tension corners of the opening were well contained. A horizontal crack formed in the flange near the upper tension corner of the opening. At 9.2 kips the flexural cracks at the midspan region were quite wide. The mild longitudinal reinforcement below the opening and at the midspan region yielded. At 10.4 kips the beam failed in

flexure at midspan. Figure 3.2.4.2 shows a photograph of BEAM D1 after unloading.

The load-deflection curve at midspan is shown in Fig. 3.2.4.3. Close to 3.2 kips when the first crack formed at the lower tension corner of the opening the slope of the load-deflection curve changes. This change of slope corresponds to 2.66 kips. The mild longitudinal reinforcement below the opening and at midspan yielded at 8.47 kips and 7.96 kips respectively as indicated on the load-deflection curve. At failure, a maximum midspan deflection of 8.60 in. was recorded.

Axial force in the top strut determined from test data is presented in Fig. 3.2.4.4. Figure 3.2.4.5 shows the shear force carried by the top strut as determined from test data. Near failure, the top strut carried 60% of the total shear.

BEAM D2 was tested with 40 x 8 in. openings. Figure 3.2.4.6 shows the crack pattern of BEAM D2 at failure. Initial cracking occurred at the lower tension corner of the opening as an extension of a shrinkage crack. Simultaneously a flexural crack formed at the bottom strut. The cracking load was 3.2 kips corresponding to 30% of the failure load. At 4.0 kips flexural cracks were observed at the midspan region and at the bottom strut. As load increased to 4.4 kips, cracking took place at the web-

flange junction in the upper tension corner of the opening. At 6.0 kips, flexural cracks that had formed close to the edge of the opening at the support side developed into inclined cracks. Flexural cracks at the midspan region elongated toward the flange.

Below 5.23 kips corresponding to the service load level, flexural cracks developed in the flange at the upper tension corner region of the opening. An inclined crack developed from the lower compression corner of the opening to the flange.

At 8.8 kips inclined cracks occurred at the bottom strut. Flexural cracks that had formed at the shear span between the support and first loading position developed into inclined cracks and reached the flange. Near failure, a horizontal crack formed at the flange close to the upper tension corner of the opening. The mild longitudinal reinforcement below the opening yielded. The flexural cracks at the midspan were noticeably widened. Failure occurred at 10.5 kips when the flexural capacity was reached at midspan. Figure 3.2.4.7 shows a photograph of BEAM D2 after unloading.

The load-deflection curve is shown in Fig. 3.2.4.8. Cracking is indicated by a change of slope in the load-deflection curve at 2.72 kips. Yielding of mild longitudinal reinforcement below the opening is also shown

on the diagram. A maximum midspan deflection of 9.55 in. was detected at failure.

Figure 3.2.4.9 shows the axial force in the top strut versus the applied load. The values of the shear force carried by the top strut as determined from test data are presented in Fig. 3.2.4.10. Of the total shear, 64% was carried by the top strut near failure.

BEAM D3 was provided with 24 x 8 in. openings. Figure 3.2.4.11 shows the crack pattern at failure. The first cracks formed at lower tension corner of the opening and at the bottom strut. The cracking load was 3.6 kips corresponding to 33% of the failure load. At 4.4 kips flexural cracks occurred at the midspan region and a flexural crack formed at the middle of the bottom strut, penetrating its full depth.

At 5.40 kips corresponding to the service load level, inclined cracks developed close to both edges of the opening. Flexural cracks that had formed in the bottom strut developed into inclined cracks.

Beyond the service load level, cracking occurred at the upper tension corner of the opening but did not elongate significantly. Flexural cracks were observed at the flange in that region. Inclined cracks formed at the shear span between the support and first loading position and extended toward the flange. Near failure, cracks at

midspan widened substantially and extended into the flange. The mild longitudinal reinforcement at midspan and below the opening yielded. At 10.8 kips, failure occurred by loss of flexural capacity at midspan. Figure 3.2.4.12 shows a photograph of BEAM D3 after unloading.

The load-deflection curve is shown in Fig. 3.2.4.13. Cracking is evident at 3.37 kips as shown by the change of slope in the load-deflection curve. The load under which the mild longitudinal reinforcement at midspan yielded is specified on the diagram. At failure a midspan deflection of 7.42 in. was recorded.

The relationship between the axial force in the top strut and the applied load is shown in Fig. 3.2.4.14. Figure 3.4.2.15 shows the relationship of shear force carried by the top strut to the total shear at the opening. Near failure, the top strut carried 41% of the total shear.

3.3 Shears in Top and Bottom Struts.

The top strut of all specimens contained demec points cemented on the upper and lower surfaces, as shown in Fig. 3.3.1, to provide information on the strains at specific cross-sections. These measured strains were used to calculate axial and shear forces in the struts.

The values of the aveage strain at the top and bottom
fibers at each load step, were determined from:

$$(S_t)_i^n = \sum_{j=1}^{2} (s_t)_{i,j}^n \qquad (3.1)$$

$$(S_b)_i^n = \sum_{j=1}^{2} (s_b)_{i,j}^n \qquad (3.2)$$

where,

i = section number

j = number of demec points across the surface

n = load step

$(S_t)_i^n$ = average top fiber strain in section i of the
top strut at load step n.

$(S_b)_i^n$ = average bottom fiber strain in section i of the
top strut at load step n.

$(s_t)_{i,j}^n$ = top fiber strain in section i at point j of
the top strut at load step n.

$(s_b)_{i,j}^n$ = bottom fiber strain in section i at point j
of the top strut at load step n.

Once the values of the average strains at each section
were determined, they were related to section and material
properties to obtain the axial force and moment. Normal
stresses in the concrete were assumed to be uniformly
distributed across the cross-section and were determined

from the stress-strain curve for concrete. By integrating
normal compressive stresses along the cross-section, the
axial compressive force at that particular cross-section
was determined. The axial compressive force at load step n
was determined from:

$$C^n = \frac{\sum\limits_{i=1}^{m} C_i^n}{m}$$ (3.3)

where,

C^n = average axial compressive force in the top strut
at load step n.

C_i^n = axial compressive force in the top strut in
section i at load step n.

m = number of cross sections considered.

By integrating normal tensile stresses along the cross-
section, the axial tensile force in the uncracked top strut
was determined. After cracking of the top strut, the axial
tensile force was assumed equal to the force in the
steel. The moment was then calculated based on equilibrium
conditions for each section. Values of shear force in the
strut were determined by the following expression:

$$V_{i,k}^n = \frac{M_i^n + M_k^n}{x_{i,k}}$$ (3.4)

where,

$V_{i,k}^n$ = shear force calculated from moments acting at sections i and k in the top strut at load step n.

M_i^n = moment at section i at load step n.

M_k^n = moment at section k at load step n.

$x_{i,k}$ = distance between sections i and k.

The value of the shear force in the top strut at load step n was determined from average values of all possible combinations of $V_{i,k}^n$. Thus,

$$V^n = \frac{\sum\limits_{i=1}^{m} \sum\limits_{k=i+1}^{m} V_{i,k}^n}{\sum\limits_{r=1}^{m} (m-r)} \qquad (3.5)$$

where,

V^n = average shear force in the top strut at load step n.

m = number of cross-sections considered.

$V_{i,k}^n$ = shear force in the top strut acting at sections i and k at load step n.

Table 3.1.1 Principal Test Results

Beam	P_{cr} (kips)	Location of First Cracking	P_{test} (kips)	$\dfrac{P_{test}}{P_{calc}}$	Type of Failure
A1	3.6	Midspan	10.93	1.12	Shear
A2	4.0	Midspan	11.22	1.15	Flexure
B1	3.2	Lower Tension Corner	11.03	1.02	Full Hinging Mechanism
B2	2.8	Lower Tension Corner	11.40	1.17	Partial Hinging Mechanism
B3	3.2	Lower Tension Corner	11.45	1.17	Partial Hinging Mechanism
C1	1.6	Lower and Upper Tension Corner	10.0	1.02	Partial Hinging Mechanism
C2	2.0	Lower and Upper Tension Corner	10.57	1.08	Shear followed by Strand Debonding
C3	2.4	Lower Tension Corner	10.50	1.07	Partial Hinging Mechanism
D1	3.2	Lower Tension Corner	10.40	1.06	Flexure
D2	3.2	Lower Tension Corner	10.50	1.07	Flexure
D3	3.6	Lower Tension Corner	10.80	1.10	Flexure

Note: P_{test} = maximum load carried by the specimen.
P_{calc} = calculated ultimate load

Support Side
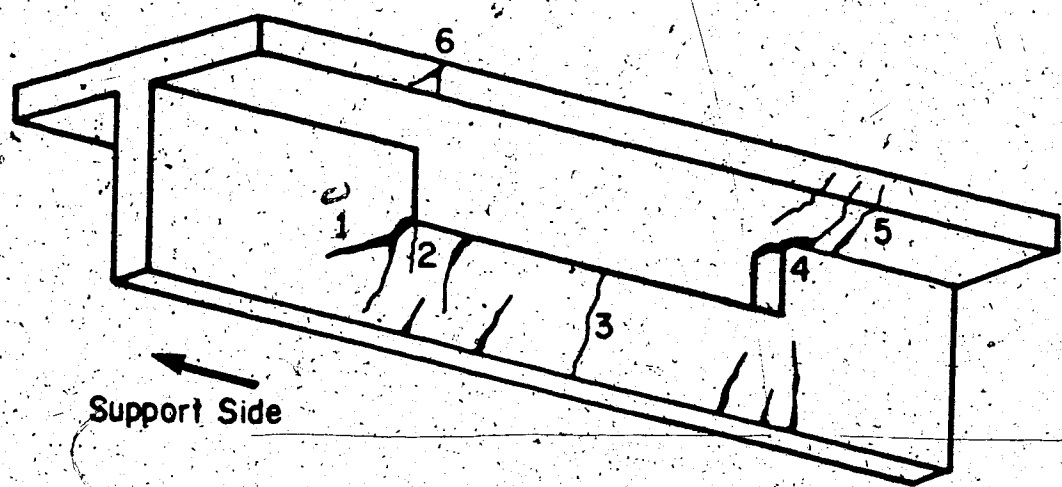
Crack	Type and Location
1	inclined crack at the lower tension corner of the opening.
2	vertical crack at the lower tension corner of the opening
3	flexural crack in the bottom strut
4	crack at the upper tension corner of the opening
5	crack in the flange near the upper tension corner of the opening
6	crack in the flange near the upper compression corner of the opening

Figure 3.1.1. Location of Cracks at the Opening.

Support Side

Figure 3.2.1.1. Crack Pattern — BEAM A1.

Figure 3.2.1.2   BEAM A1 after unloading.
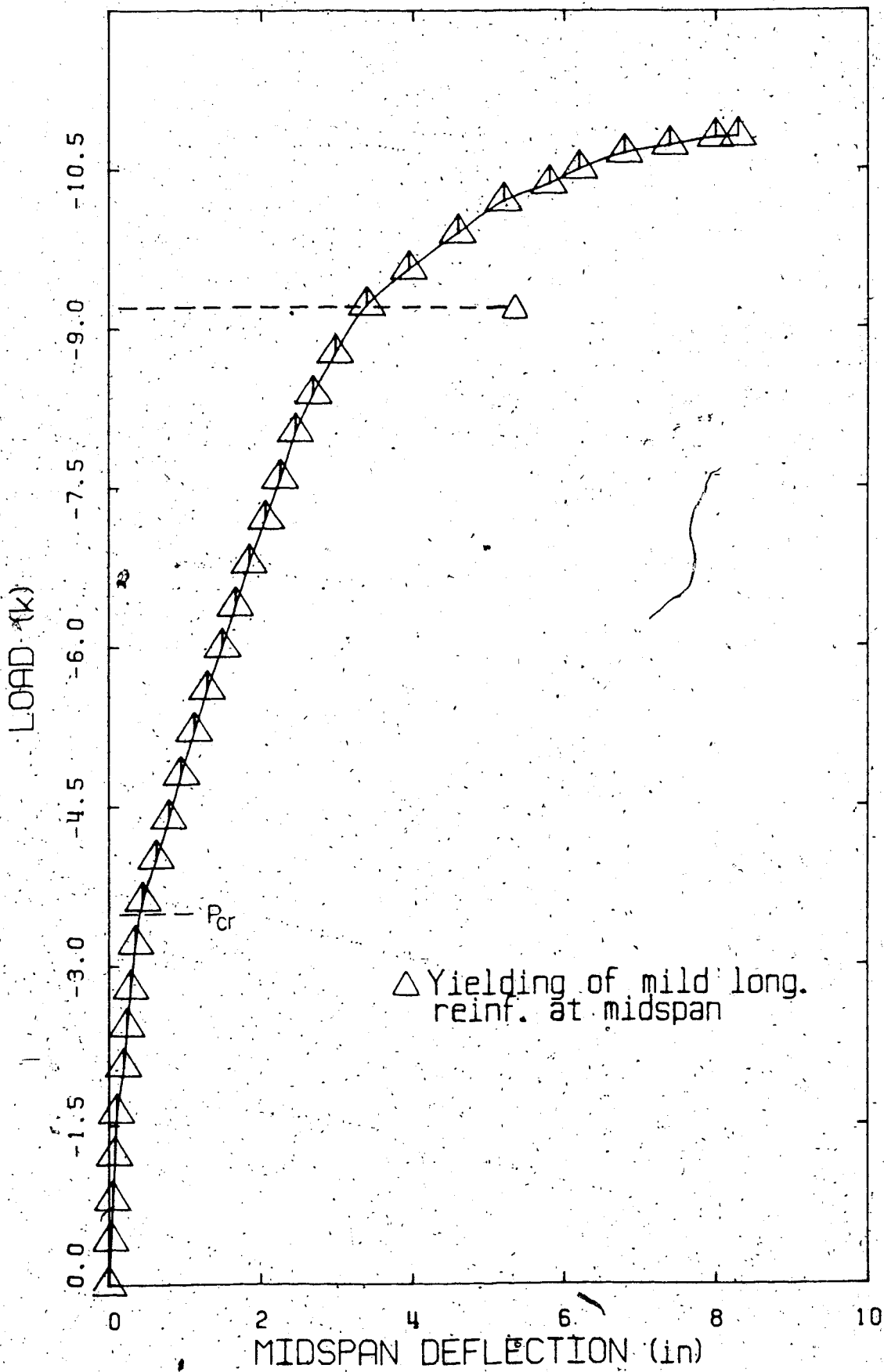
Figure 3.2.1.3   Load-Deflection Curve BEAM A1.
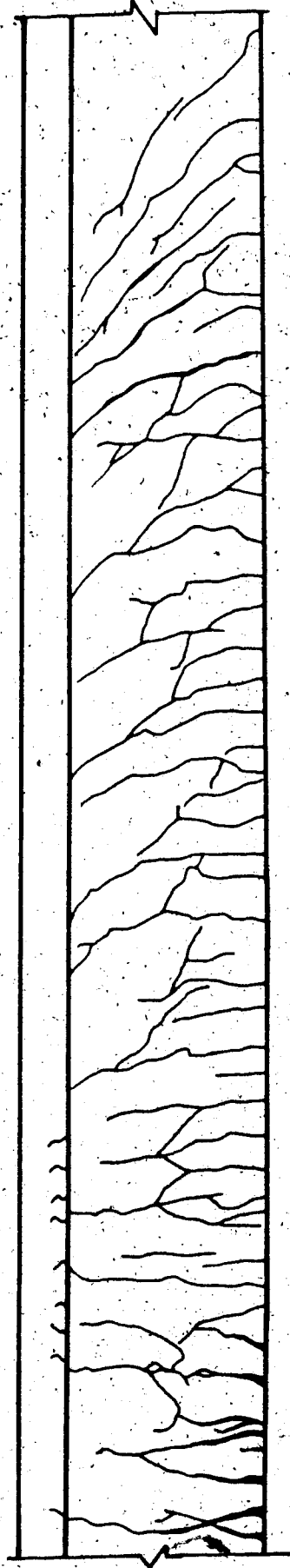
Support Side

Figure 3.2.1.4   Crack Pattern - BEAM A2.
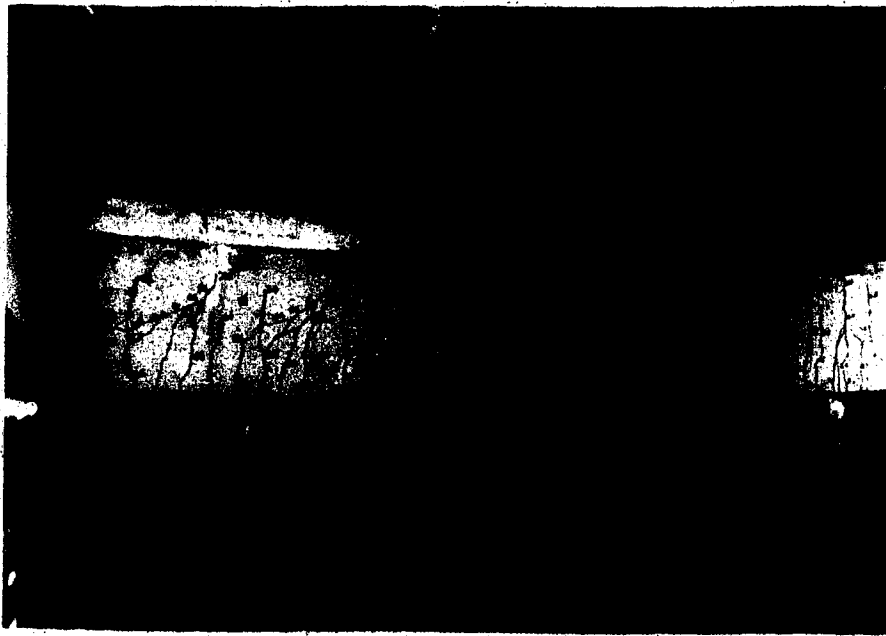
Figure 3.2.1.5   BEAM A2 after Unloading.
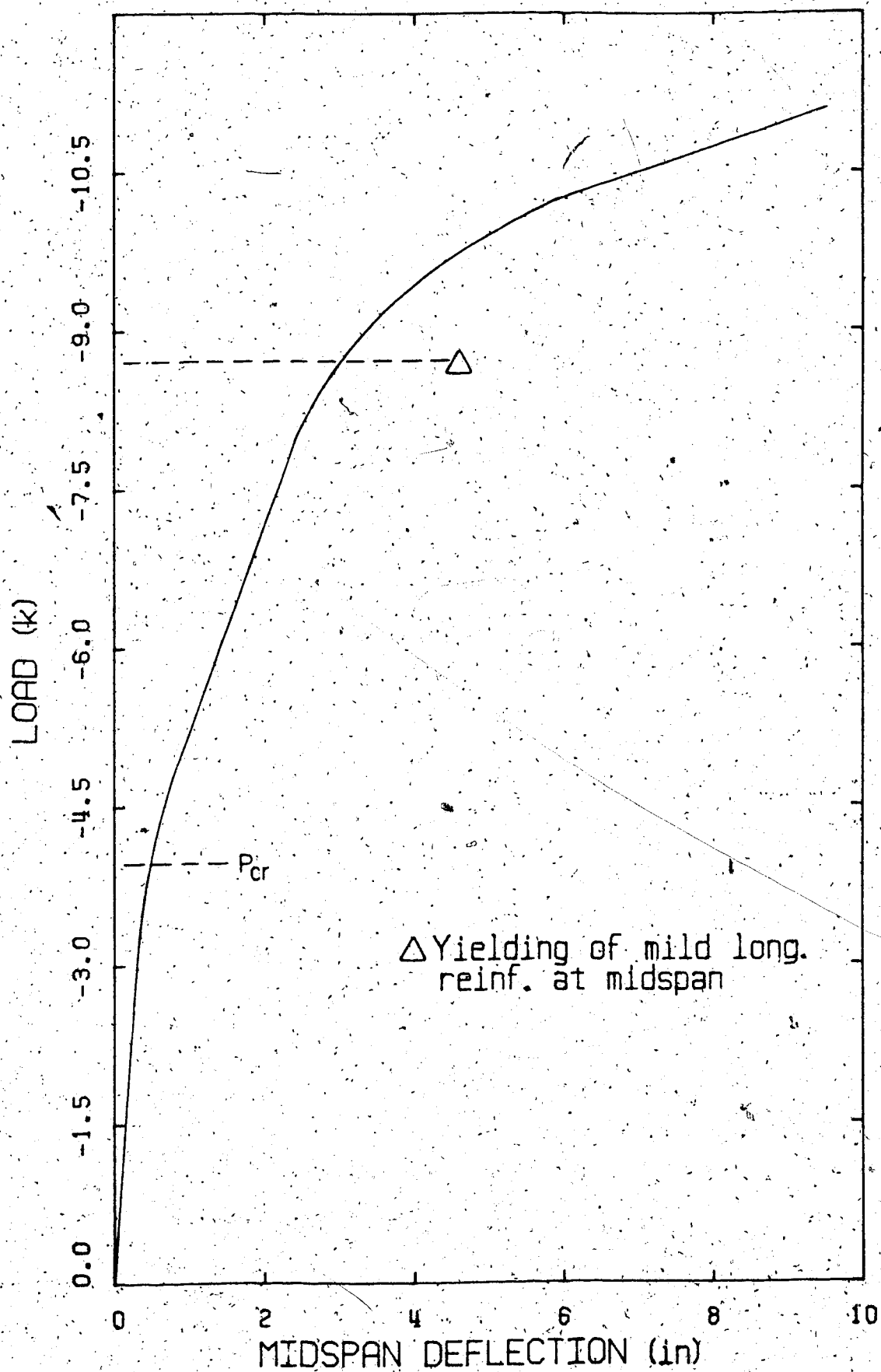
Figure 3.2.1.6   Load-Deflection Curve BEAM A2,
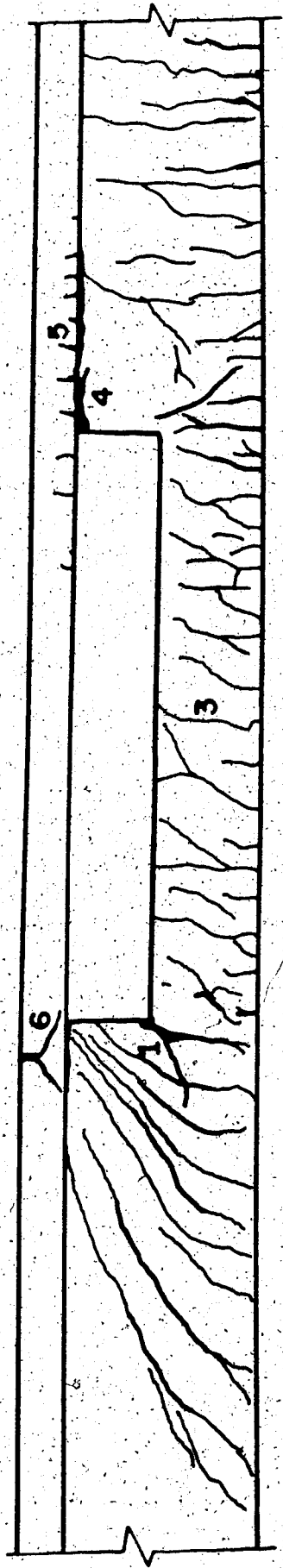
Support Side

Figure 3.2.2.1   Crack Pattern - BEAM B1.

Figure 3.2.2.2   BEAM B1 after Unloading.
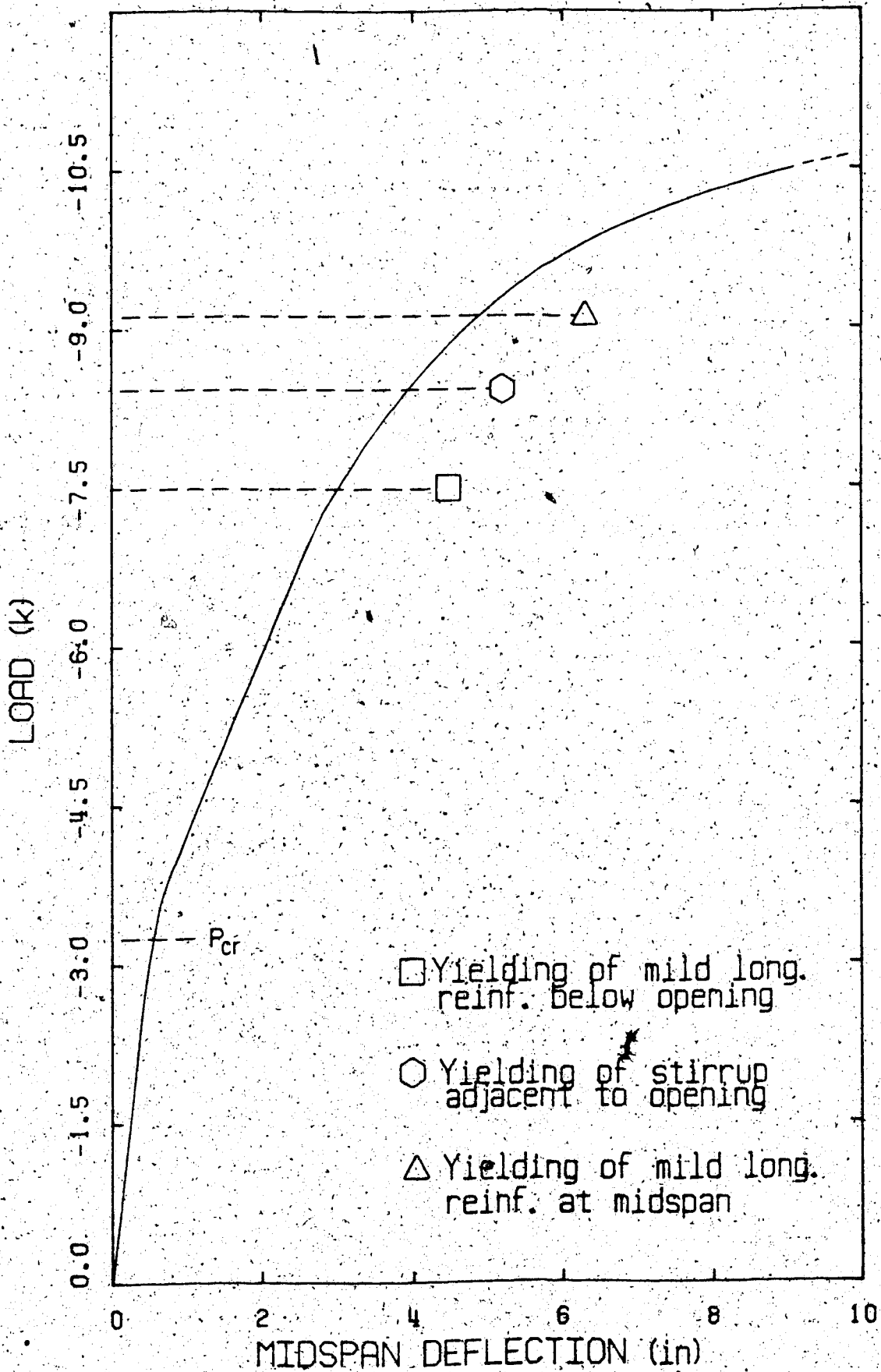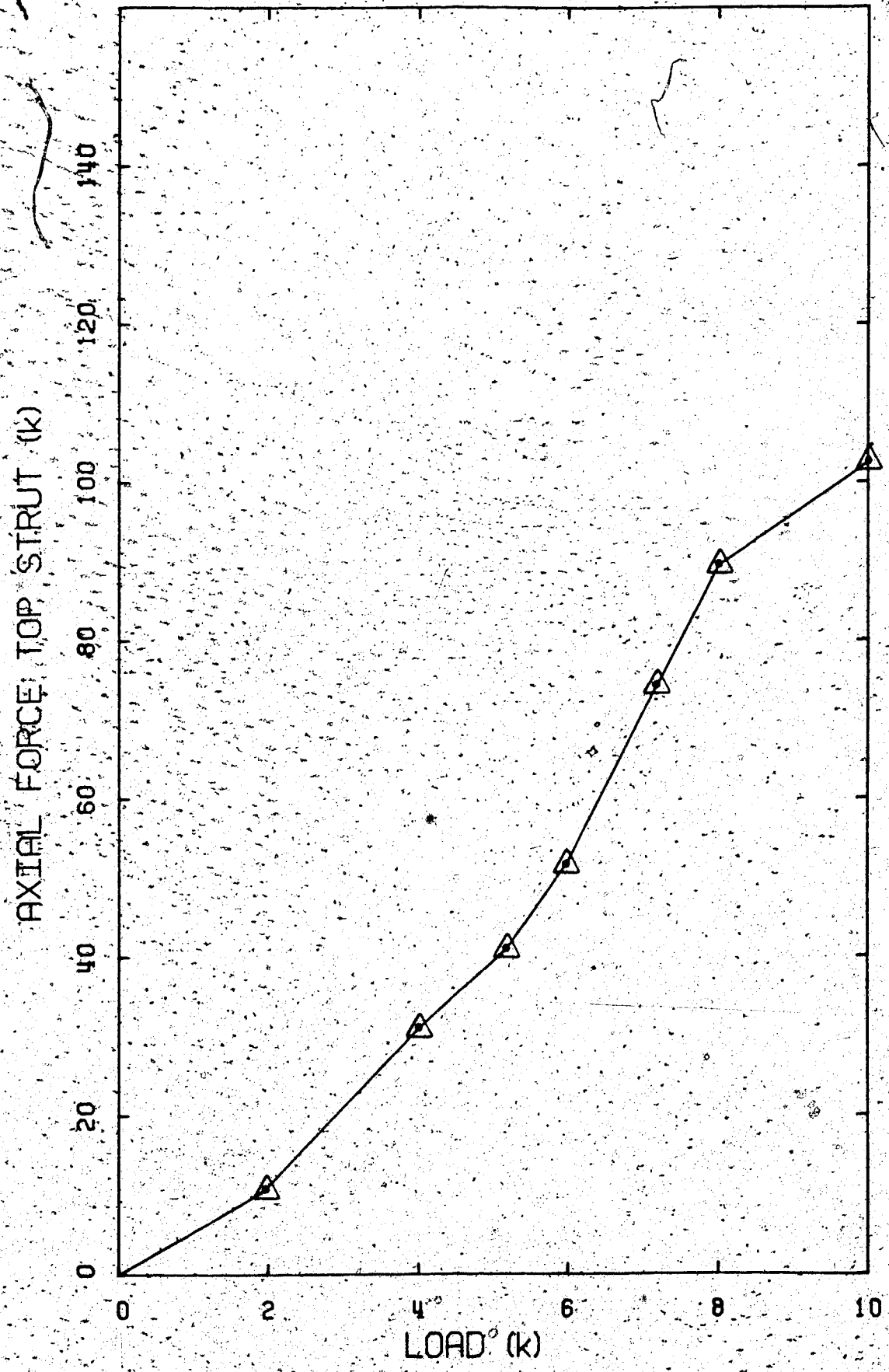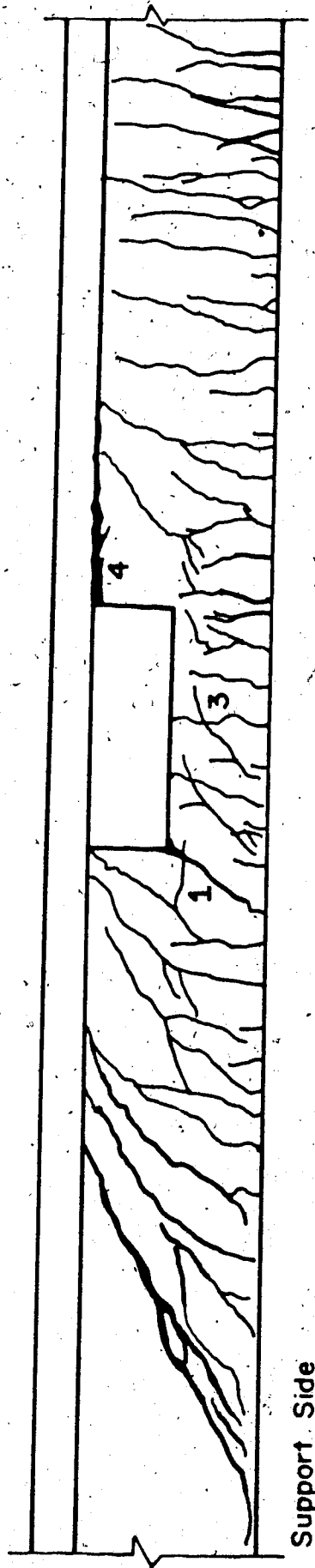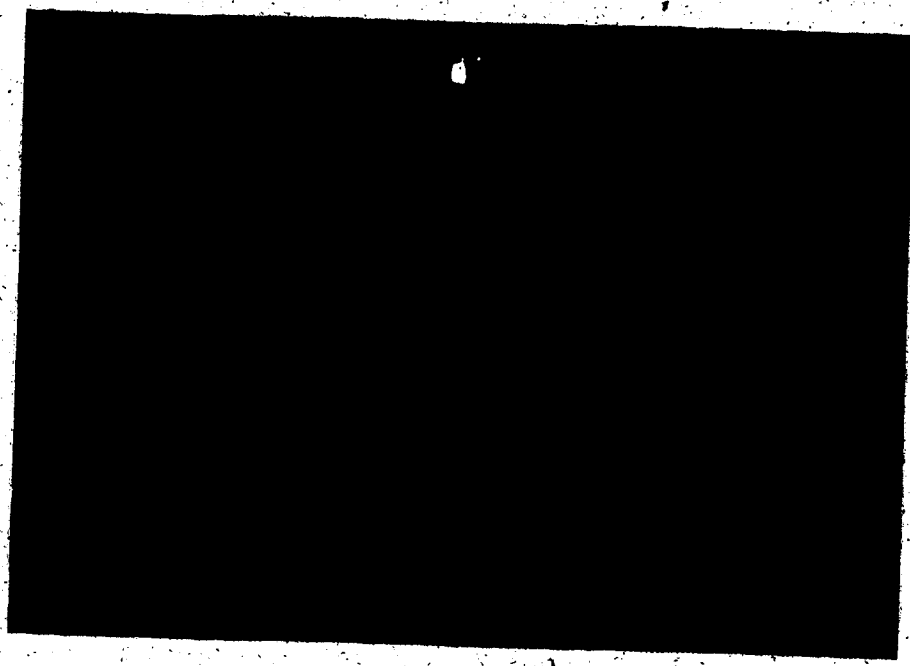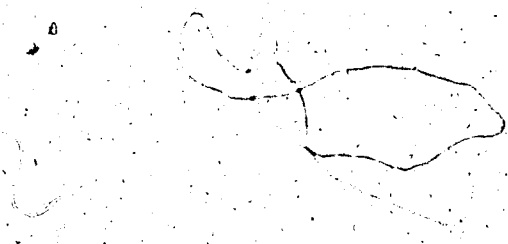
Figure 3.2.2.3   Load-Deflection Curve - BEAM B1.
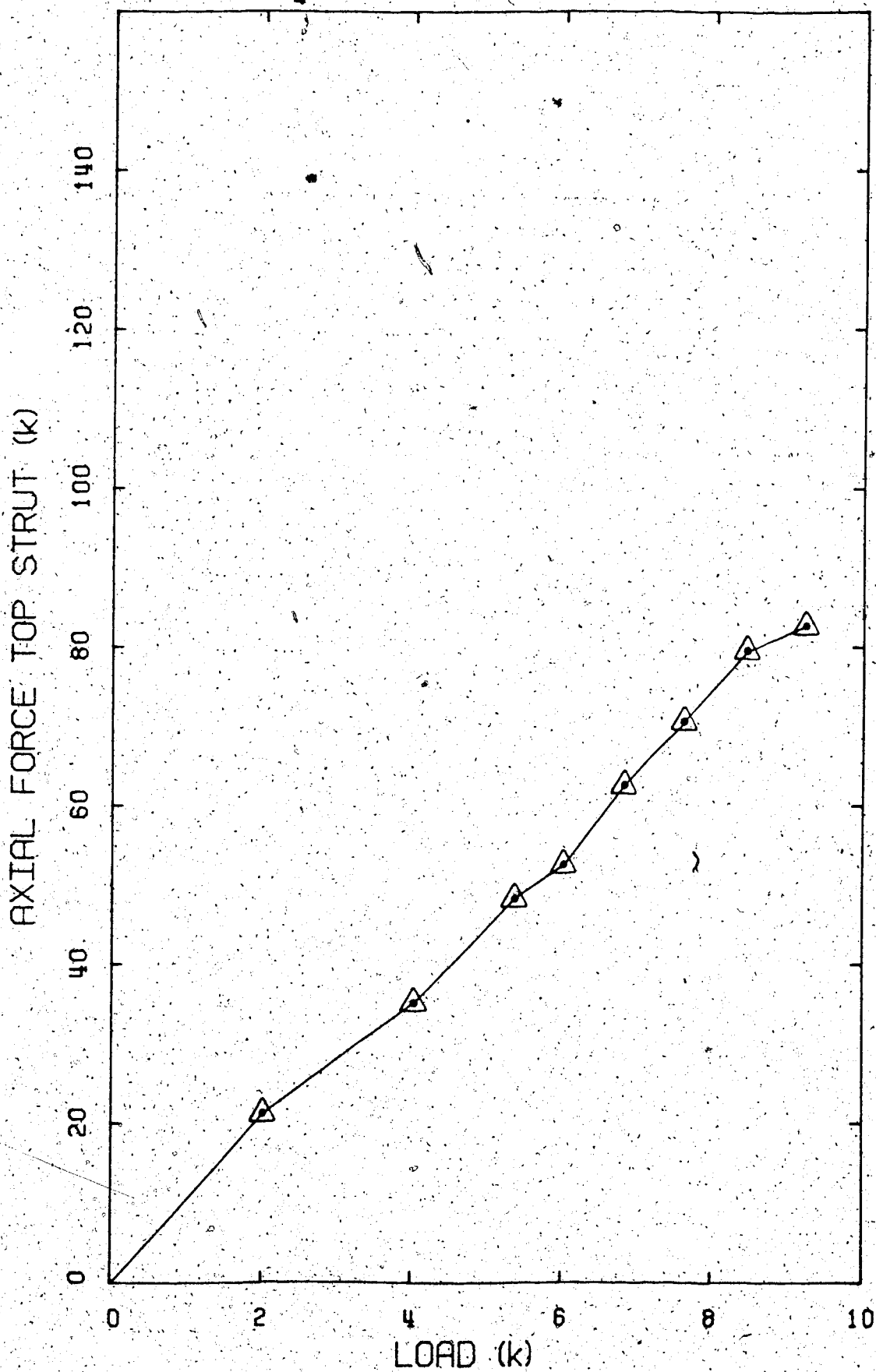
Figure 3.2,2.4   Axial Force in the Top Strut BEAM B1.
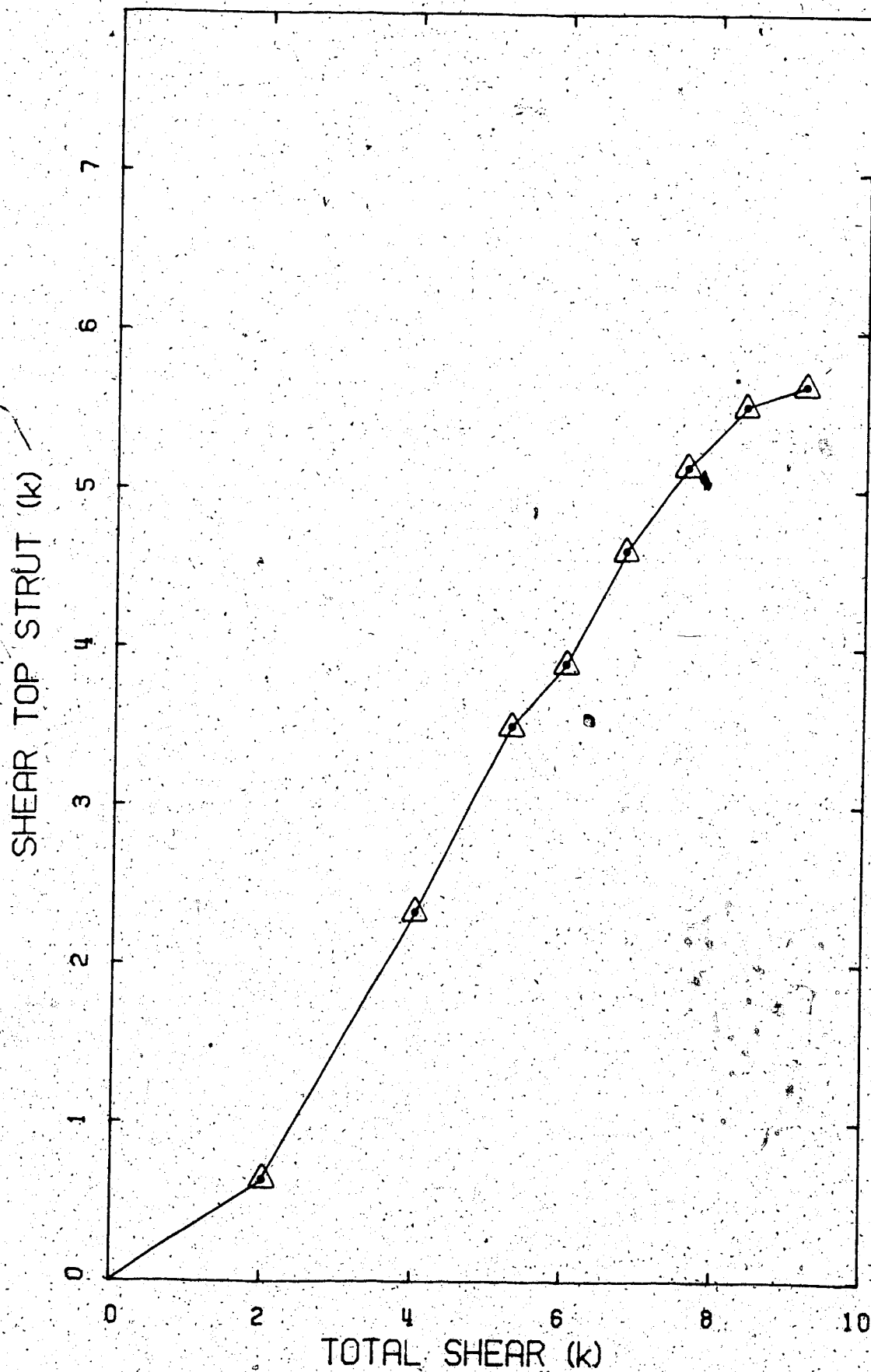
Figure 3.2.2.5   Shear Force in the Top Strut BEAM B1.

Support Side
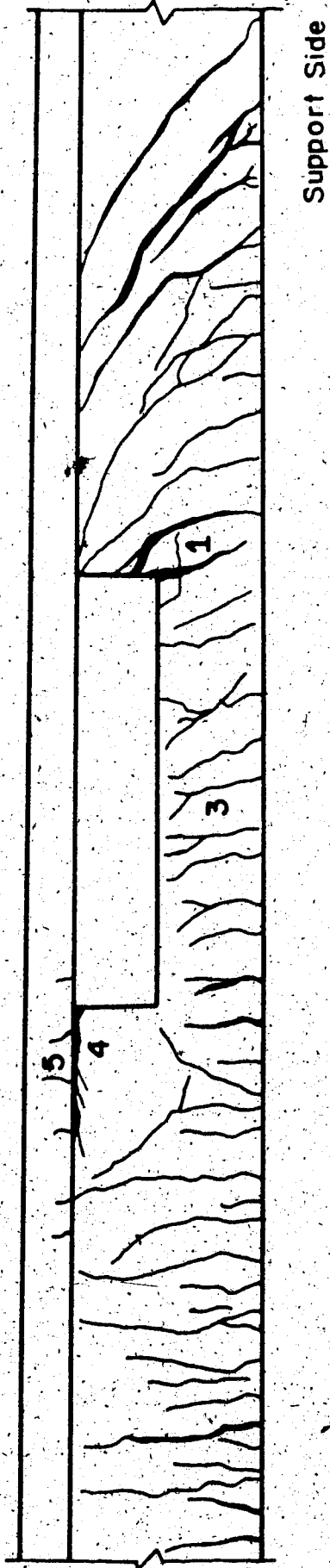
Figure 3.2.2.6. Crack Pattern - BEAM B2.
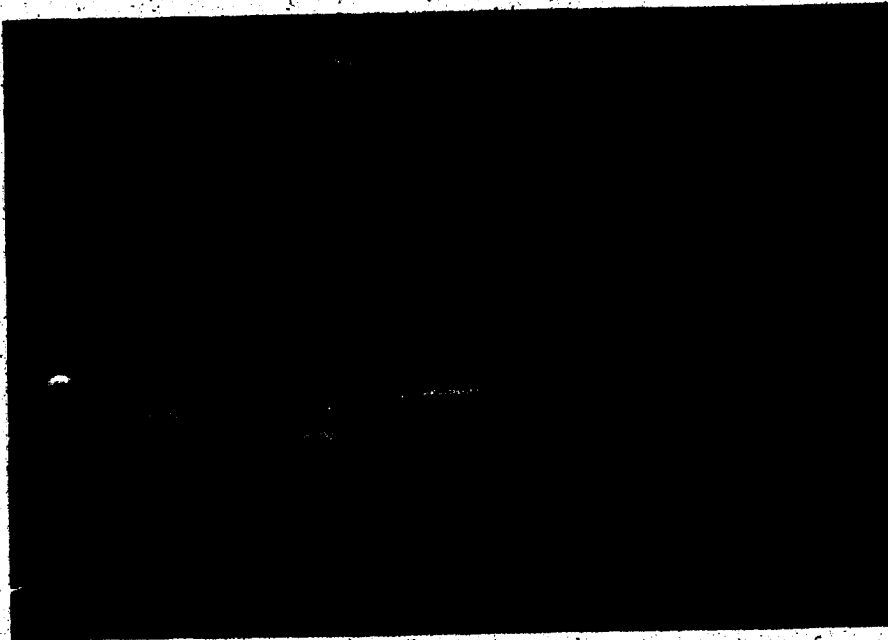
Figure 3.2.2.7   BEAM B2 after Unloading.
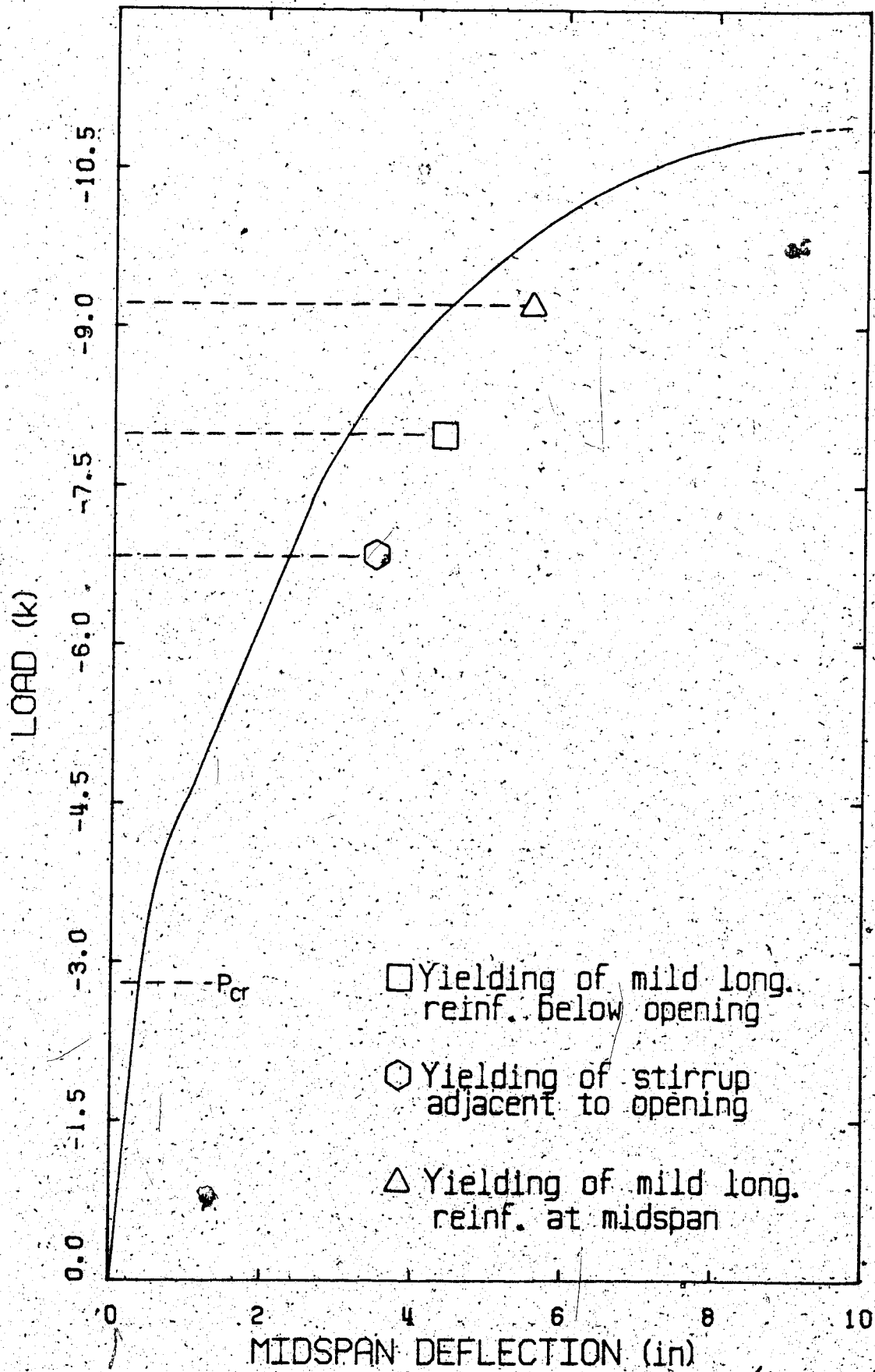
Figure 3.2,2.8   Load-Deflection Curve - BEAM B2.

Figure 3.2.2.9 - Axial Force in the Top Strut - BEAM B2.
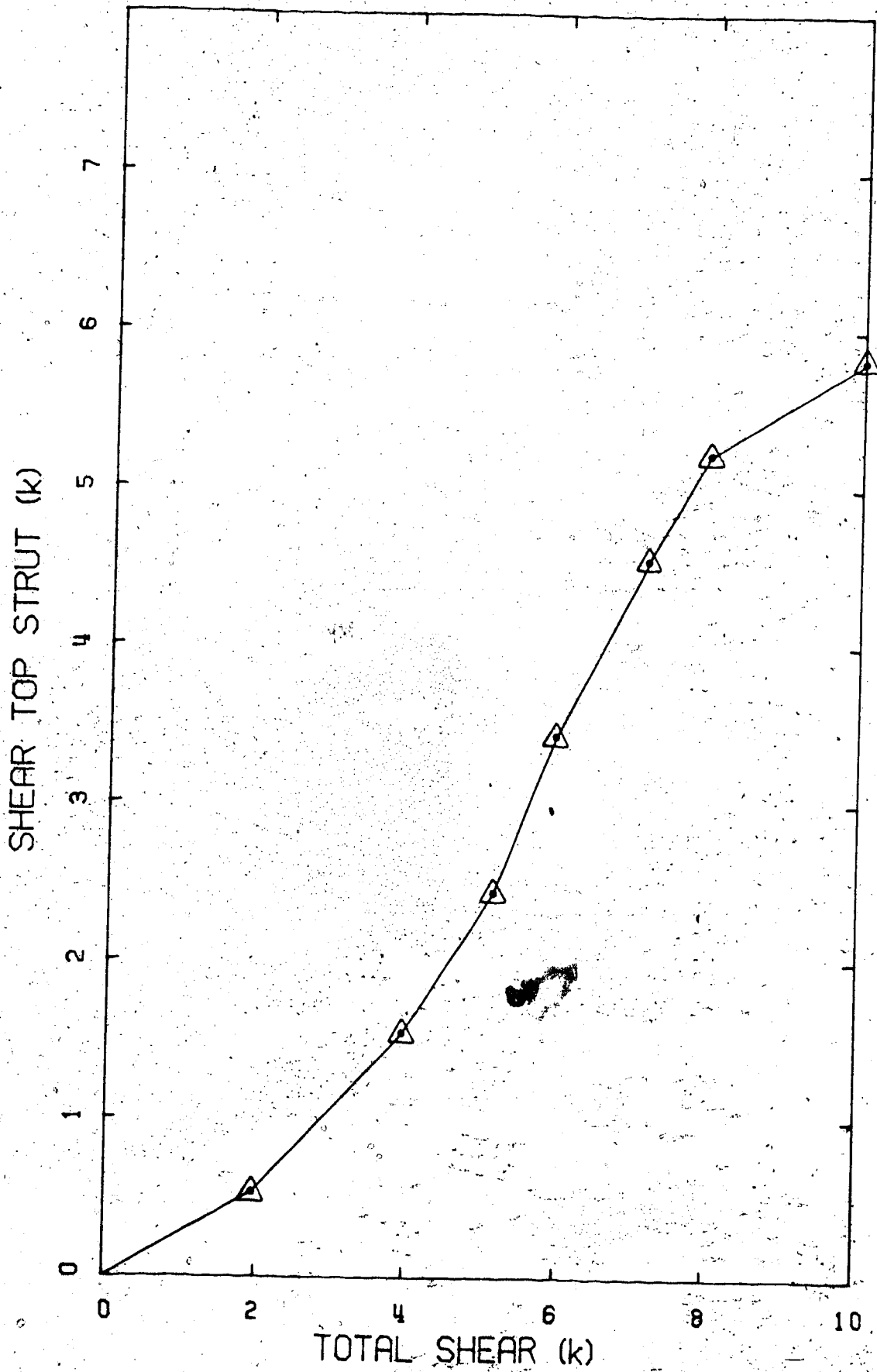
Figure 3.2.2.10   Shear Force in the Top Strut - BEAM B2

94

Support Side

Figure 3.2.2.11 Crack Pattern – BEAM B3.
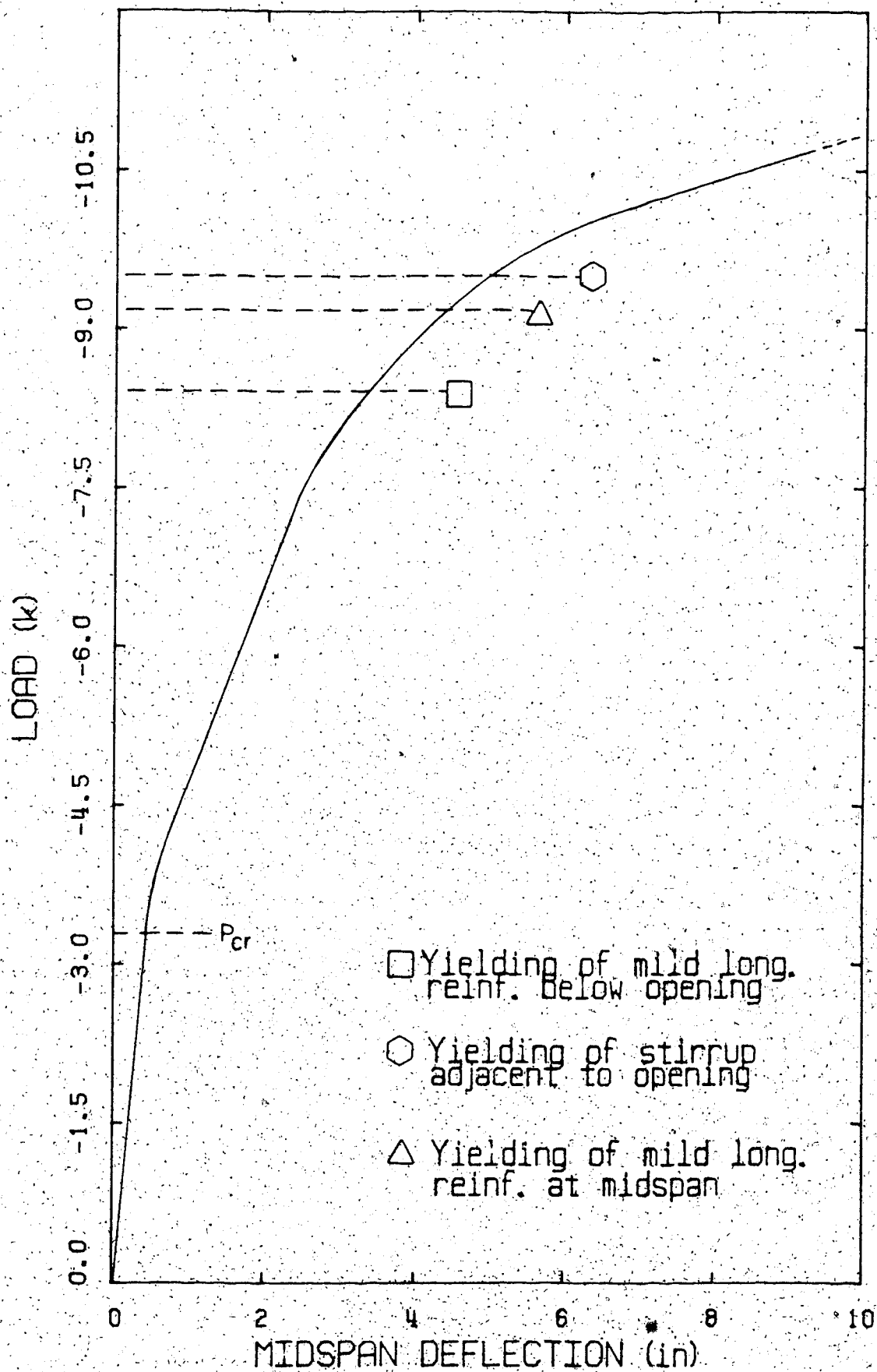
Figure 3.2.2.12   BEAM B3 after Unloading.
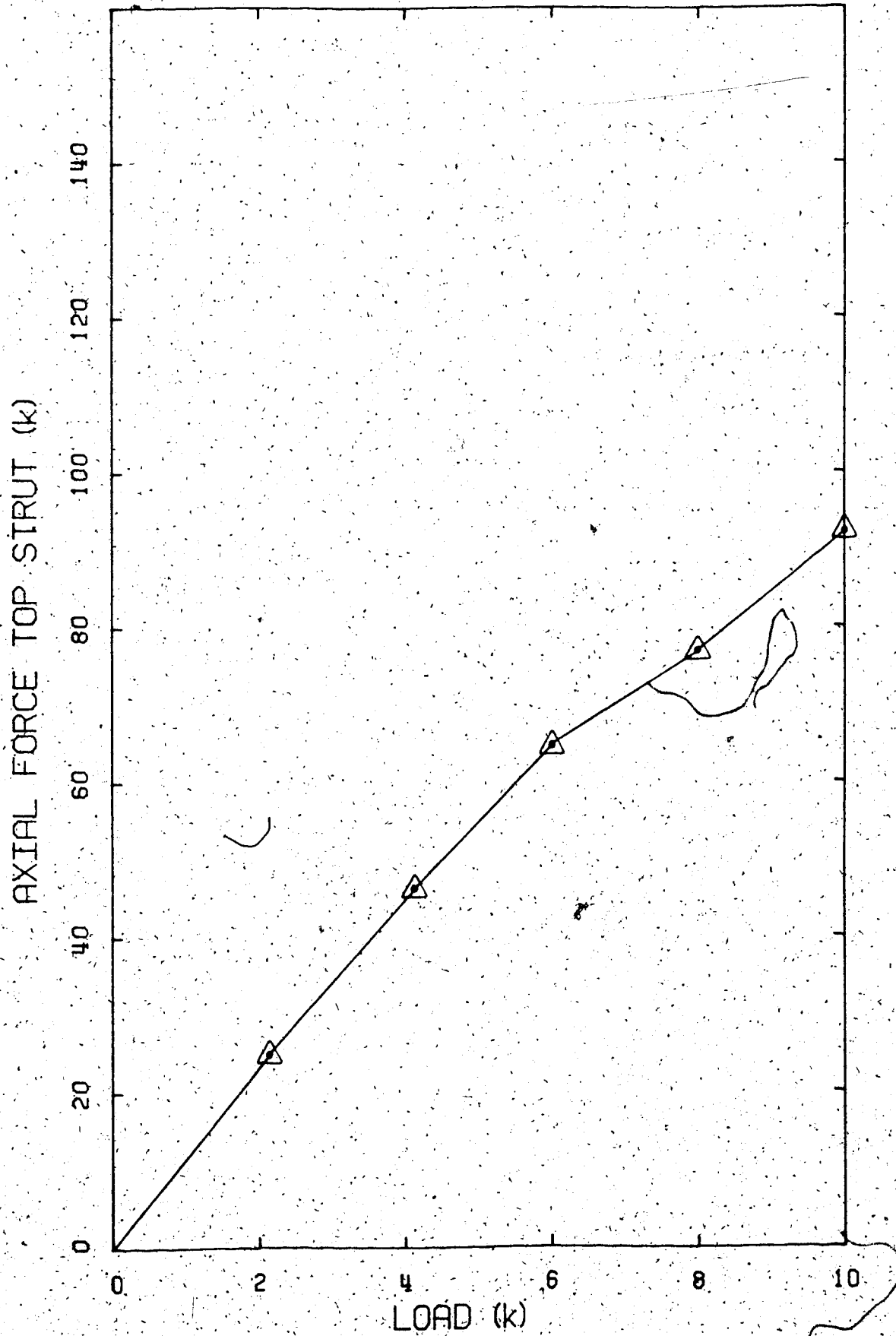
Figure 3.2.2.13 Load-Deflection Curve - BEAM B3.
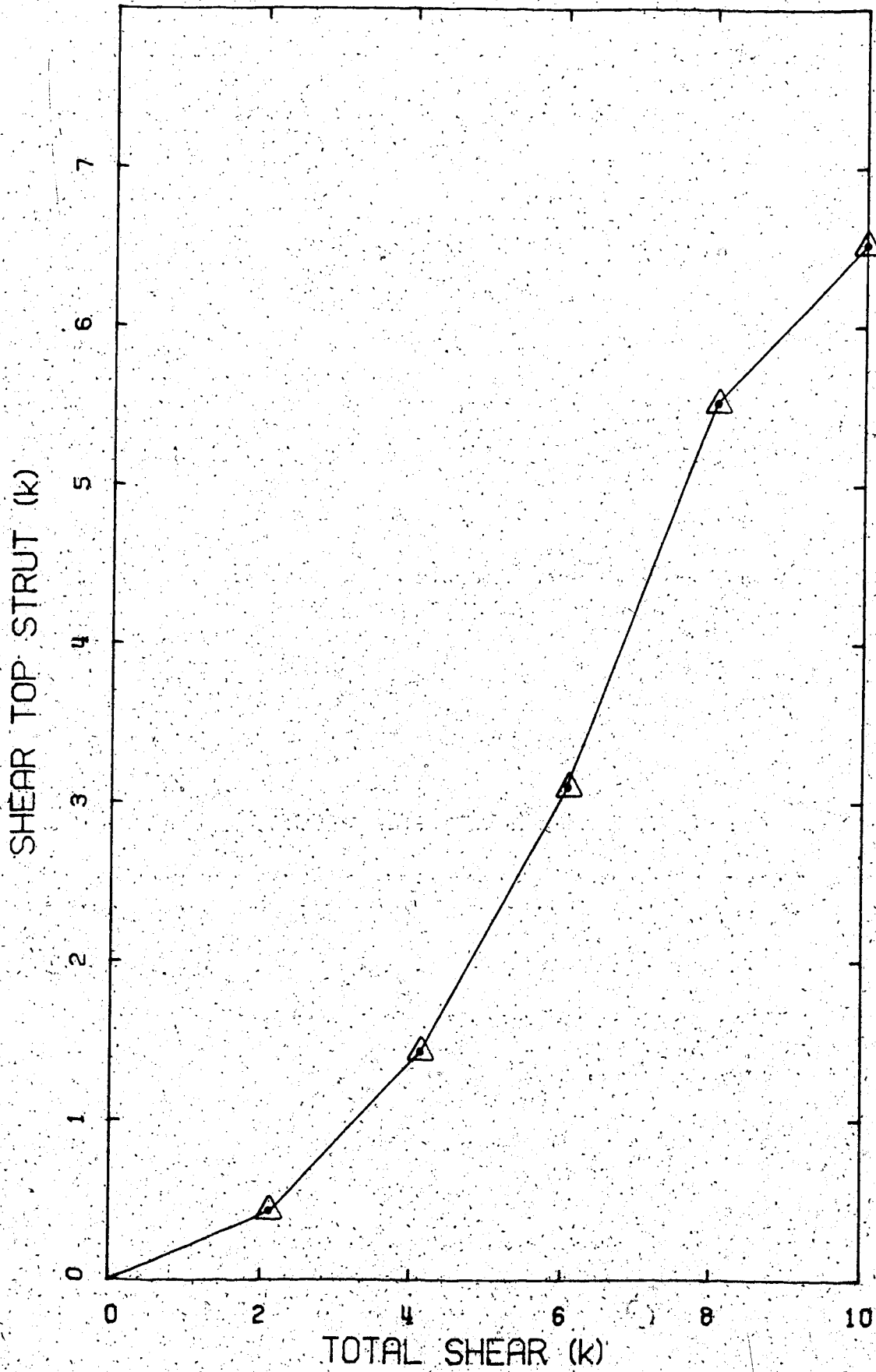
Figure 3.2.2.14 Axial Force in the Top Strut – BEAM B3.

Figure 3.2.2.15 Shear Force in the Top Strut - BEAM B3.

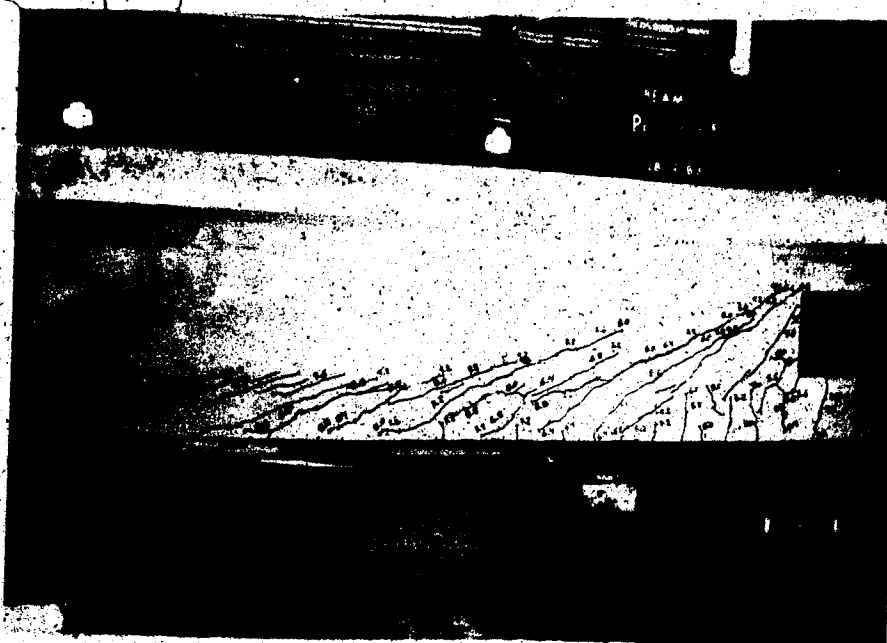Figure 3.2.3.1   Crack Pattern - BEAM C1.

Figure 3.2.3.2 : BEAM C1 after Unloading.

Figure 3.2.3.3   Load-Deflection Curve - BEAM Cl.

Figure 3.2.3.4   Axial Force in the Top Strut — BEAM C1.

Figure 3.2.3.5   Shear Force in the Top Strut – BEAM C1.

Support Side

Figure 3.2.3.6   Crack Pattern — BEAM C2.

Figure 3.2.3.7   BEAM C2 after Unloading.
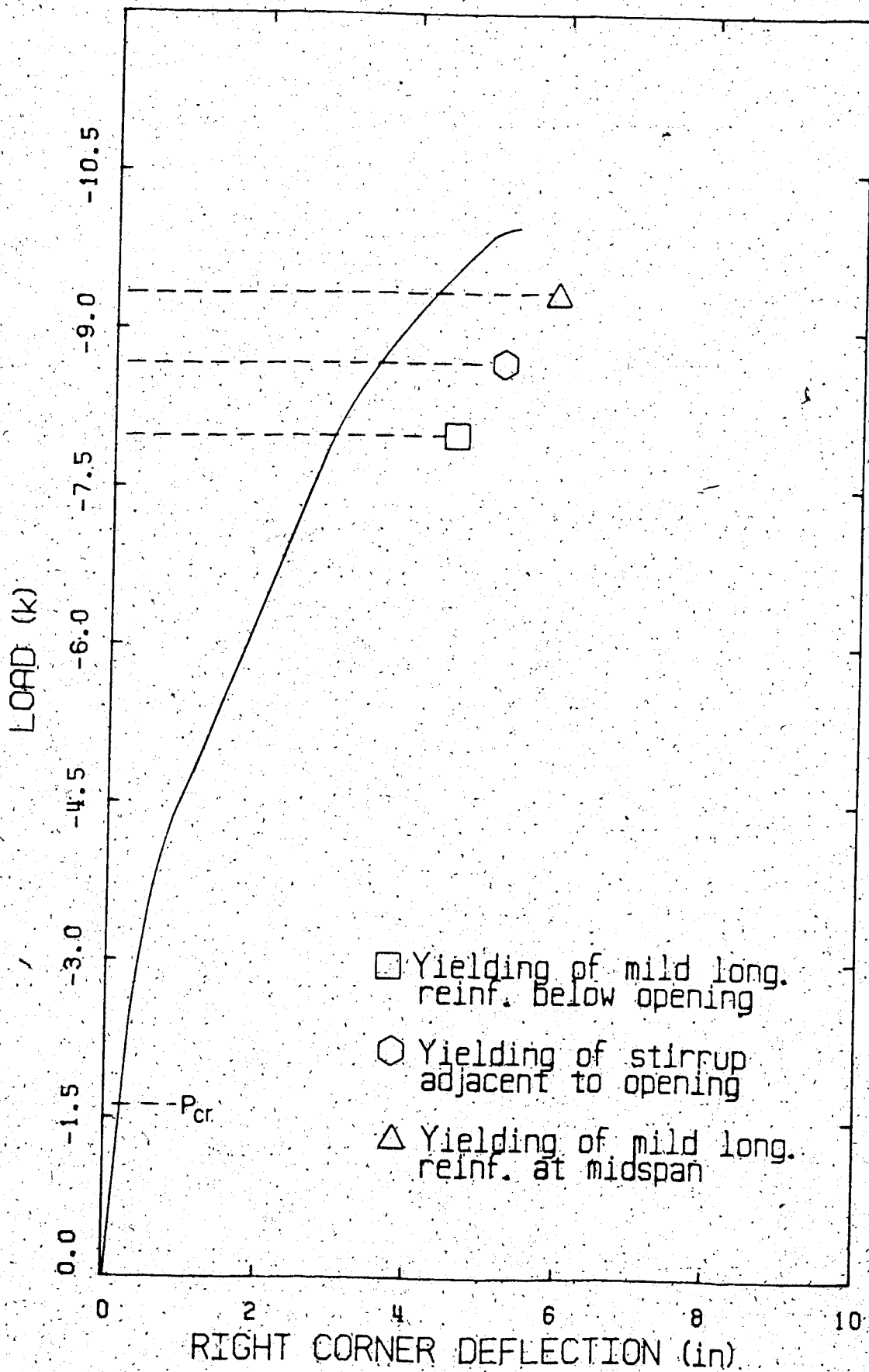
Figure 3.2.3.8   Load-Deflection Curve - BEAM C2.

Figure 3.2.3.9   Axial Force in the Top Strut - BEAM C2.

Figure 3.2.3.10   Shear Force in the Top Strut - BEAM C2.

109

Support Side

Figure 3.2.3.11 Crack Pattern - BEAM C3.

Figure 3.2.3.12 BEAM C3 after Unloading.

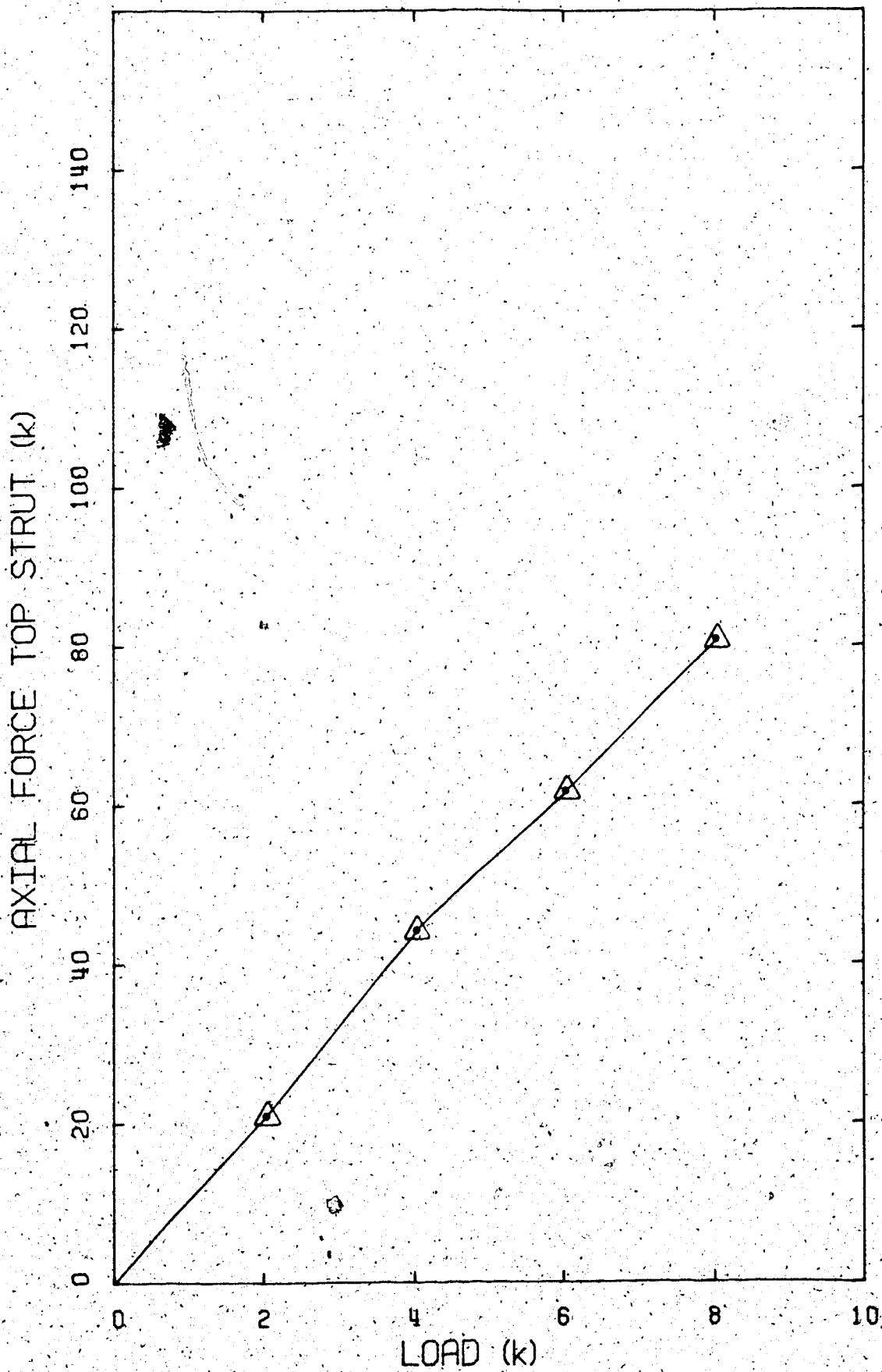Figure 3.2.3.13 Load-Deflection Curve - BEAM C3.
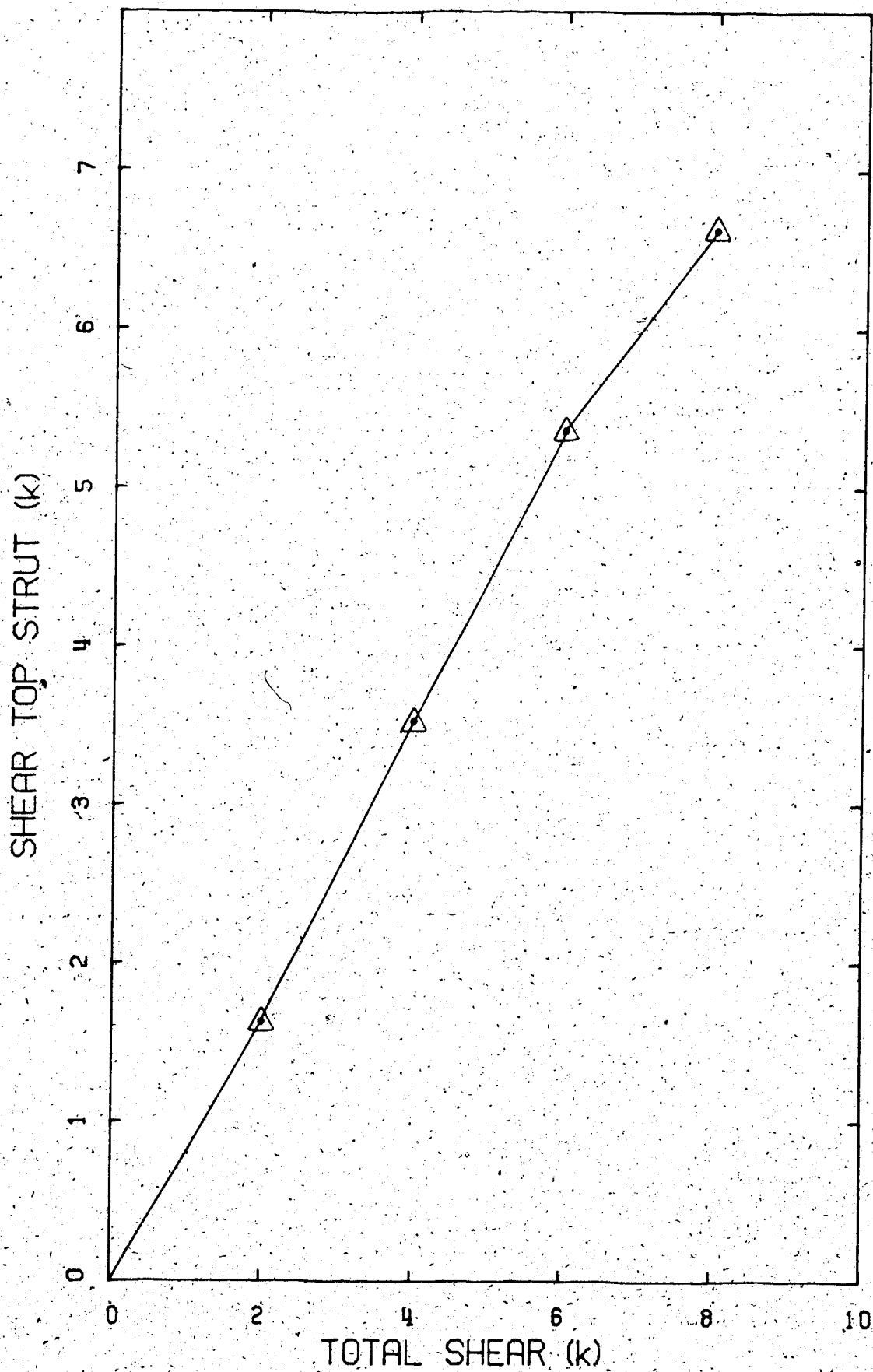
Figure 3.2.3.14 Axial Force in the Top Strut - BEAM C3.

Figure 3.2.3.15 Shear Force in the Top Strut - BEAM C3.
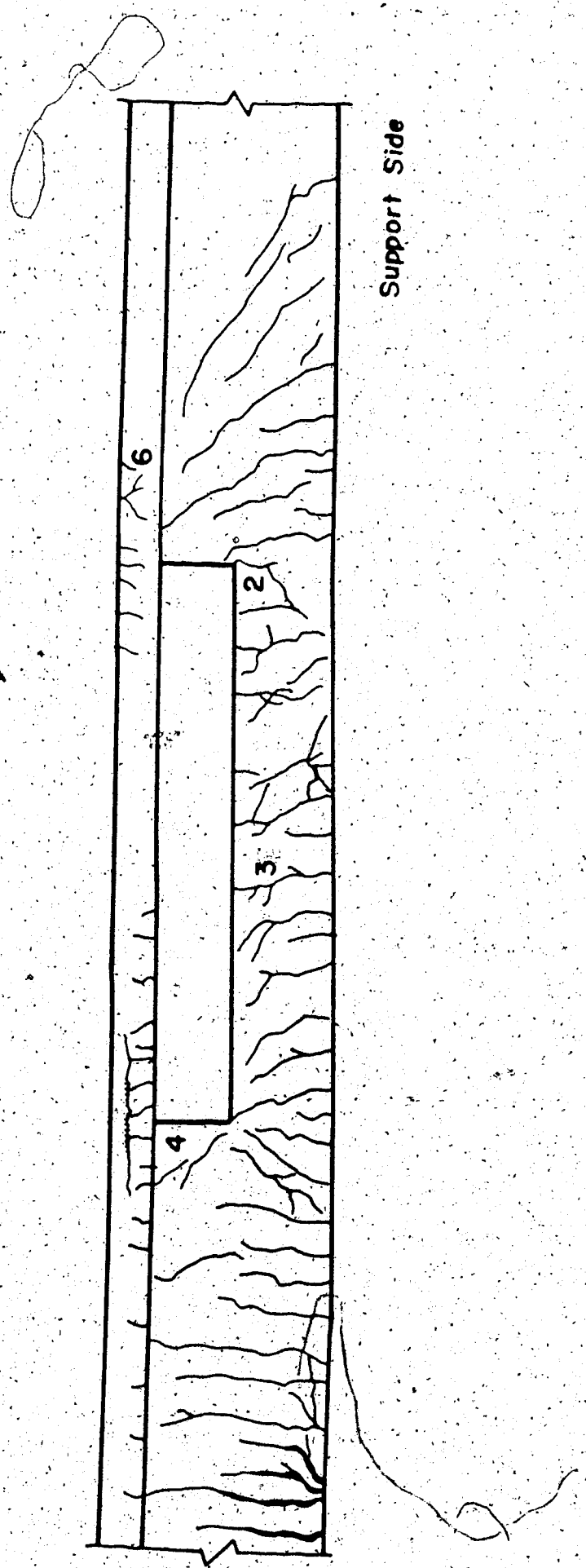
Figure 3.2.4.1   Crack Pattern - BEAM D1.

Figure 3.2.4.2   BEAM D1 after Unloading.

Figure 3.2.4.3   Load-Deflection Curve - BEAM D1.

Figure 3.2.4.4 Axial Force in the Top Strut - BEAM D1.
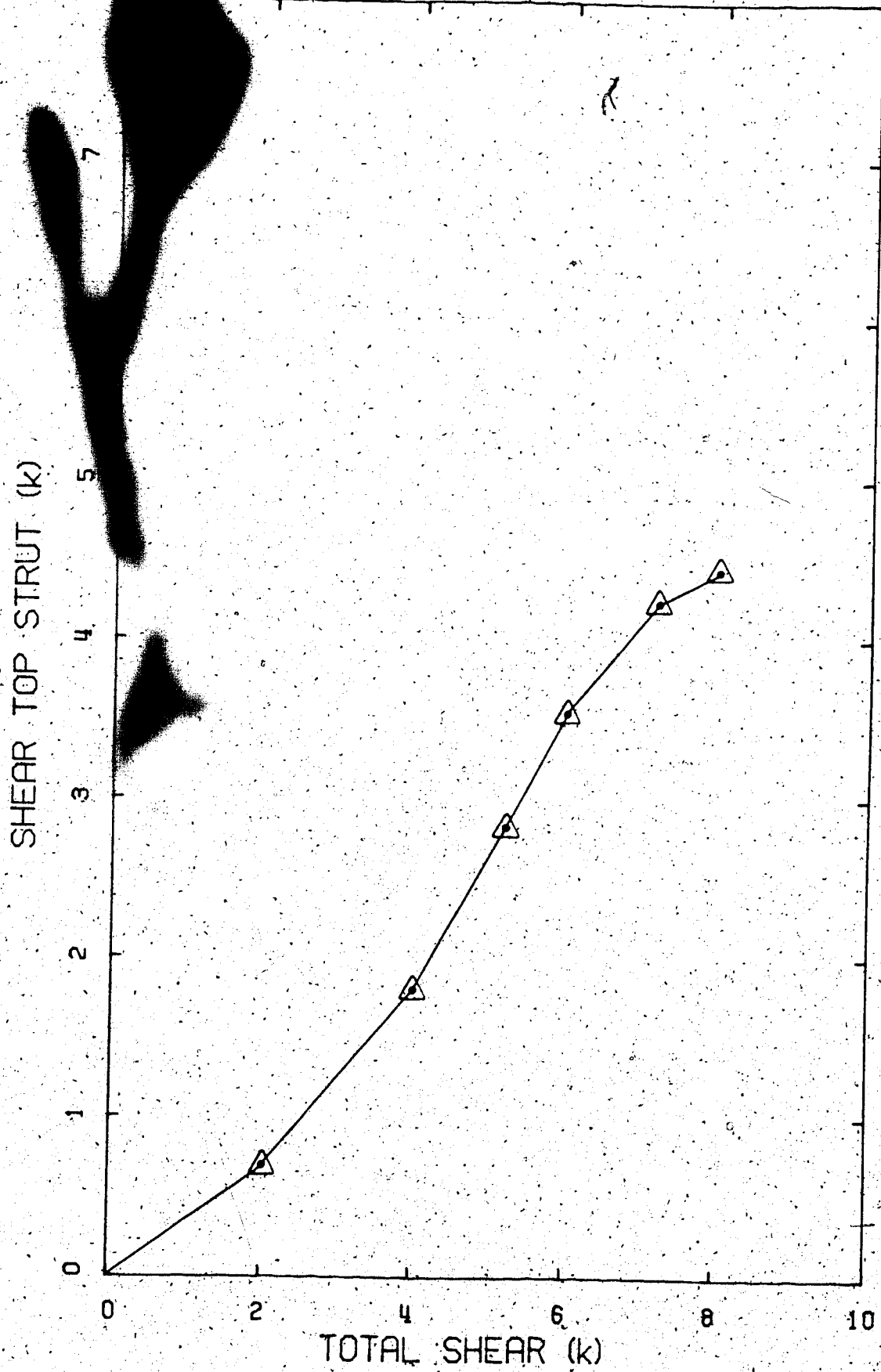
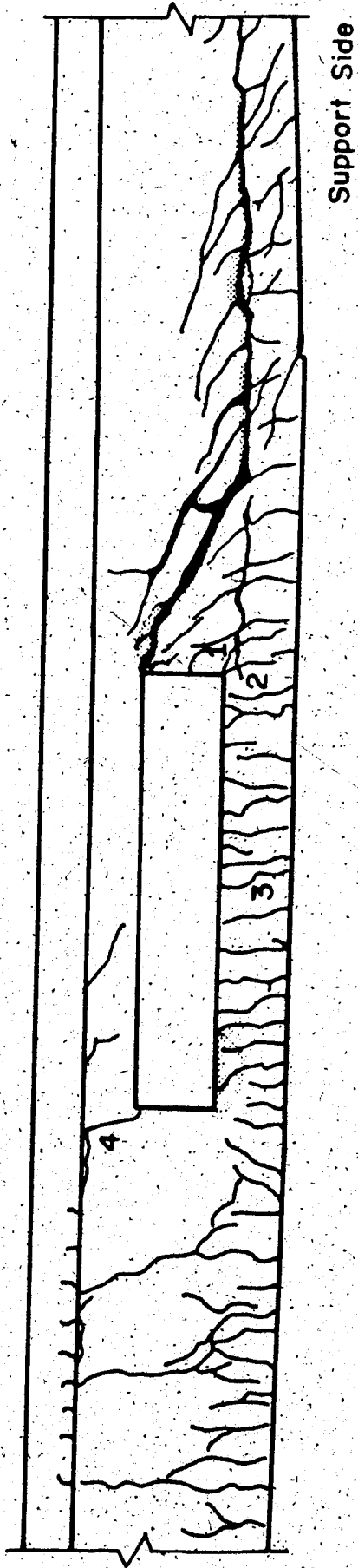Figure 3.2.4.5.   Shear Force in the Top Strut - BEAM D1.
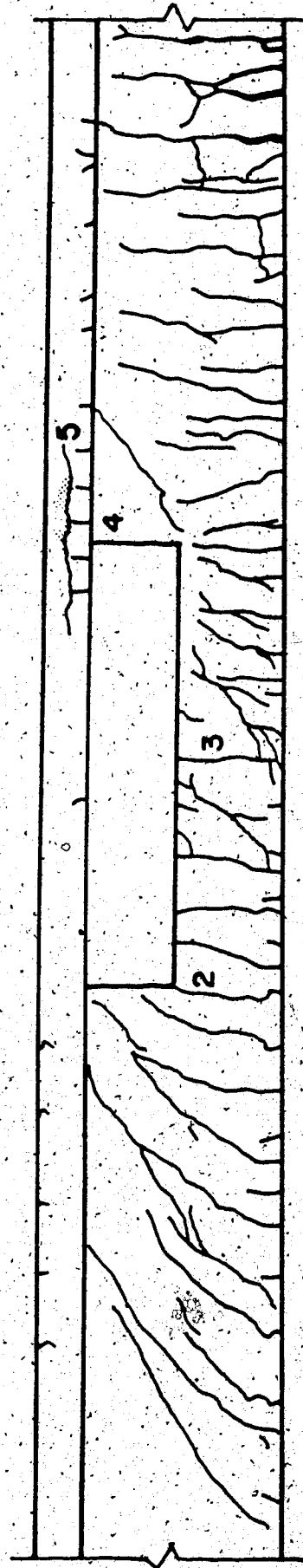
Figure 3.2.4.6.   Crack Pattern — BEAM D2.

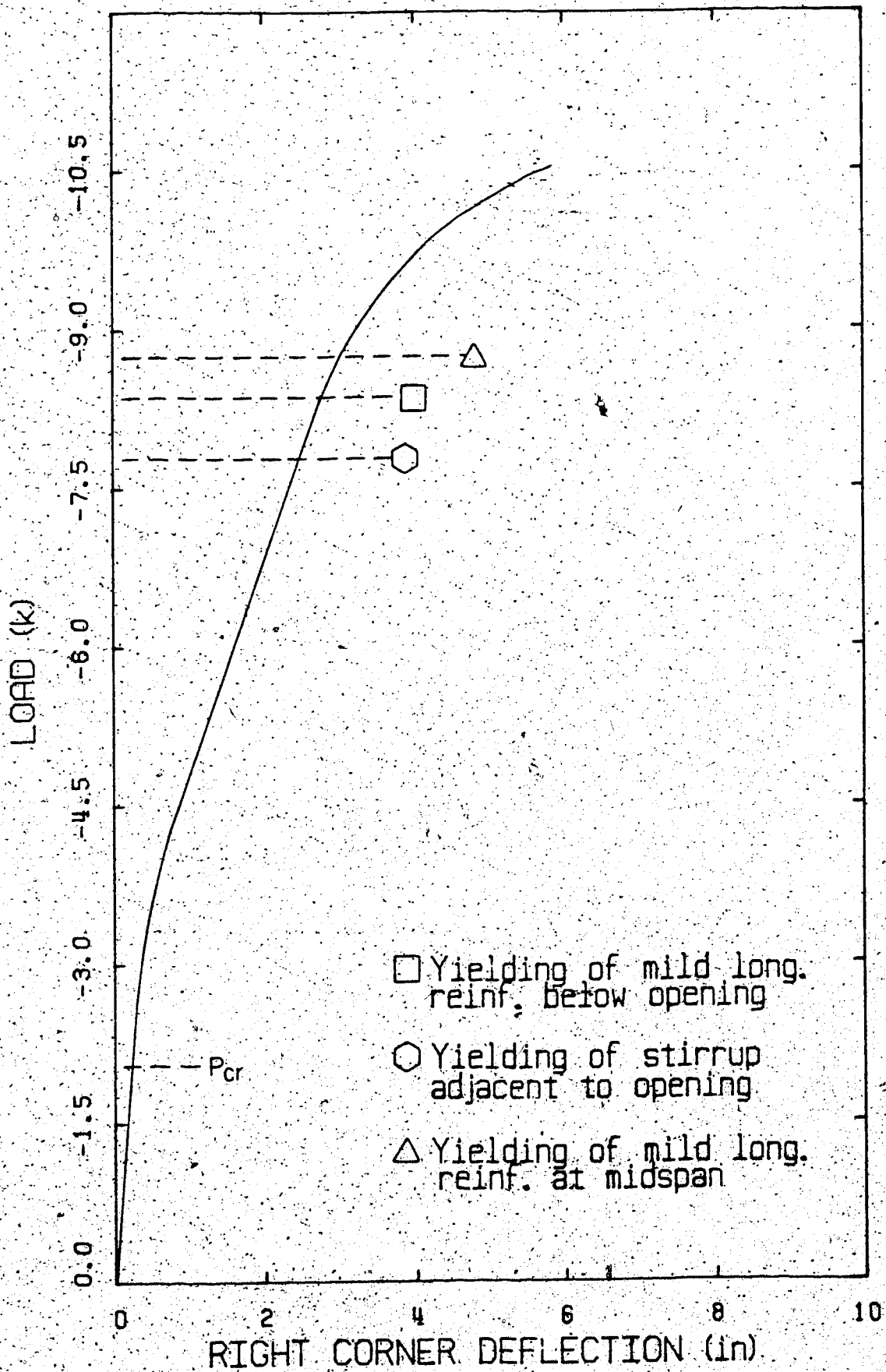Figure 3.2.4.7   BEAM D2 after Unloading
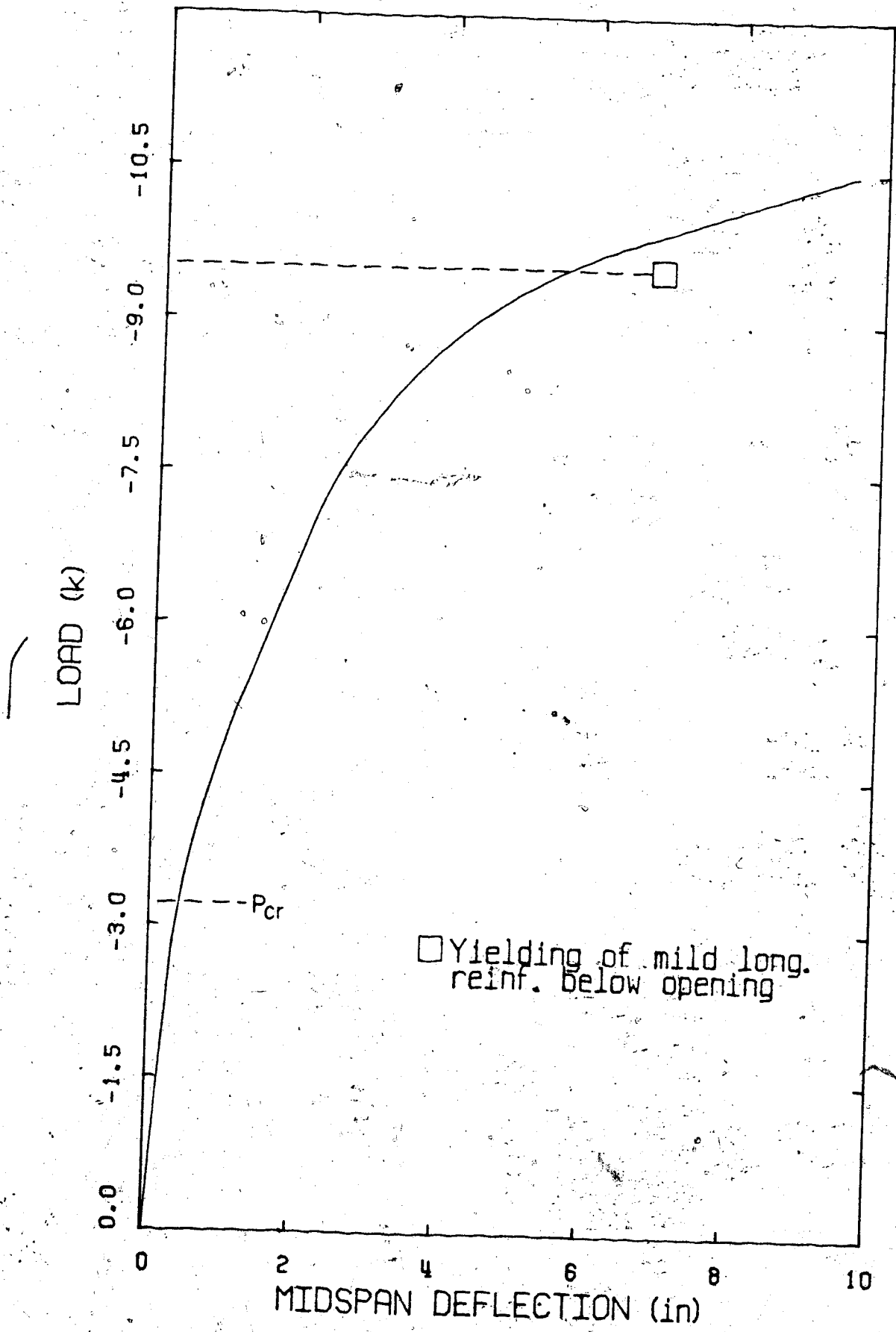
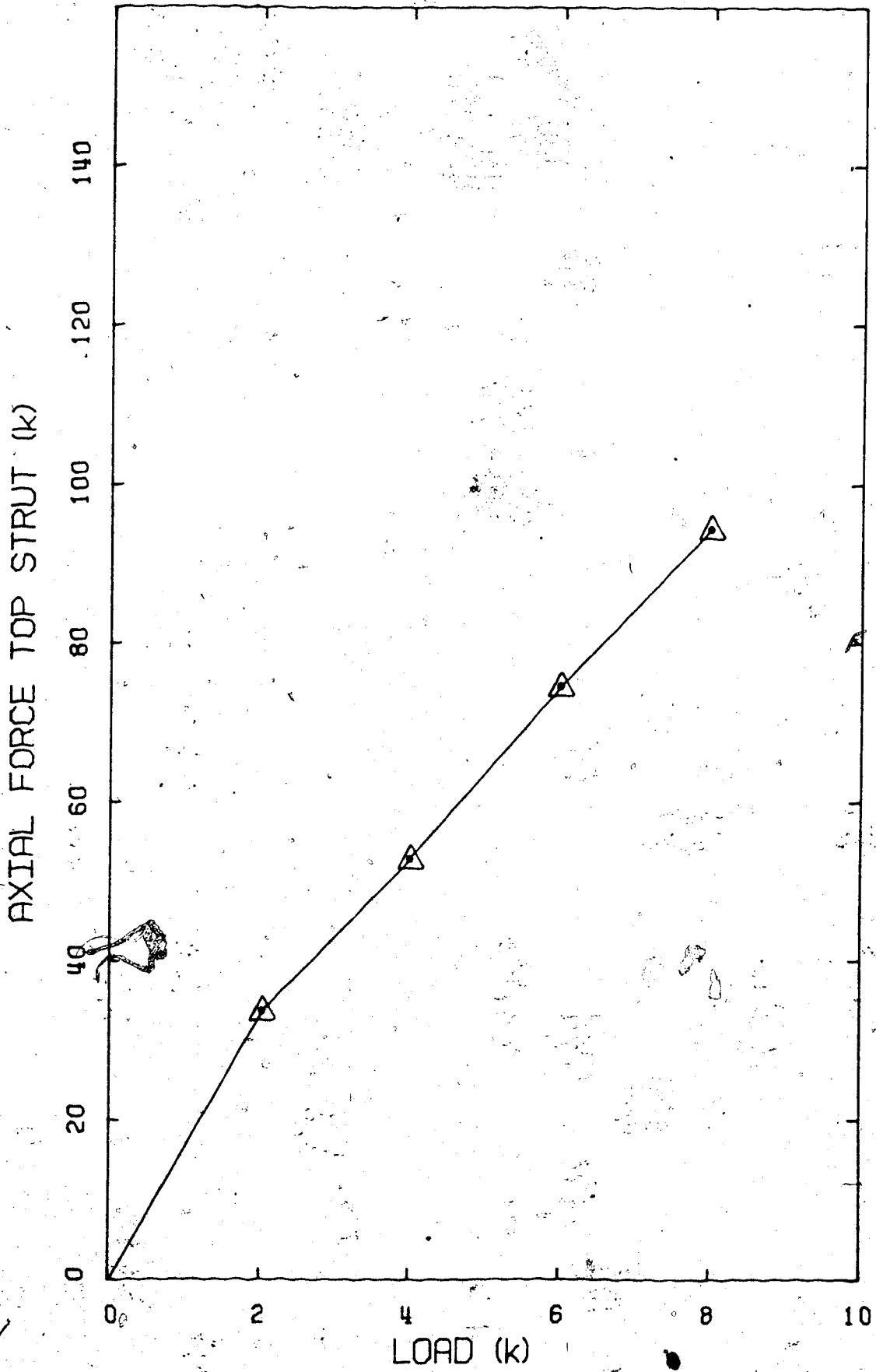Figure 3.2.4.8   Load-Deflection Curve - BEAM D2.
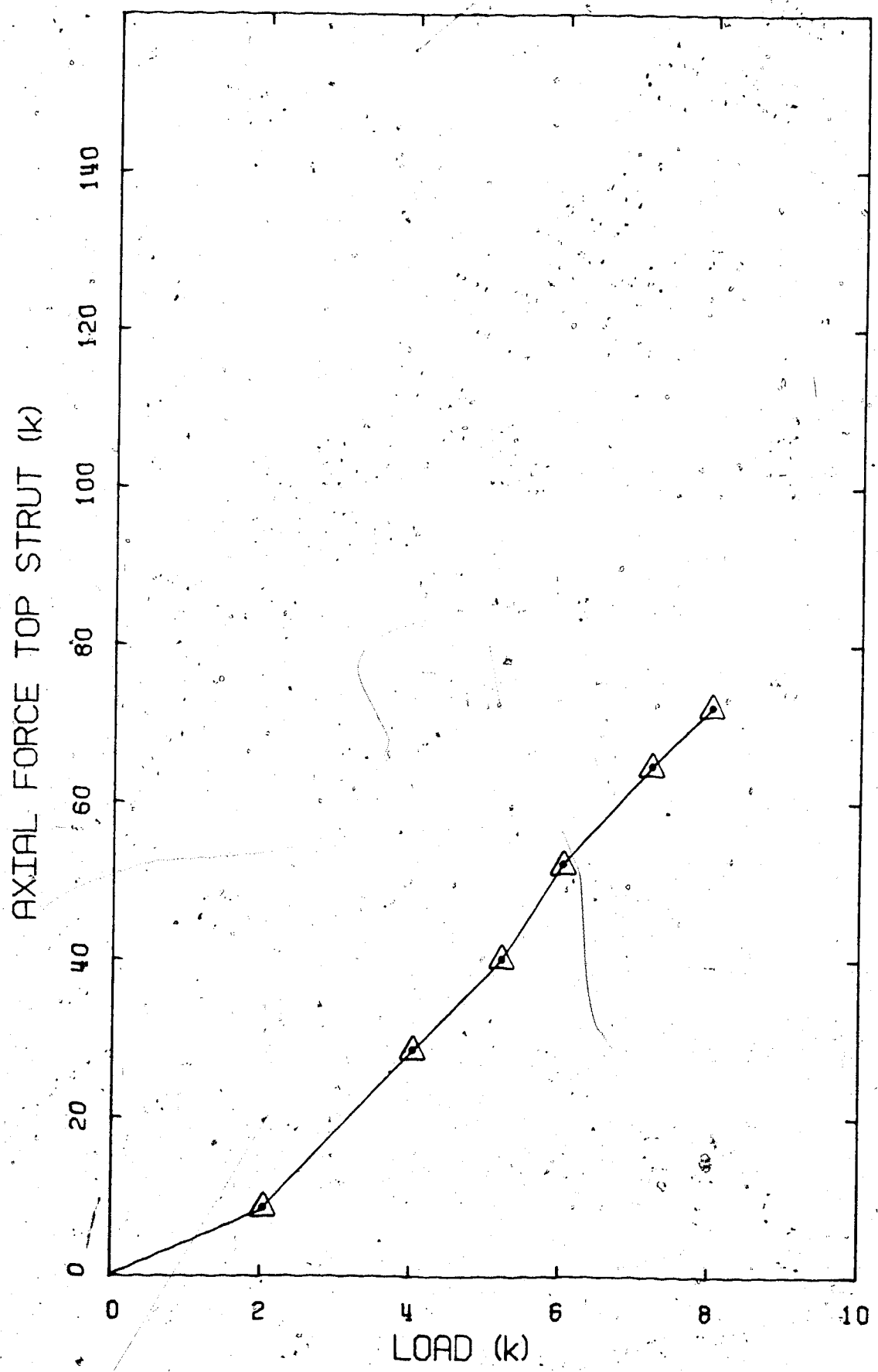
Figure 3.2.4.9   Axial Force in the Top Strut – BEAM D2.
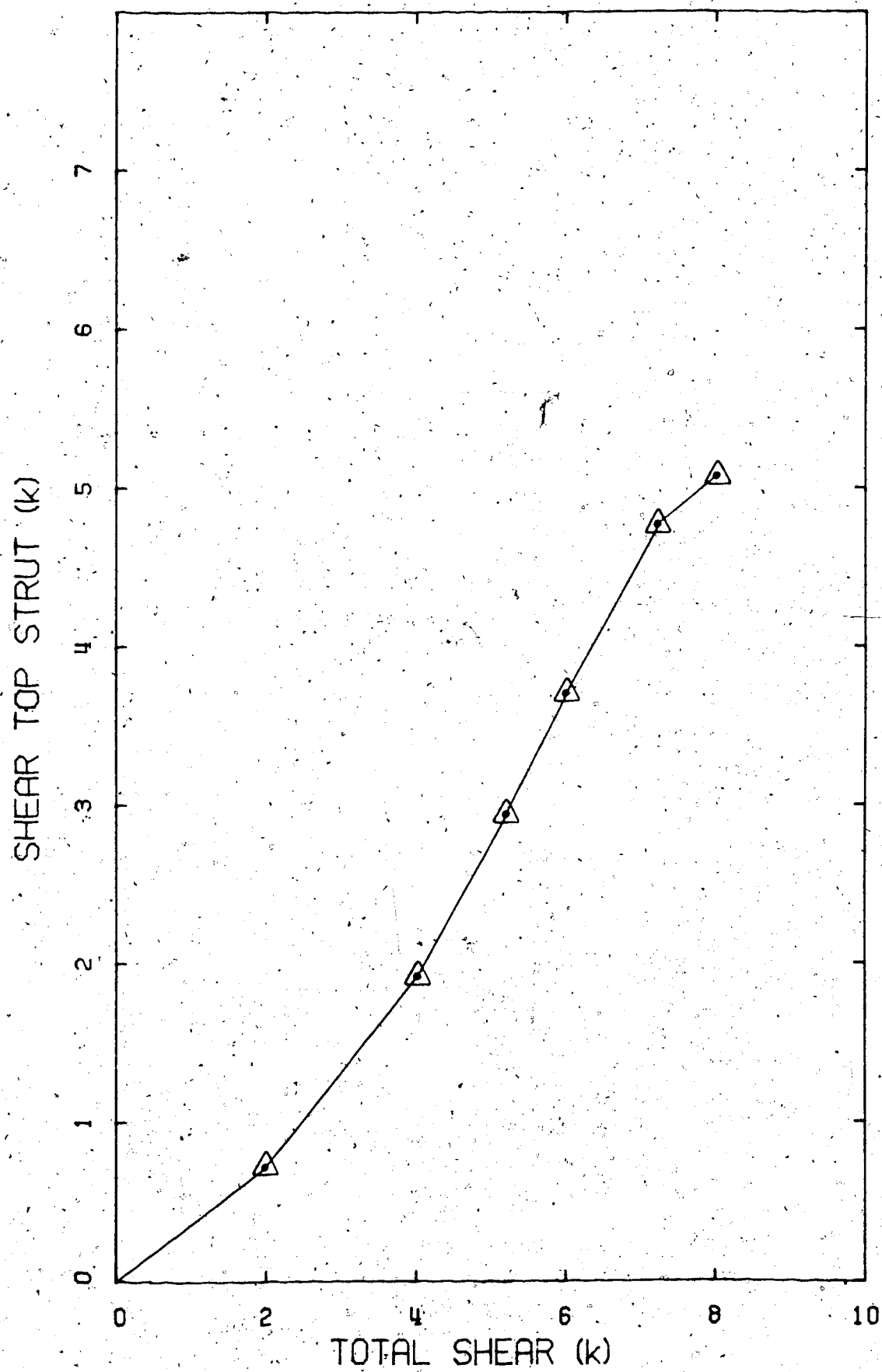
Figure 3.2.4.10 Shear Force in the Top Strut - BEAM D2.

124

Support Side
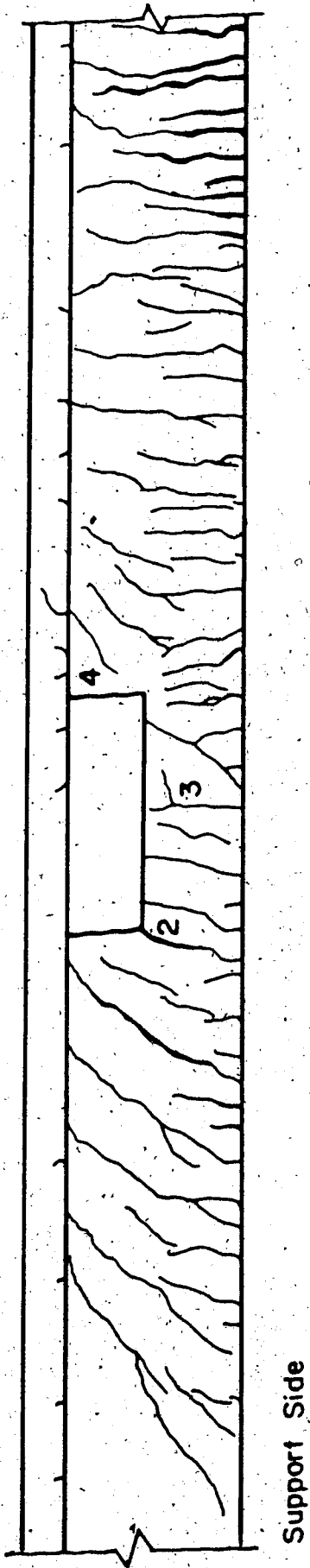
Figure 3.2.4.11 Crack Pattern — BEAM D3.
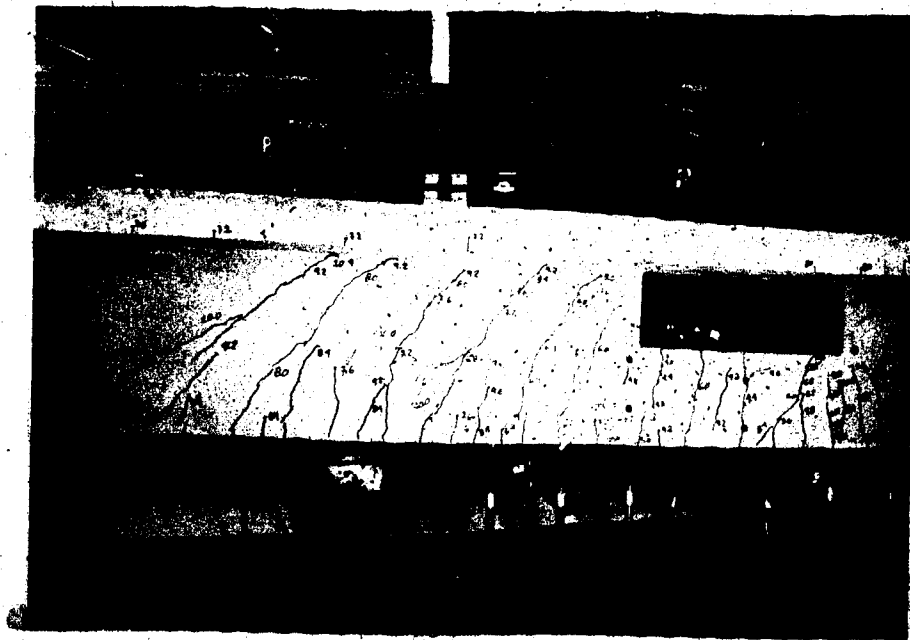
Figure 3.2.4.12 BEAM D3 after Unloading.
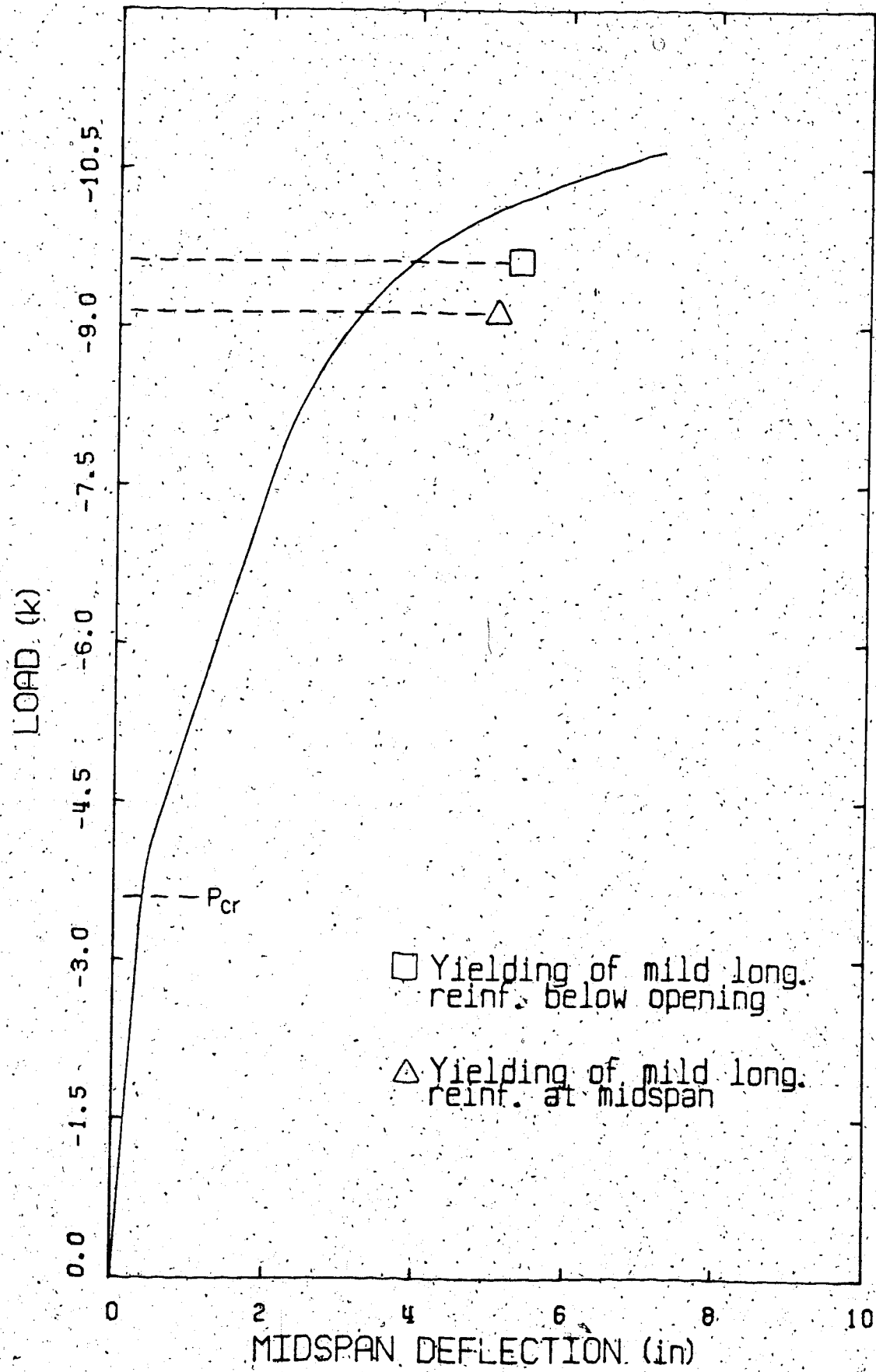
Figure 3.2.4.13 Load-Deflection Curve - BEAM D3.

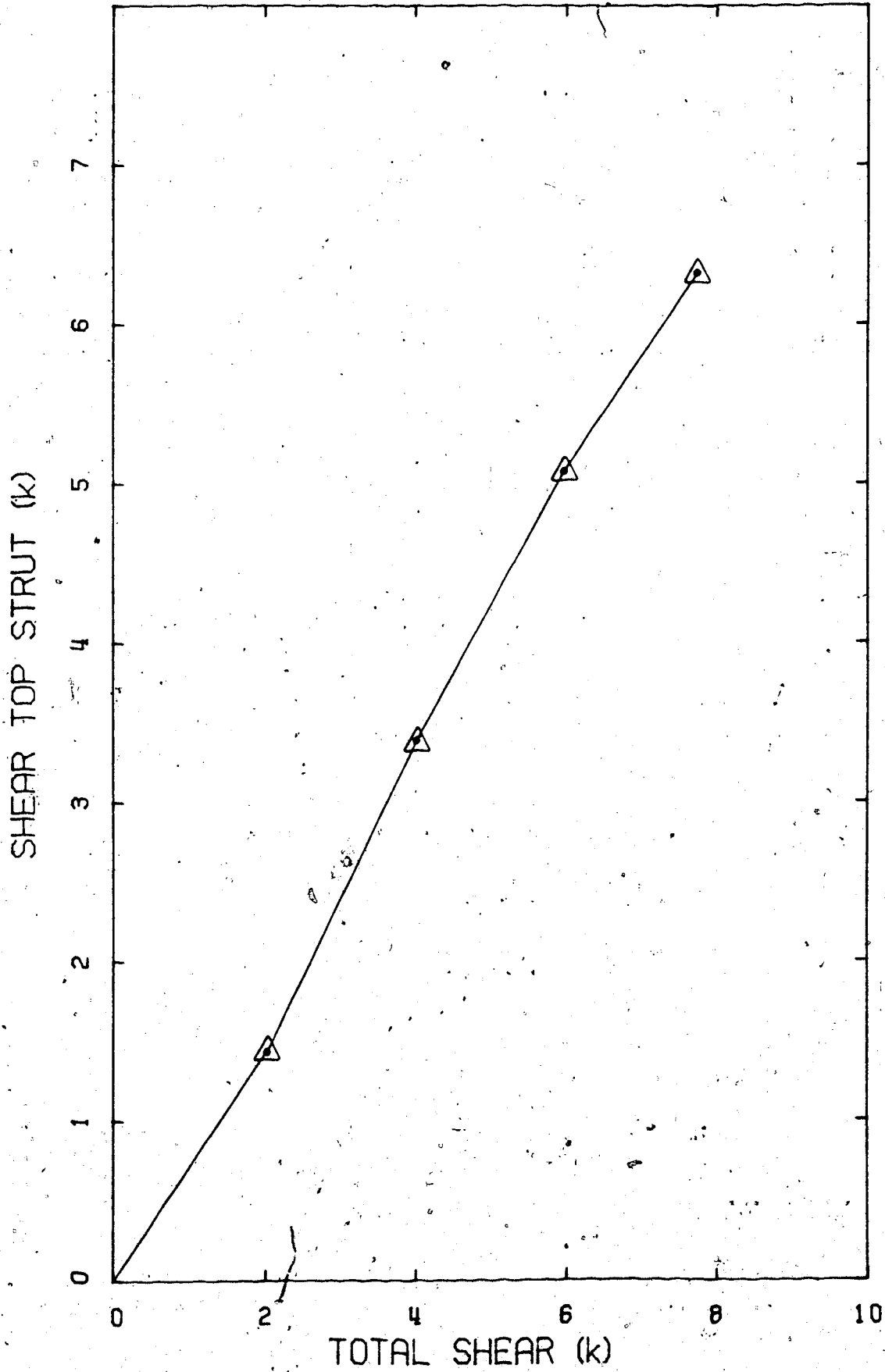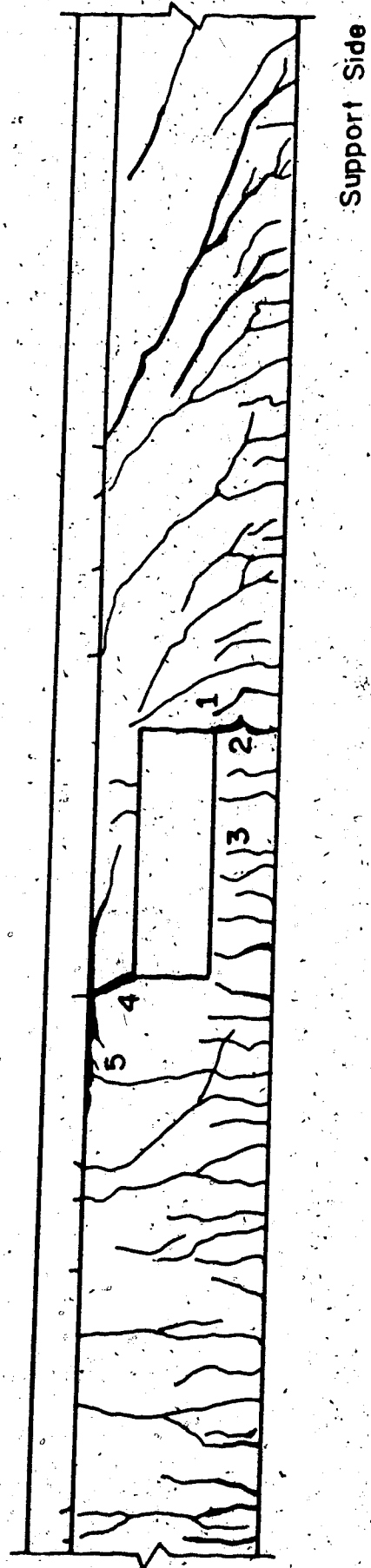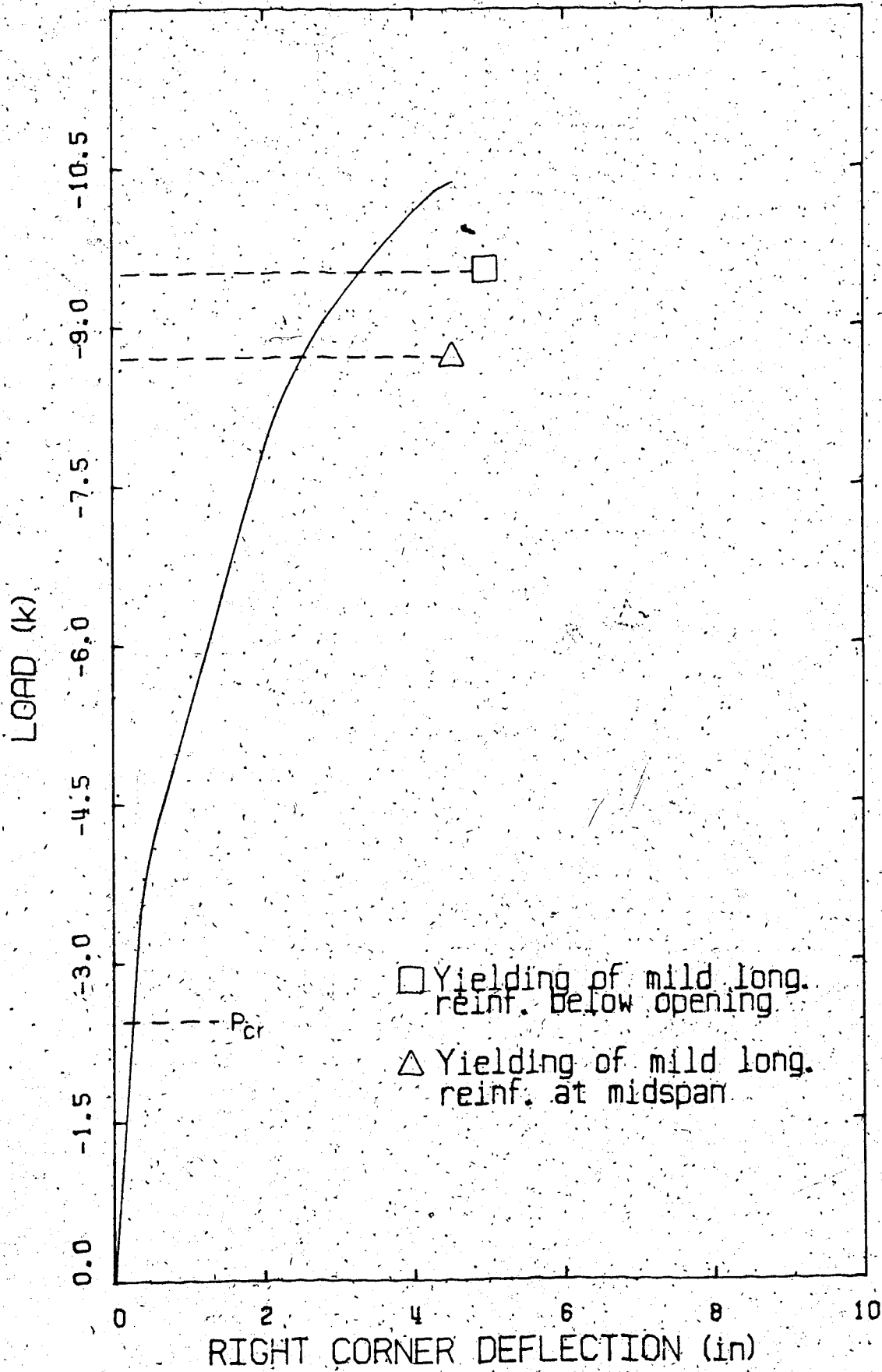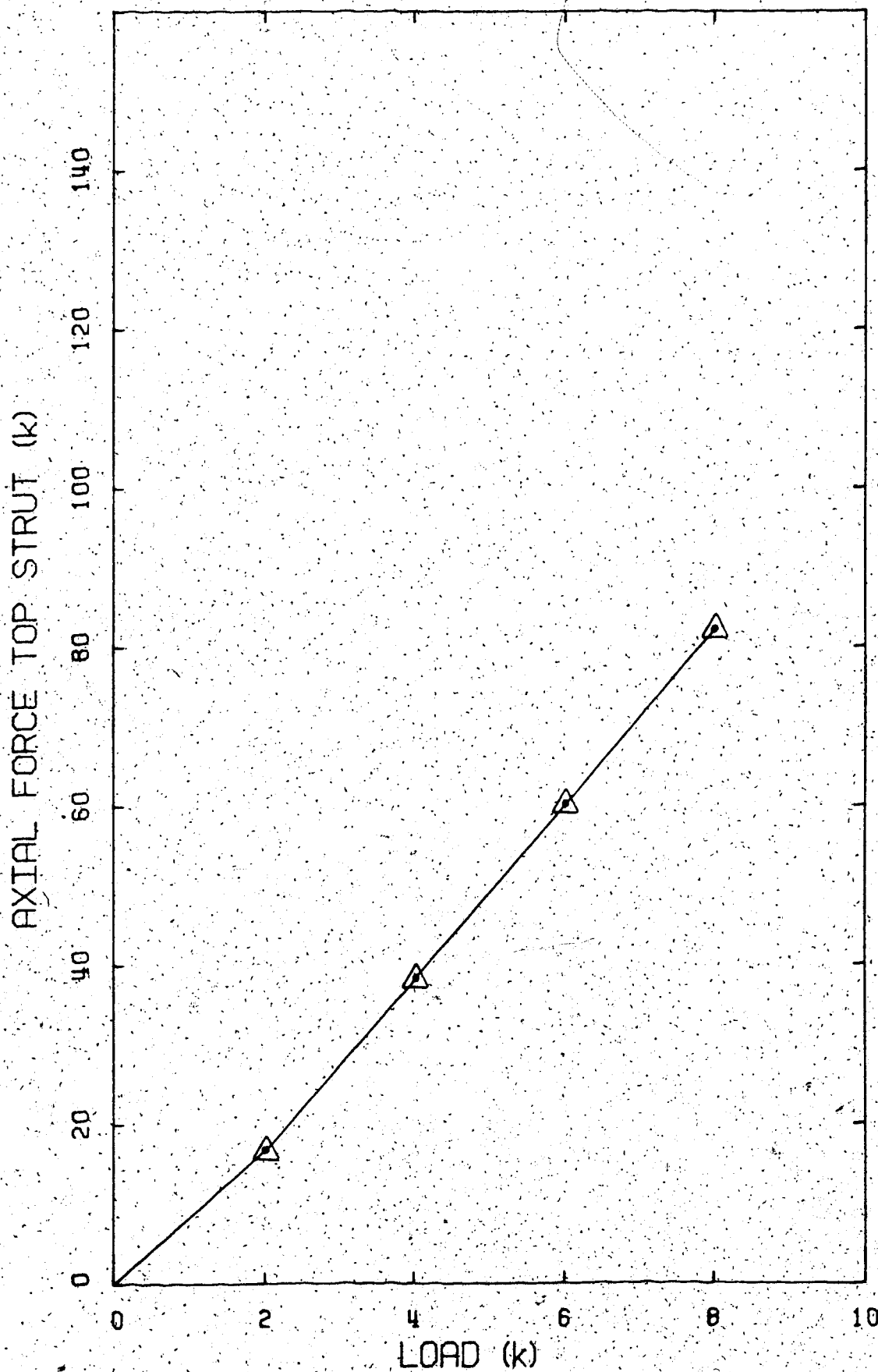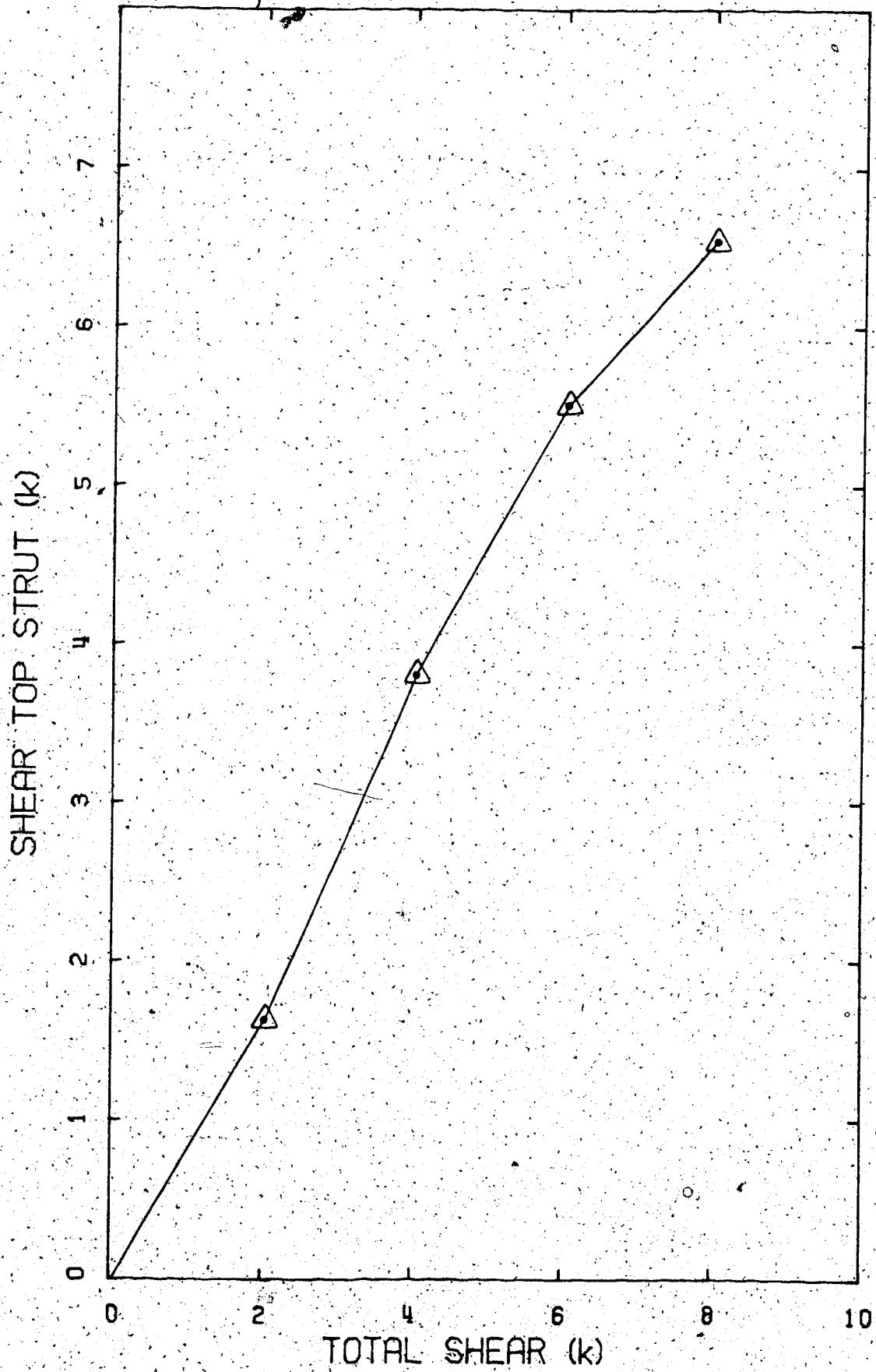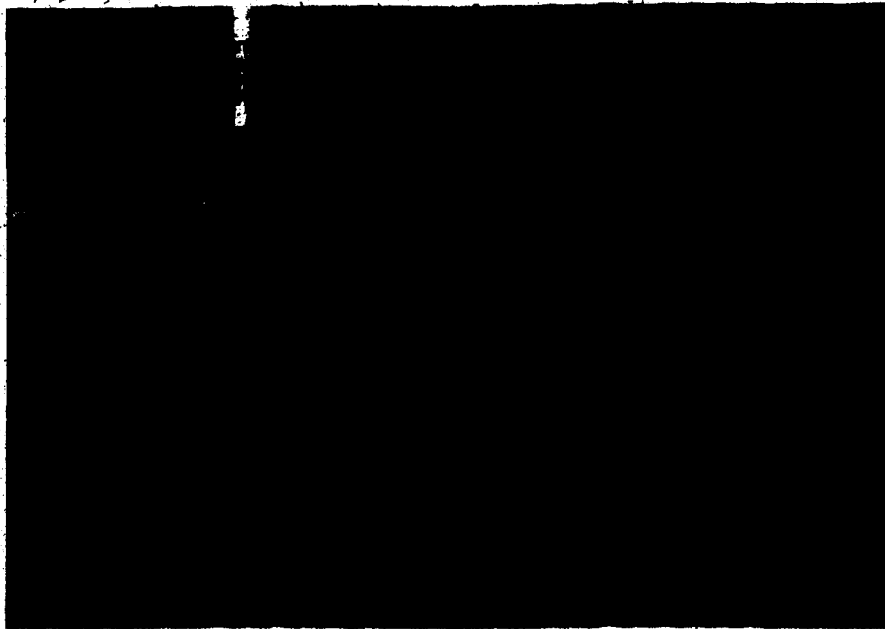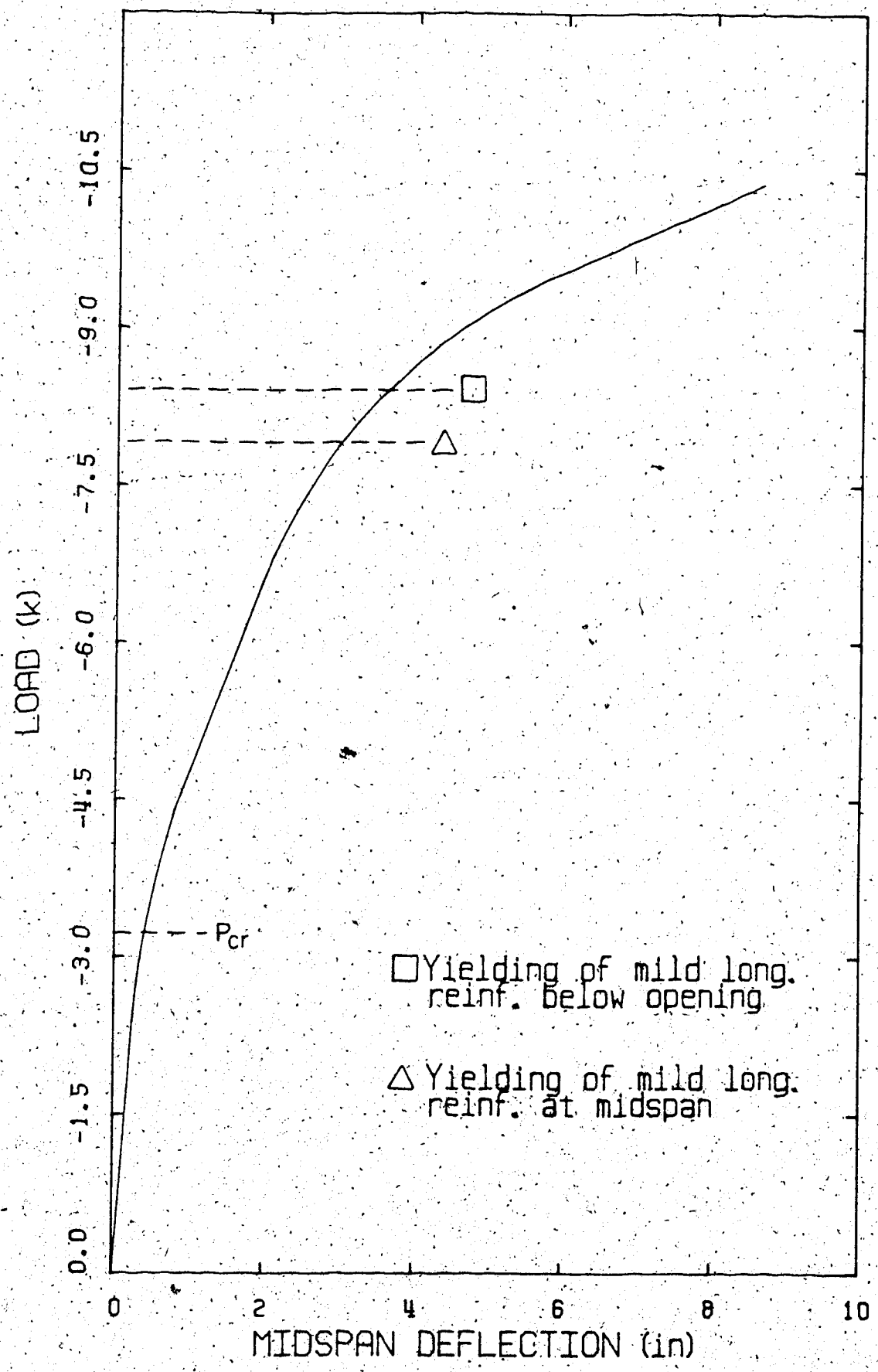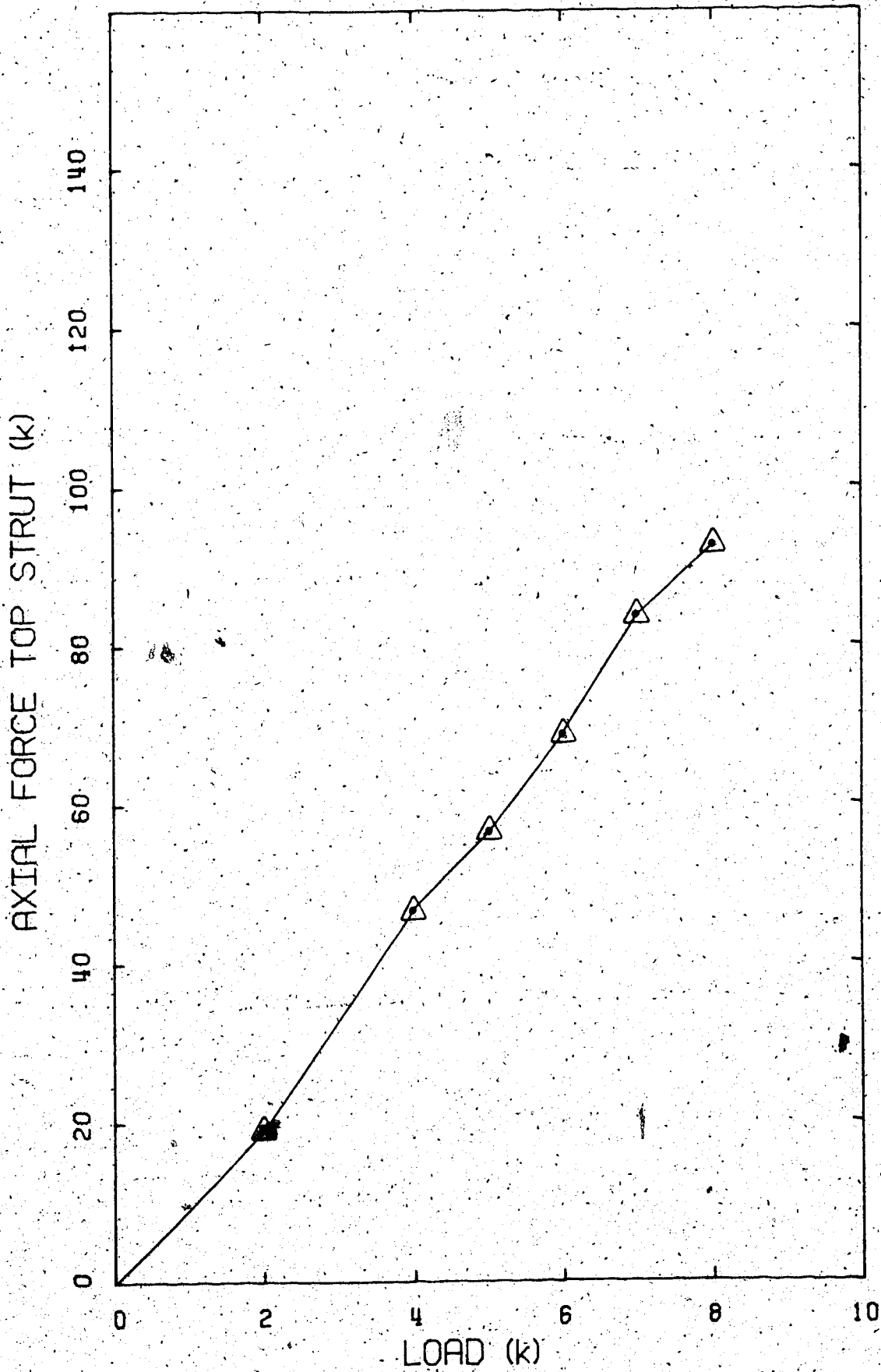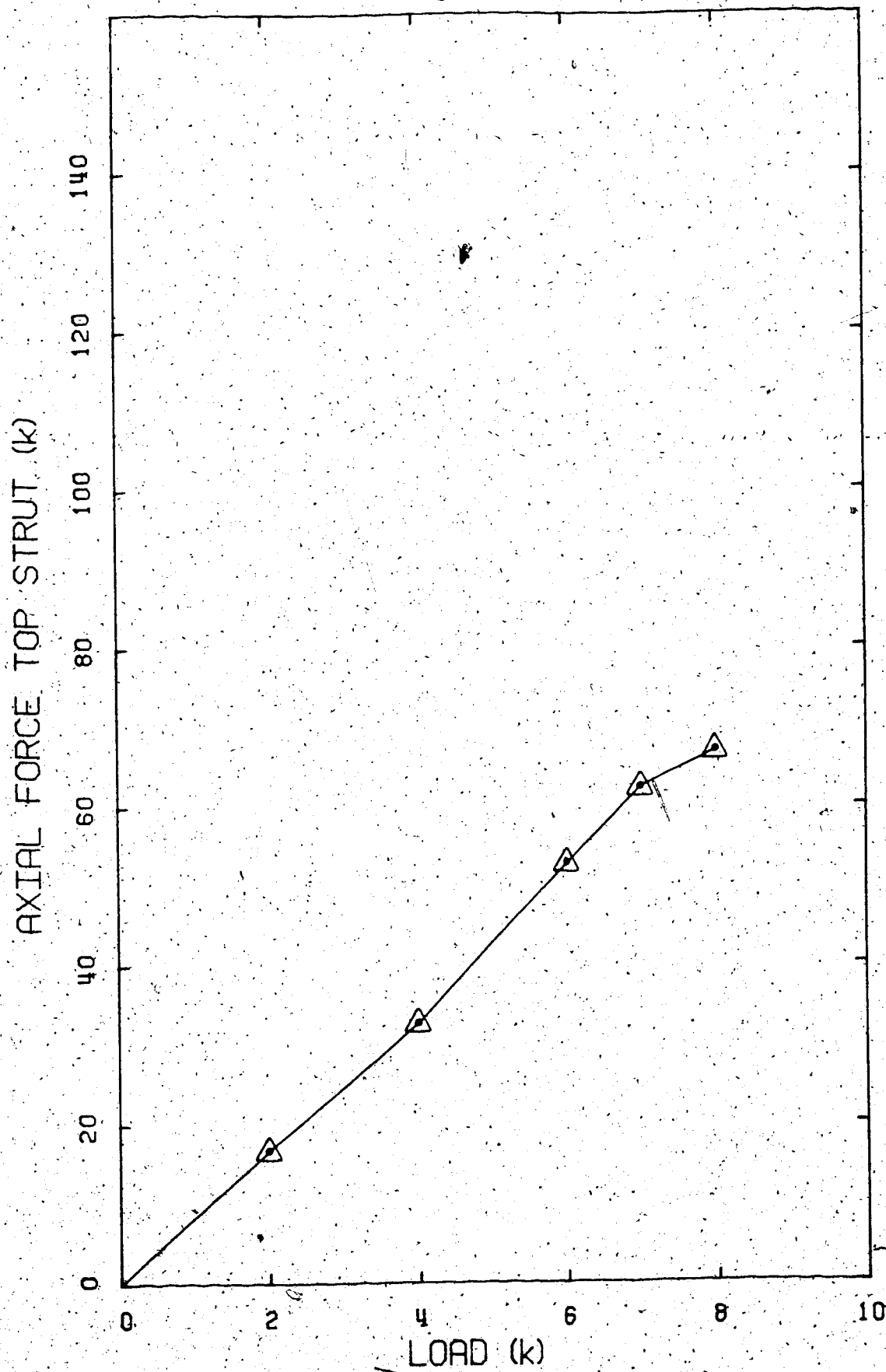Figure 3.2.4.14 Axial Force in the Top Strut - BEAM D3.
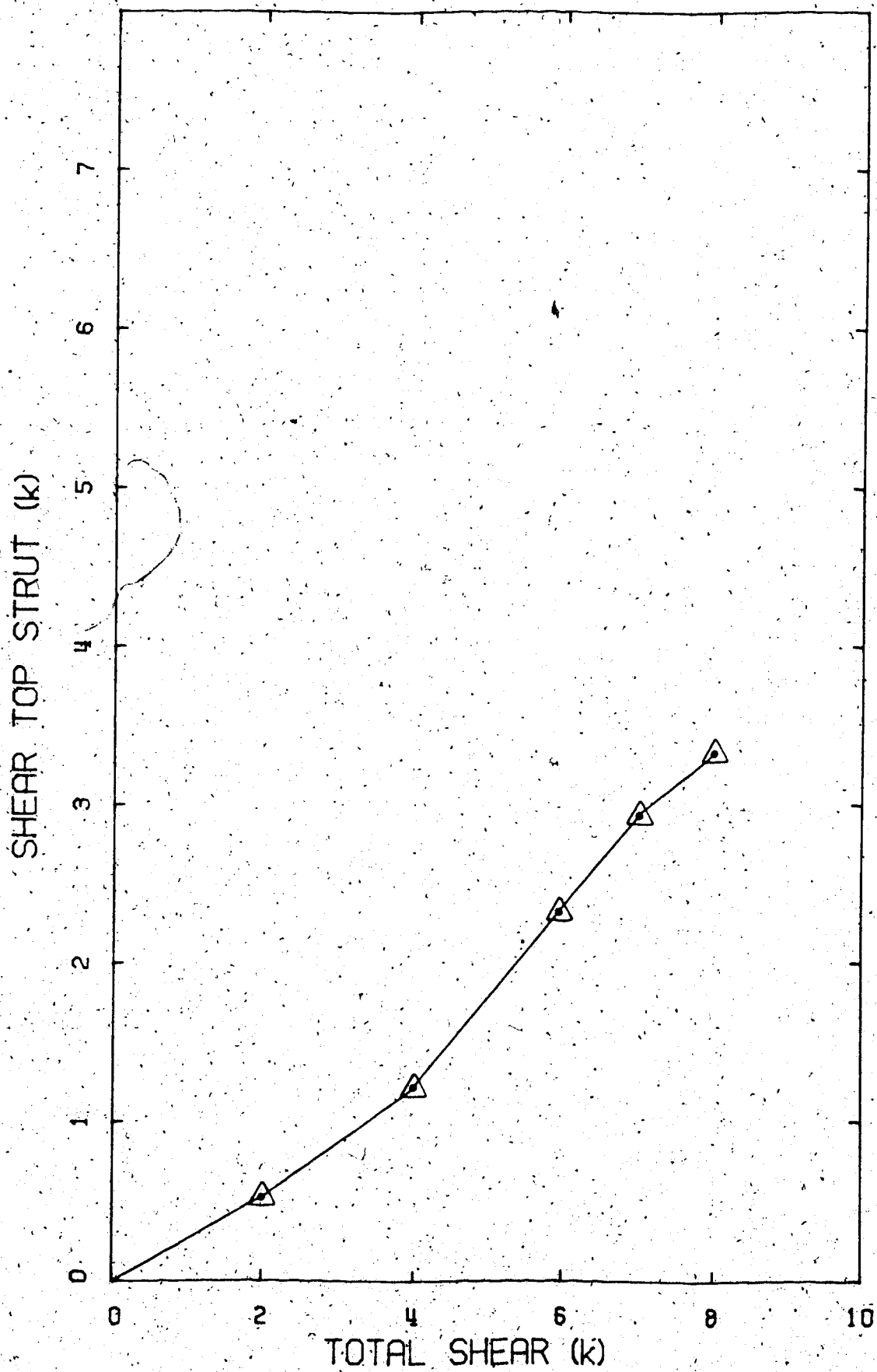
Figure 3.2.4.15 Shear Force in the Top Strut - BEAM D3.

Plan view

56 x 8 in. Opening
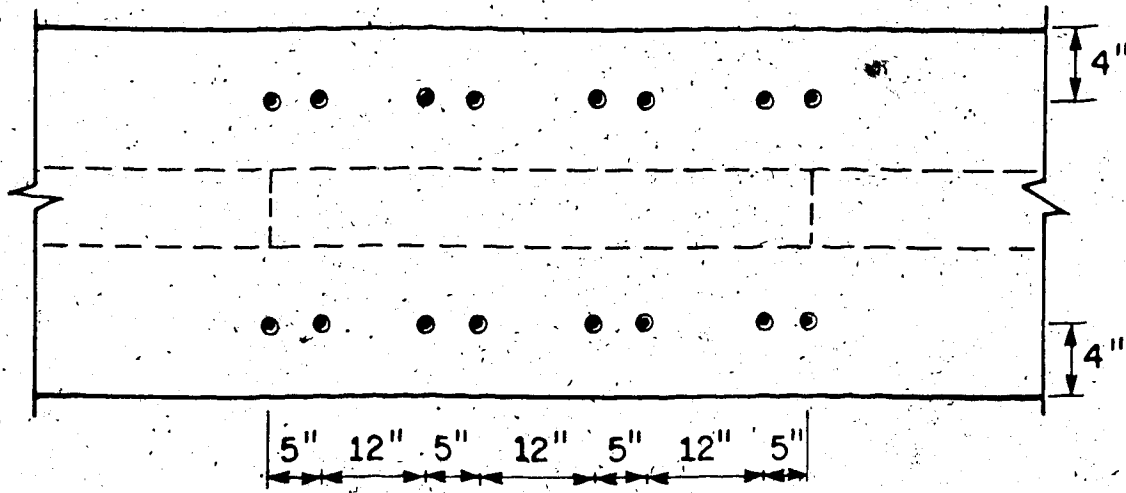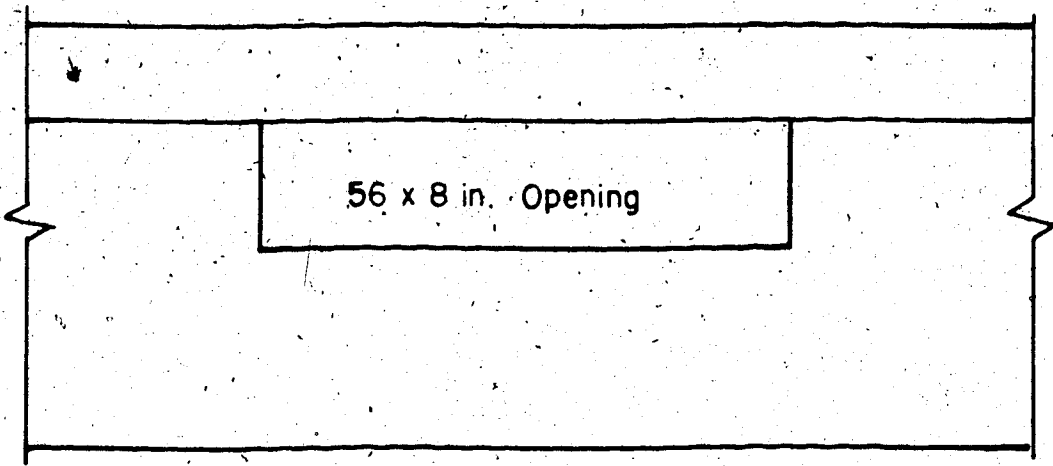
Beam elevation

Figure 3.3.1 Demec Points on Top Strut – BEAM B1

4. EVALUATION OF THE EFFECTS OF SELECTED PARAMETERS

4.1 Introduction

In this chapter, an evaluation is made of the effects of selected parameters on the behavior of the test beams. Parameters varied in the study were: length of opening, vertical position of the opening, and shear reinforcement details. Particular attention is paid to the effect of each parameter on the extent of cracking in the struts, distribution of shear between top and bottom struts, yielding of reinforcement, and failure mode.

4.2 Effect of Length of Opening.

Length of openings considered in this test program were 56 in., 40 in. and 24 in. All web openings were centered at 104.4 in. from supports.

Since cracking was detected through a visual inspection on the specimens, difficulties were found in differentiating shrinkage cracks from cracking caused by loading. Therefore the cracking loads reported are not regarded as precise. It is clear, however, that opening length affected cracking of the struts. As can be observed

130

on load-deflection curves presented in Figure 4.2.1, the slope after cracking is smaller for specimens provided with longer openings indicating greater loss of flexural stiffness of the struts.

The effect of the length of the opening on the shear distribution in the struts for Series B, Series C and Series D are shown in Fig. 4.2.2, Fig. 4.2.3 and Fig. 4.2.4, respectively. Figure 4.2.2 indicates that after cracking, the top strut of BEAM B1, which had the longest opening, carried the total increase in shear caused by loading. This is indicated by the slope of the post-cracking shear distribution curve being approximately parallel to the reference line. As the opening length decreased, near ultimate, the top strut carried an increase in shear greater than the total increase in shear caused by loading as indicated by greater slope of the post-cracking distribution curves. After cracking of the bottom strut, its stiffness decreased and consequently the bottom strut had a tendency to carry a smaller portion of the increase in shear caused by loading. As the flexural stiffness of the bottom strut decreased with increase in length of opening a smaller portion of the shear in that strut was transferred to the top strut. When the top strut was near its flexural-shear capacity there was a transfer of shear from the top to the bottom strut. Since

the bottom strut was not able to carry any additional shear due to its reduced shear capacity a mechanism was developed in the struts. The effect of opening length on the change in shear distribution after cracking in specimens of Series C was minimal. This result is discussed in the next section. Figure 4.2.4 indicates that the top strut of BEAM D1 and BEAM D2 carried approximately the same increase in shear caused by loading. The top strut of BEAM D3, which had the shortest opening length, carried an increase in shear less than the increase in shear caused by loading. Therefore some of that increase in shear was carried by the bottom strut. This is indicated by a smaller slope of the post-cracking shear distribution curve corresponding to BEAM D3.

The Vierendeel action in each strut results in additional moment at the edges of the opening, equal to the product of the portion of shear carried by the strut times the opening half-length. It is clear that the moment in the strut increases with opening length.

Opening length also affected the failure mode of the specimens in Series B. BEAM B1, with the longest opening of Series B, failed by formation of a full hinging mechanism involving two hinges in the bottom strut and two hinges top strut. BEAM B2 and BEAM B3, with shorter developed a partial hinging mechanism with

two hinges in the bottom strut and one hinge close to the upper tension corner of the opening. Both specimens failed in shear at the shear span between the support and first loading position. A partial hinging mechanism developed in the struts because the flexural-shear capacities of the struts were not reached before shear failure at the shear span. None of the specimens of Series C and Series D failed by developing a full hinging mechanism. For the specimens of these two series containing the longest opening, the main longitudinal reinforcement beneath the opening yielded at 80% of the failure load.

Opening length did not affect the failure mode of specimens in Series C and Series D. All specimens in Series C failed in shear at the shear span between the support and first loading position. All specimens in Series D failed in flexure at the midspan.

4.3 Effect of Vertical Position of Opening

Test results for specimens of Series B and Series C indicate the effect of the vertical position of the opening on the behavior and failure of the specimens. As discussed in Chapter 2 the specimens of Series B had the openings positioned immediately below the flange, while in Series C they were shifted by 4 in. towards the bottom of the

specimen.   Web reinforcement consisting of W2.9 wire double-legged stirrups was provided in the top strut of specimens in Series C.

Cracking in the struts was affected by the vertical position of the opening. In specimens of Series B, cracks formed at the bottom and top struts at higher loads than Series C. This reflects the effect of reduction in the flexural stiffness of the bottom strut of the specimens in Series C.

The effect of the vertical position of the opening on the shear distribution of the struts for the three opening lengths considered is shown in Fig. 4.3.1, Fig. 4.3.2 and Fig. 4.3.3. It can be observed that the top strut of the specimens in Series C carried a larger portion of the total shear than the specimens in Series B. This would be expected since cracking in the bottom strut of specimens in Series C was more severe and occurred at loads between 50 to 75% of cracking loads of specimens in Series B, leading to a higher transfer of shear from the bottom strut to the top strut. This fact reflects the greater ratio of flexural stiffness of the top strut to the bottom strut for specimens in Series C than in Series B.

With the exception of BEAM B1, which developed a full hinging mechanism, all other specimens in Series B and C developed a partial hinging mechanism.   The mild

longitudinal reinforcement in the bottom strut of specimens
in Series C yielded at lower loads than in Series B.

4.4 Effect of Shear Reinforcement Details at Opening.

To evaluate the effect of shear reinforcement details
on the behavior of the specimens tested a comparison of
test results for specimens in Series B and Series D is
made.

The specimens in these two series were provided with
different types and amounts of shear reinforcement. As
reported in Chapter 2, specimens in Series B were provided
with minimum web shear reinforcement as specified by the
ACI Building Code (318-77)[1]. The reinforcement consisted
of vertical double-legged stirrups bent from W2.9 wires and
spaced such that a stirrup was placed at each side adjacent
to the opening. The specimens in Series D contained the
same minimum web shear reinforcement as BEAM A2 plus
additional 0.44 in. diameter inclined bars placed at each
tension corner of the opening.

The type and amount of shear reinforcement
significantly affected the behavior and failure mode of the
specimens. The web shear reinforcement provided in the
specimens in Series B was not effective in limiting the
propagation of cracks formed at the lower and upper tension

corners of the opening. As load increased to 80% of failure load, these cracks widened considerably. The crack formed at the upper tension corner of the opening, extended and penetrated into the flange causing web-flange separation. The failure of BEAM B1 occurred through the formation of a hinging mechanism in both struts, while a partial hinging mechanism was developed in BEAM B2 and BEAM B3.

The specimens in series D developed their calculated flexural capacity at midspan. The additional 0.44 in. diameter inclined bars prevented significant widening of cracks that formed at the upper and lower tension corners of the opening. These cracks were well contained and web-flange separation did not occur. The vertical stirrups placed at each side and adjacent to the opening were stressed to a significantly higher level in the specimens in Series B than those in Series D.

Figures 4.4.1, 4.4.2 and 4.4.3 show the top strut shear for the three opening lengths considered. As can be observed, the top strut of BEAM B1 and BEAM B3 carried a larger portion of the total shear, at ultimate, than BEAM D1 and BEAM D3 respectively. BEAM B2 and BEAM D2 had similar shear distribution. It is clear that the specimens in Series D were able to reach their flexural capacity at midspan before the formation of a hinging mechanism in the

struts. This was due to the shear reinforcement provided at the opening that restricted cracking within the struts and avoided web-flange separation at the upper tension corner of the opening.

4.5 Summary

Based on the evaluation of test results, it can be concluded that the selected parameters affected various aspects of the behavior of the specimens, in different degrees.

The opening length had some effect on the extent of cracking in the struts which is related to the loss of flexural rigidity of the struts. It also affected the shear distribution between the top and bottom struts, and the failure mode of the specimens in Series B. For the other series the effect was minimal.

Cracking in the struts and shear distribution between the top and bottom struts were significantly affected by the vertical position of the opening.

The shear reinforcement details at the opening significantly affected the propagation of cracks at the corners of the opening, the shear distribution between the top and bottom struts, and the failure mode.
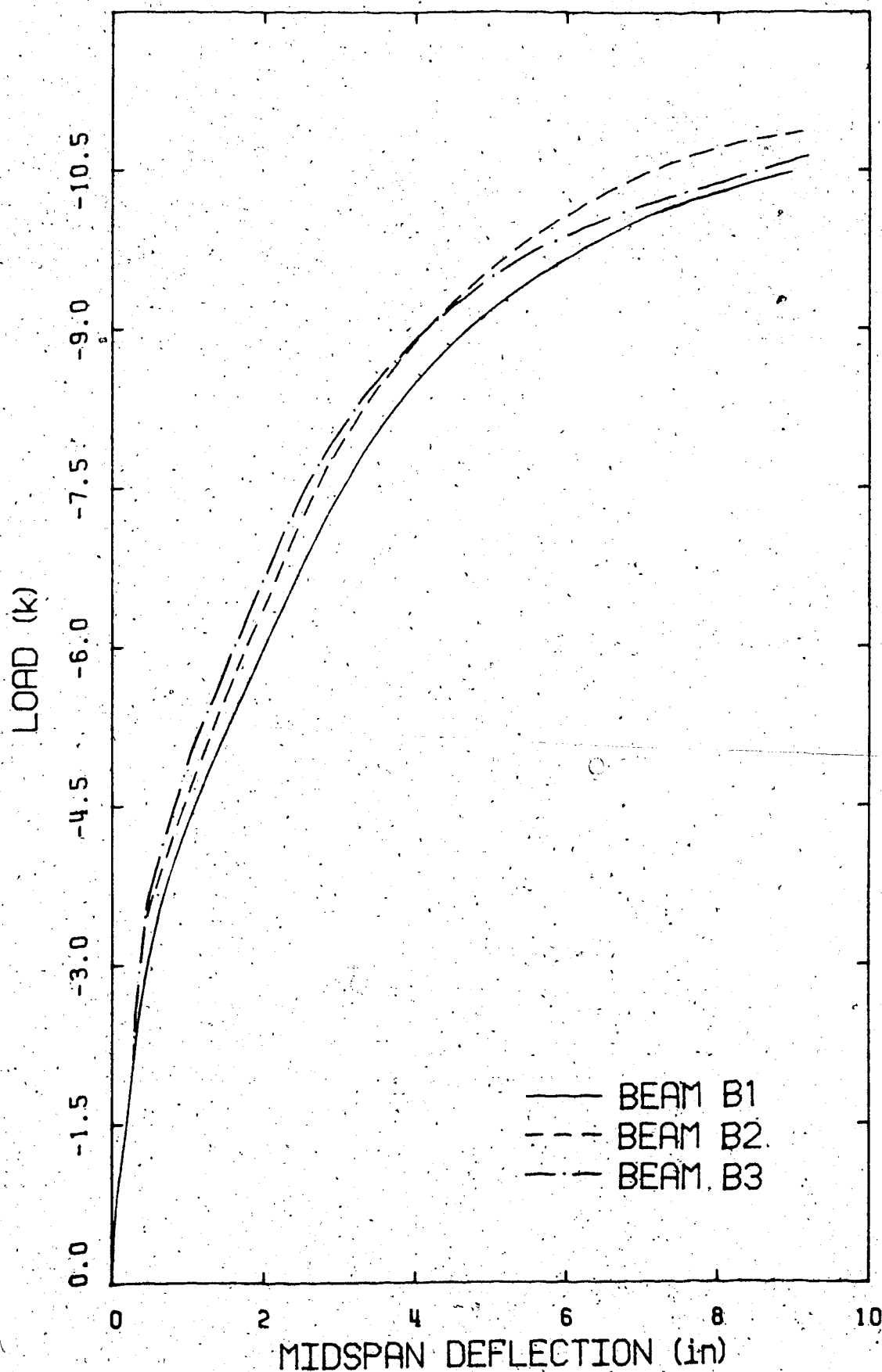
Figure 4.2.1 Load-Deflection Curve - BEAM B1 - BEAM B2 and

BEAM B3
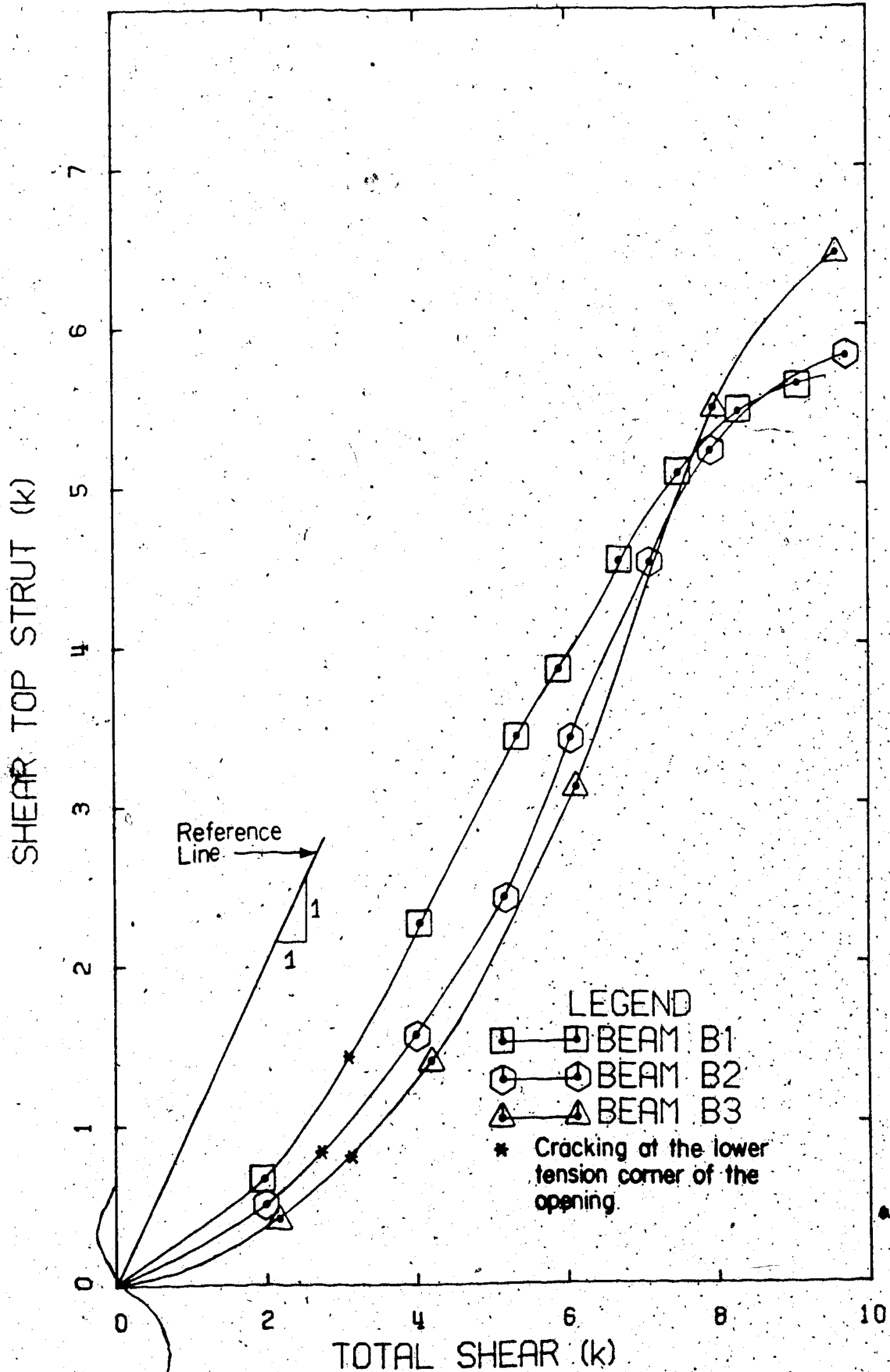
Figure 4.2.2   Effect of Opening Length on Shear in the Top Strut.
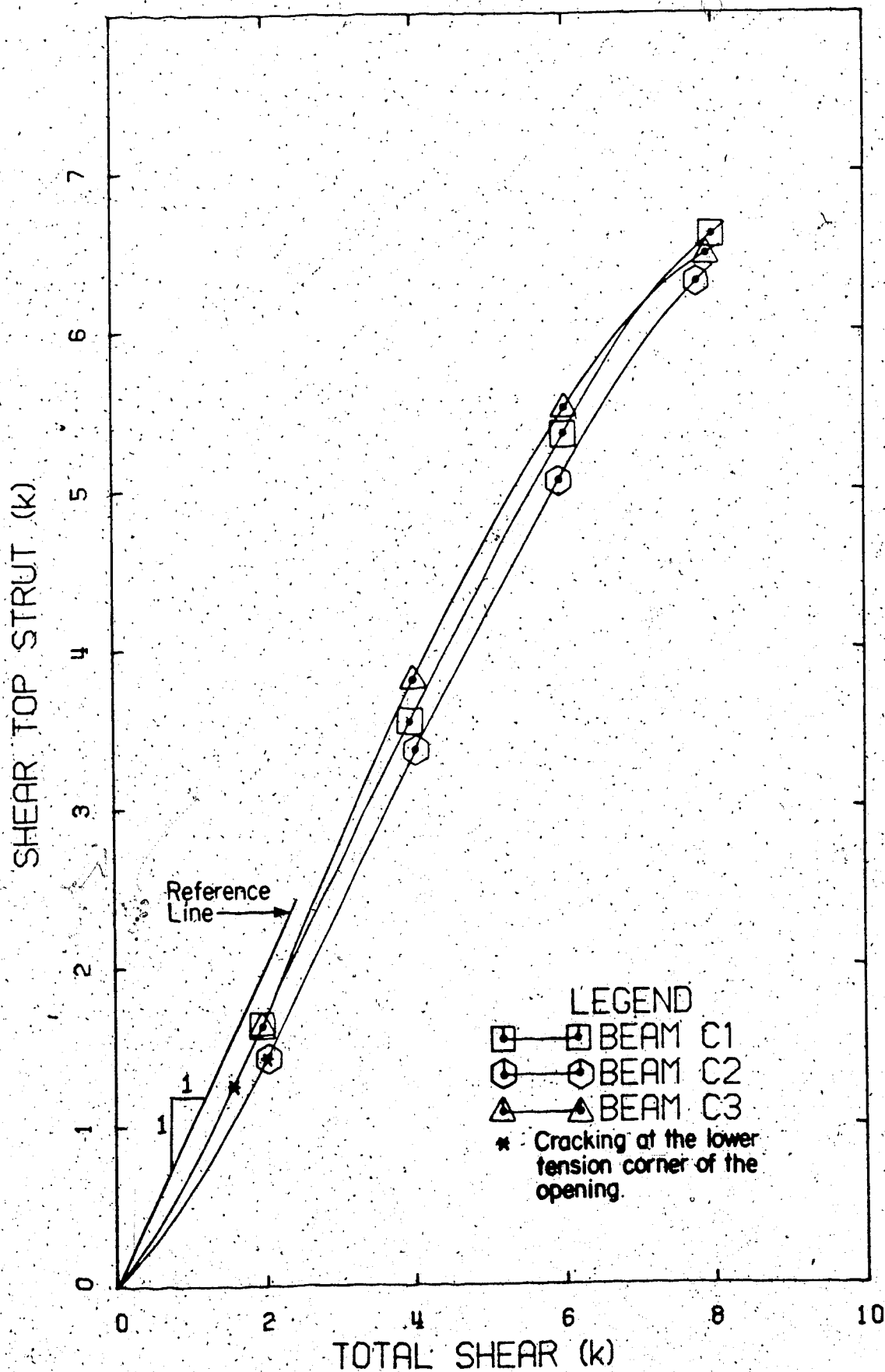
Figure 4.2.3   Effect of Opening Length on Shear in the

Top Strut.

Figure 4.2.4   Effect of Opening Length on Shear in the
Top Strut.

Figure 4.3.1   Effect of Opening Vertical Position on

Shear in the Top Strut.
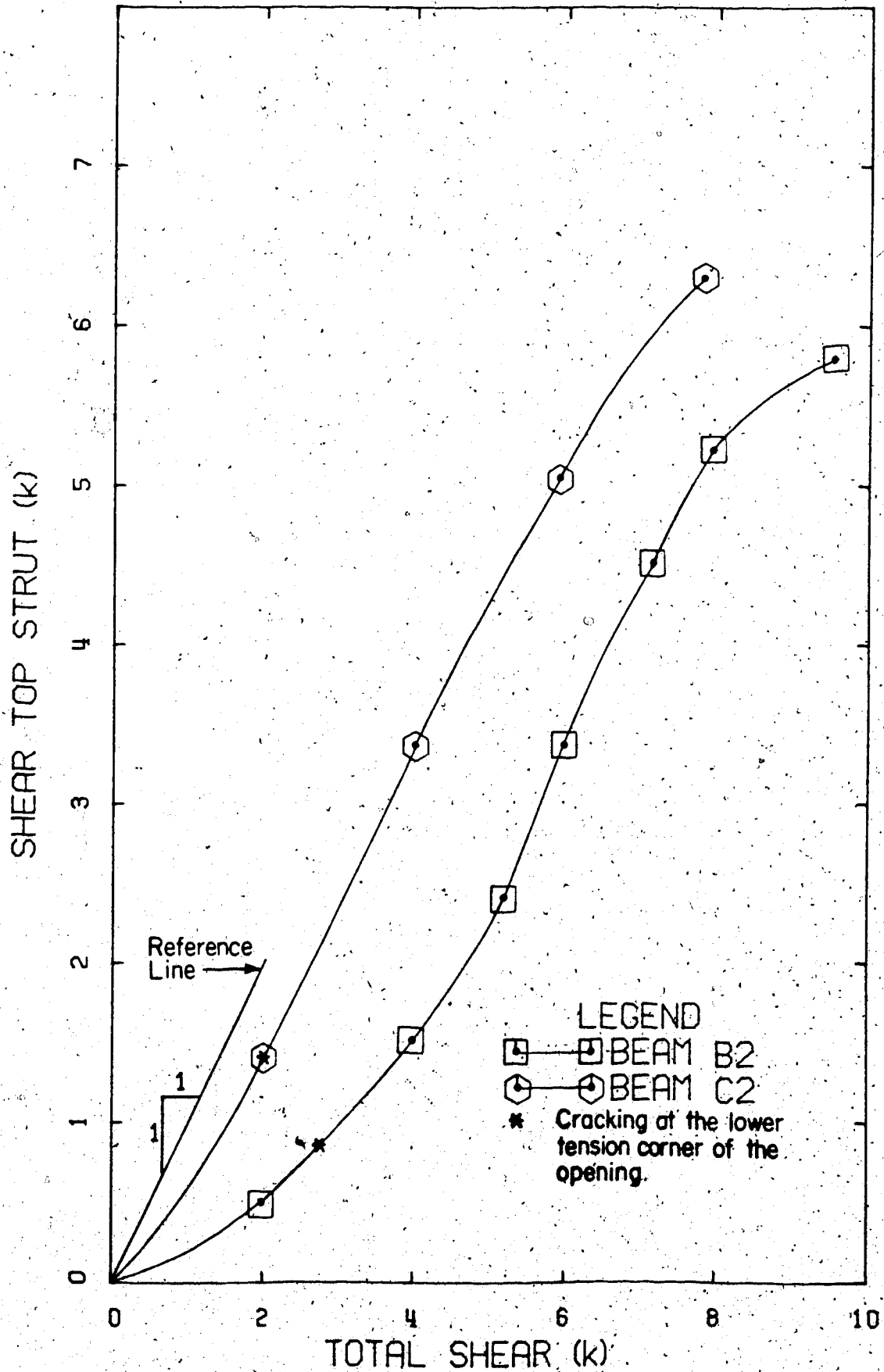
Figure 4.3.2   Effect of Opening Vertical Position on

Shear in the Top Strut.
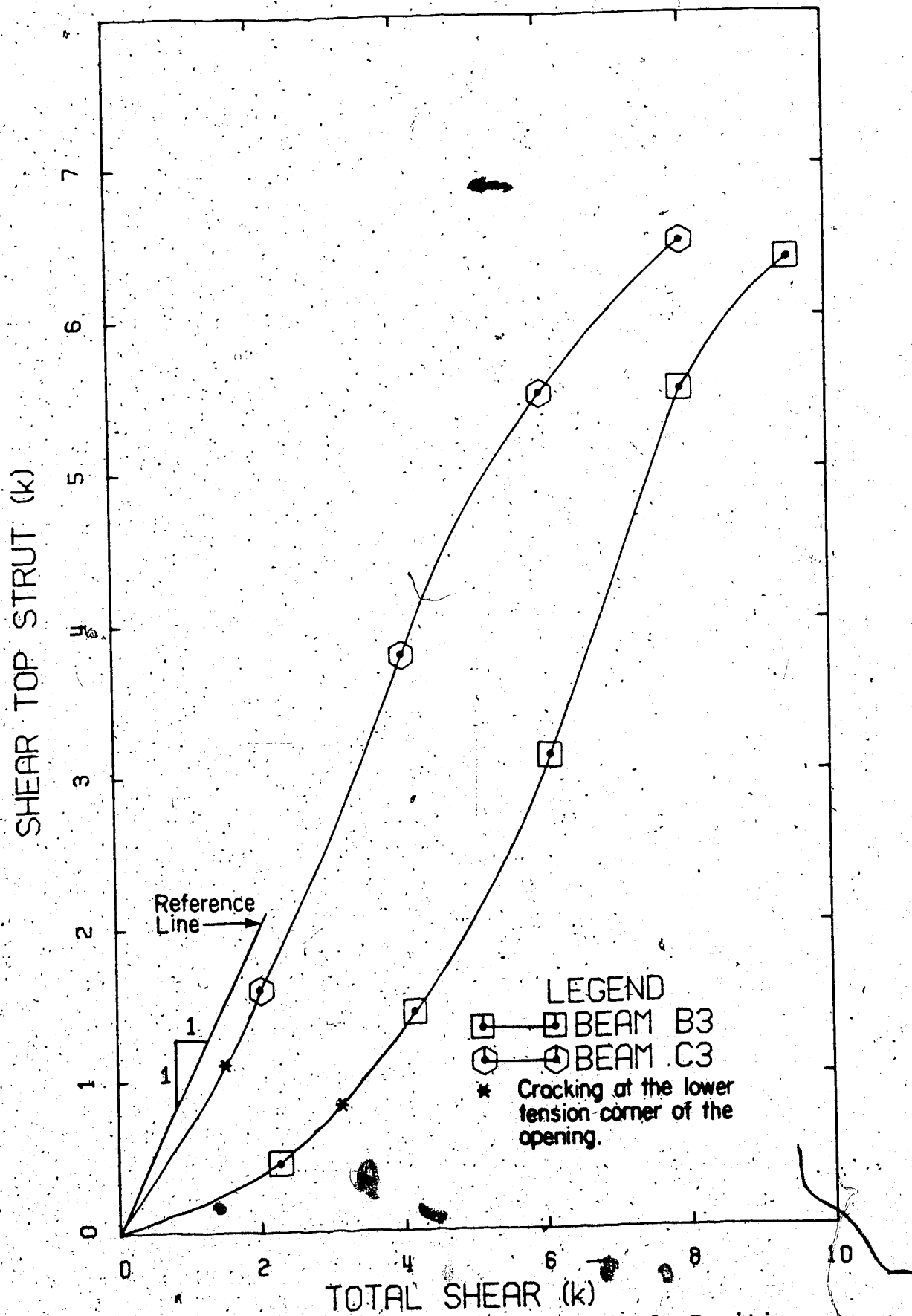
Figure 4.3.3   Effect of Opening Vertical Position on Shear in the Top Strut.
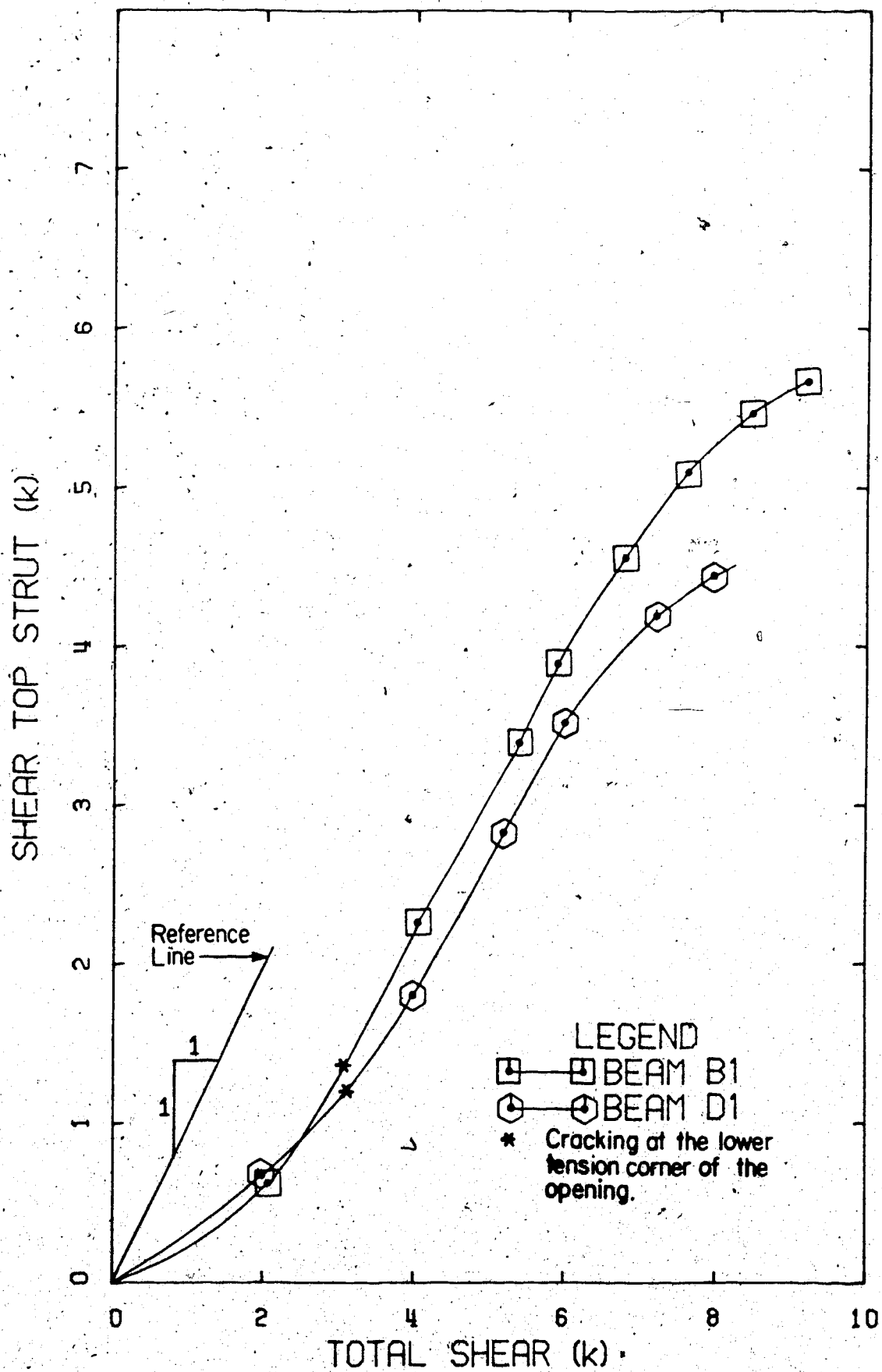
Figure 4.4.1   Effect of Shear Reinforcement on Shear in
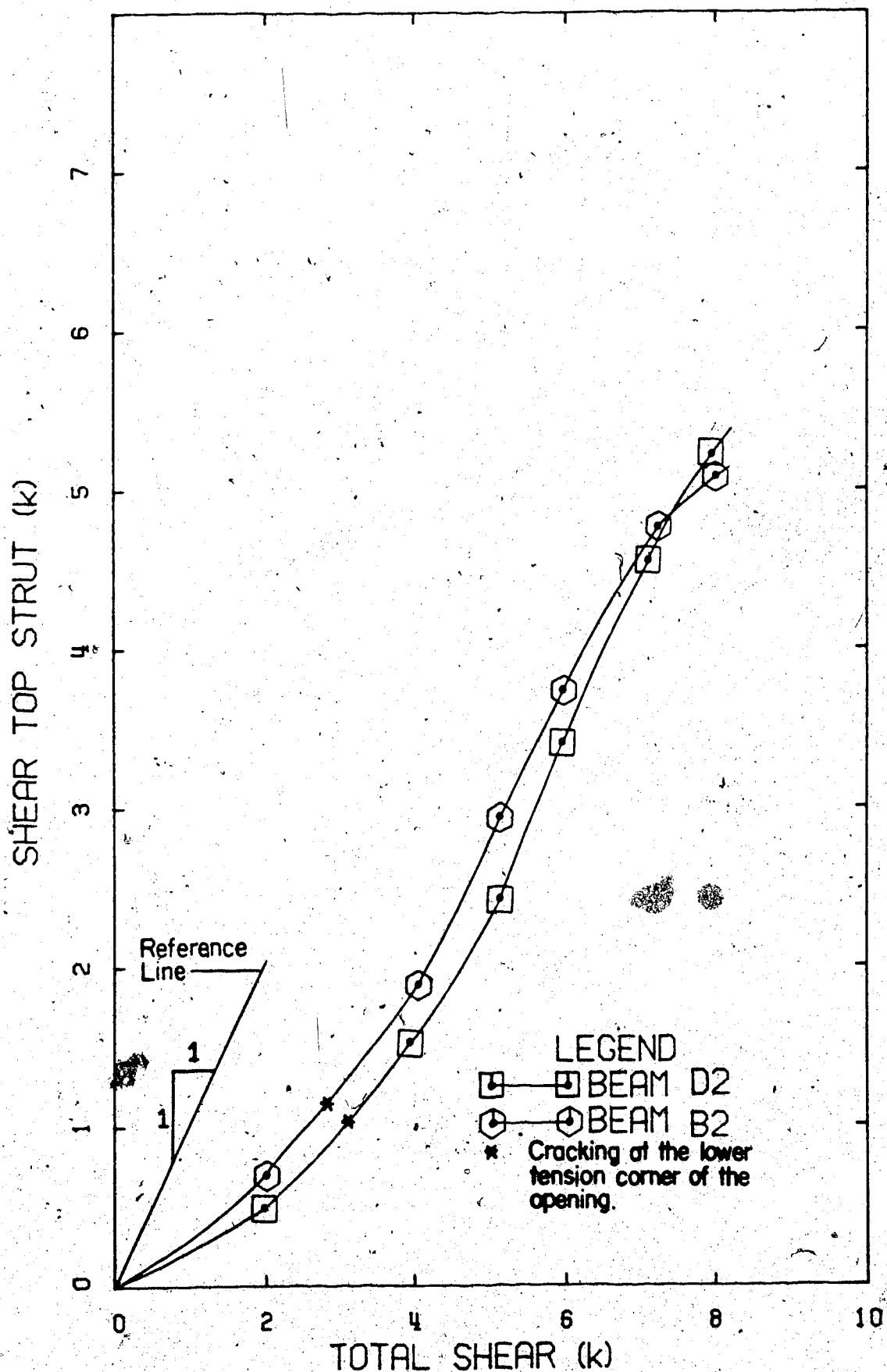
the Top Strut.

Figure 4.4.2   Effect of Shear Reinforcement on Shear in
the Top Strut.
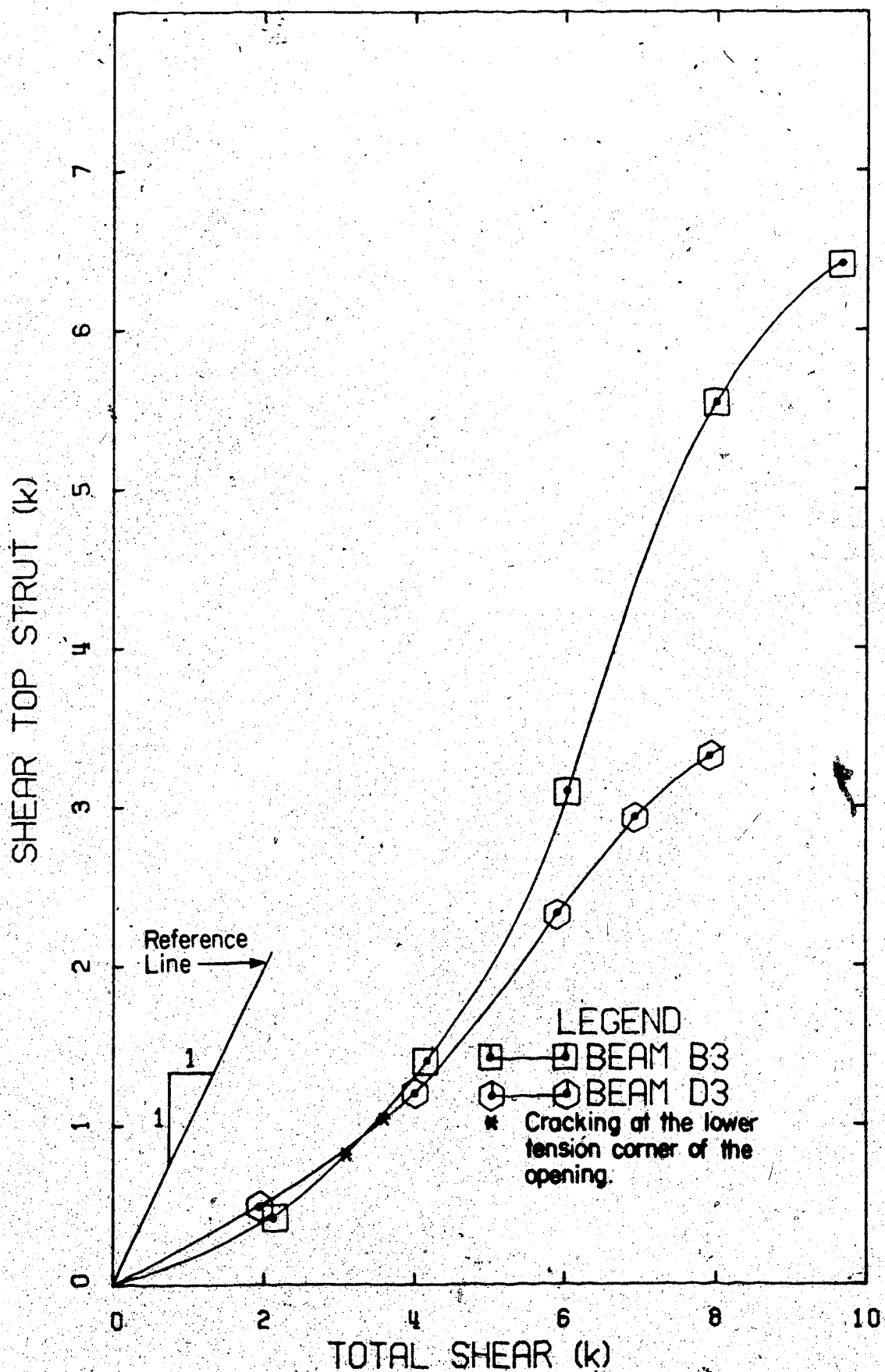
Figure 4.4.3   Effect of Shear Reinforcement on Shear in
the Top Strut.

5. ANALYTICAL MODEL

5.1 Introduction

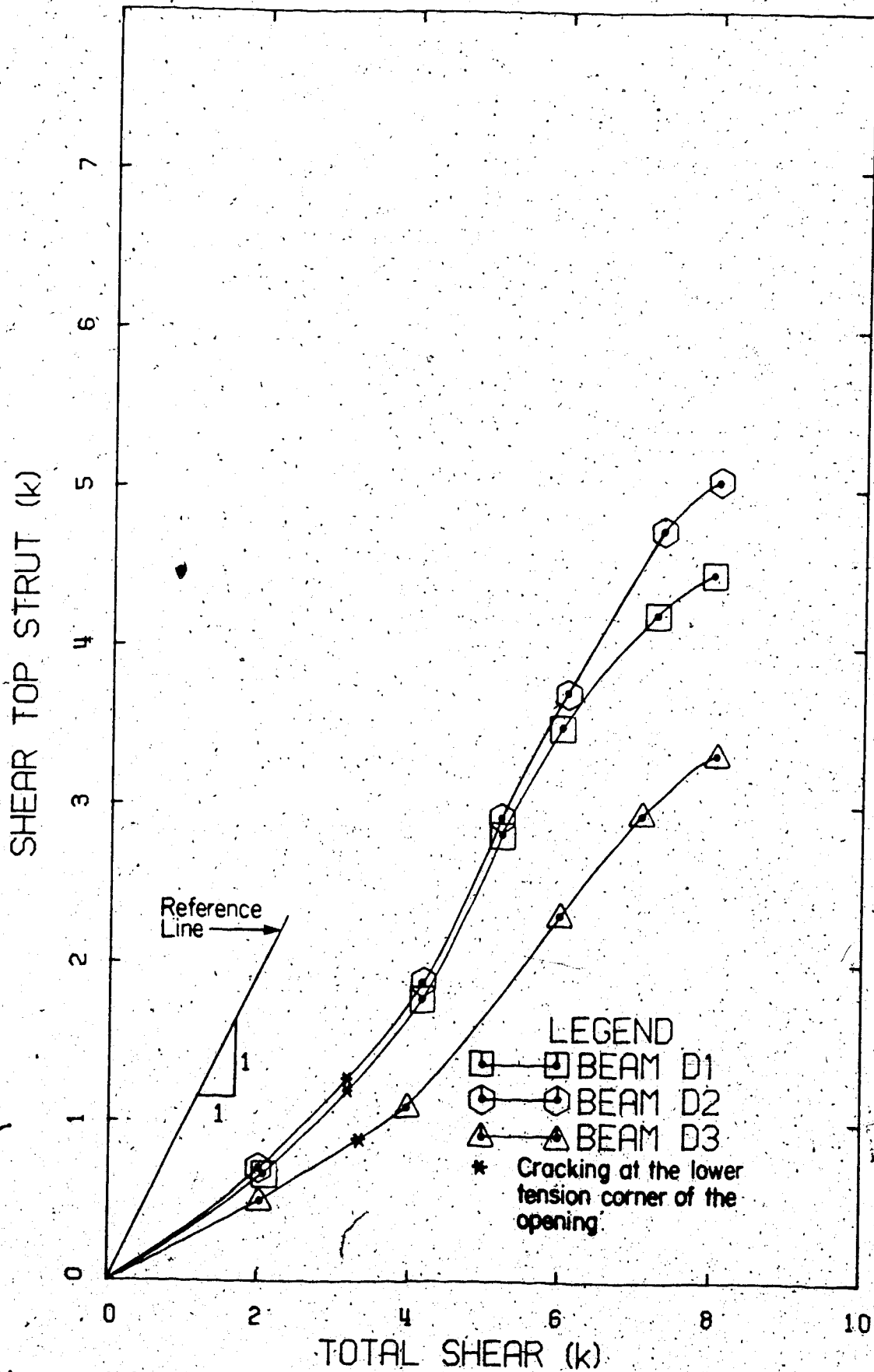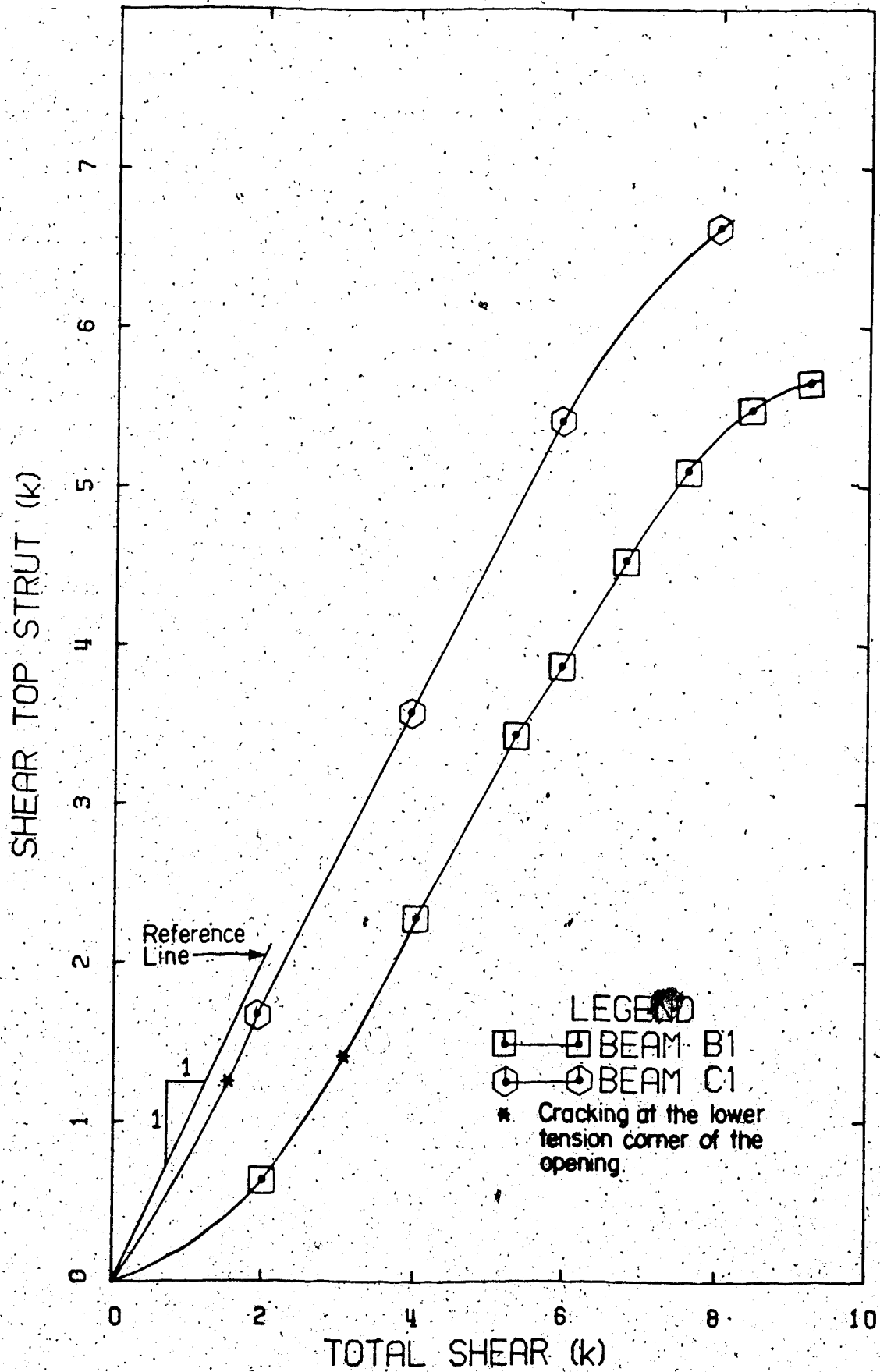The analytical model described in this chapter provides a method for determining the load-deflection response of prestressed concrete beams with large rectangular web openings up to first yielding of the reinforcement. The analysis is based on a truss model that includes the effects of progressive cracking. Post-cracking response is based on application of the effective moment of inertia concept.

A comparison between analytical results and experimental results in the service load range is presented, and limitations of the model are discussed.

5.2 Assumptions and Basis

Reinforced concrete and prestressed concrete structures at service load levels are expected to exhibit essentially linear elastic behavior in terms of stress-strain response of steel and compressive stress-strain response of concrete. Load-deflection behavior becomes nonlinear however if cracking occurs in the concrete. The ACI

Building Code (318-77)[1] recognizes this nonlinearity through the use of Branson's effective moment of inertia procedure[5] for calculating beam deflections. Prestressed concrete beams with large openings in the web require special attention because of the significant discontinuity in beam stiffness that occurs at the opening, where the behavior more closely resembles that of a Vierendeel truss than a simple beam. Consequently, in this particular case, simple beam theory is not strictly applicable.

Significant advances have been made over the past fifteen years in the application of finite element methods of analysis of concrete structures as outlined in a recent state-of-the-art report[26]. The finite element approach permits detailed stress analysis of reinforced and prestressed concrete structures including effects of cracking and other nonlinearities. However, these refined analytical techniques are quite complex and may not be warranted for many applications.

An alternative to the use of beam theory or finite element methods is available through the use of truss models. Some of the earliest attempts to model reinforced concrete behavior, particularly behavior in shear, were based on truss models. This approach has seen new developments in recent years including work related to shear and torsion,[7] and as an aid to proper detailing[22].

The truss model presented herein is attractive in that
it is conceptually simpler than the more refined finite
element models and at the same time provides more
versatility than simple beam theory.

Figure 5.2.1 shows a simply supported prestressed
concrete beam with web opening and the respective truss
model. Locations of top and bottom chord members are
selected to suit the geometry of the beam, particularly the
details of the opening. For the section below opening, the
top chord truss member is located at the top reinforcing
steel level and the bottom chord member is located at the
prestressing strand centroid. For the section above the
opening, the top chord member is located at the centroid of
concrete compression zone and the bottom chord member is
located at the reinforcing steel centroid. For the solid
cross-section, the locations of the top and bottom chord
members were the same as those corresponding to the top
chord member for the section above the opening and to the
bottom chord member for the section below the opening,
respectively. Locations of web truss members are defined
by positions of beam stirrups. To simulate the effect of
prestressing, horizontal forces P_t and P_b are applied to
the top and bottom chord members respectively, at each end
of the truss. Forces P_t and P_b are determined to provide
at the end of the truss a total axial force and moment

statically equivalent to the actual prestressing force and moment in the beam. The force P_t applied at the top chord member of the truss is:

$$P_t = -P_e \frac{e}{h} + P_e \frac{h_2}{h} \qquad (5.1)$$

and the force applied at the bottom chord member of the truss is:

$$P_b = P_e \frac{e}{h} + P_e \frac{h_1}{h} \qquad (5.2)$$

where,

P_e -effective prestress force

e -eccentricity of strand

h -depth of truss model

h_1 -distance from centroid of bottom chord to centroid of beam section

h_2 -distance from centroid of top chord to centroid of beam section

Truss members are assumed to have a modulus of elasticity equal to that for concrete. It is then necessary to determine areas of truss members to produce a flexural stiffness equivalent to that of the beam. Since it is assumed that deformations due to shear can be

neglected in comparison with flexural deformations, the areas of web members are assumed to be unchanged by cracking.

5.3 Application of the Model

Initially it is assumed that the beam is uncracked. Once the properties of truss members are determined, a linear elastic analysis is made for loading due to prestress, dead load and live load.

By comparing the tensile stress at sections along the beam with the tensile strength of concrete, it is possible to scale the applied load to the value at which cracking first occurs. The moment and axial force producing the tensile stress at a section are obtained from truss member forces.

The analysis can then be repeated at selected load levels above the load to cause first cracking, after truss chord areas are adjusted to produce the same moment of inertia as the beam section. The load-deflection response as affected by progressive cracking is traced.

5.3.1 Uncracked Section

Figure 5.3.1.1 shows beam cross sections and equivalent top and bottom truss chord members. Areas of top and bottom chord members are calculated to provide the

same moment of inertia as the beam within each truss panel. Top and bottom chord cross-sectional areas are assumed to be equal and are determined by the following expression:

$$I_g = A_t \ (h/2)^2 + A_b(h/2)^2 \qquad\qquad (5.3)$$

$$A_t = A_b \qquad\qquad (5.4)$$

Where,

I_g = gross moment of inertia of beam section

h = depth of truss model

A_t = area of top chord truss member

A_b = area of bottom chord truss member

Areas of web members are determined from the tributary area of concrete based on truss panel spacing. Figure 5.3.1.2 shows beam stirrups position and corresponding web members. Areas of vertical web members are determined by the following expression:

$$A_v = (\frac{s_1 + s_2}{2}) \ w \qquad\qquad (5.5)$$

where,

A_v = area of vertical web members

s_1, s_2 = lengths of adjacent truss panels

w = width of beam web

Areas of diagonal web members are determined by the following expression:

$$A_d = (\frac{s_1 + s_2}{2}) \, w \, \sin\theta \qquad\qquad (5.6)$$

where,

θ = angle between diagonal and bottom chord member.

From truss member forces shown in Fig. 5.3.1.3, moment and axial forces at a section at mid-panel are obtained as follows:

$$P = T_t + W_h - C_t \qquad\qquad (5.7)$$

$$M = C_t \frac{h}{2} + T_t \frac{h}{2} + W_h(0) \qquad\qquad (5.8)$$

where,

P - net axial force at a mid-panel section

M - net moment at a mid-panel section

T_t - tensile force in the truss bottom chord

C_t - compressive force in the truss top chord

W_h - horizontal component of force in the diagonal truss, member

h - truss height

In this particular investigation, the horizontal component of force in the diagonal truss member was considered in the calculation of the net axial force, and

the error induced was less than 1%. The tensile stress
acting at the corresponding beam section and compared to
the tensile strength of concrete is determined by the
following expression:

$$\sigma_t = \frac{P}{A} \pm \frac{M}{S} \qquad\qquad (5.9)$$

where,

A - cross-sectional area

S - section modulus

If the calculated tensile stress exceeds the tensile
strength of concrete, truss chord areas are re-calculated
based on I_e as discussed as follows in the next section of
this chapter.

5.3.2 Cracked Section

Behavior after cracking can be illustrated by the
strain diagram shown in Fig. 5.3.2.1 and the moment-
curvature relationship shown in Fig. 5.3.2.2. The
curvature after cracking should be considered as the
average curvature in a constant moment cracked zone.
Application of the prestressing force produces a curvature
ϕ_p corresponding to the moment $M_p = - P_e$ e. Applied moment
of opposite sign to the prestressing moment decreases the

net moment till zero moment and zero curvature are present at the cross-section. Further application of moment leads to zero stress at the bottom fiber when the net moment is $M_O = P_e r^2/C_2$ with curvature ϕ_O. Application of additional moment $M_{cr} = f_r S_2$ produces cracking at the bottom fiber. Further application of load leads to progressive decrease in stiffness as indicated. Assuming as a first approximation that cracks close completely on unloading, unloading of the beam from point D would occur along DBOA. In Branson's form of the I_e equation,

$$I_e = (\frac{M_{cr}}{M_n})^3 I_g + (1 - (\frac{M_{cr}}{M_n})^3) I_{cr} \qquad (5.10)$$

M_{cr} was taken as $M_{cr} = f_r S_2$. This is identical to the expression used for non-prestressed beams. The corresponding value of the difference between moment due to the applied load and the sum of the decompression and prestress moments is given by $M_n = M_a - P_e(\frac{r^2}{C_2} + e)$ where M_a is the moment due to applied load.

This procedure for calculating I_e differs from the procedure given by Branson and Trost[5], who replace M_{cr} by the term $M'_{cr} = M_{cr} + P_e r^2/C_2$ with a corresponding modification to M_n. In either case, however, the effective moment of inertia expression provides a gradual transition from I_g to I_{cr} as progressive cracking takes place.

Using an incremental loading procedure, the value of I_e at each panel is determined. At each stage the moment and axial force at a beam section are obtained from truss member forces. Truss chord areas are assumed equal and then adjusted to produce the same moment of inertia, I_e, according to the following expression:

$$I_e = A_t(h/2)^2 + A_b(h/2)^2 \qquad (5.11)$$

where,

I_e = effective moment of inertia of beam section

h = depth of truss model

A_t = area of top chord truss member

A_b = area of bottom chord truss member.

Once the truss chord areas are adjusted, the analysis is repeated at the same load level. The analysis is stopped when the force in the truss bottom chord equals the force corresponding to yielding of mild longitudinal reinforcement, or fracture of the prestressing strand.

5.4 Comparison of Analytical and Experimental Results

To assess the accuracy of the analytical model, numerical results were compared with experimental results for six of the beams tested as part of this investigation, as well as three of the beams tested by Barney[4].

In each case, load-deflection readings were taken after prestress and beam self-weight were applied. For purposes of comparison therefore, prestress and self-weight effects were subtracted from numerical results before plotting the load-deflection curve. While the beams were all tested to failure, the analysis is terminated when the force in the truss bottom chord equals the force corresponding to yielding of mild longitudinal reinforcement. Figures 5.4.1 to 5.4.3 show details of three of the specimens analyzed.

The load-deflection curves at midspan and at the left corner of the opening for BEAM B1 are shown in Fig. 5.4.4 and Fig. 5.4.5, respectively. First cracking is predicted by the model at the lower tension corner of the opening, at 2.0 kips. The change of slope in the load-deflection curve recorded during testing reflects the formation of a crack at the lower tension corner of the opening at 3.2 kips. As can be observed in Fig. 5.4.4 and Fig. 5.4.5, there is good agreement between analytical and experimental results up to 8.2 kips, when yielding of mild longitudinal reinforcement beneath the opening is predicted by the model.

Figure 5.4.6 and Fig. 5.4.7 show the load-deflection curves at midspan and at left corner of the opening, for BEAM B3. First cracking is predicted by the model at the lower tension corner of the opening, at 2.4 kips. The

linear portion of the load-deflection curve plotted during testing shows evidence of first cracking at 3.2 kips. The agreement between analytical and experimental results for BEAM B3 is slightly better than for BEAM B1. Yielding of mild longitudinal reinforcement beneath the opening is predicted by the model at 7.6 kips.

The load-deflection curves at mispan and at the left corner of the opening, for BEAM C1, are presented in Fig. 5.4.8 and Fig. 5.4.9, respectively. The analytical model predicts first cracking at the lower tension corner of the opening at 1.7 kips and cracking at the upper tension corner of the opening at 2.4 kips. However, during testing, first cracks formed simultaneously at the lower and upper tension corner of the opening, at 1.6 kips. As indicated in Fig. 5.4.8 the model overestimates deflections at midspan for loads higher than approximately 2.4 kips, corresponding to cracking predicted by the model at the upper tension corner of the opening. The analysis of BEAM C1 is stopped at 8.7 kips, corresponding to yielding of mild longitudinal reinforcement beneath the opening.

Figures 5.4.10 and 5.4.11 show the load-deflection curves at midspan and at the right corner of the opening, for BEAM C2. First cracking is predicted by the model at the lower tension corner of the opening, at 1.83 kips, and cracking at the upper tension corner of the opening at 2.4.

kips. During testing, first cracking occurred simultaneously at the lower and upper tension corners of the opening, at 2.0 kips. As shown in Fig. 5.4.10, midspan deflections are overestimated by the model for loads higher than 4.0 kips. However, good agreement between analytical and experimental results are obtained for the right corner of the opening. Yielding of mild longitudinal reinforcement below the opening is predicted by the model at 9.0 kips.

The load-deflection curves at midspan and at the left corner of the opening, for BEAM D1 are shown in Fig. 5.4.12 and Fig. 5.4.13, respectively. The analytical model predicts first cracking at the lower tension corner of the opening at 2.5 kips. The slope of the load-deflection curve, recorded during testing, changes at 2.66 kips, reflecting the formation of first cracking. As indicated in Fig. 5.4.12 and Fig. 5.4.13 the load-deflection curves predicted by the model and plotted during testing are almost coincident until approximately 8.15 kips. At 8.25 kips, yielding of mild longitudinal reinforcement at midspan is predicted by the model.

Figures 5.4.14 and 5.4.15 show the load-deflection curves at midspan and at right corner of the opening, for BEAM D2. First cracking is predicted by the model at the lower tension corner of the opening, at 2.65 kips.

Cracking is indicated by a change of slope in the load-deflection curve plotted during testing, at 2.72 kips. As can be observed in Fig. 5.4.14 and Fig. 5.4.15 excellent agreement between analytical and experimental results are obtained until approximately 8.15 kips. For higher loads results become divergent. Yielding of mild longitudinal reinforcement at midspan is predicted by the model, at 8.4 kips.

The load-deflection curve at the right corner of the opening for BEAM B7 is shown in Fig. 5.4.16. First cracking is predicted by the model at the lower tension corner of the opening, at 2.16 kips. During testing first crack formed at the lower tension corner of the opening at 2.7 kips. Figure 5.4.16 indicates that for loads higher than 3.75 kips, the difference between analytical and experimental results increases with load. The analysis of BEAM B7 is stopped at 6.65 kips corresponding to fracture of prestressing strand beneath the opening.

Figure 5.4.17 shows the load-deflection curve at the right corner of the opening, for BEAM B5. The analytical model predicts first cracking at the lower tension corner of the opening at 2.0 kips. During testing first crack occurred at the lower tension corner of the opening at 2.04 kips. As shown in Fig. 5.4.17 good agreement between analytical and experimental results are obtained up to 3.18

kips. As load increases analytical and experimental results diverge. Fracture of prestressing strand beneath the opening is predicted by the model at 5.62 kips.

The load-deflection curve at the right corner of the opening, for BEAM B4, is shown in Fig. 5.4.18. Test results indicate that first cracking occurred at the lower tension corner of the opening at 2.04 kips. The analytical model predicts first cracking at the lower tension corner of the opening at 2.4 kips. Figure 5.4.18 indicates that for loads higher than 3.37 kips the difference between analytical and experimental results increases with load. The analysis of BEAM B4 is stopped at 6.38 kips corresponding to fracture of prestressing strand beneath the opening.

It can be observed, by comparing Fig. 5.4.4 and Fig. 5.4.8 against Fig. 5.4.12 that analytical results are closer to experimental results for BEAM D1 than for BEAM B1 and BEAM C1. This is expected since the analytical model does not model widening of cracks at corners of the opening and in BEAM B1 and BEAM C1 cracks at tension corners of the opening extended and widened considerably with load. However, since BEAM D1 was provided with diagonal reinforcing bars at the opening region, cracks at tension corners of the opening were restricted and excellent agreement between analytical and experimental results is obtained.

The differences among Barney's three beams presented in this chapter were length of the opening and shear reinforcement near openings. BEAM B7 and BEAM B5 contained 10 x 60 in. openings and BEAM B4 contained 10 x 45 in. openings. Shear reinforcement near opening consisted of welded wire fabric was provided in BEAM B5 and BEAM B4. Additional no.3 vertical stirrups near openings were provided in BEAM B7.

As indicated in Fig. 5.4.16 to Fig. 5.4.18, the discrepancy between analytical and experimental results is not affected significantly by the type of shear reinforcement near opening in those three specimens.

5.5 Statistical Analysis of the Results

Table 5.5.1 presents the ratio of test-to-predicted cracking load and measured-to-predicted deflection at the service load level and at the level corresponding to yielding of longitudinal reinforcement or fracture of prestressing strand for all specimens. Ratios of loads corresponding to detected and predicted yielding of longitudinal reinforcement are also listed.

For test-to-predicted cracking load, a standard deviation of 0.15 was found with a corresponding coefficient of variation of 12%. For test-to-predicted deflections at the service load level, a standard deviation

of 0.20 was found with a corresponding coefficient of variation of 18.8%. For test-to-predicted deflections at the level corresponding to yielding of longitudinal reinforcement, a standard deviation of 0.19 and a coefficient of variation of 20% were determined. It should be noted that the model gives the best predictions for beams in Series D where widening of cracks at corners of openings was restricted by the presence of diagonal web reinforcing bars. The correlation obtained between test and predicted deflections appears to be consistent with results reported by ACI Committee 435[2].

For test-to-predicted loads corresponding to yielding of longitudinal reinforcement or fracture of prestressing strand, a standard deviation of 0.06 and a coefficient of variation of 6.2% were determined. This indicates that the model can predict yielding of longitudinal reinforcement or fracture of prestressing strand with acceptable accuracy.

5.6 Model Limitations

The basic assumption made in developing the analytical model is that the areas of the top and bottom chord members are calculated to provide the same moment of inertia as the beam within each truss panel. The areas of web members are determined from the tributary area of concrete based on truss panel spacing and are assumed to be unchanged by cracking.

The effect of cracking on shear deformations is neglected. This assumption is consistent with the usual assumption that shear deformations can be neglected when calculating deflection of slender beams. Consequently widening of diagonal cracks at corners of the opening is not modelled. However with proper detailing, significant widening of cracks would not be expected at service load levels.

The effective moment of inertia concept as applied to the truss model makes the procedure valid only for loads up to yielding of reinforcement. No yielding in steel and only linear stress-strain relationship for concrete are considered. Therefore, as results indicate, the model cannot simulate behavior in the post-yield range. However, the extension of the modeling technique into the post-yield range is possible and could provide useful insight into the behavior of prestressed concrete members, particularly in terms of the localized behavior in highly stressed zones as in the vicinity of openings.

5.7 Summary

Comparison between analytical and experimental results indicates that the proposed truss model provides an efficient method for determining the load-deflection response at service load levels, and up to first yield of

prestressed concrete beams with large web openings. Post-cracking response is based on application of the effective moment of inertia concept. Limitations of the model are discussed.

Table 5.5.1   Statistics for Test-to-Predicted Cracking Load,
Deflection and Load at Yielding Ratios.

Specimen	Cracking Load $\dfrac{P_{test}}{P_{predicted}}$	Service Load $\dfrac{\Delta_{test}}{\Delta_{predicted}}$	Yielding of Long. Reinf. $\dfrac{P_{test}}{P_{predicted}}$	Yielding of Long. Reinf. $\dfrac{\Delta_{test}}{\Delta_{predicted}}$
BEAM B1	1.52	1.08	0.92	0.96
BEAM B2	1.36	1.17	0.95	1.08
BEAM B3	1.19	1.16	1.09	1.38
BEAM C1	1.11	0.74	0.92	0.80
BEAM C2	1.06	0.83	0.92	0.78
BEAM C3	1.04	0.85	0.92	0.75
BEAM D1	1.25	0.99	0.95	1.12
BEAM D2	1.22	1.00	1.00	1.02
BEAM D3	1.20	1.00	1.03	1.05
BEAM B4	1.15	1.40	0.96	-
BEAM B5	1.07	1.26	-	-
BEAM B7	1.21	1.30	0.90	-
Mean Value	1.20	1.06	0.96	0.99
Standard Deviation	0.15	0.20	0.06	0.20
Coefficient of Variation	12%	18.8%	6.2%	20%

Beam elevation.
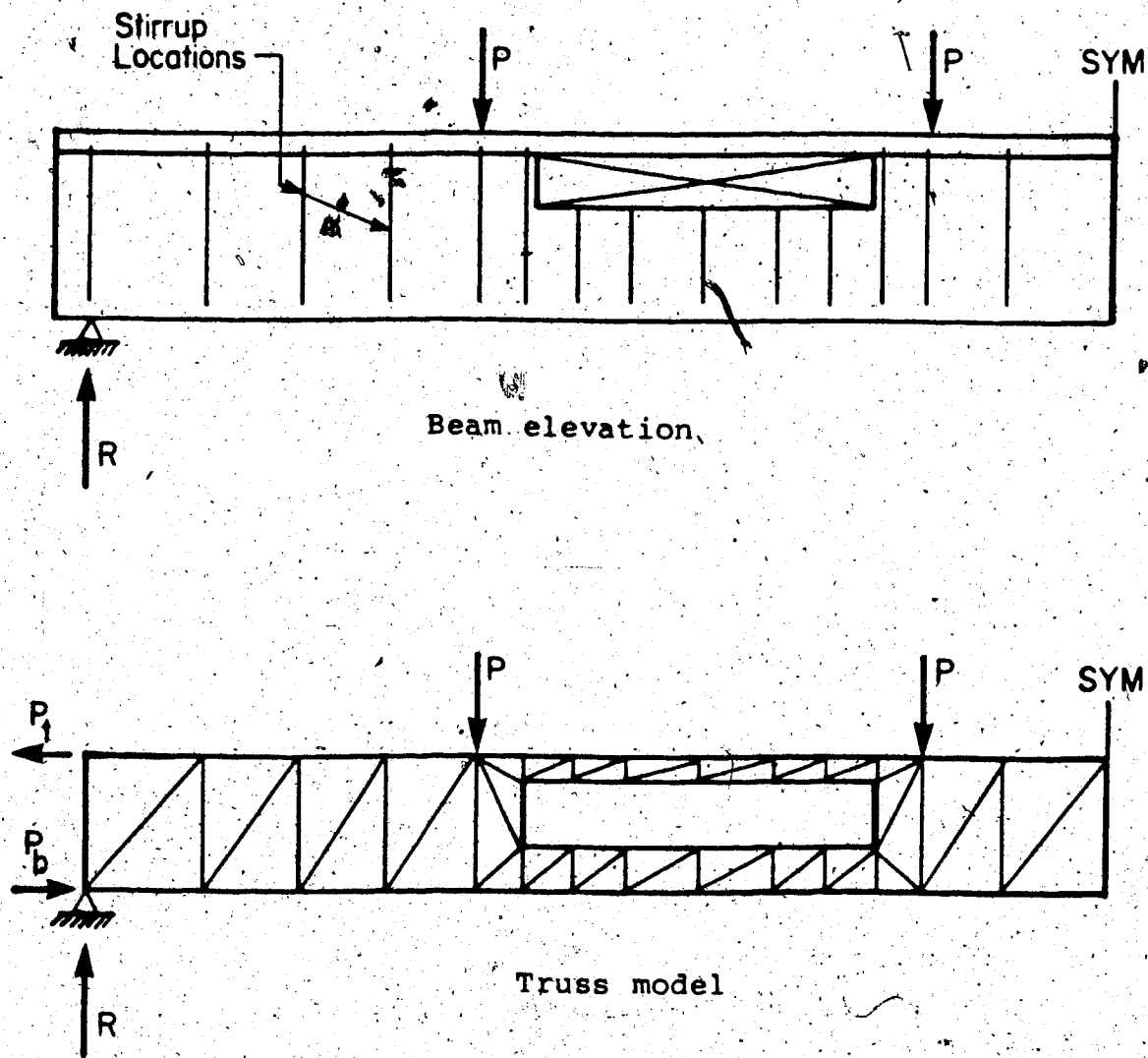
Truss model

Figure 5.2.1   Prestressed Beam with Web Opening and
Respective Truss Model.
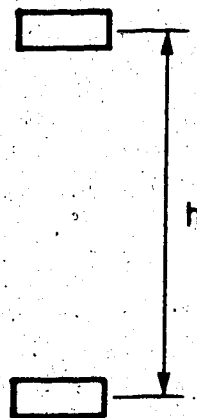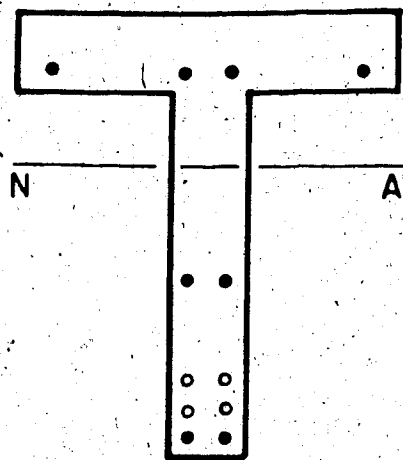
Solid cross-section
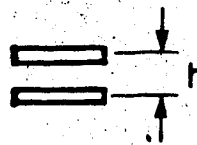
Cross-section above opening
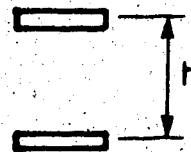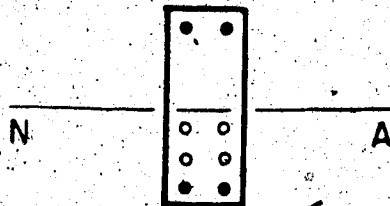
Cross-section below opening

Figure 5.3.1.1 Beam Cross-Sections Equivalent Bottom and
Top Truss Chord Members.

stirrups

S_1 S_2 S_3

Stirrup position

$\dfrac{S_1 + S_2}{2}$

Vertical truss memʟ

$\left(\dfrac{S_1 + S_2}{2}\right) \sin\theta$

θ

$\dfrac{S_1 + S_2}{2}$

Diagonal truss member
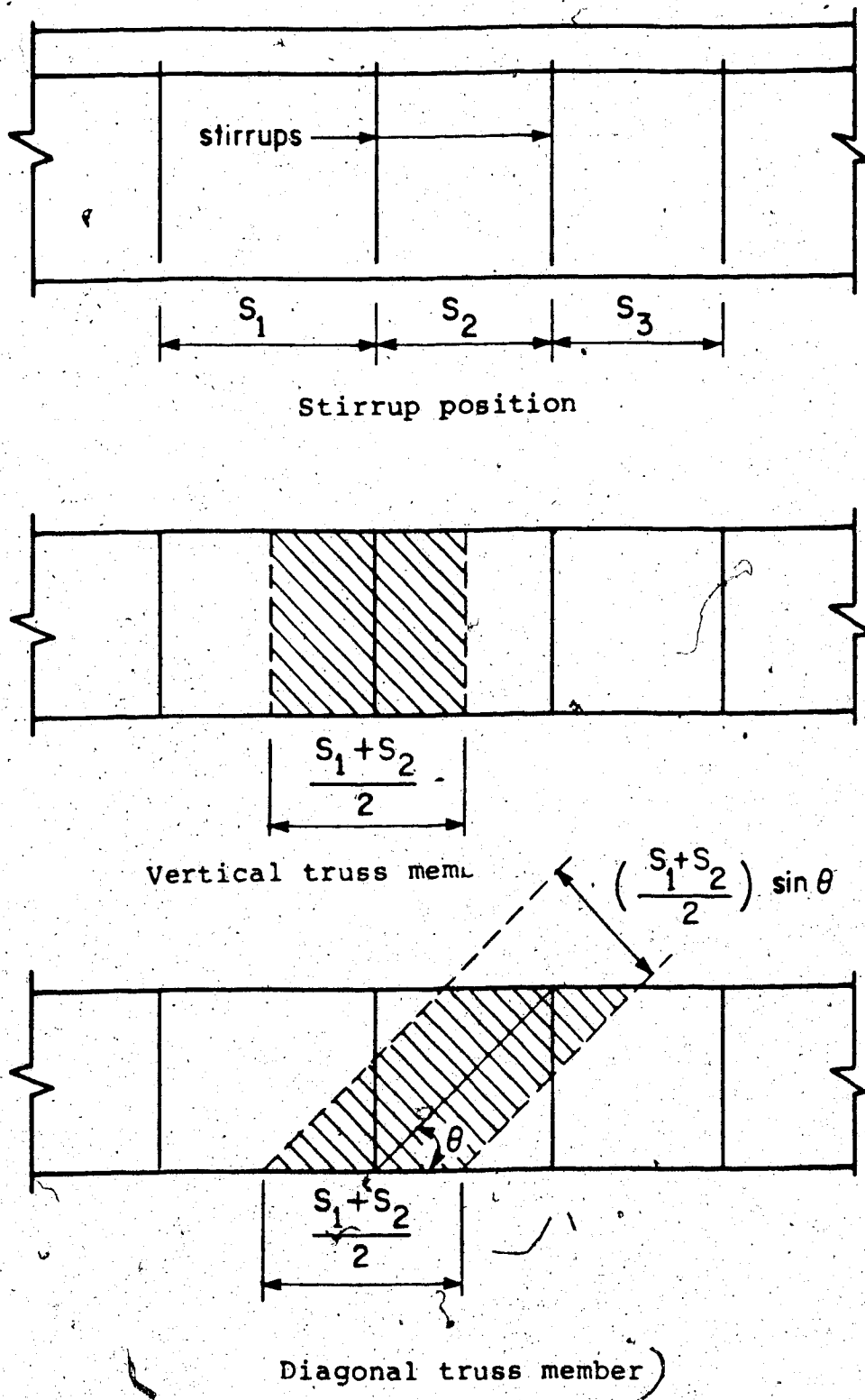
Figure 5.3.1.2 Beam Stirrup Position and Corresponding Web Members.
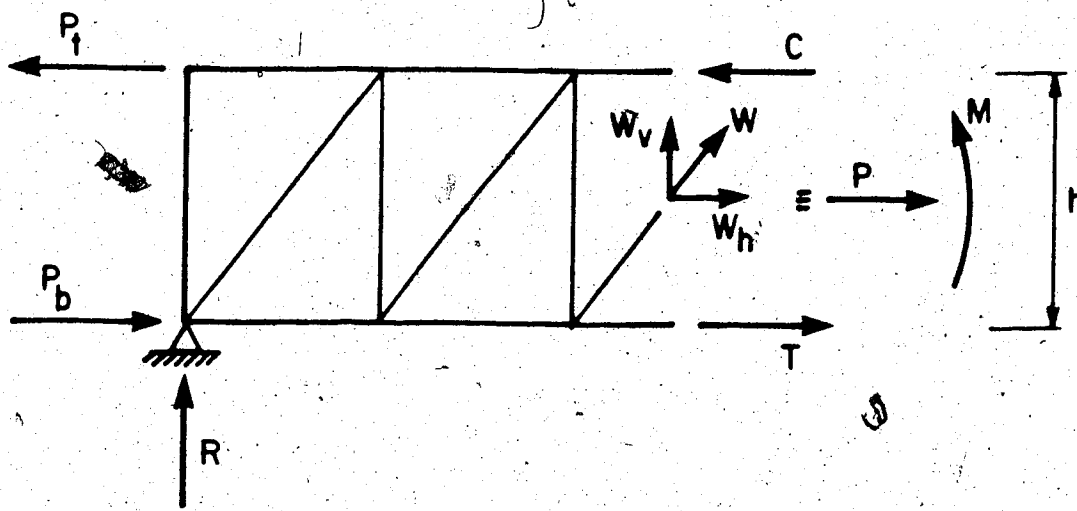
Figure 5.3.1.3 Forces at a Mid-Panel Section.
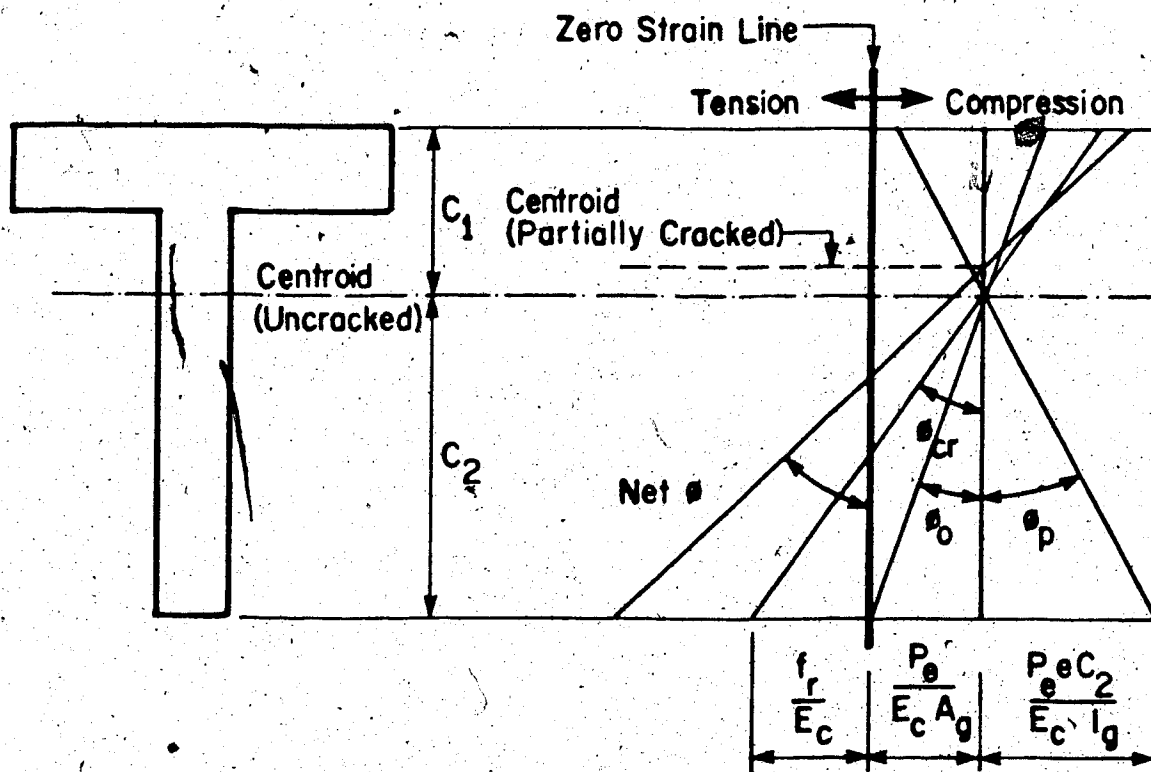
Figure 5.3.2.1 Strain-Diagram.
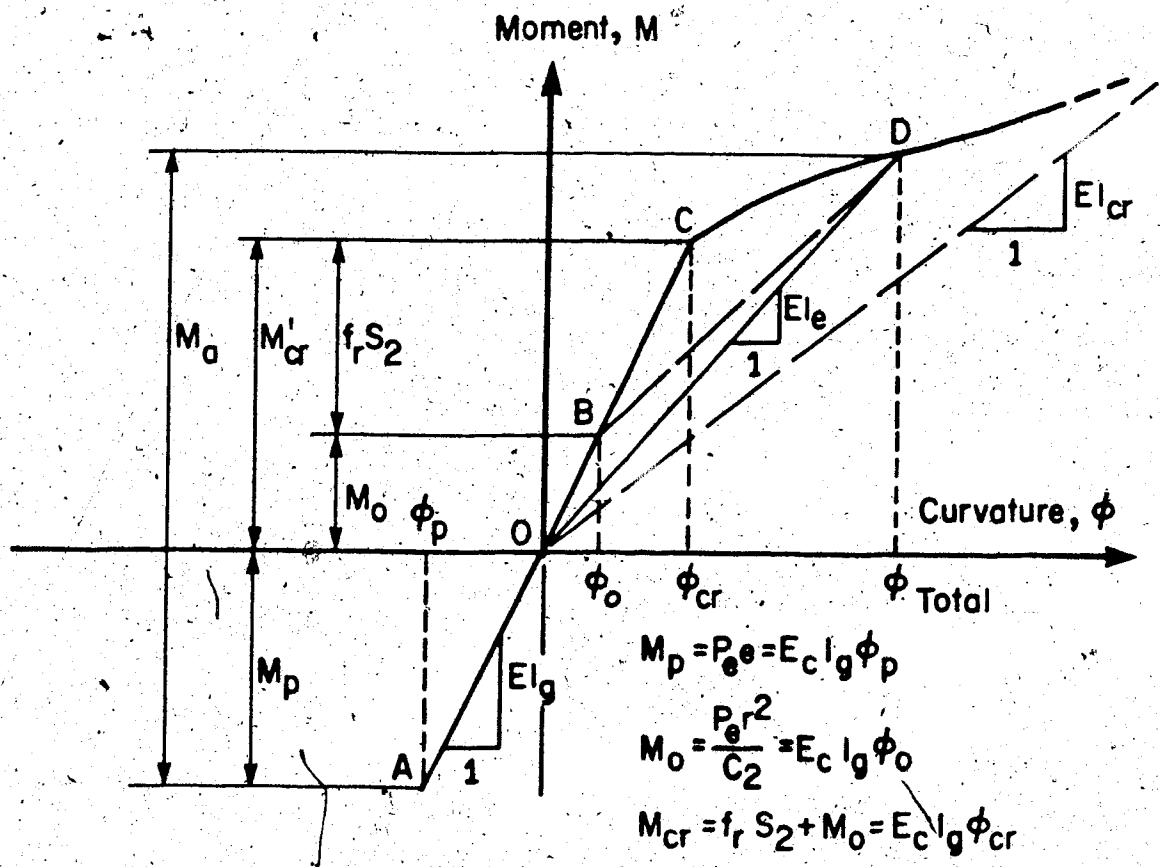
Figure 5.3.2.2 Moment-Curvature Relationship.

$$M_p = P_e e = E_c I_g \phi_p$$

$$M_o = \frac{P_e r^2}{C_2} = E_c I_g \phi_o$$

$$M_{cr} = f_r S_2 + M_o = E_c I_g \phi_{cr}$$

P   P   SYM

69.6"   69.6"   34.8"

174"

6"

R

Beam elevation

P   P   SYM

R

Truss model

0.44 in. Dia. Bars

0.44 in. Dia. Bars

$\frac{3}{8}$" Dia. 250 k Strands

Cross-section details
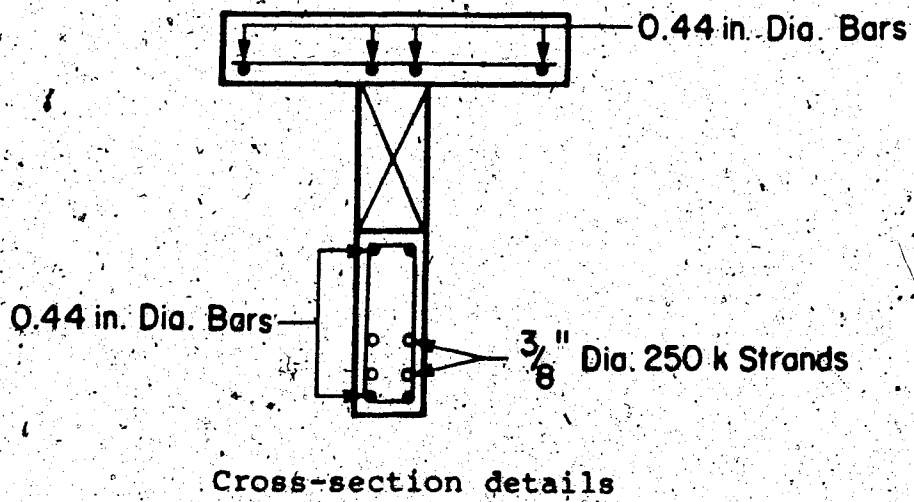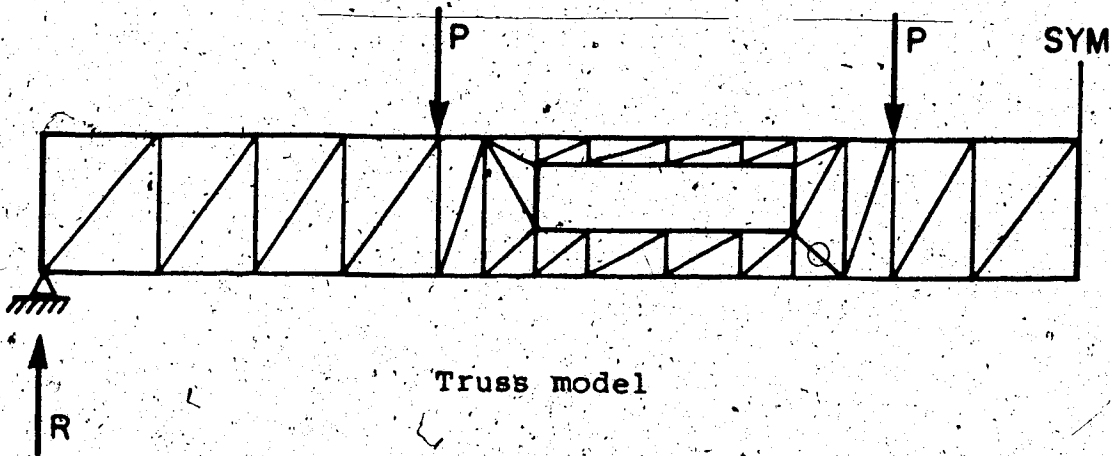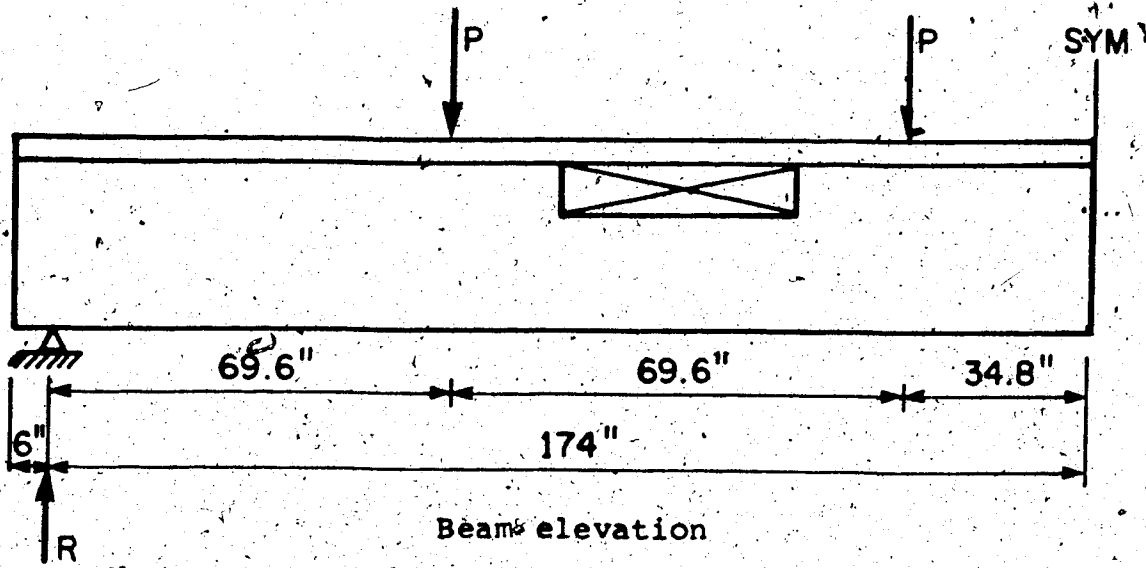
Figure 5.4.1   Details of BEAM B2.

P P SYM

69.6" 69.6" 34.8"

174"

Beam elevation

6"

R

P P SYM

Truss model

R

0.44 in. Dia. Bars

W 2.9 Wires

0.44 in. Dia. Bars

$\frac{3}{8}$" Dia. 250 k Strands
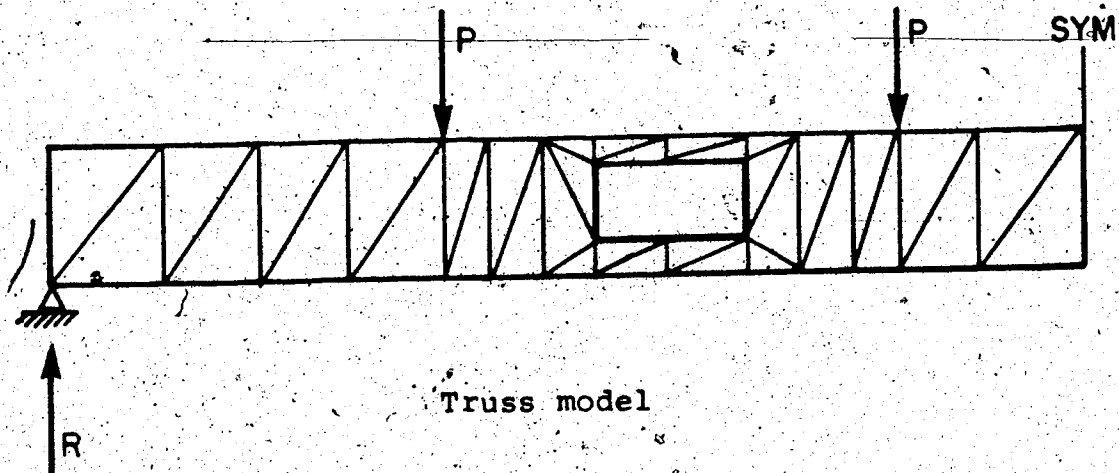
Cross-section details

Figure 5.4.2   Details of BEAM C3.
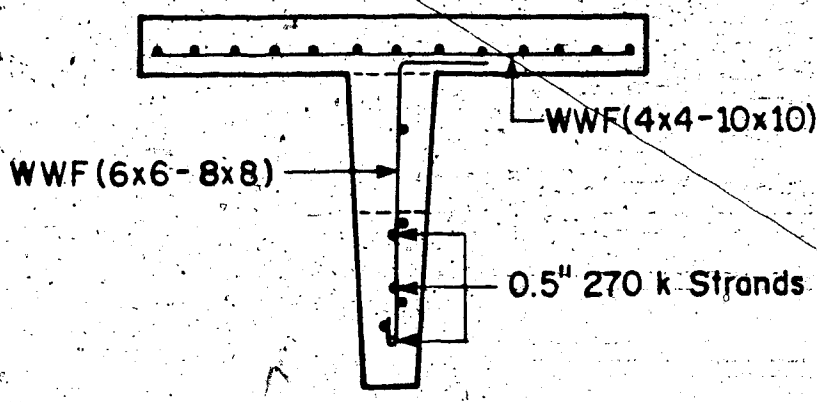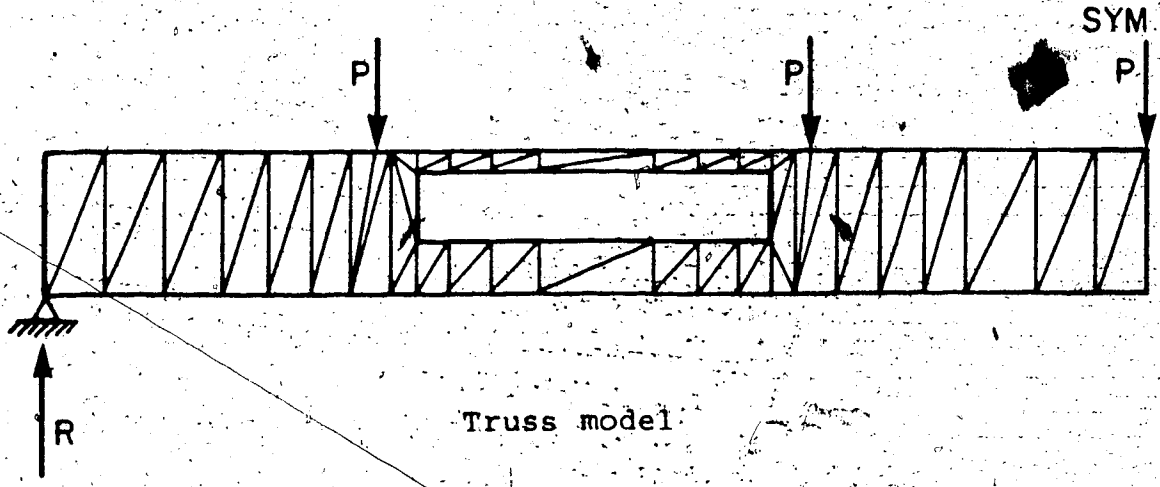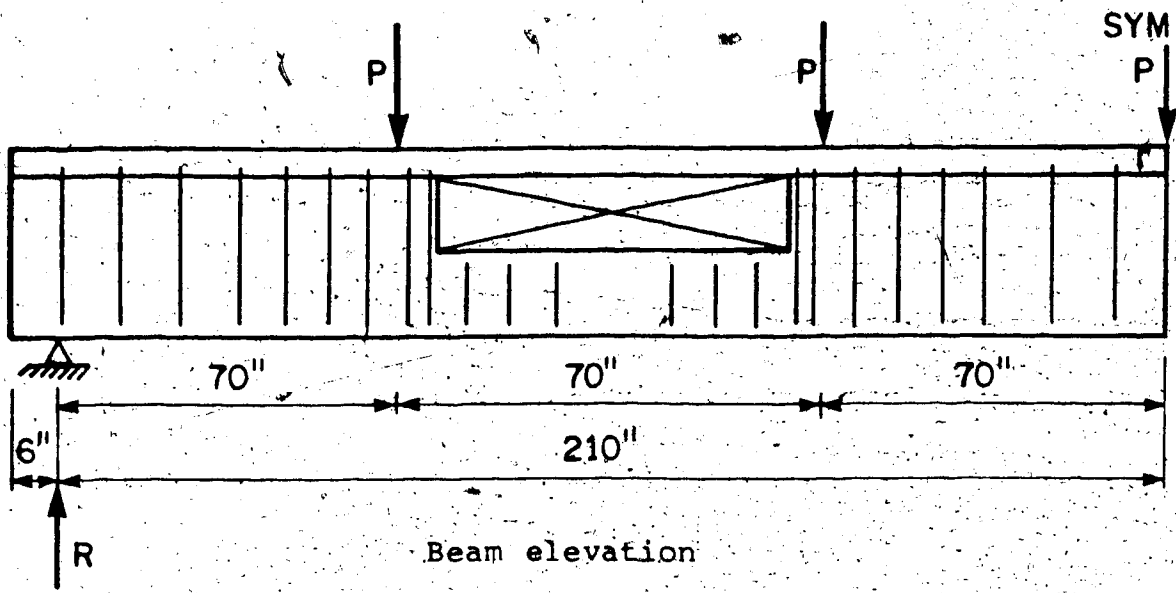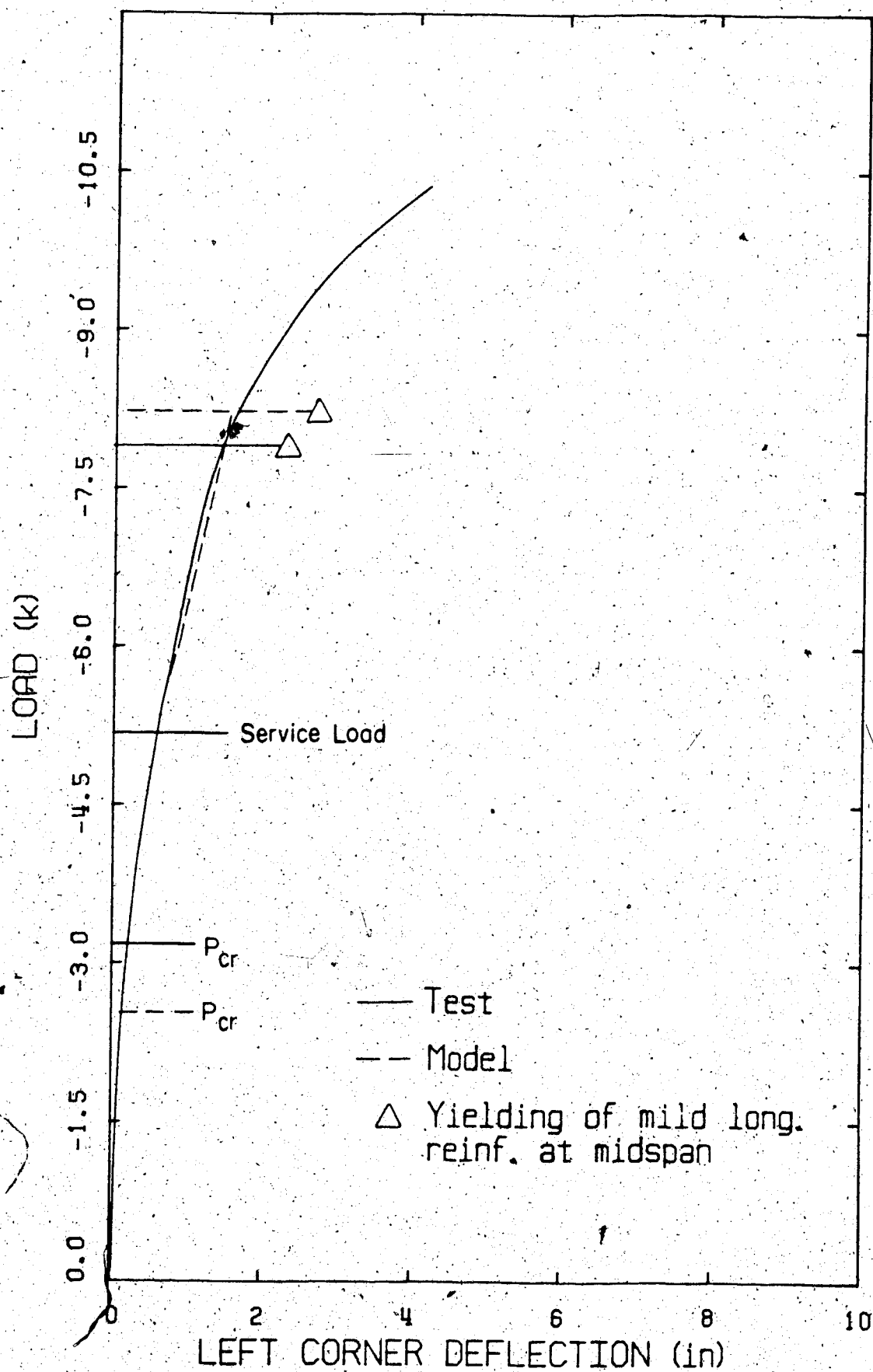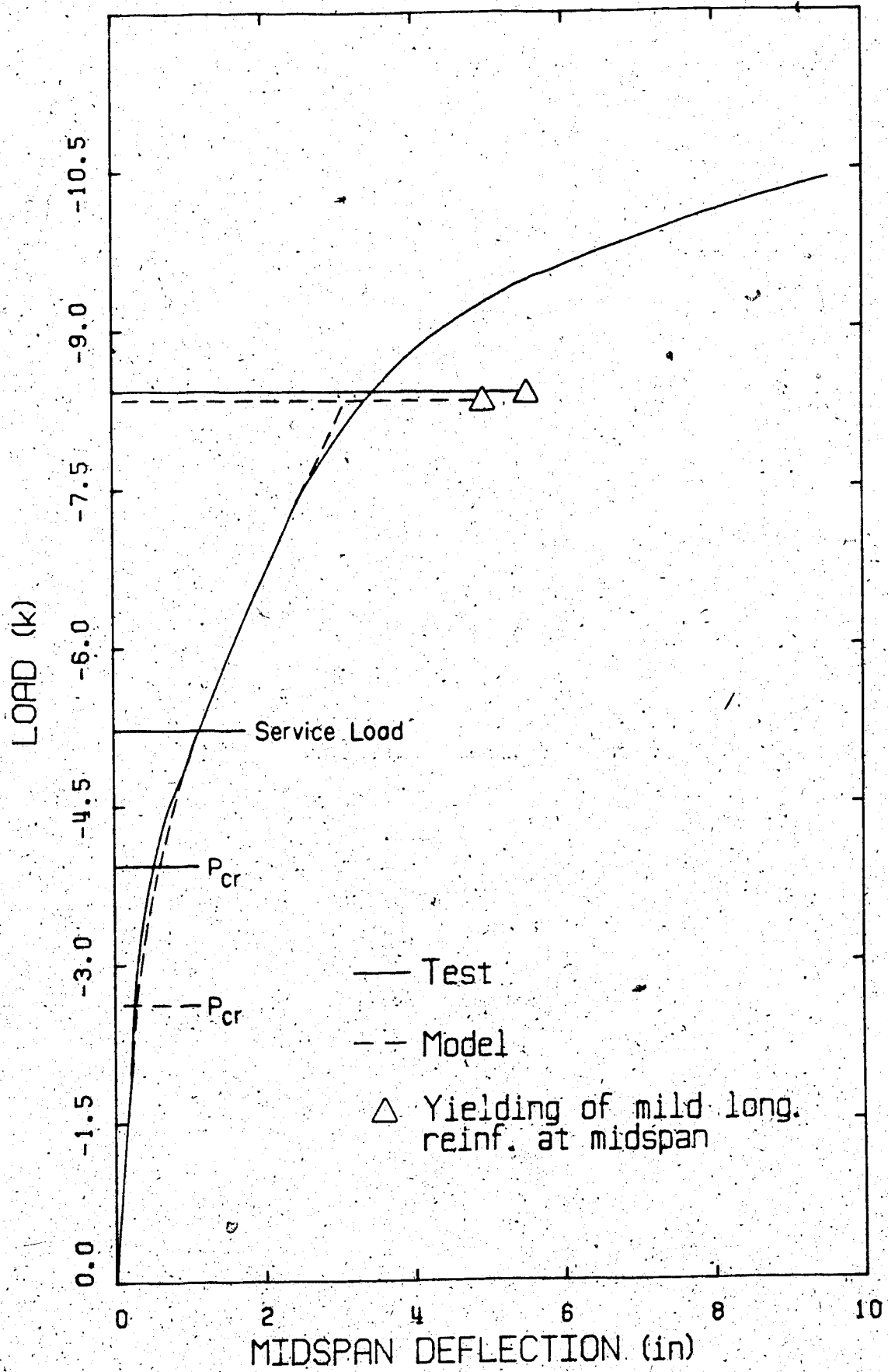
Figure 5.4.3   Details of BEAM B7 (Ref. 4).
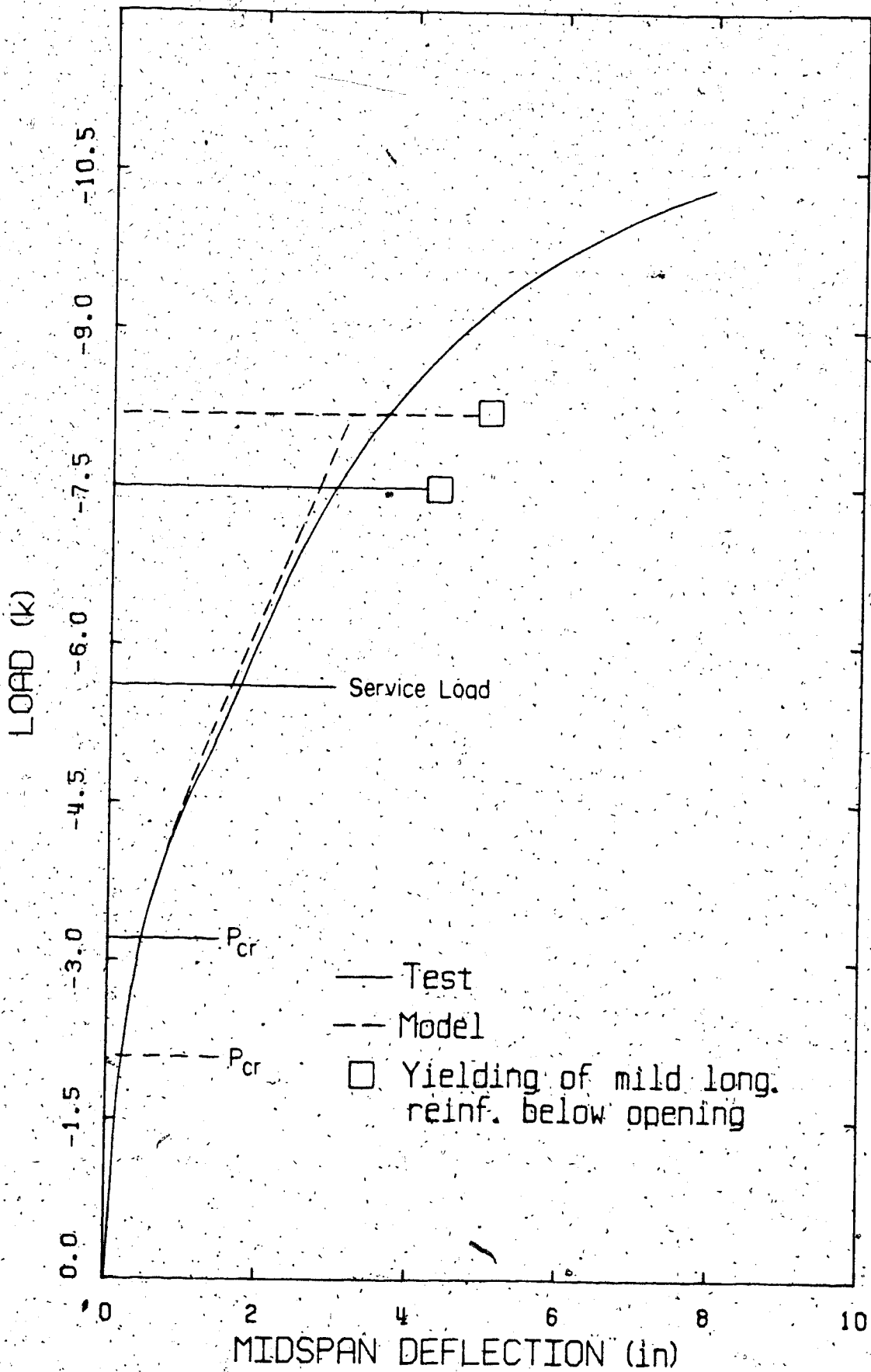
Figure 5.4.4   Load-Deflection Curve - BEAM B1.
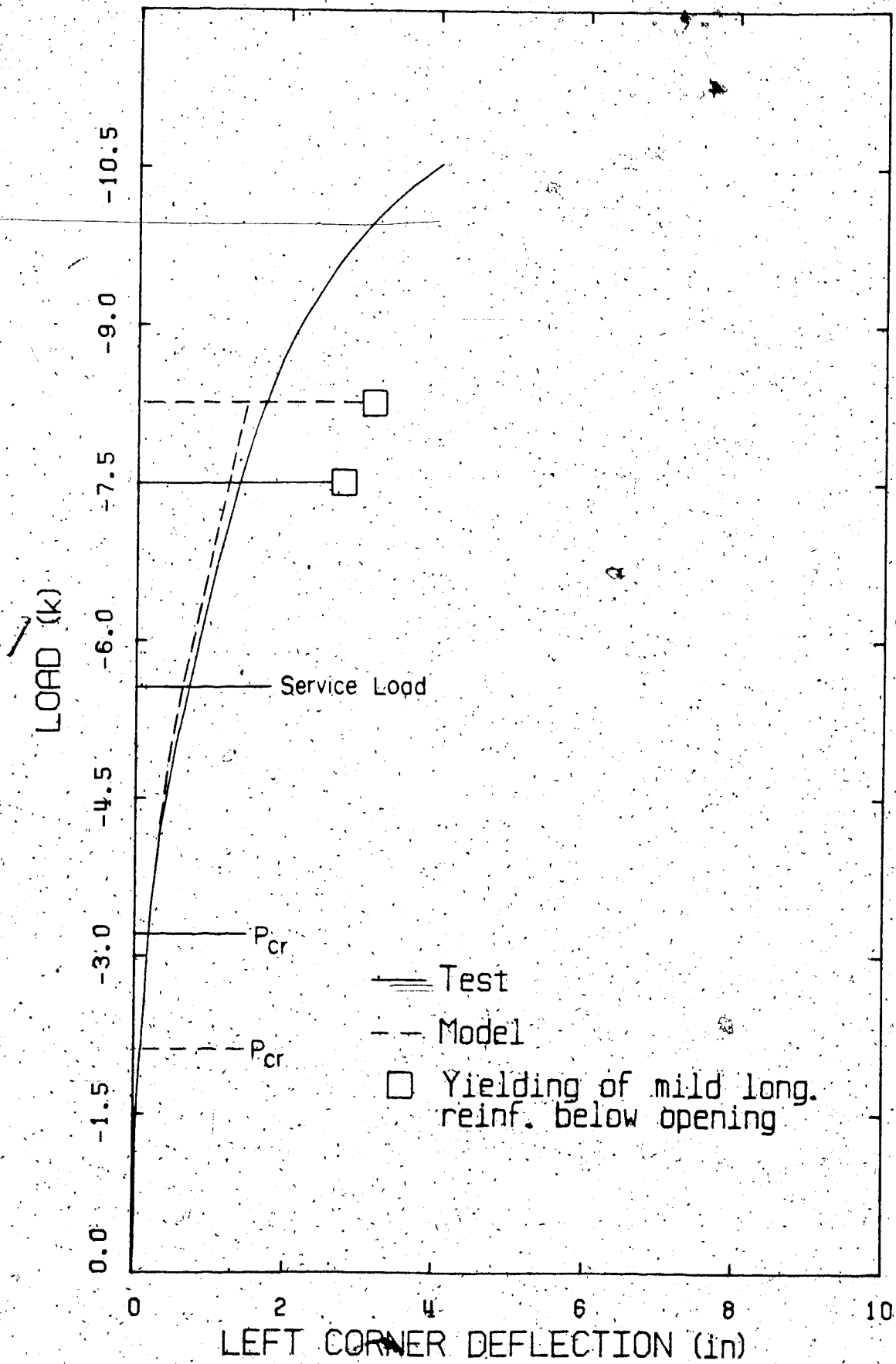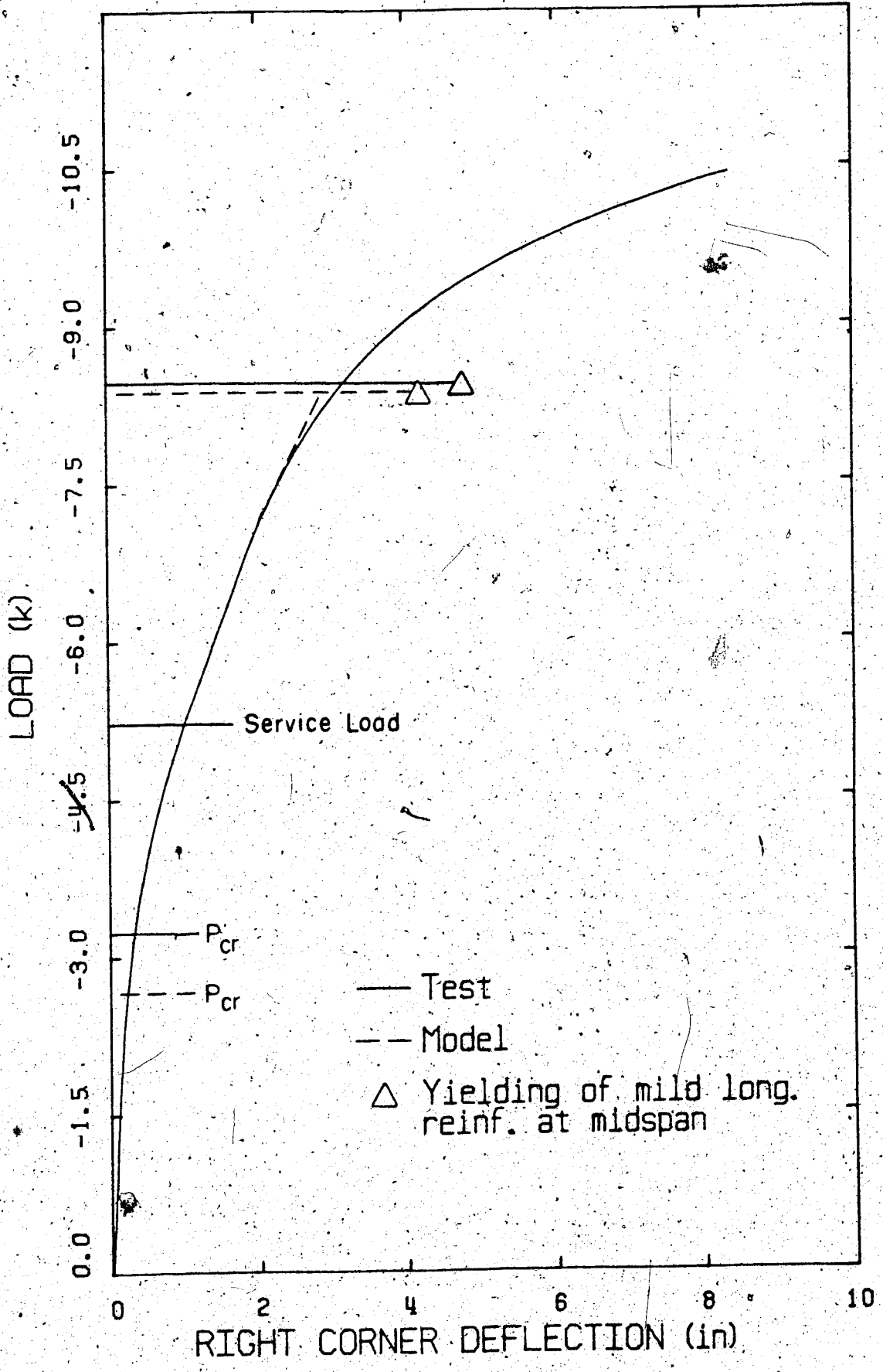
Figure 5.4.5   Load-Deflection Curve - BEAM B1.
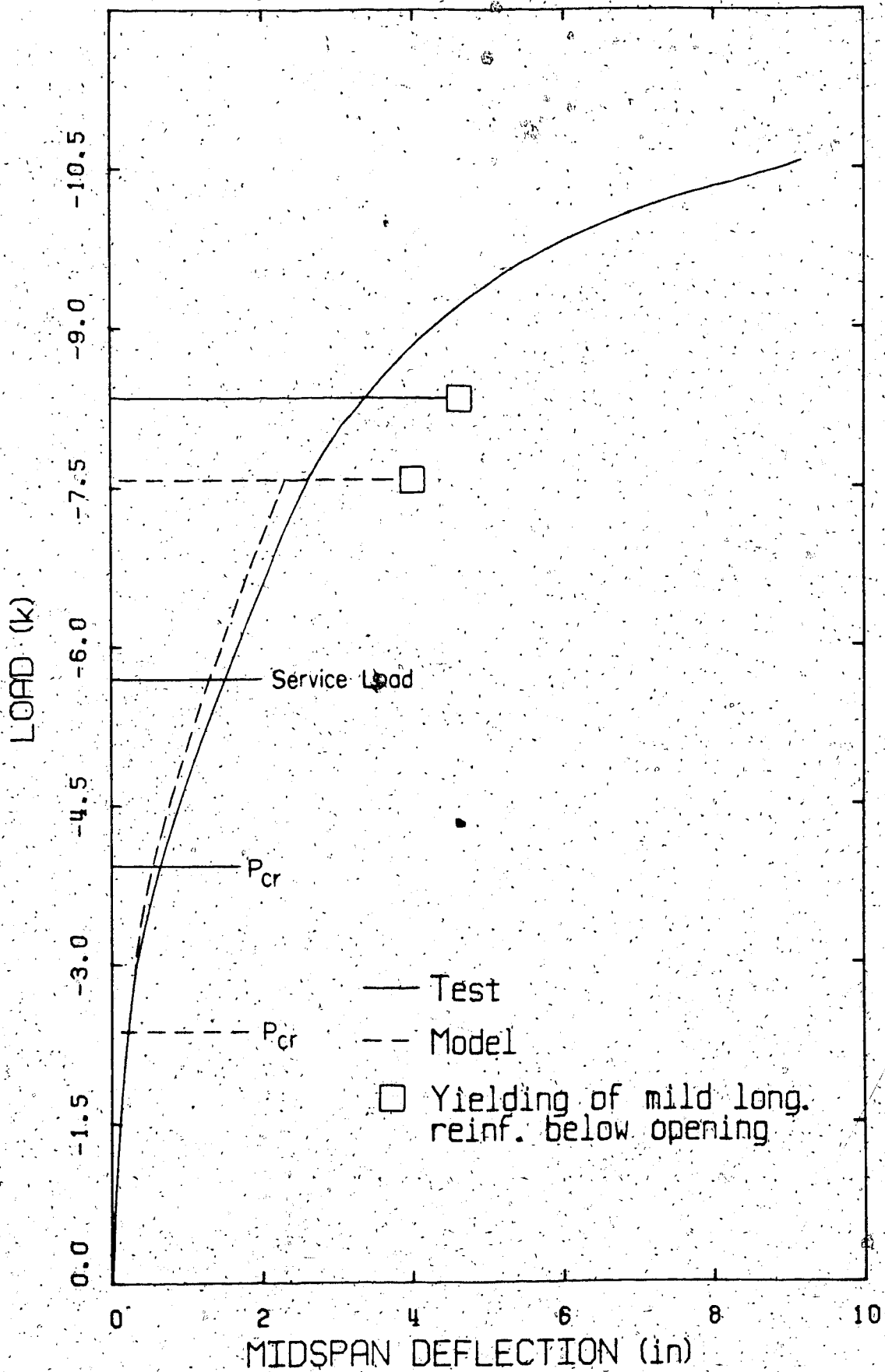
Figure 5.4.6   Load-Deflection Curve - BEAM B3.
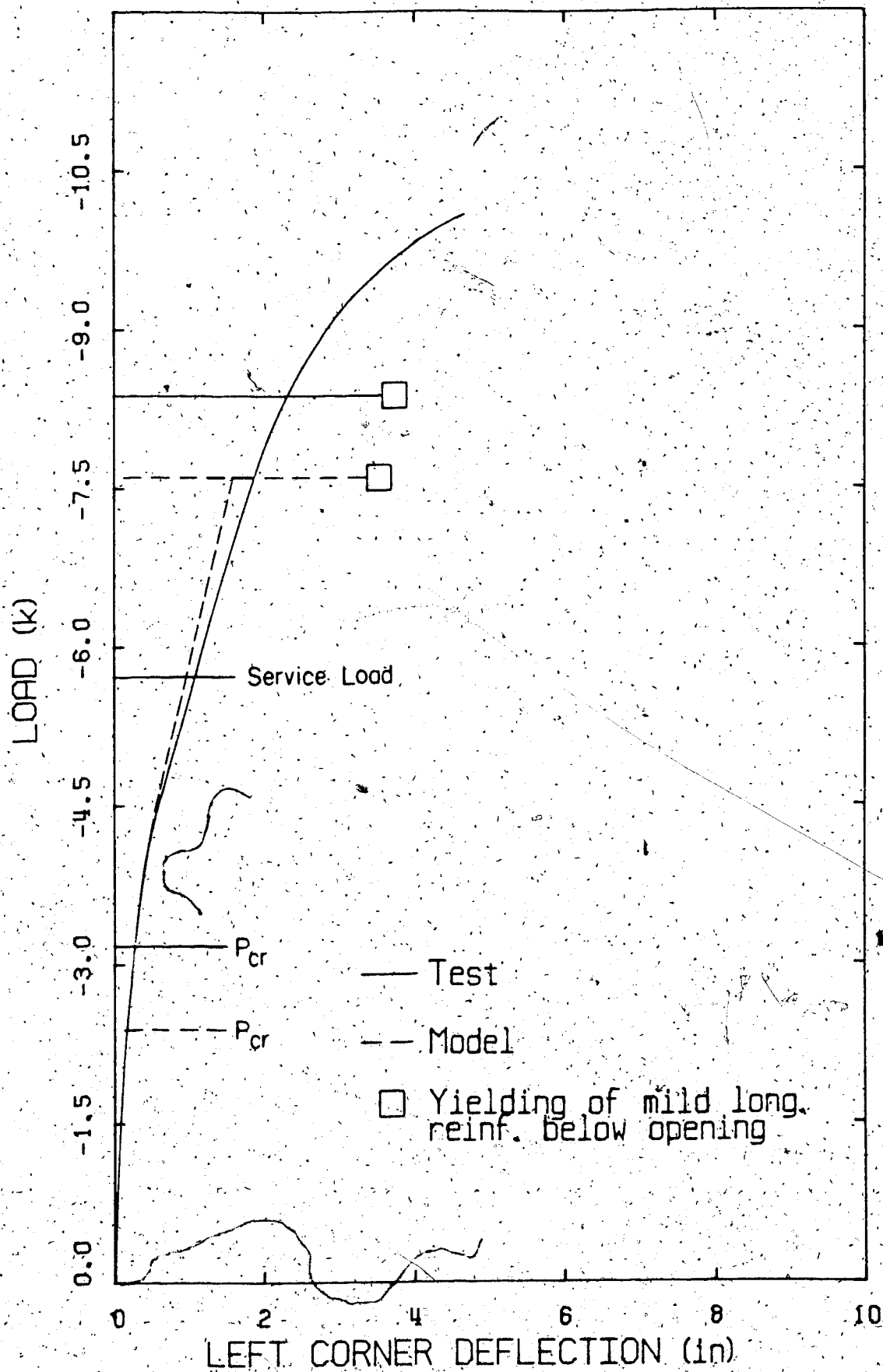
Figure 5.4.7   Load-Deflection Curve - BEAM B3.
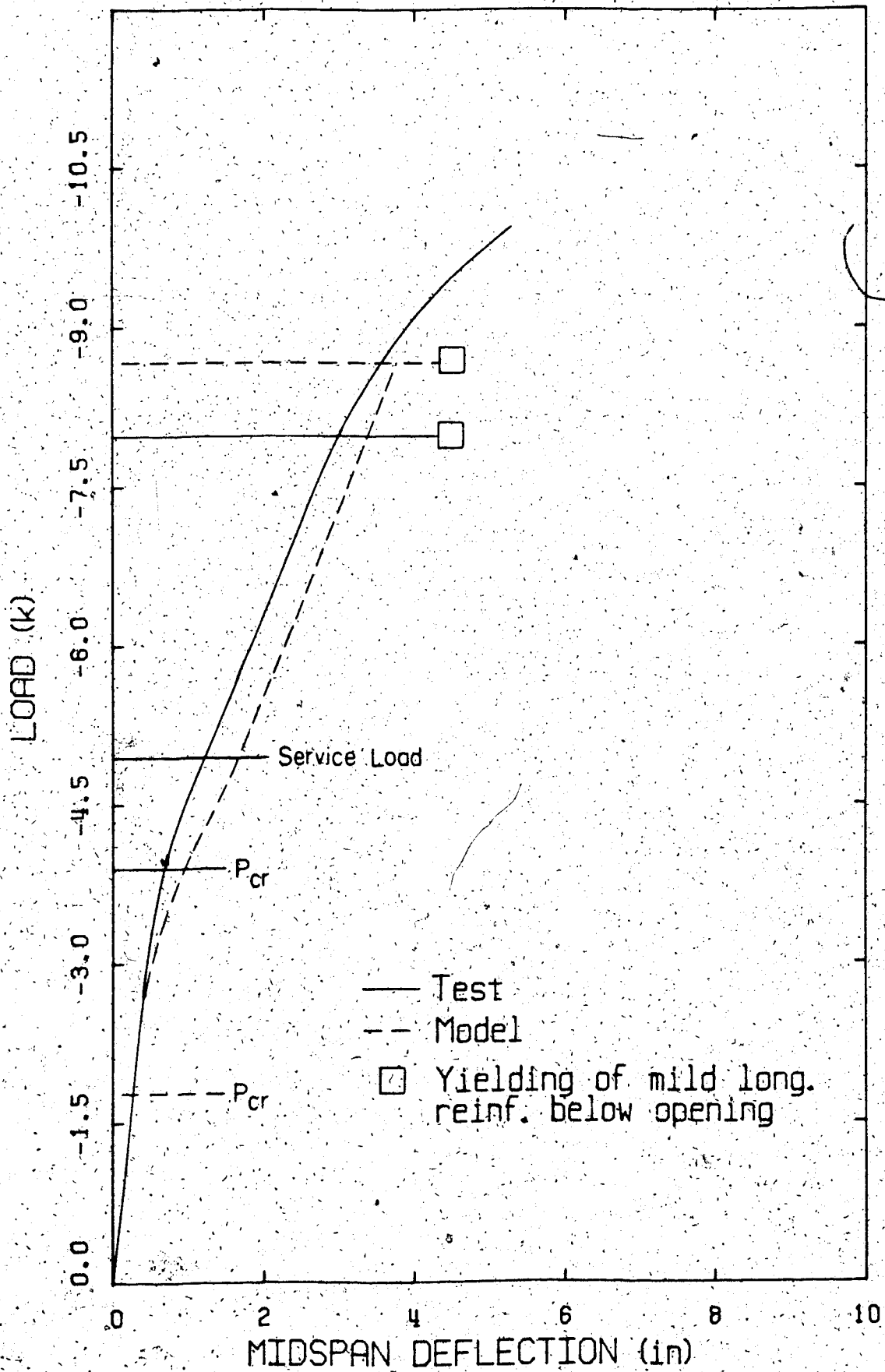
Figure 5.4.8   Load-Deflection Curve - BEAM C1.

182
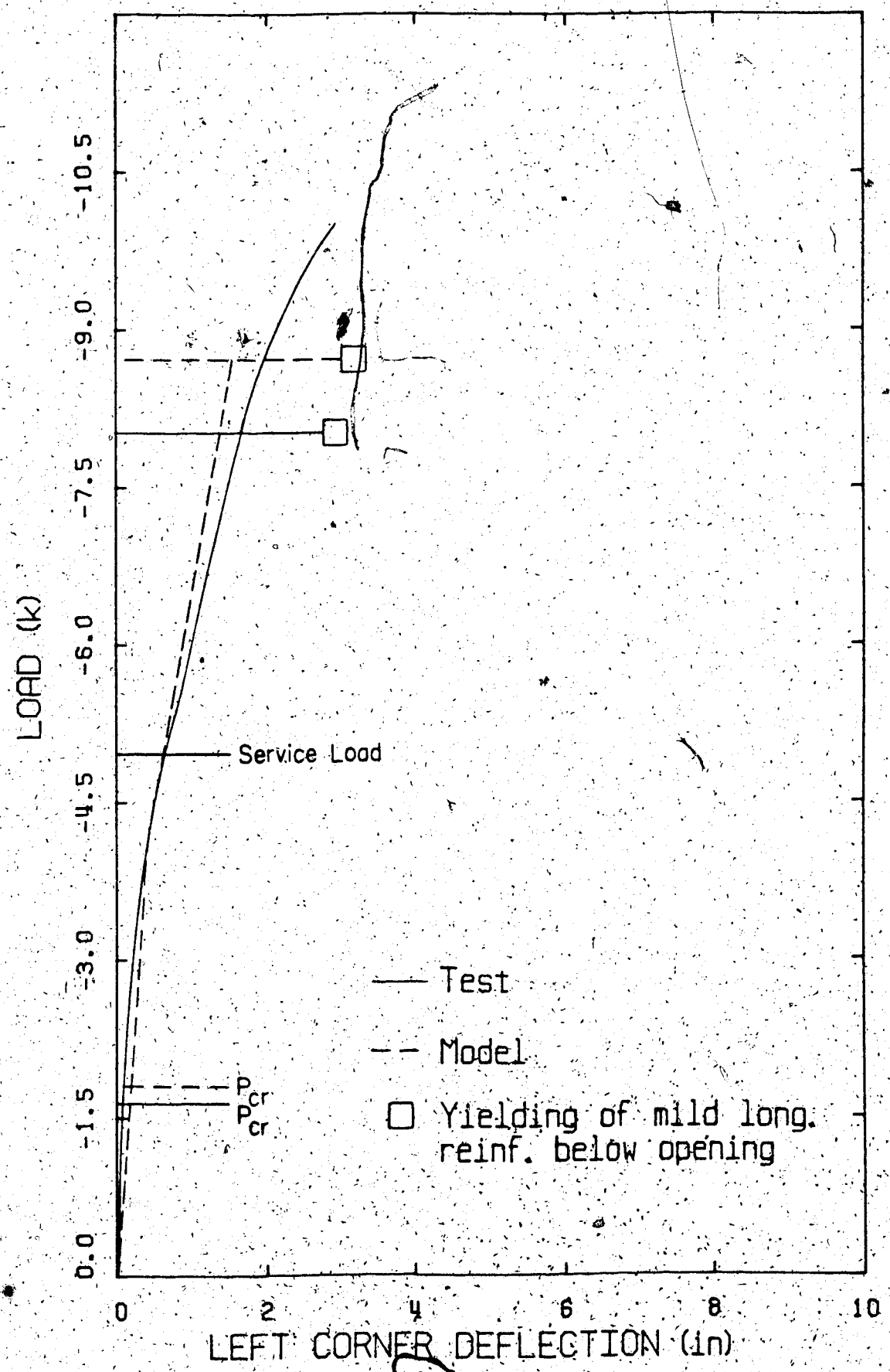
Figure 5.4.9   Load-Deflection Curve - BEAM C1.
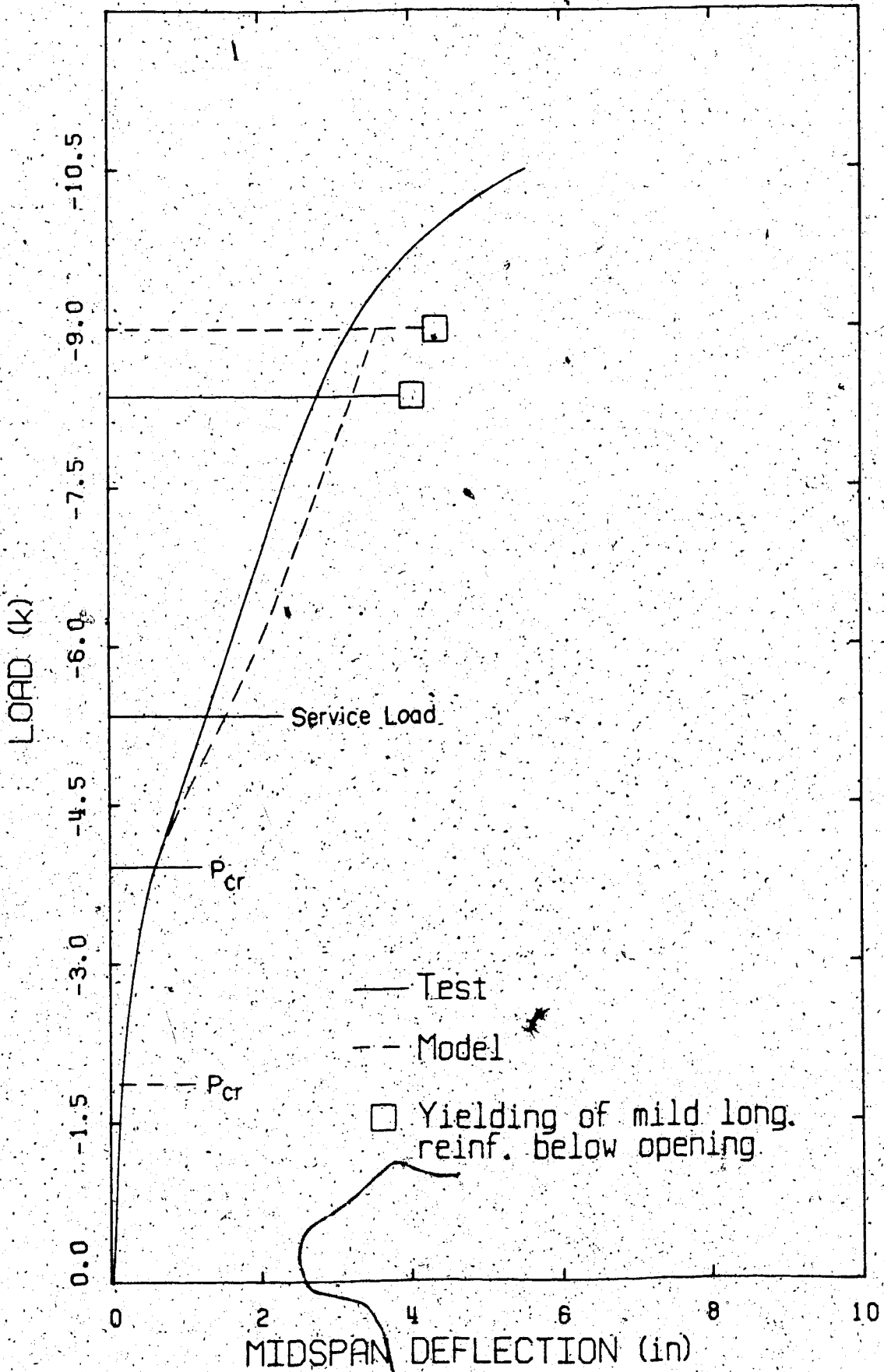
Figure 5.4.10   Load-Deflection Curve - BEAM C2.
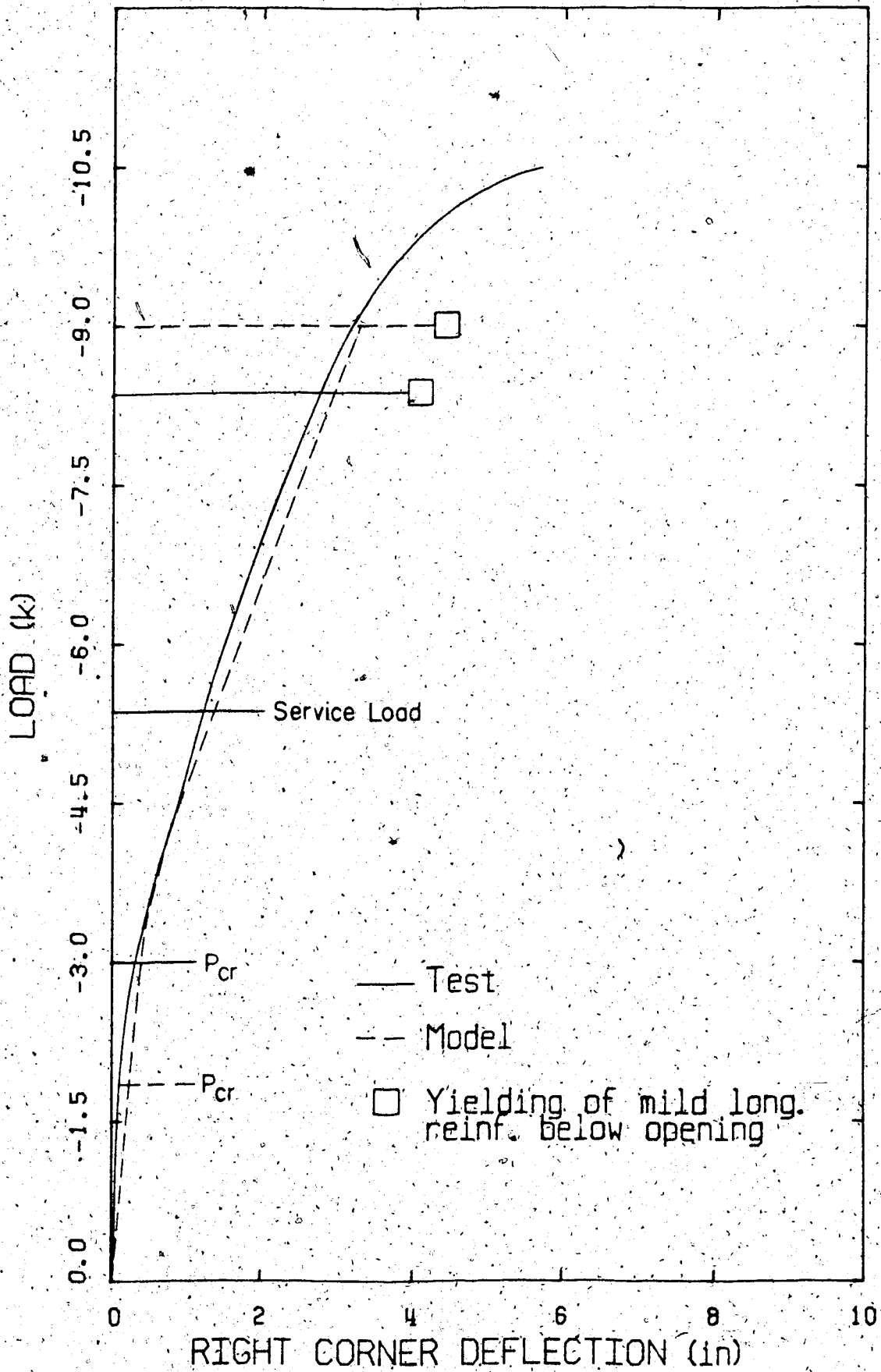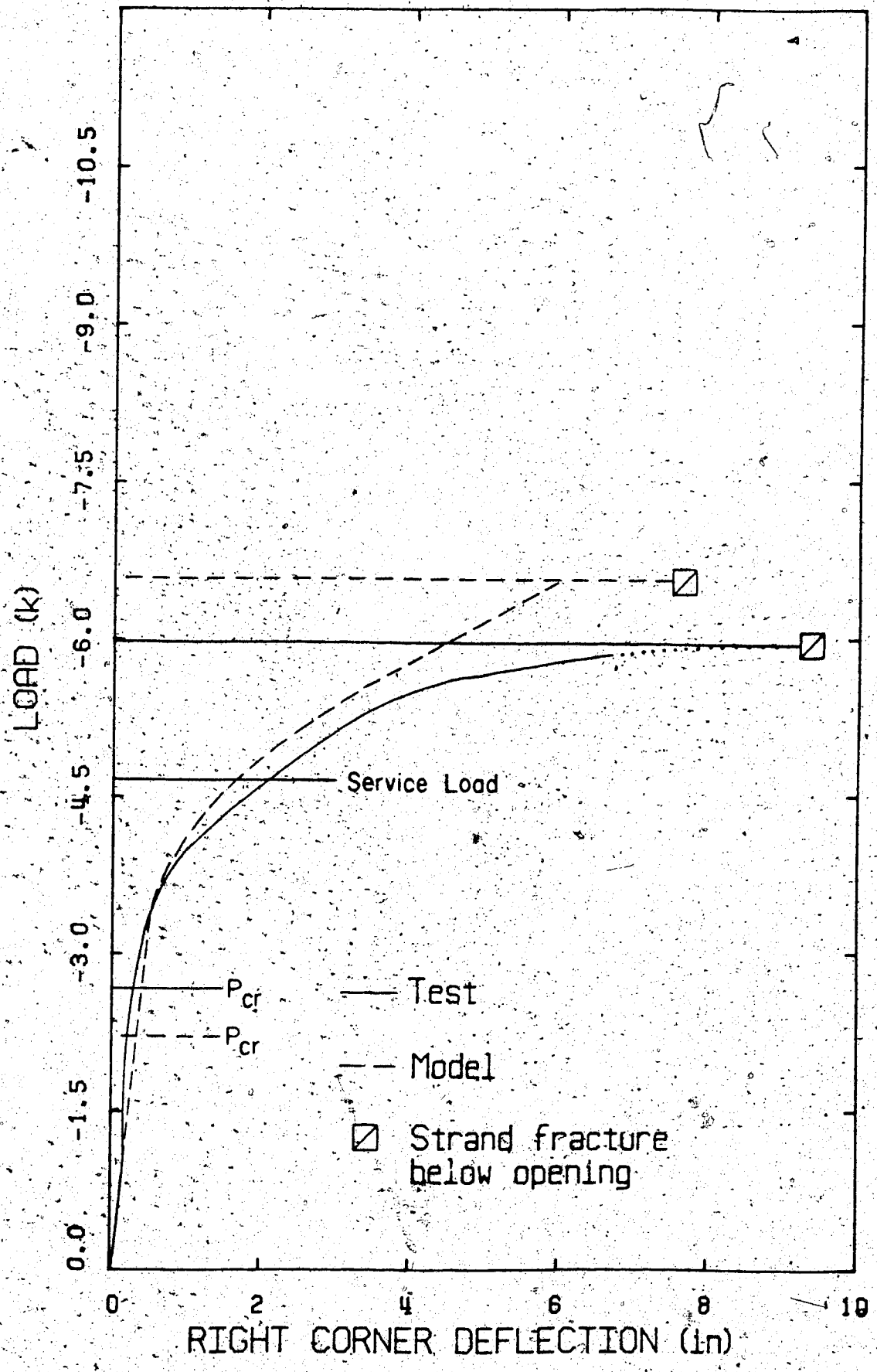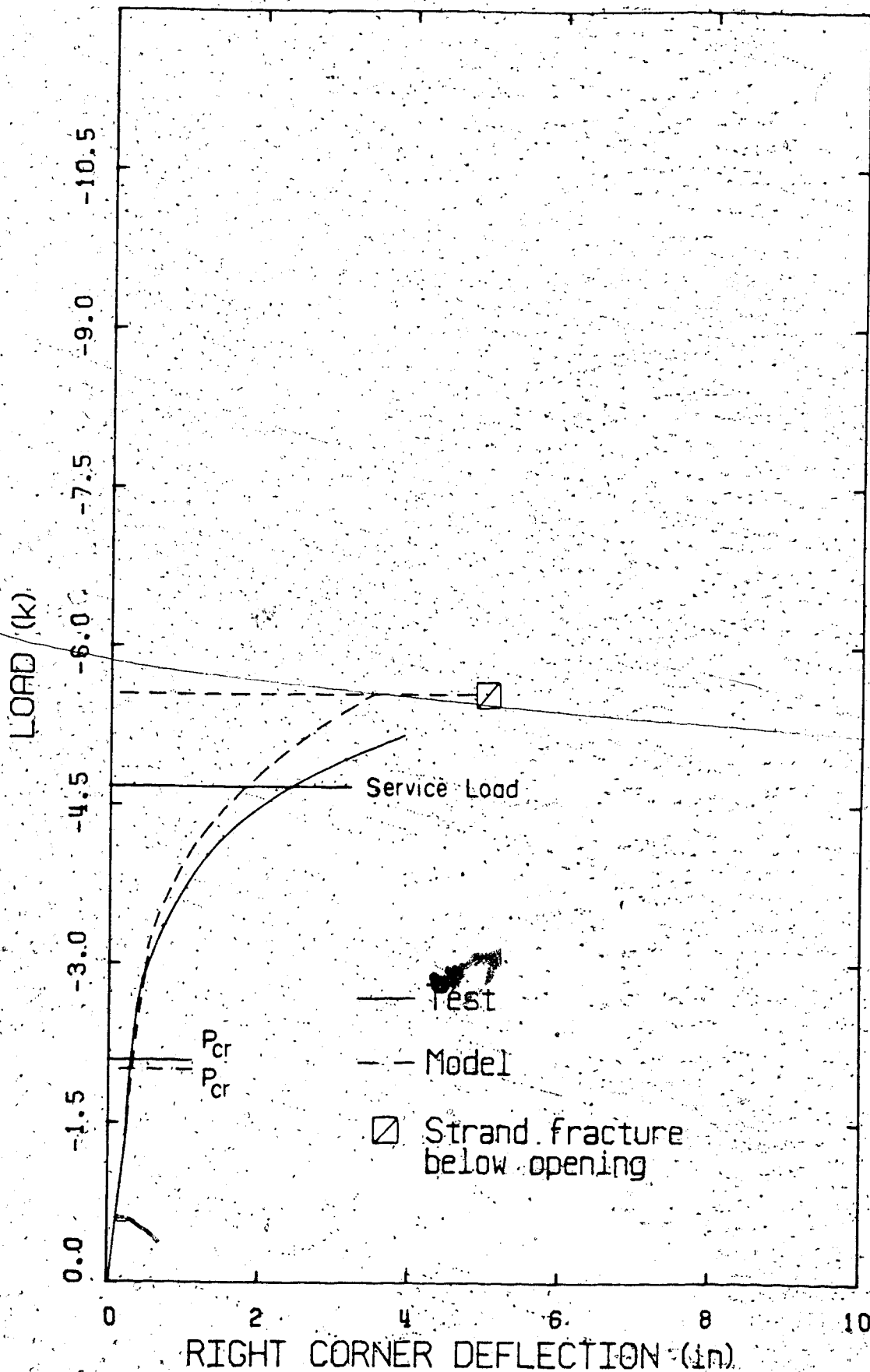
Figure 5.4.11   Load-Deflection Curve - BEAM C2.
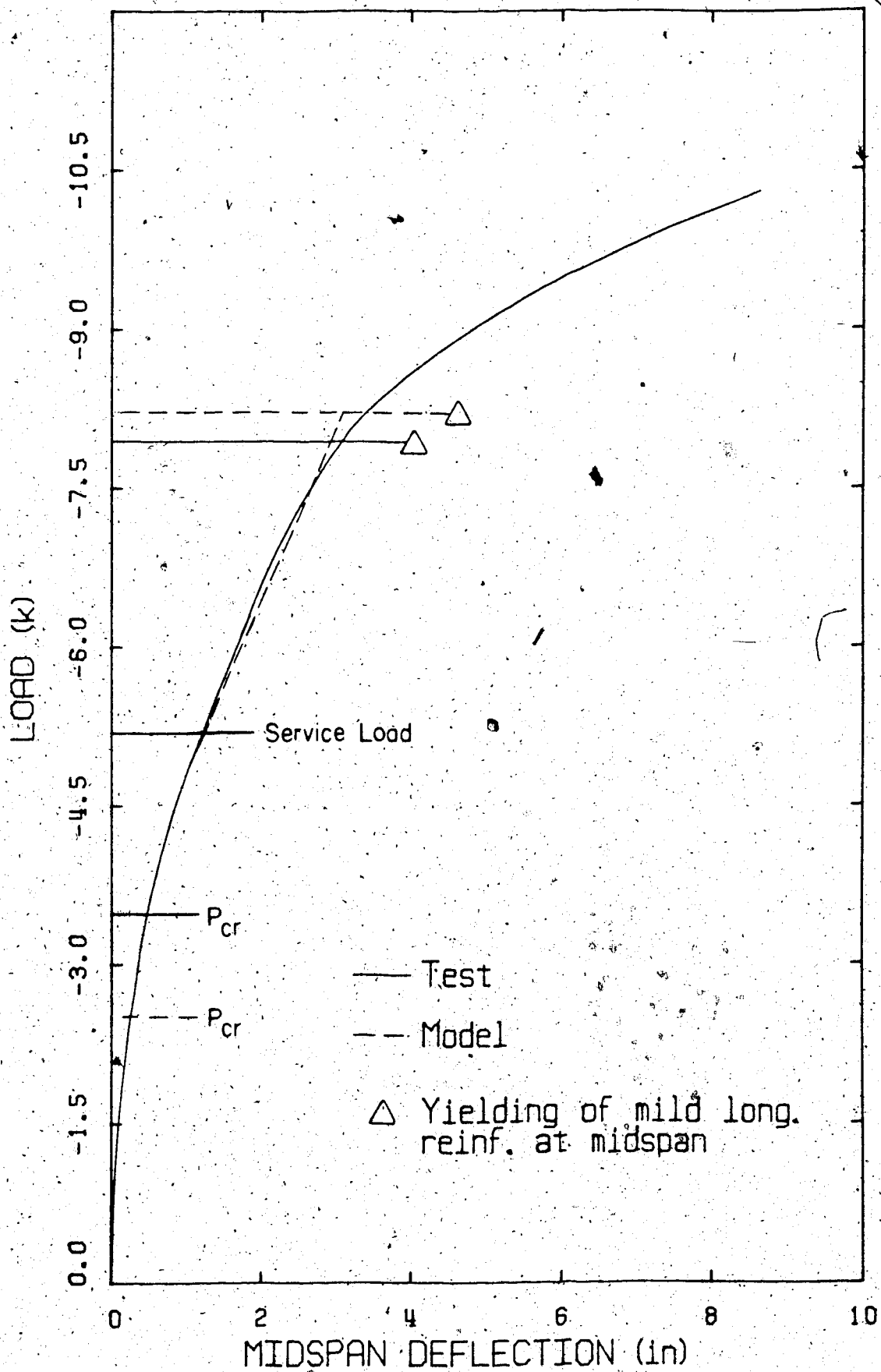
Figure 5.4.12   Load-Deflection Curve - BEAM D1.

Figure 5.4.13   Load-Deflection Curve - BEAM D1.

Figure 5.4.14   Load-Deflection Curve - BEAM D2.

Figure 5.4.15   Load-Deflection Curve - BEAM/D2.

Figure 5.4.16   Load-Deflection Curve - BEAM B7 (Ref. 4).

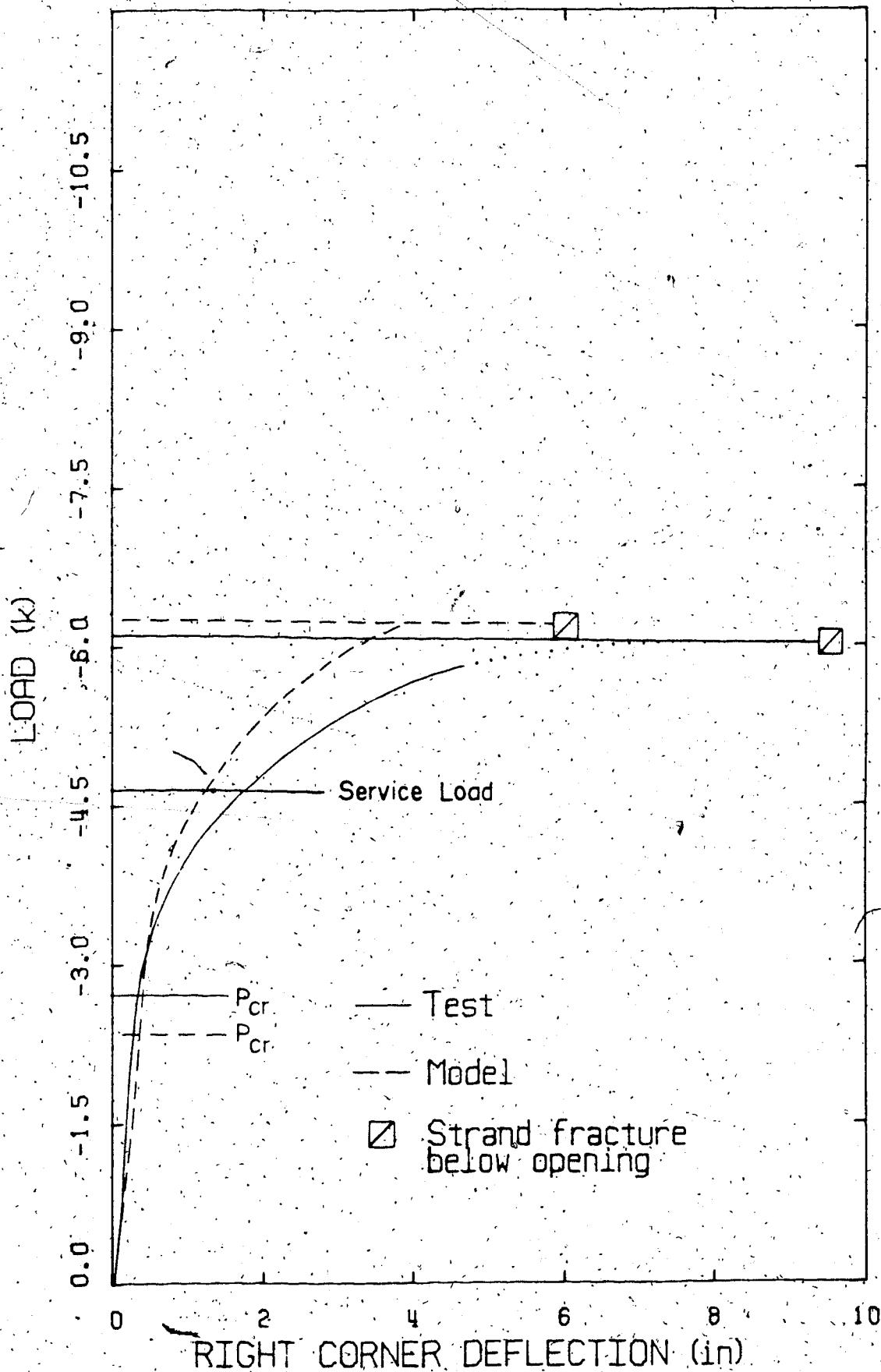Figure 5.4.17   Load-Deflection Curve - BEAM B5 (Ref. 4).

Figure 5.4.18   Load-Deflection Curve — BEAM B4 (Ref. 4).

6. EVALUATION OF STRENGTH AND SERVICEABILITY OF PRESTRESSED BEAMS WITH WEB OPENINGS

6.1 Introduction

In this chapter, considerations related to evaluation of design and deflections of prestressed concrete beams with web openings are discussed in light of the results of the analytical and experimental work described in previous chapters.

Design for strength requires that critical sections have adequate strength to resist applied design loads. In the case of beams with openings it is necessary to determine forces in the top and bottom struts associated with the ultimate limit state. Once these forces have been determined the struts must be designed to have adequate strength to resist the forces. In addition, design and detailing should be aimed at providing ductile rather than brittle failure modes. In this respect, flexural failure, rather than shear and bond failure, is the desired mode. For prestressed beams with web openings the critical section for flexural failure may occur at the solid section or in the struts above and below openings, depending on the geometry and location of openings.

192

Serviceability refers to performance at working load levels, particularly in terms of deflections. For beams with openings, deflections may be critical as a result of decreased stiffness in the vicinity of the openings.

6.2 Strength

6.2.1 Failure Modes

As mentioned in Chapter 3, failure modes observed in this test program were:

-full hinging mechanism involving two hinges in the bottom strut and two hinges in the top strut.

-development of a partial hinging mechanism consisting of two hinges in the bottom strut and one hinge in the top strut, followed by a shear failure away from the opening.

-shear failure at solid shear span followed by strand debonding.

-flexural failure at midspan.

These failure modes are illustrated in Fig. 6.2.1.1. Another possible failure mode in prestressed concrete beams with web openings is strand slip. When openings are placed in high shear regions and the inclined crack formed at the lower tension corner of the opening is allowed to extend

into the required strand embedment length, the strand may slip. To avoid this undesirable type of failure, openings must be located outside the required strand embedment length and adequate shear strength must be provided within the strand embedment length.

A significant factor that must be considered as well as the strength of prestressed concrete beams with web openings is ductility. This means ensuring that the beam does not fail in a brittle fashion without warning but is capable of large deformations near the maximum load-carrying capacity. To ensure ductile behavior special attention must be given to detailing, ensuring that all brittle failure modes are avoided. Therefore, flexural failure, rather than shear and bond failure and strand slip, is the desired failure mode.

6.2.2 Evaluation of Forces in Struts Due to Applied Loads at Ultimate

The design of a prestressed concrete beam with large web openings requires an evaluation of the forces acting in the struts so that the struts can be designed to resist the applied loads. Due to the loads applied on the beam, a shear force V and a moment M are produced at the middle section of the opening. Figure 6.2.2.1 shows the forces

acting on a cross-section of a prestressed concrete beam with web openings. The top strut carries a portion V_t and the bottom strut carries a portion V_b of the total shear force acting at the section, at the ultimate load level. The prestress force P_p and the moment M produce an axial tensile force T in the bottom strut and an axial compressive force C in the top strut. The axial forces C and T are assumed to be applied at the centroids of the top and bottom struts respectively and are calculated, at ultimate, from equilibrium conditions at the middle section of the opening, where a point of inflection is assumed to occur in each strut. The axial compressive force acting in the top strut is determined according to the following expression:

$$C = \frac{M - P_p(d_p)}{d_{st}} \qquad (6.1)$$

where

$$P_p = 0.7 \, f_{pu}A_p \qquad (6.2)$$

The axial tensile force acting in the bottom strut is determined as follows:

$$T = \frac{M - P_p(d_{st} + d_p)}{d_{st}} \qquad (6.3)$$

where,

M − moment at the center of the opening due to applied loads

f_{pu} − tensile strength of prestressing strand

A_p − area of prestressing strand

d_p − distance between centroid of prestressing strand and bottom strut centroid

d_{st} − distance between centroids of top and bottom struts

The shears V_t and V_b depend on the relative flexural stiffnesses of the top and bottom struts at ultimate. If a full mechanism occurs at the opening, the shear in each strut is that associated with the smaller shear corresponding to the flexural and shear capacities of each strut. The moment capacities in turn are affected by the presence of axial forces C and T. The shears in the top and bottom members may however be limited by the shear capacity of one or both struts. This is particularly the case for the bottom strut where the presence of the tensile force reduces the ability of the concrete to contribute to shear carrying capacity of the strut.

In Section 6.2.2.1 the method of calculating the shears corresponding to a full flexural mechanism at the opening is described. The shear capacity of the axially

loaded struts is determined by expressions given in the ACI Building Code (318-77)[1] as outlined in Section 6.2.2.2. The shears are then compared with shears obtained from the tests.

6.2.2.1 Shears Corresponding to Full Hinging Mechanism at Opening.

Once the axial force in a strut is calculated, the corresponding flexural capacity can be determined by considering strain compatibility and equilibrium conditions for the strut cross-section. To accomplish this, a computer program developed by Shushkewich[24] was used. The solution is based on a bilinear stress-strain curve for mild reinforcement and a mathematical stress-strain relationship proposed by Mattock[15] for the prestressing steel. The stress-strain relationship for concrete is based on equivalent rectangular stress block.

Figure 6.2.2.1.1 shows free-body diagrams for the struts above and below an opening at formation of a full hinging mechanism. The end moments M_1 through M_4 represent the flexural capacities corresponding to the calculated axial forces in the members. The strut shears V_t and V_b corresponding to these moments can be calculated from equilibrium conditions as:

$$V_{bf} = \frac{M_1 + M_2}{\ell} \qquad\qquad (6.4)$$

$$V_{tf} = \frac{M_3 + M_4}{\ell} \qquad\qquad (6.5)$$

where,

V_{bf} - shear carried by bottom strut

V_{tf} - shear carried by top strut

M_1, M_2 - moments at the ends of bottom strut

M_3, M_4 - moments at the ends of top strut

ℓ - opening length

6.2.2.2 Shear Strength of Strut Based on ACI Design
           Equations

The presence of the axial tensile force in the bottom strut increases the longitudinal tensile stress and the resulting tendency for inclined cracking. On the contrary the addition of the axial compressive force in the top strut decreases the longitudinal tensile stress and the tendency for inclined cracking.

Since shear is associated with the phenomenon of diagonal tension, it is expected that axial compression will increase and axial tension will decrease the shear capacities of the struts.

The basis for the ACI Building Code (318-77) approach to the design of flexural members subjected to axial forces

is that in web reinforced members the nominal shear strength provided by concrete can be carried together with the shear resisted by the truss mechanism with 45° diagonal struts. The ACI Building Code proposes a semi-empirical equation, based on principal stress concepts, which conservatively predicts the diagonal cracking load. This equation is suitably modified to take into account the effect of axial forces. However, because it is frequently difficult to be applied in design, the ACI Building Code (318-77) allows the use of simplified equations to compute the shear carried by the concrete beams subjected to axial forces.

Thus, the shear corresponding to the shear capacity of the bottom strut determined according to ACI Building Code is given by:

$$V_{bs} = 2[1 + (\frac{-T}{500 \ A_b})] \ \sqrt{f'_c} \ b_w d \ + \ \frac{A_s \ f_y \ d}{s} \qquad (6.6)$$

where,

V_{bs} - shear at bottom strut

T - tensile axial force in the bottom strut

A_b - area of bottom strut

f'_c - compressive strength of concrete

b_w - web width

d - distance from extreme compression fiber to centroid

of longitudinal tension reinforcement

A_s - area of shear reinforcement

f_y - yield strength of shear reinforcement

s - spacing of shear reinforcement

When the calculated shear strength provided by concrete is found negative it is assumed to be zero. The shear corresponding to the shear capacity of the top strut determined according to ACI Building Code (318-77) is given by:

$$V_{ts} = 2[1 + 0.0005 \left(\frac{C}{A_t}\right)] \sqrt{f_c'} \, b_w d + \frac{A_s f_y d}{s}$$

where,

V_{ts} - shear at top strut

C - compressive axial force in the top strut

A_t - area of top strut

6.2.3 Comparison Between Shear Carried by Struts at Failure and Calculated Shear Capacities.

Strut shear forces corresponding to strut flexural capacity (formation of hinging mechanism) and strut shear capacity are listed in Table 6.2.3.1 for the twelve specimens with openings considered in this study.

Calculations of strut shear capacities are given in Appendix D. It can be seen that in some cases flexural capacity governs while in other cases shear capacity governs the shear force that can be carried by each strut. To estimate the total shear capacity at the opening, the smaller values of each of the top and bottom struts were added together and listed in Table 6.2.3.1. Also shown in this table are the test results for shear in each strut and total shear at the opening. The procedure used to obtain test results for strut shear is outlined in Section 3.3.

For all beams in the study, the shear in the bottom as limited by the strut shear capacity rather than l capacity. In all but two cases flexural capacity ed the shear carrying capacity of the top strut. In cases the total calculated shear capacity at the ning was greater than the total shear at failure. ever it should be noted that in only one case, BEAM B1, failure associated with formation of a full hinging chanism. In all other cases, partial hinging mechanisms re developed at the opening with failure of the beam occurring by flexure at midspan or by shear in the end shear span.

In the case of BEAM B1, the shear at failure was 86% of the calculated shear carrying capacity. The top strut

attained 84% of its calculated shear carrying capacity while the bottom strut attained 89% of its calculated shear carrying capacity.

In all other beams failure occurred before the top strut reached its load-carrying capacity whereas at failure the bottom strut shear was in the vicinity of its calculated value. As outlined in Chapter 3, for all beams the bottom strut was extensively cracked at failure and it is apparent that the bottom strut was at or close to its load-carrying capacity when failure occurred. The test results therefore provide an indication of the accuracy of the ACI design equation for calculating capacity of the bottom strut.

Statistical analysis of the ratios of test-to-calculated capacity values of bottom strut shear indicates a mean value of 1.11 with a coefficient of variation of 30% and a range of 0.69 to 1.90. The statistics are given in Table 6.2.3.2. Since the ACI equation is semi-empirical and is intended to be a conservative estimate of shear capacity based on test results, the relatively high coefficient of variation is not unexpected. However one would expect not only that the mean value would be greater than unity as is the case, but that all values would be greater than unity. For those beams with test-to-calculated ratios less than unity (B1, C1, C2, D1, B4), the following comments are related to the apparent discrepancy.

BEAM D1 was provided with diagonal bars at the corners of openings to control cracking at the lower and upper tension corners. As a result BEAM D1 sustained significantly less damage in the form of wide cracks than those beams without the extra diagonal bars. It is quite likely therefore that the bottom strut had some reserve capacity to carry additional shear at the load causing flexural failure at midspan.

BEAM B4 tested by Barney[4] failed by strand fracture at the bottom strut. As was the case for BEAM D1 it is therefore likely that the lower strut had reserve shear capacity at the load causing failure by strand fracture. BEAMS B1, C1 and C2 sustained significant damage in the bottom struts due to wide cracks at the lower tension corner, while the top strut was still capable of carrying additional load. The low shears obtained from test results are most likely the result of softening of response due to extensive cracking causing transfer of shear to the top strut, and premature failure of the bottom strut.

These results suggest that, if premature failure of the bottom strut is prevented by the proper detailing in the vicinity of the opening, the bottom strut can be expected to carry its calculated shear capacity based on the semi-empirical ACI design equations. The remaining design shear can then be assigned to the top strut. For

comparison, in Barney's proposed design procedure[4] for high values of tensile force in the bottom strut such as those in the present test program no shear would be assigned to the bottom strut and the total shear would have to be resisted by the top strut.

6.2.4 Detailing to Prevent Brittle Failure.

Based on the failure modes observed in this test program and in test programs of other authors[4,16] it is clear that proper reinforcement detailing around the opening is needed to avoid premature failure.

Widening and extension of inclined cracks at the tension corners of the opening can be efficiently restricted by placing inclined bars adjacent to each side of the opening. The force to be resisted by the diagonal bars can be determined by equilibrium conditions for the free body diagram shown in Fig. 6.2.4.1. For the sake of simplification the shear force V' is neglected. The tensile force T_i to be carried by inclined bars is determined as follows:

$$\Sigma F_v = 0$$

$$T_i = \frac{V_b}{\cos \alpha} \qquad\qquad (6.8)$$

where,

V_b -shear force at the corner of the opening

α -angle of inclination of the diagonal bar to the vertical.

The inclined bars are placed at the lower and upper tension corners of the opening as shown in Fig. 6.2.4.2. The angle of inclination of the crack formed at the corner of the opening varied between 40° and 60° for the specimens of Series B and Series C. For the specimens in Series D, which were provided with inclined bars, that angle varied between 80° and 85°. The main advantage of placing the bars at a 45° angle is that they can intercept cracks emanating from the corner over a wide range of angle of inclination. The tendency is for cracking to occur at approximately 45°. The diagonal bars will therefore cross the potential crack at approximately 90°. This is the most desirable situation since immediately after cracking the bar is subjected to direct tension.

Since the main objective is to control crack propagation and crack width, the steel stress should be kept to a relatively low level rather than allowing the steel to yield at ultimate load[2]. For the beams in the test program the shear in the bottom strut ranged from 2.38

kips to 6.78 kips. Assuming a value of 5 kips as being representative, the steel stress in the diagonal bars at the ultimate load level is:

$$f_s = \frac{V_b}{A_s \cos\alpha} = \frac{5}{0.30 \times 0.707} = 23.5 \text{ ksi} \qquad (6.9)$$

The beams in Series D exhibited satisfactory behavior at this stress level, therefore a steel stress of 24 ksi is recommended for design. Note that this is the permissable service load stress specified in the ACI Buiding Code (318-77) for the Alternate Design Method (design using unfactored service loads).

6.3 Serviceability

Large web openings may produce a significant decrease in beam stiffness as compared to a beam without openings. Further decrease in stiffness will occur when cracking occurs. Deflections may therefore become a critical design consideration for beams with large web openings.

In Chapter 5, it was shown that the analytical model developed based on a truss analogy can predict deflections with reasonable accuracy at service load levels and up to loads causing yielding. Such a model however is too complex for routine design. In the following, a simpler

approach is developed based on standard beam analysis procedures.

The midspan deflection caused by live load is estimated as the result of adding the deflection caused by prestress and the deflection caused by live load. Each of these deflections has two components:

1 - flexural deformation of specimen as a whole

2 - additional deflection due to localized bending of the struts

Using moment-area principles, according to Fig. 6.3.1 midspan deflection due to prestress is determined to be:

$$\Delta p = \frac{1}{20} \frac{P_e e}{EI_2} [(4L-10\ell)(8L-5\ell)+(6L-10\ell)(3L-5\ell)+\frac{1}{10} \frac{P_e e}{EI_2} \ell(L+2\ell)$$

(6.10)

L- span length

ℓ- opening length

I_2- gross moment of inertia of a section through the opening

I_1- gross moment of inertia of beam section

P_e- effective prestress force

e- strand eccentricity

Since in this test program all specimens were provided with straight strands, shear in the struts due to prestress is zero. Consequently the additional deflection due to

localized bending of the struts caused by prestress is also zero.

According to Fig. 6.3.2 midspan deflection of the specimen as a whole due to lateral loading is given by the following expression:

$$\Delta_\ell =$$

$$\frac{2}{75}\frac{M_1}{EI_1}L^2 + \frac{1}{20}\frac{M_1}{EI_e}(2L-10\ell)(5L-5\ell) + \frac{2}{30}\frac{(M_2-M_1)}{EI_e}(L-5\ell)(3L-5\ell) +$$

$$+\frac{M_2}{EI_{cr}}(\ell)(3L) + \frac{2}{30}\frac{(M_3-M_2)}{I_{cr}}(\ell)(9L+5\ell) + \frac{1}{20}\frac{M_3}{EI_e}(2L-10\ell)(7L+5\ell) +$$

$$+\frac{2}{30}\frac{(M_4-M_3)}{EI_e}(L-5\ell)(5L) + \frac{9}{200}M_4L^2$$

$$(6.11)$$

where,

E — concrete modulus of elasticity

I_e — effective moment of inertia of beam section

I_g — gross moment of inertia of beam section

I_{cr} — cracked moment of inertia of a section through the opening

According to Fig. 6.3.3 additional deflection at midspan due to localized bending moment of the struts is given by:

$$\Delta_s = \frac{V\ell^3}{12E(I_{b_e} + I_{t_e})} \qquad (6.12)$$

where,

V - shear at the opening due to applied live load

E - modulus of elasticity of concrete

ℓ - opening length

I_{b_e} - bottom strut effective moment of inertia

I_{t_e} - top strut effective moment of inertia

The total deflection at midspan caused by live load is given by:

$$\Delta_m = -\Delta_p + \Delta_\ell + \Delta_s \qquad (6.13)$$

Table 6.3.1. presents predicted and measured deflections at midspan and the ratio of measured-to-predicted deflection at the service load level for all specimens. The mean value of the ratio of test-to-predicted deflections was found to be 1.04. A standard deviation of 0.11 was found with a corresponding coefficient of variation of 11%. This level of correlation can be compared to the conclusion of ACI Committee 435[3] that under controlled laboratory conditions there is a 90% chance that the deflection of a particular beam will be within the range of 20% less than to 30% more than the

calculated value using the effective moment of inertia approach as outlined in the ACI Building Code (318-77).

6.4 Proposed Design Procedure

Based on the experimental and analytical results for prestressed concrete T-beams with web openings described in this thesis, the following design procedure is proposed. The proposed design procedure is limited to slender beams with no significant concentrated loads applied to the top strut, and beams for which slenderness effects in the top strut are not significant.

1. Design the beam for flexure and shear according to the ACI Building Code (318-77) or Canadian Standard A23.3 as if the beam contained no web openings.

2. Insure that openings are placed outside the code specified strand embedment length.

3. Provide in the bottom strut, vertical stirrups of the same size and spacing as the beam without openings. Ensure that a vertical stirrup is placed in the solid section immediately adjacent to each side of the opening.

4. Determine axial forces in the struts from equilibrium conditions in the middle section of the opening, as outlined in Section 6.2.2.

5. Determine moment capacities in the top and bottom struts corresponding to the calculated axial forces based on axial force-moment interaction.

6. Determine, from equilibrium considerations, shear forces corresponding to moment capacities calculated in step 5.

7. Determine shear capacities of the top and bottom struts according to the design equations for members subjected to axial force as provided by ACI Building Code (318-77) or Canadian Standard A23.3.

8. Determine the shear that can be transferred by each strut as the smaller of the values calculated in steps 6 and 7.

9. Check that the total applied shear does not exceed the total shear capacity as determined from step 8. Increase the shear-carrying capacities of the struts if required.

10. Provide inclined reinforcing bars at the upper and lower tension corners of the opening to carry the factored shear in each strut at a stress of 24 ksi as outlined in Section 6.2.4.

11. Check deflections at service load levels. Deflections can be estimated by means of the truss analysis or the beam analysis developed in this thesis.

The major difference between the design procedure proposed herein and that proposed by Barney[4] is in the assignment of shear carrying capacity to the top and bottom struts. The procedure proposed by Barney is conservative and involves simpler calculations, primarily because there is no calculation of axial force - moment interaction required. In many cases the shear-carrying capacity of the bottom strut would be ignored by Barney's procedure and the total shear would be assigned to the top strut. However from Barney's tests and the present test program it is clear that a significant amount of shear can be carried by the bottom strut. The procedure proposed in this thesis provides a rational approach to assigning a portion of shear to the bottom strut.

It has also been shown that ductile behavior of the beam can be assured by attention to detailing at the corners of the opening. In the present procedure a rational approach has been proposed for determining the amount of reinforcement required.

Finally, two approaches have been proposed for estimating deflections of beams with openings. Since openings tend to decrease the stiffness of the beam, deflection may be a critical design consideration.

Table 6.2.3.1 Shear Force in Top and Bottom Struts.

Specimen	Shear Corresponding to Strut Flexural Capacity (kips) by Strain-Compatibility(24)		Shear Corresponding to Strut Shear Capacity (kips)[1] by ACI		Total Calculated Shear Capacity at Opening (kips)	Test Results Shear (kips)		
	Top Strut	Bottom Strut	Top Strut	Bottom Strut		Top Strut	Bottom Strut	Total
BEAM B1	7.15	7.21	15.80	5.70	12.85	6.0	5.03	11.03
BEAM B2	10.15	9.71	15.68	4.69	14.84	6.21	5.19	11.40
BEAM B3	16.35	16.16	15.12	3.57	18.69	6.82	4.63	11.45
BEAM C1	9.37	7.59	10.0	3.46	12.83	7.62	2.38	10.0
BEAM C2	13.64	9.84	9.39	2.81	12.20	7.80	2.77	10.57
BEAM C3	19.53	16.49	8.43	2.14	10.57	7.40	3.10	10.50
BEAM D1	7.11	7.63	15.30	5.70	12.81	5.45	4.95	10.40
BEAM D2	9.48	10.53	14.53	4.69	14.17	5.60	4.90	10.50
BEAM D3	16.08	17.10	14.86	3.57	18.43	4.02	6.78	10.80
BEAM B4	10.15	17.20	29.78	2.63	12.78	6.00	2.05	12.08
BEAM B5	6.19	12.80	28.20	5.34	11.53	4.75	5.94	10.70
BEAM B7	7.18	14.09	30.0	5.57	12.75	5.69	6.30	11.99

Table 6.2.3.2   Statistics for Test-to-Calculated Capacity
Values of Shear in the Bottom Strut.

Specimen	$V_{calc.}$ [1]	V_{test} [2]	$V_{test}/V_{calc.}$
BEAM B1	5.70	5.03	0.89 [3]
BEAM B2	4.69	5.19	1.11 [4]
BEAM B3	3.57	4.63	1.30 [4]
BEAM C1	3.46	2.38	0.69 [4]
BEAM C2	2.81	2.77	0.99 [4]
BEAM C3	2.14	3.10	1.45 [4]
BEAM D1	5.70	4.95	0.87 [4]
BEAM D2	4.69	4.90	1.04 [4]
BEAM D3	3.57	6.78	1.90 [4]
BEAM B4	2.63	2.05	0.79 [4]
BEAM B5	5.34	5.94	1.11 [3]
BEAM B7	5.57	6.30	1.13 [4]
Mean Value			1.11
Standard Deviation			0.33
Coefficient of Variation			30%

Notes:

(1) $V_{calc.}$ is the calculated shear capacity based on the ACI design equation given in Section 6.2.2.2. This value is intended to provide a conservative estimate of the shear capacity of the member rather than a prediction of the actual shear strength.

(2) V_{test} is the shear in the bottom strut at failure based on test results.

(3) Failure occurred at the opening.

(4) Failure occurred away from the opening.

Table ... flection at Midspan at Service Load Level

Section	Deflection at Midspan		
	Predicted	Test	Test/Predicted
BEAM B1	1.54	1.63	1.05
BEAM B2	1.35	1.60	1.18
BEAM B3	1.25	1.40	1.12
BEAM C1	1.46	1.30	0.89
BEAM C2	1.32	1.25	0.95
BEAM C3	1.26	1.15	0.92
BEAM D1	1.28	1.20	0.93
BEAM D2	1.13	1.15	1.01
D3	0.95	0.90	0.94
BEAM B4	1.40	1.75	1.25
BEAM B5	2.05	2.37	1.15
BEAM B7	1.98	2.12	1.07
Mean Value			1.04
Standard Deviation			0.11
Coefficient of Variation			11%

Full hinging mechanism
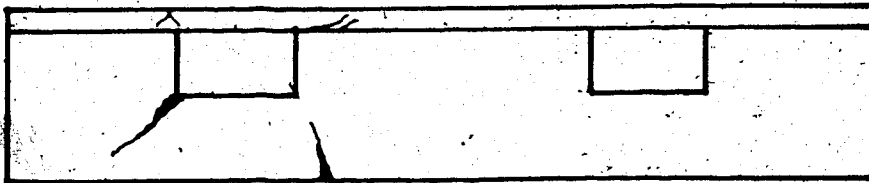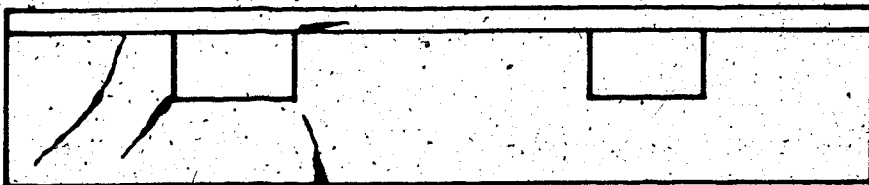
Beams:
B1

Partial hinging mechanism

Beams:
B2, B3
C1, C3
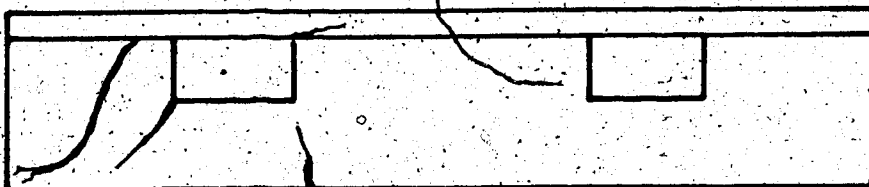
Shear failure followed by strand debonding

Beams:
A1, C2

Flexural failure at midspan

Beams:
A2, D1
D2, D3

Figure 6.2.1.1 Primary Crack Pattern Associated with
Failure Modes Observed in Tests.
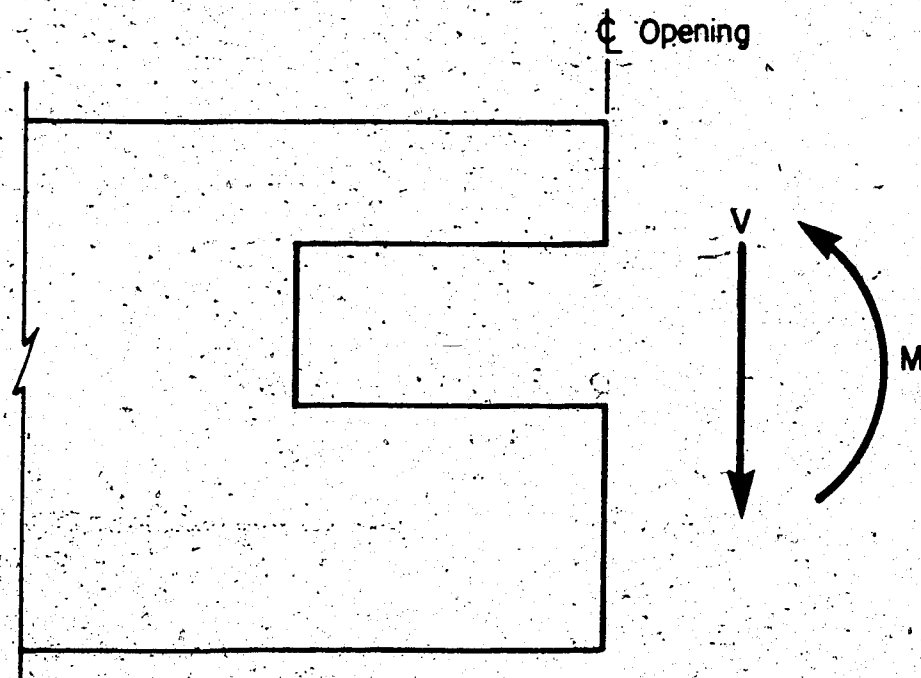
Shear and Moment at Center Line of Opening Due to Applied Loads
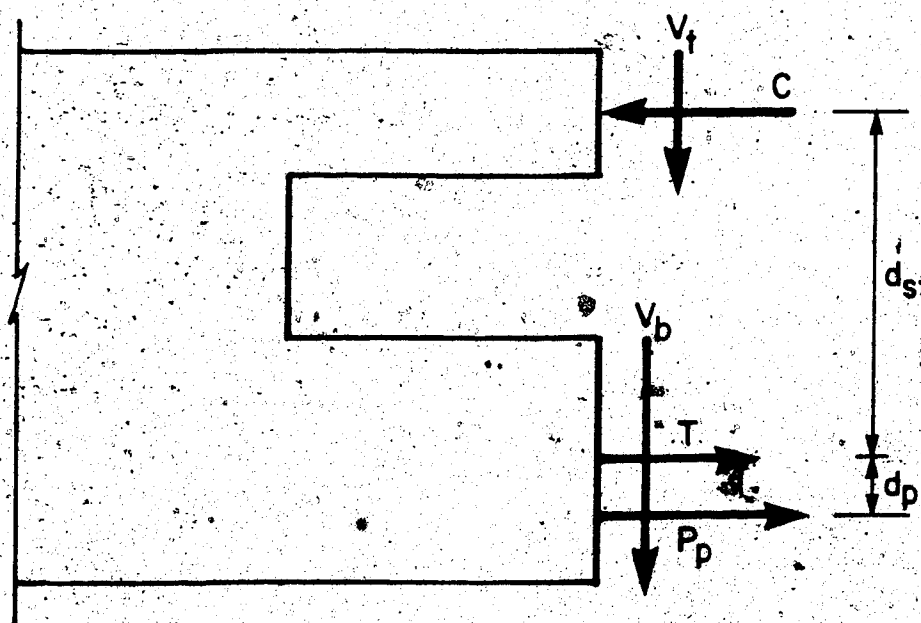
Forces in Top and Bottom Struts at Center Line of Opening

Figure 6.2.2.1   Forces at Middle Section of the Opening.
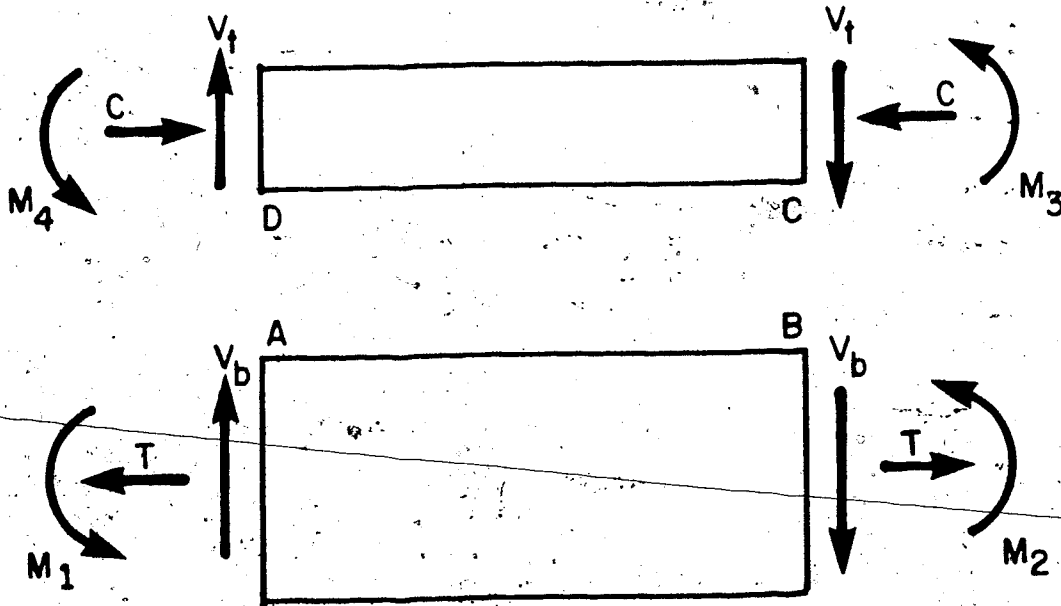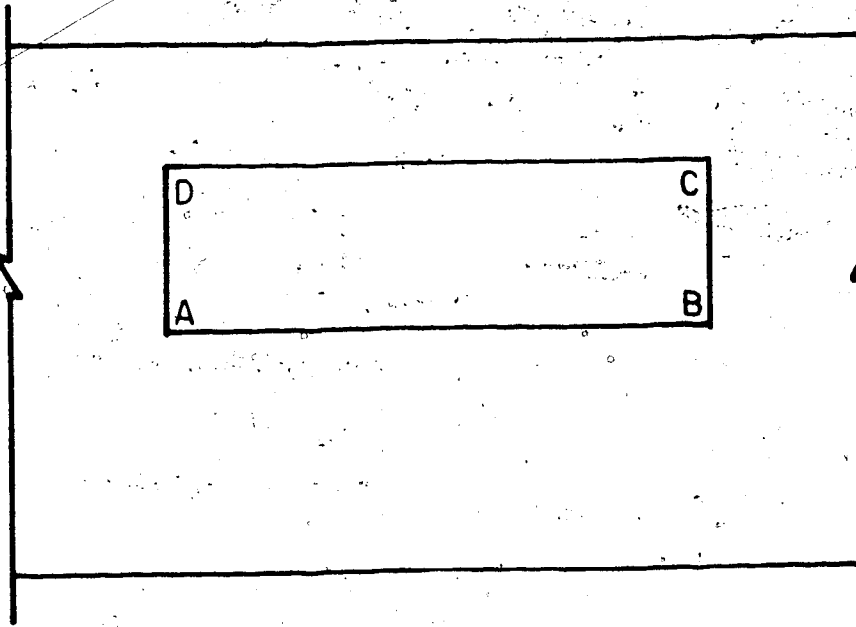
Figure 6.2.2.1.1 Moment Capacities at the Struts
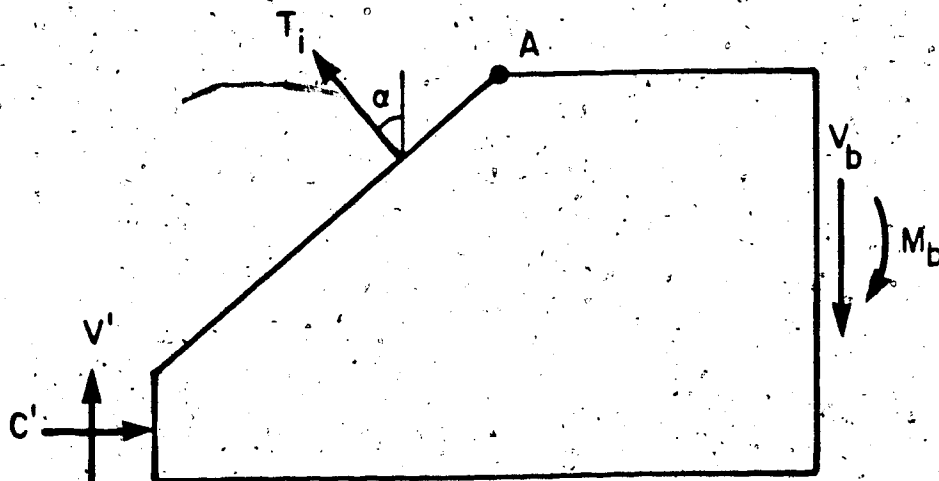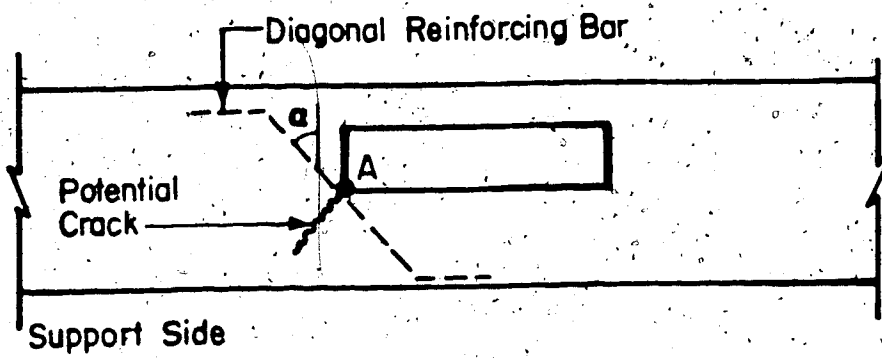
Figure 6.2.4.1 Free Body Diagram for the Cracked Bottom Strut.
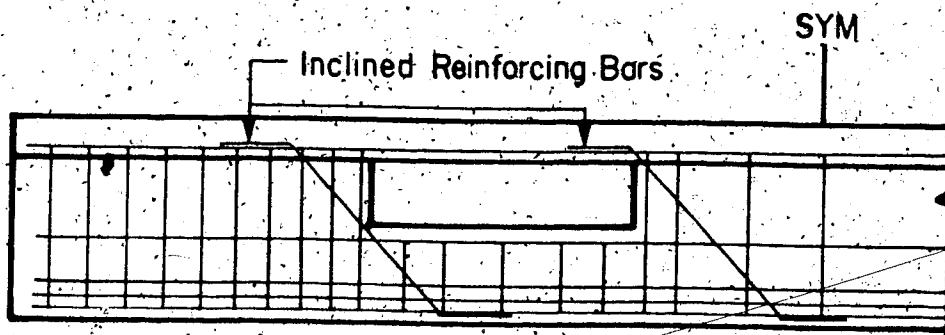
Figure 6.2.4.2   Inclined Reinforcing Bars at the Corners
of the Opening
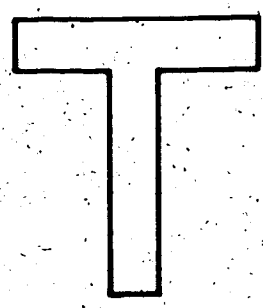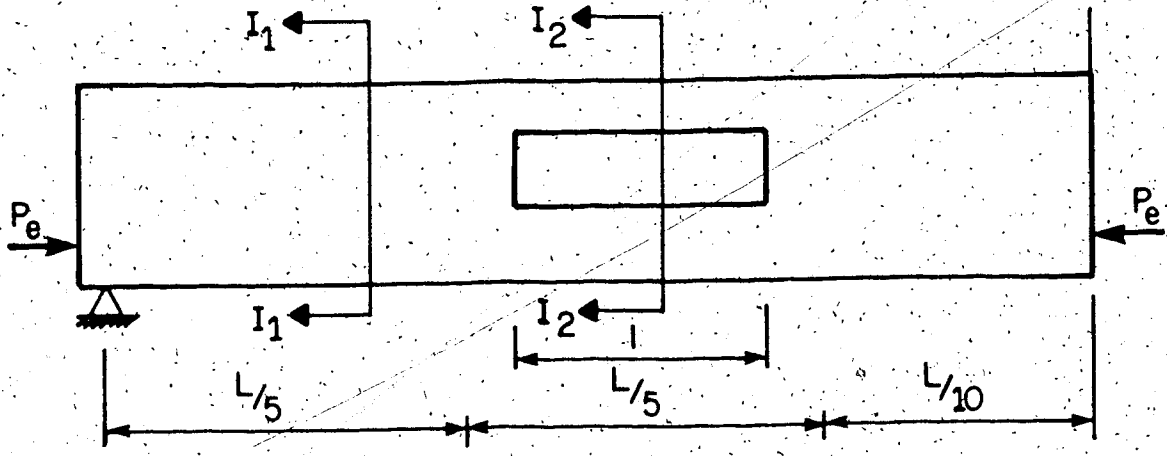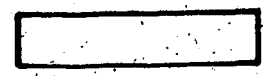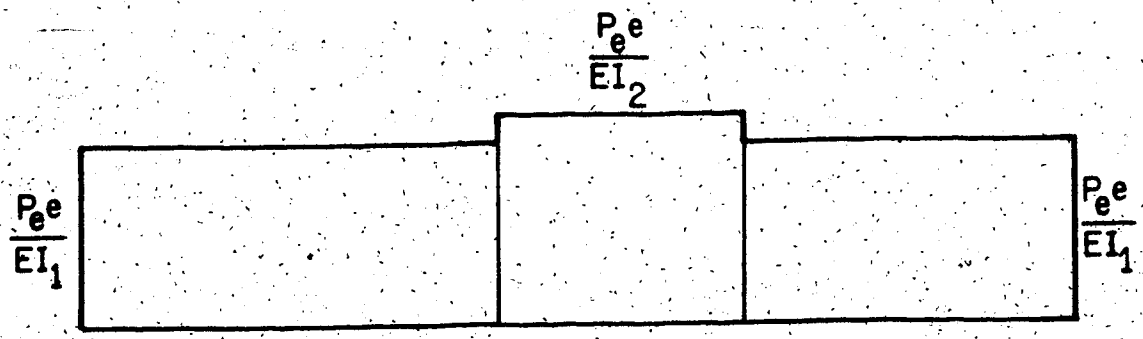
Figure 6.3.1   M/EI Diagram Due to Prestress.
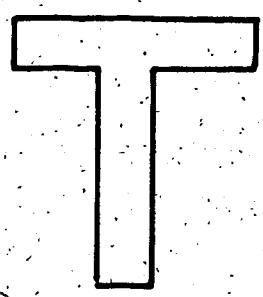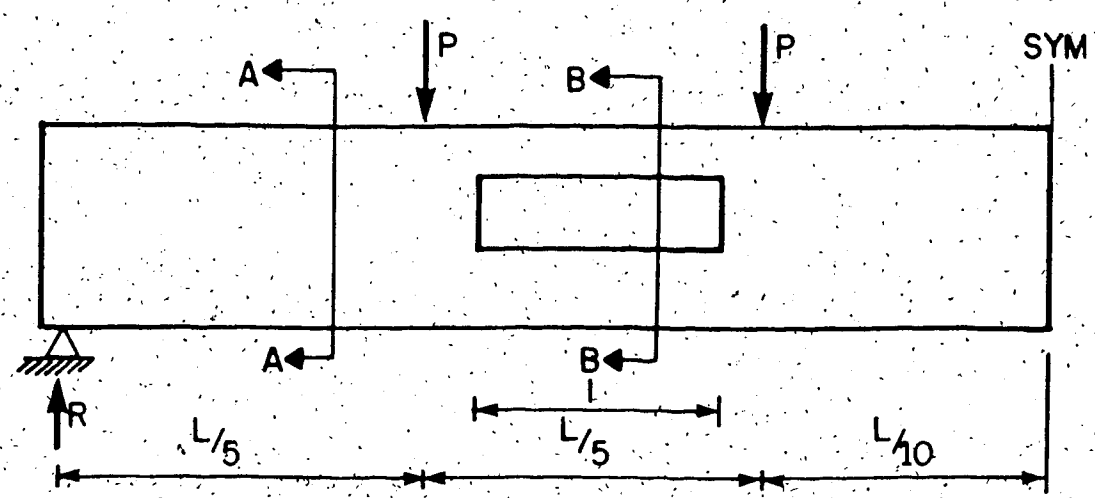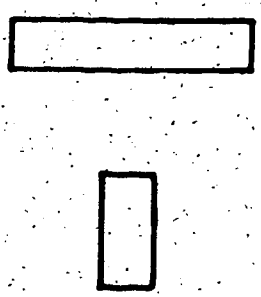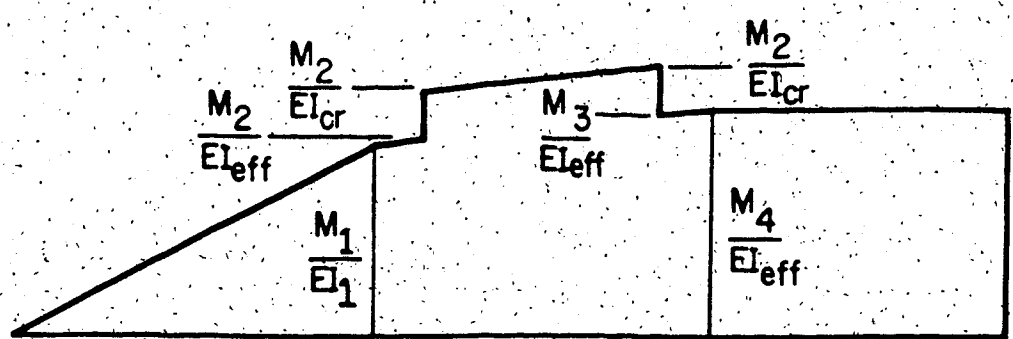
Figure 6.3.2   M/EI Diagram Due to Applied Load.
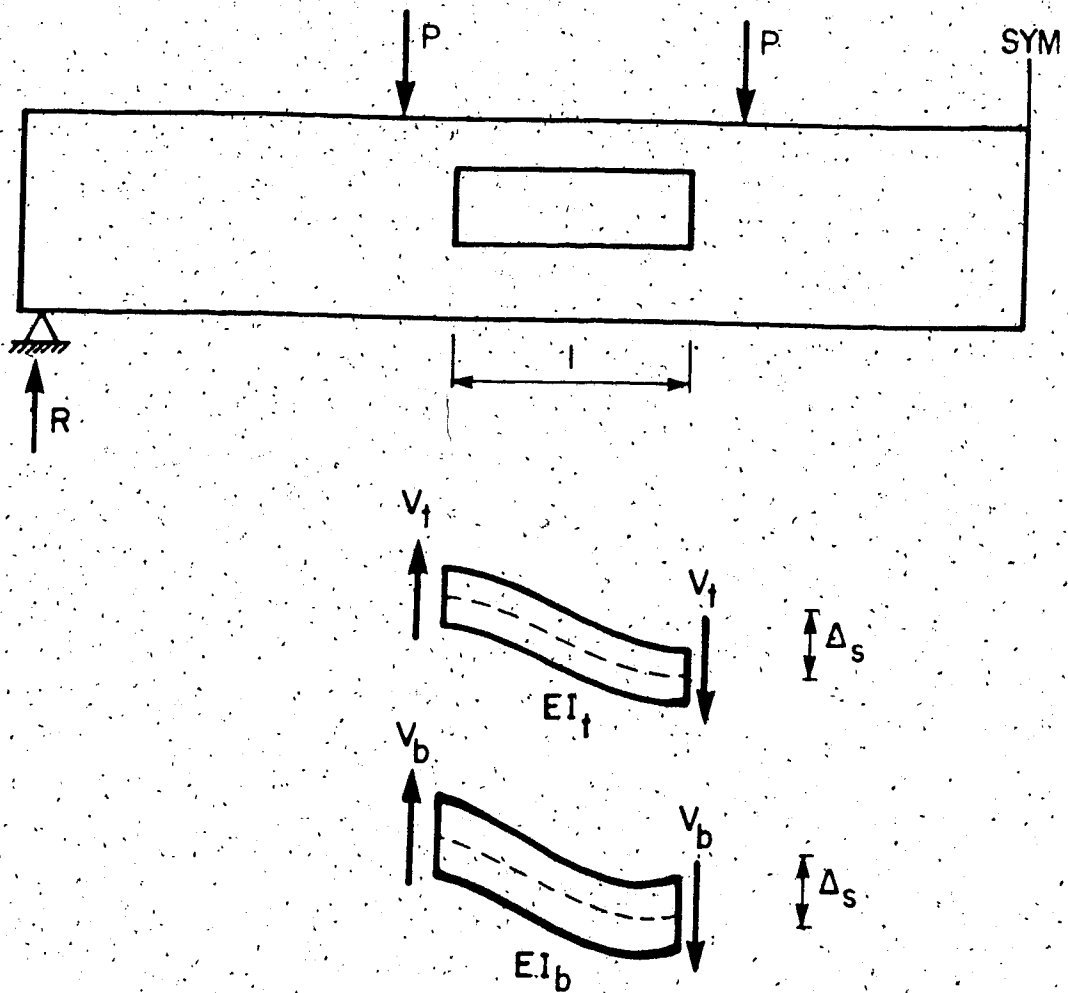
Figure 6.3.3   Localized Deformation of Struts.

7. SUMMARY CONCLUSIONS AND RECOMMENDATIONS

7.1 Summary

A combined experimental and analytical investigation was undertaken to study the behavior of prestressed concrete T-beams with web openings and to provide a basis for design recommendations. The experimental program consisted of tests to failure of eleven beams, nine with web openings and two without web openings. In the analytical investigation a truss analysis was developed to trace the load-deflection response of the beams into the post-cracking range, up to first yielding of the reinforcement. The test specimens were designed for flexure and shear according to the requirements of the ACI Building Code (318-77)[1] as beams without openings subjected to four point loads. Openings were provided in the webs and web reinforcement consisting of vertical stirrups, of the same size and spacing as the beam without openings, was provided in the bottom strut. The specimens were instrumented to obtain strain and deflection readings throughout the full load range up to failure.

Of primary interest in the test program were the modes of failure, distribution of shear between top and bottom struts, and load-deflection response. Effects on behavior of length of opening, depth of top strut, and reinforcement details around the opening were studied.

A truss model was developed to trace the load-deflection response up to the load causing post yield using Branson's effective moment of inertia concept to model the degradation of flexural stiffness with progressive cracking.

Based on the results of this investigation a design procedure that assigns shear forces to the top and bottom struts on a rational basis is proposed. The proposed procedure also contains recommendations for detailing around the openings, and deflection calculations.

7.2 Conclusions

Based on the observed behavior of eleven prestressed concrete beams with large rectangular openings and on the analytical model developed, the following conclusions are presented:

1. Failure modes observed in this test program were:

a) full hinging mechanism involving two hinges in each strut,

b) partial hinging mechanism consisting of two hinges in the bottom strut and one hinge in the top strut followed by a shear failure away from the opening,

c) shear failure at solid shear span followed by strand debonding,

d) flexural failure at midspan.

2. Opening length affects the extent of cracking in the struts. As the length of opening increases, the local strut moments also increase, causing an increase in cracking. The slope of the load-deflection curve is smaller for specimens provided with longer openings due to the reduced flexural stiffness in the vicinity of the struts. Opening length also affects the shear distribution between the top and bottom struts. After cracking of the bottom strut a redistribution of shear takes place involving transfer of shear from the bottom to the top strut. The amount of shear transferred decreased as the opening length increased.

3. Vertical position of opening affected development of cracking in the struts. When the opening is shifted

towards the bottom of the specimen cracks form at the bottom strut at lower loads, reflecting a reduction in the flexural stiffness of the bottom strut. Vertical position of the opening also affected the shear distribution of the struts. If the bottom strut has its depth reduced, the top strut carries a larger portion of the total shear. This reflects a greater ratio of flexural stiffness of the top strut to the bottom strut.

4. The shear reinforcement details at the opening significantly affected the propagation of cracks at the corners of the opening, the shear distribution between the top and bottom struts, and failure mode. If the web shear reinforcement at the opening is not effective in limiting the propagation of cracks at the corners of the opening, web-flange separation and loss of bond occur causing brittle failure. Proper detailing of reinforcement around the opening is essential to prevent brittle failure and widening of cracks. Inclined reinforcement placed at the tension corners of the opening is shown to be effective in restricting extension and widening of the inclined crack formed at the corner of the opening, preserving the struts connection and allowing redistribution of forces in the struts.

5. Based on the comparisons between calculated flexural and shear capacity of the struts and the portion of shear carried by each strut, it is concluded that a reasonable estimate of the shear carried by the bottom strut is that corresponding to its calculated shear capacity. Consequently the rest of total shear at the opening is carried by the top strut.

6. Comparison between analytical and experimental results indicates that the proposed truss model provides an efficient method for determining the load-deflection response of prestressed concrete beams with large rectangular openings. The effective moment of inertia concept as applicable to the truss model makes the procedure valid only for loads in the service load range although good agreement was obtained between analytical and experimental results up to the load at first yield.

7. Large web openings may produce a significant decrease in beam stiffness compared to a beam without openings, particularly if cracking occurs at the service load levels. Deflections may therefore become a critical design consideration for beams with large web

openings. Although the analytical model based on a truss analogy can predict deflections with reasonable accuracy at working load levels, such a model is considered too complex for routine design.

8. A simpler approach based on standard beam analysis procedure, considering flexural deformations of the beam as a whole and additional deflection due to localized bending of the struts, also predicts deflections with reasonable accuracy at the service load range.

7.3 Recommendations.

Based on the results of this investigation, recommendations for prestressed concrete beams with large web openings are presented.

7.3.1 Design Recommendations

A design procedure for prestressed concrete beams with web openings has been proposed in Chapter 6. The main features of the proposed procedure are as follows:

1. Determine shear-carrying capacities of the top and ... m struts and ensure that the capacity available is ...te to resist the total applied shear.

2. Provide reinforcement details at the corners of the
    opening to prevent rapid propagation and widening of
    cracks likely to cause premature brittle failure.

3. Check deflections, taking into account the reduced
    flexural capacity due to the web opening and local
    flexural deformation of the top and bottom struts.

7.3.2 Recommendations for Further Research

Additional experimental work could provide useful
information concerning a number of aspects of behavior
including:

1. Effects of multiple openings with narrow posts
    separating the openings.

2. Effectiveness of alternative reinforcing details at the
    corners of openings.

3. Limits on lengths of opening before stability of the
    compression strut becomes a significant consideration.

4. Effects of varying degrees of partial prestress.

Design of test specimens should attempt to induce
failure in the struts rather than in the solid section of
the beam.

The truss model could be extended to include the
effect of yielding of reinforcement and the effect of

diagonal web cracking. Detailed examination of load transfer mechanisms around corners of openings would be of interest using advanced finite element techniques.

REFERENCES

1. ACI Committee, "Building Code Requirements for Reinforced Concrete (ACI 318-77), American Concrete Institute, Detroit, Michigan, 1977.

2. ACI Committee 224, "Control of Cracking in Concrete Structures", Concrete International, October 1980, V.2, No. 10, pp. 35-76.

3. ACI Committee 435, "Variability of Deflections of Simply Supported Reinforced Concrete Beams", ACI Journal, Proceedings, V.69, No. 1, January 1972, pp. 29-35.

4. Barney, G., "Design of Prestressed Concrete Beams with Large Web Openings", Ph.D. Thesis, Northwestern University, Evanston, Illinois, 1975.

5. Branson, D.E., and Trost, H., "Unified Procedures for Predicting the Deflection and Centroidal Axis Location of Cracked Nonprestressed and Prestressed Concrete Members", ACI Journal, Proceedings, V. 79, No. 2, March-April 1982, pp. 119-130.

6. British Standard Code of Practice (CP 110-72), London, 1972.

7. Collins, M.P. and Mitchell, D., "Shear and Torsion Design of Prestressed and Non-prestressed Concrete

Beams", PCI Journal, September-October, 1980, pp. 32-100.

8. Dunbar, A., "Prestressed Concrete T-Beams Containing Large Circular Web Openings", M.Sc. Theis, University of Alberta, Edmonton, Alberta, 1976.

9. German Concrete Code, DIN 4227.

10. Hanson, J.M., "Square Openings in Webs of Continuous Joists", Research and Development Bulletin, Portland Cement Association, Skokie, Illinois, 1969.

11. LeBlanc, E.P., "Parallelogram Shaped Openings in Prestressed Concrete T-Beams", M.Sc. Thesis, University of Alberta, Edmonton, Alberta, 1971.

12. Linder, R.A., "Large Web Openings in Prestressed Concrete T-Beams", M.Sc. Thesis, University of Alberta, Edmonton, Alberta, 1976.

13. Lorentsen, M., "Holes in Reinforced Concrete Girders", Byggastaren, Volume 41, No. 7, July 1962. Translated from the Swedish by Portland Cement Association.

14. MacGregor, J.G., and Hanson, J.M., "Proposed Changes in Shear Provisions for Reinforced and Prestressed Concrete Beams", ACI Journal, Proceedings, V. 66, No. 4, April 1969, pp. 276-288.

15. Mattock, A.H., "Flexural Strength of Prestressed Concrete Sections by Programable Calculator", PCI Journal, V. 24, No. 1, January-February 1979, pp. 32-54.

16. Nasser, K., Acavalos, A., and Daniel, H.R., "Behavior and Design of Large Openings in Reinforced Concrete Beams", ACI Journal, V. 64, No. 1, January 1967.

17. Code for the Design of Concrete Structures for Buildings, (CAN-A23.3-M77), Canadian Standard Association, Ottawa, 1977.

18. New Zealand Standard (DZ 3101-80), Wellington, 1980.

19. Ragan, H.S., and Warwaruk, J., "Tee Members with Large Web Openings", PCI Journal, V. 12, No. 4, August 1967, pp. 52-65.

20. Ramey, M.R., and Tattershall, D.W., "Reinforced Requirements for Concrete Beams with Large Web Openings", Highway Research Record Number 428, 1973, pp. 5-21.

21. Sauve, J.G., "Prestressed Concrete Tee Beams with Large Web Openings", M.Sc. Thesis, University of Alberta, Edmonton, Alberta, 1970.

22. Schlaich, J., and Weischede, D., "Detailing Reinforced Concrete Structures", Proceedings of the Canadian Structural Concrete Conference, Toronto, 1981, pp. 171-198.

23. Segner, E.P., "Reinforcement Requirements for Girder Web Openings", ASCE Journal, Proceedings, V. 90, Paper 3919, June 1964, pp. 147-164.

24. Shushkewich, K.W., "Simplified Cracked Analysis", ACI Journal, V. 80, No. 48, Nov-Dec 1983, pp 526-531.

25. Somes, N.F., and Corley, W.G., "Circular Openings in Webs of Continuous Beams", ACI Journal, V. 1, 5P-42, 1974, pp. 359-398.

26. Task Committee on Finite Element Analysis of Reinforced Concrete Structures, "State-of-the-Art Report: Finite Element Analysis of Reinforced Concrete Structures", ASCE, 1982.

Conversion Factors - SI Equivalents

1 in. = 25.4 mm

1 lb (mass) = 0.4536 kg

1 lb (force) = 4.488 N

1 lb/sq in. = 6.895 kPa

1 kip = 444.8 N

1 kip/sq in. = 6.895 MPa

1 in.-kip = 0.1130 N m

APPENDIX A

DETAILS OF OPENING GEOMETRY AND REINFORCEMENT

236

SYM

20" 3 at 16.5"   5.8"   5.8"
          2 at 8" 2 at 13" 2 at 8" 2 at 17.4"
              348"

0.44 in. Dia. Bars

0.44 in. Dia. Bars   3/8" Dia. 250 k Strands
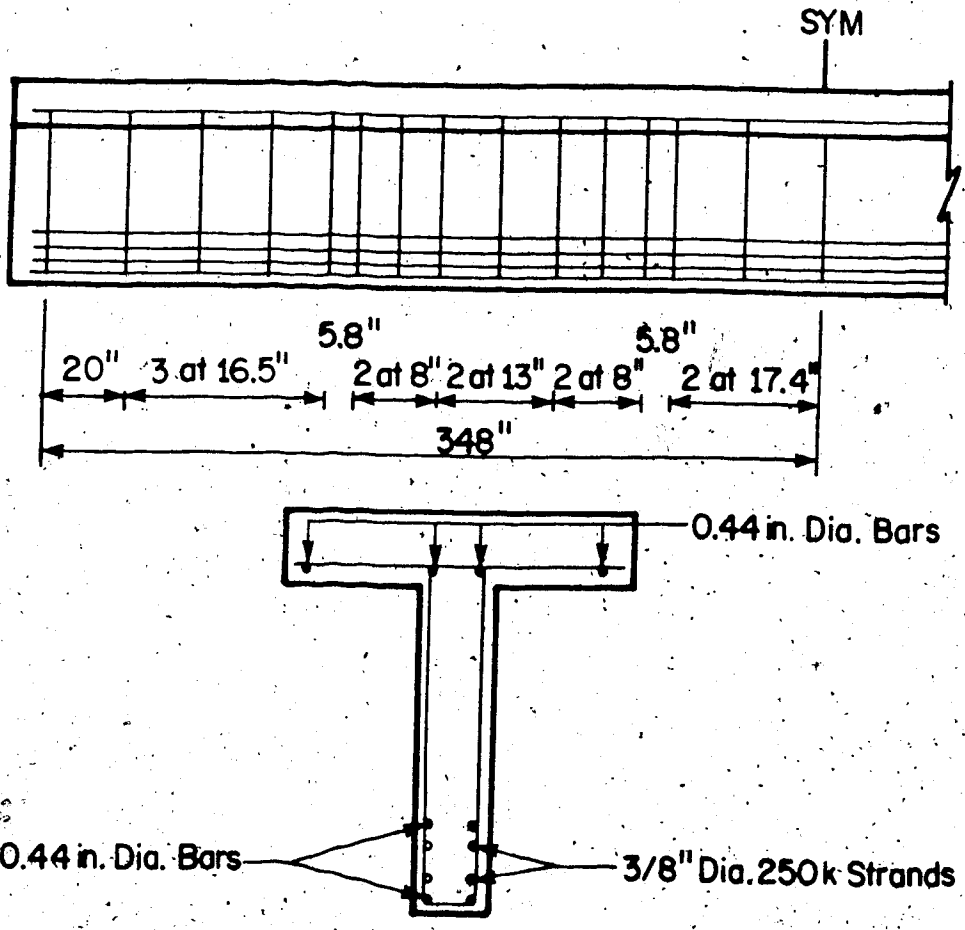
Figure A1 Reinforcement Details - BEAM A1

SYM

2 at 10"
6 at 8.25
5.8"
2 at 8" 2 at 13" 2 at 8"
5.8"
2 at 17.4"
348"

0.44 in. Dia. Bars

0.44 in. Dia. Bars

3/8" Dia. 250 k Strands
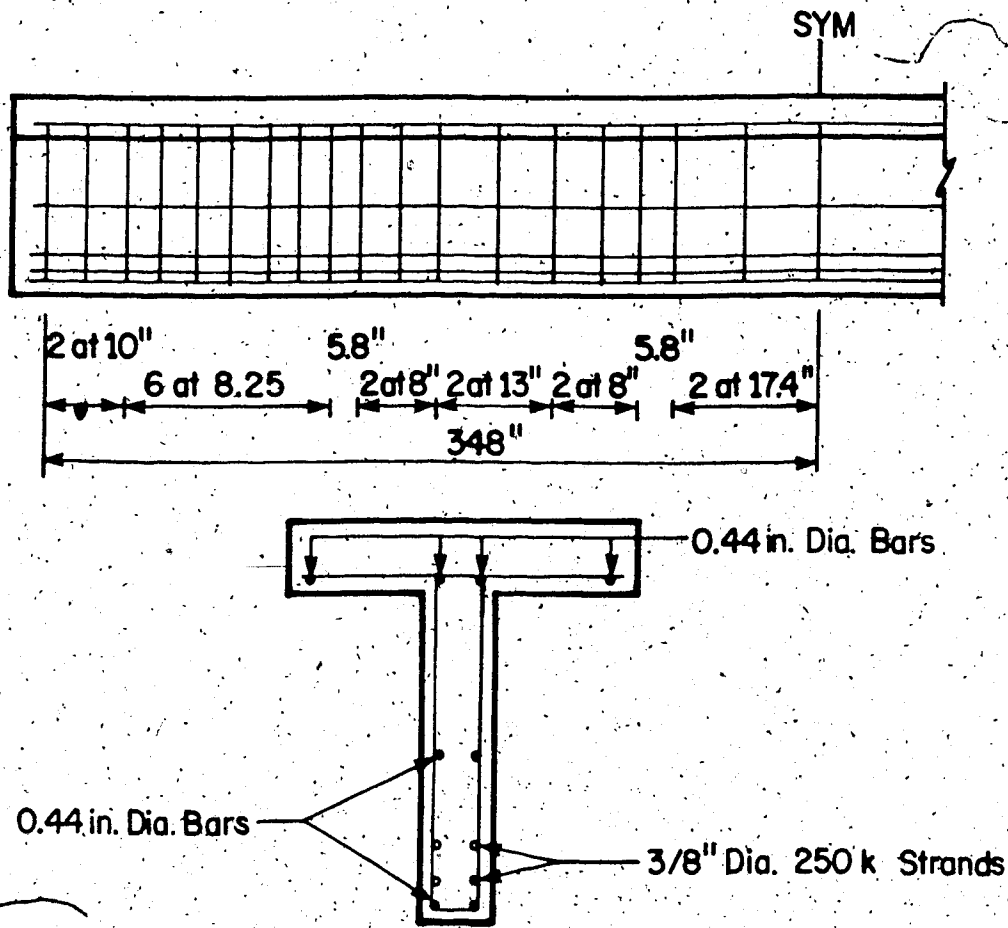
Figure A2 Reinforcement Details - BEAM A2
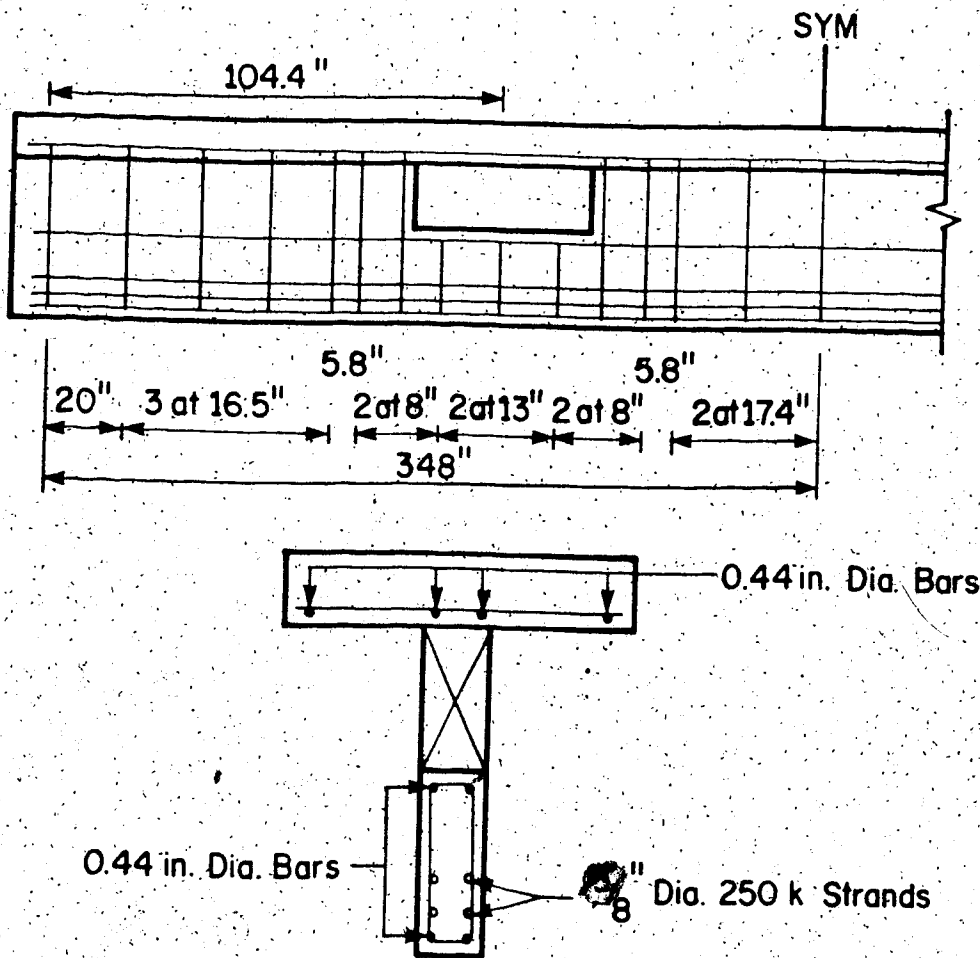
Figure A3   Reinforcement Details – BEAM B2
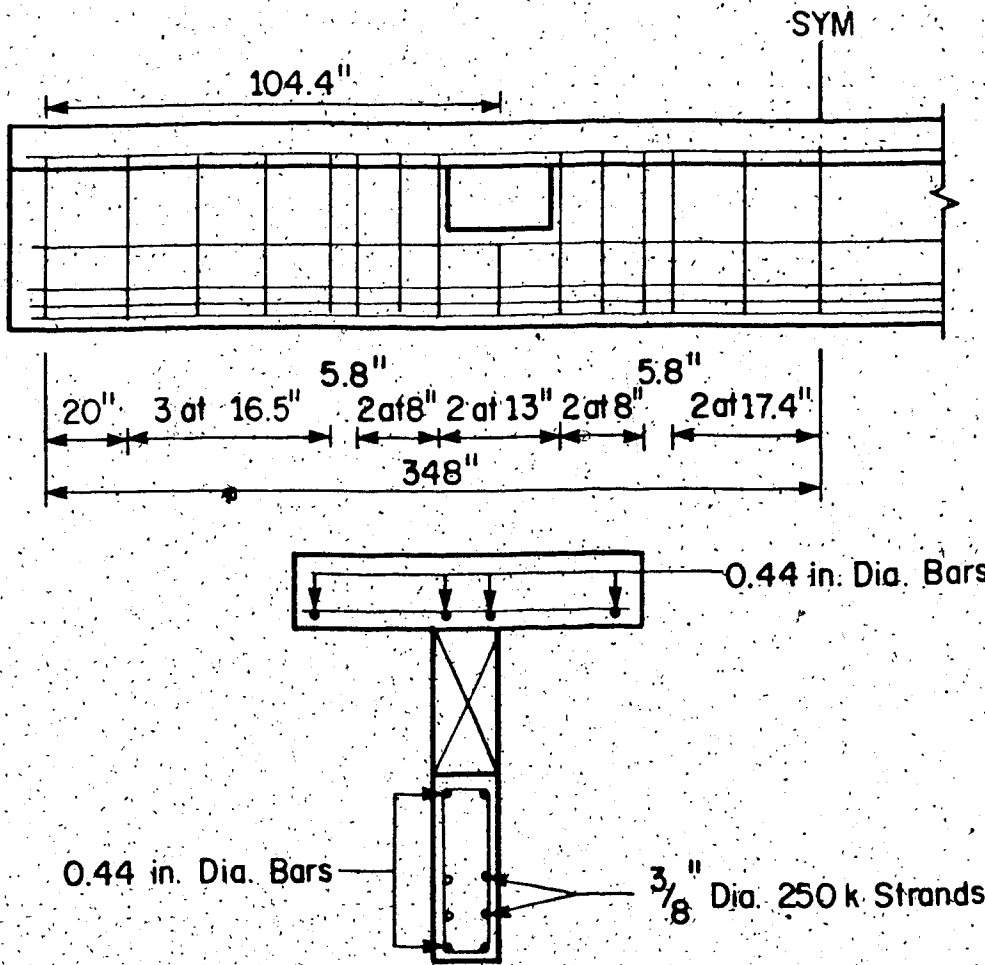
Figure A4   Reinforcement Details - BEAM B3
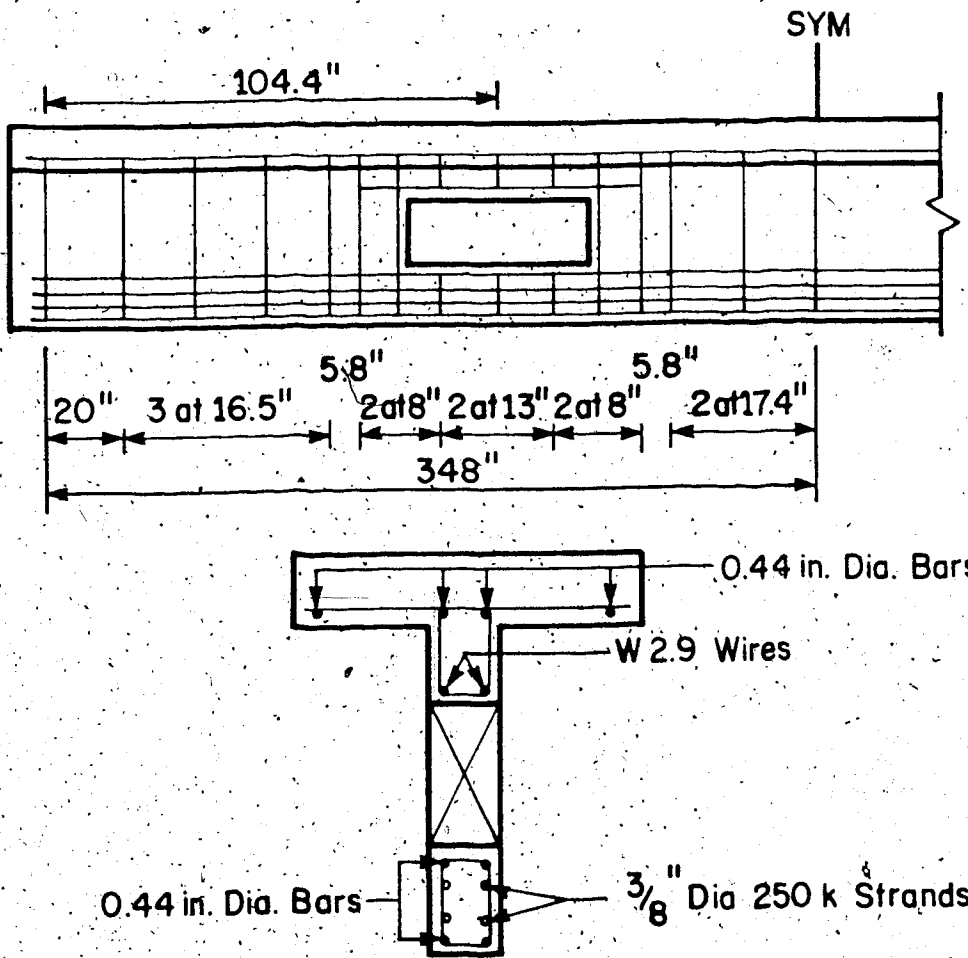
Figure A5   Reinforcement Details – BEAM C2
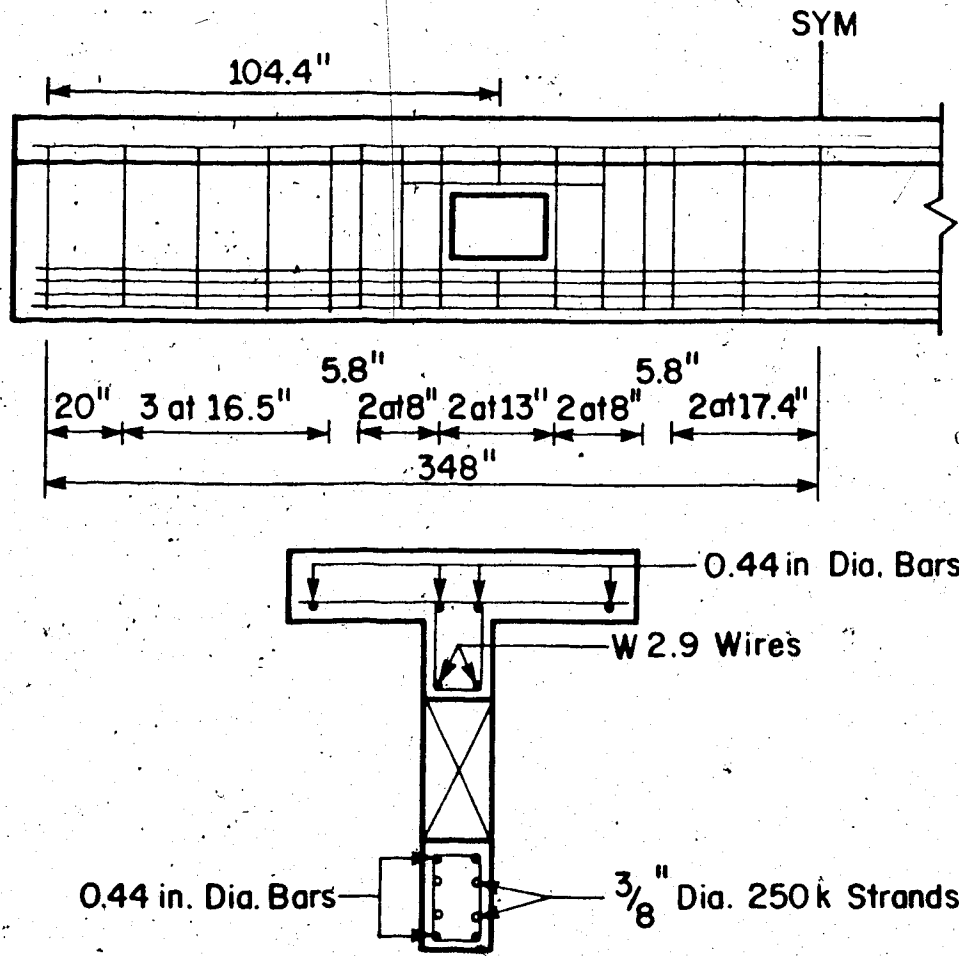
Figure A6 . Reinforcement Details - BEAM C3

104.4"

SYM

0.44 in. Dia. Bars

2 at 10"

6 at 8.25"   5.8"   2 at 8" 2 at 13" 2 at 8"   5.8"   2 at 17.4"

348"

0.44 in Dia. Bars

0.44 in. Dia. Bars

$\frac{3}{8}$" Dia. 250 k Strands
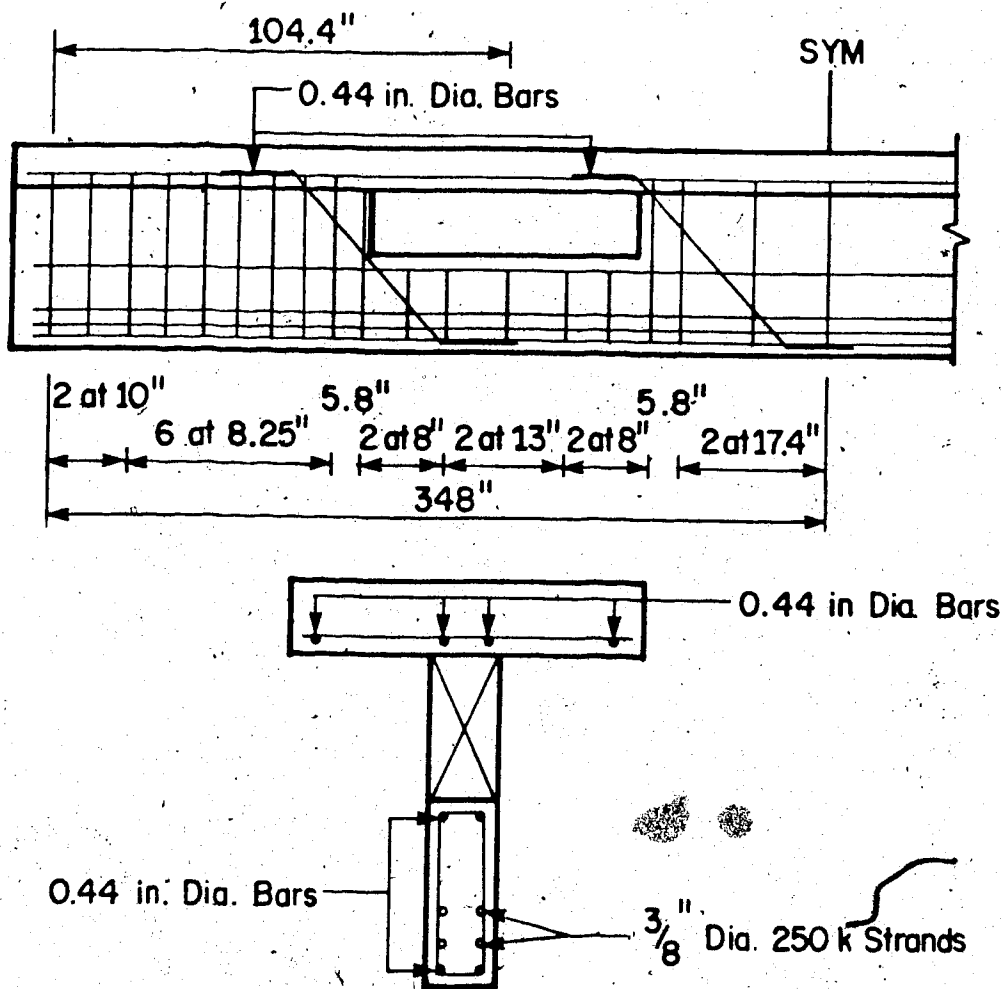
Figure A7   Reinforcement Details - BEAM D1
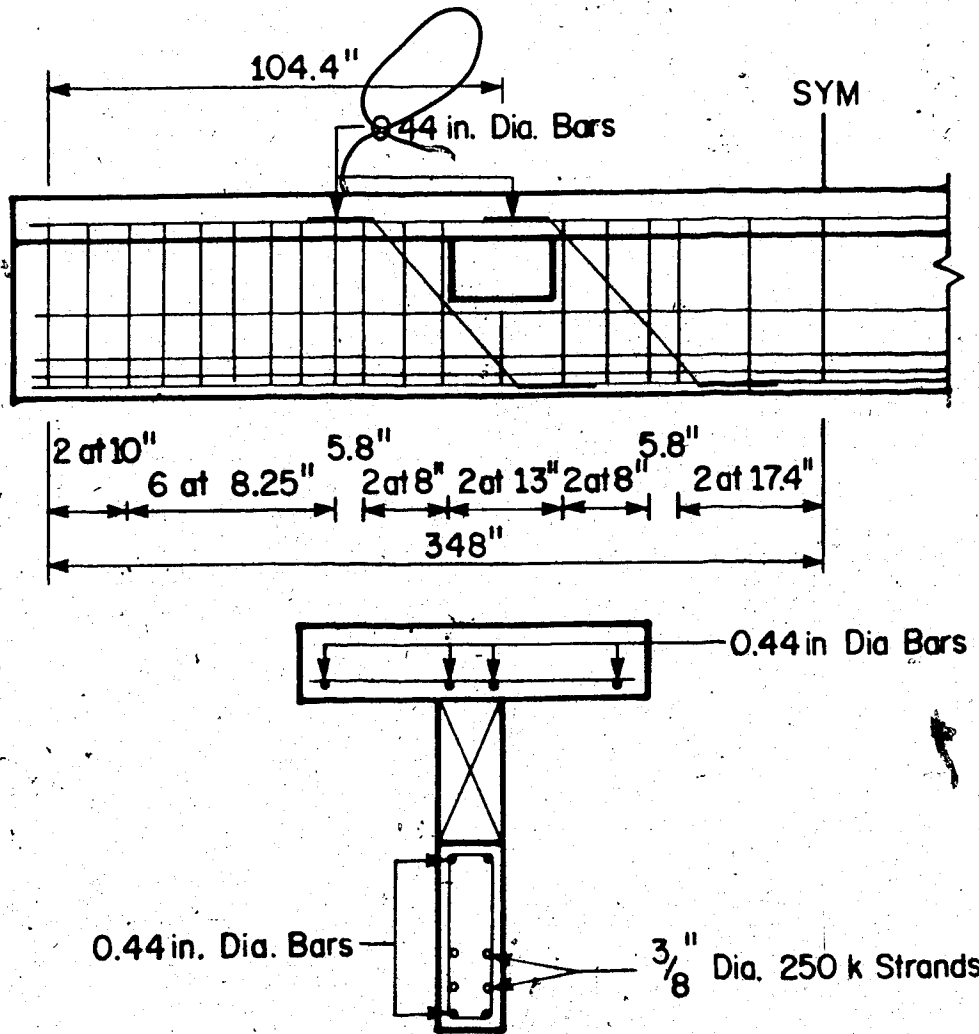
Figure A8   Reinforcement Details - BEAM D3

APPENDIX B

STRAIN-GAGE LOCATIONS FOR LONGITUDINAL REINFORCEMENT

DEMEC POINTS ON STIRRUPS AT THE OPENING

DEMEC POINTS ON TOP STRUT

245

10   12   15

40 x 8 in Opening

2   4

5   7
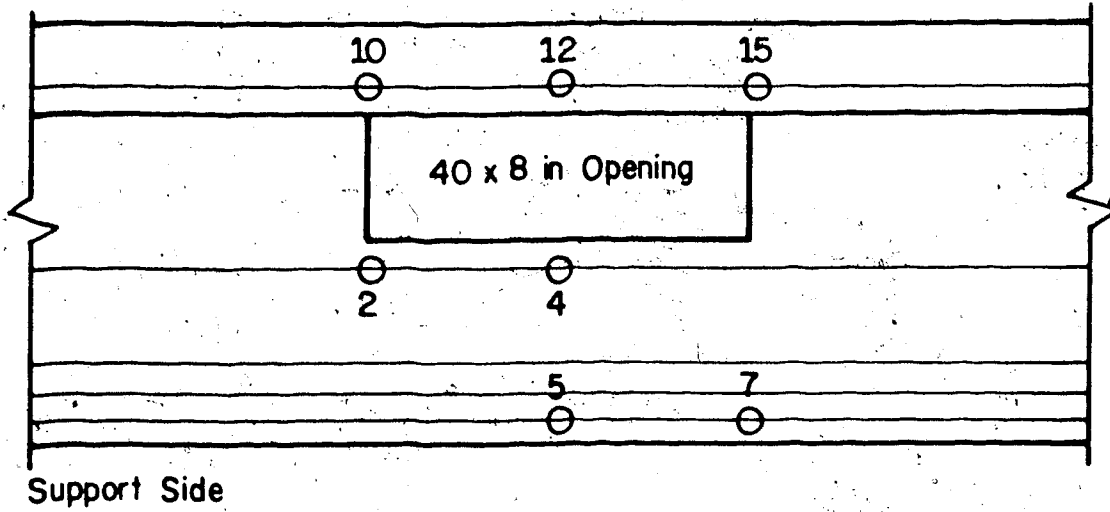
Support Side

Figure B1   Strain-Gage Locations - BEAM B2

11   12   13

24 x 8 in
Opening

3   4

5   6
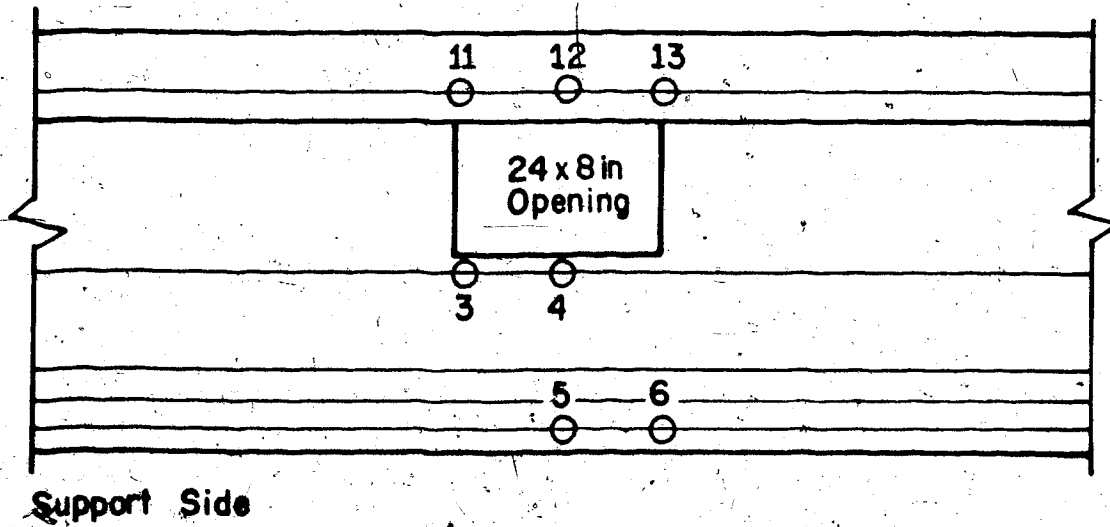
Support Side

Figure B2   Strain Gage Locations - BEAM B3
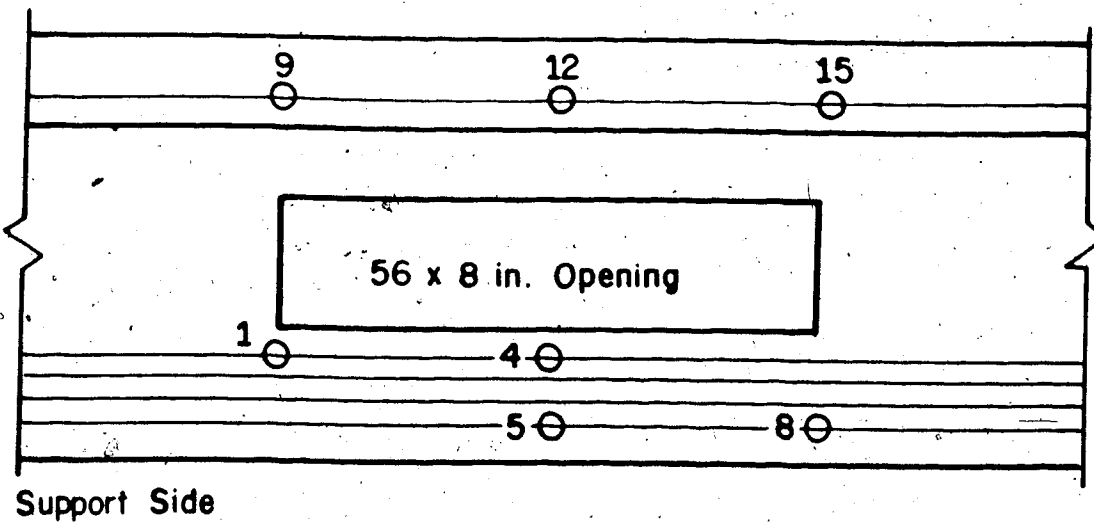
Figure B3   Strain Gage Locations - BEAM C1
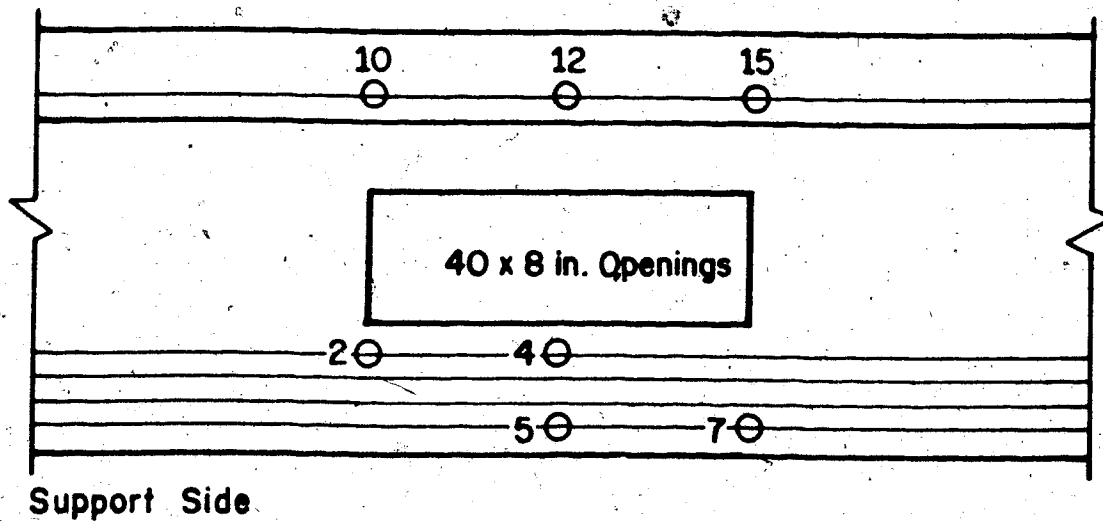
Figure B4   Strain Gage Locations - BEAM C2
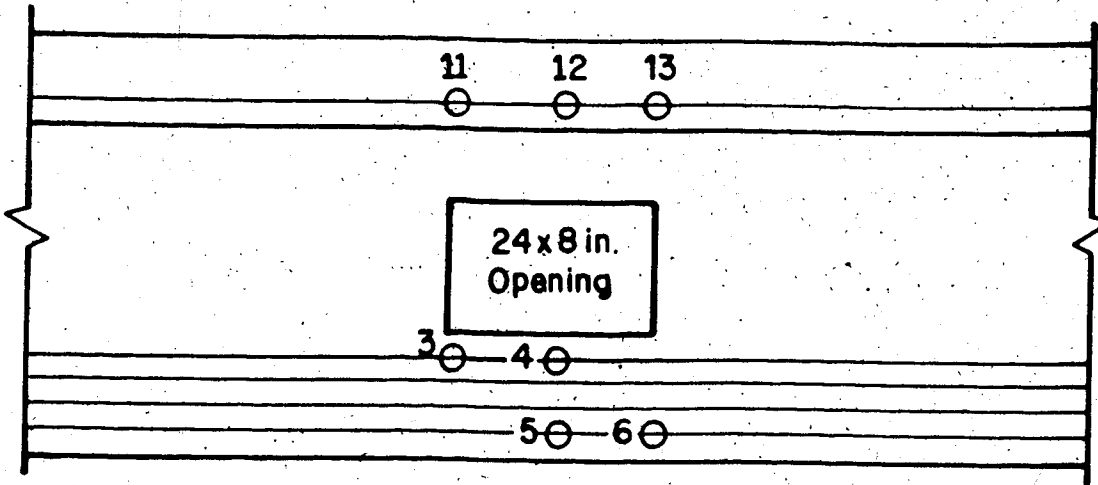
Support Side

Figure B5   Strain Gage Locations - BEAM C3
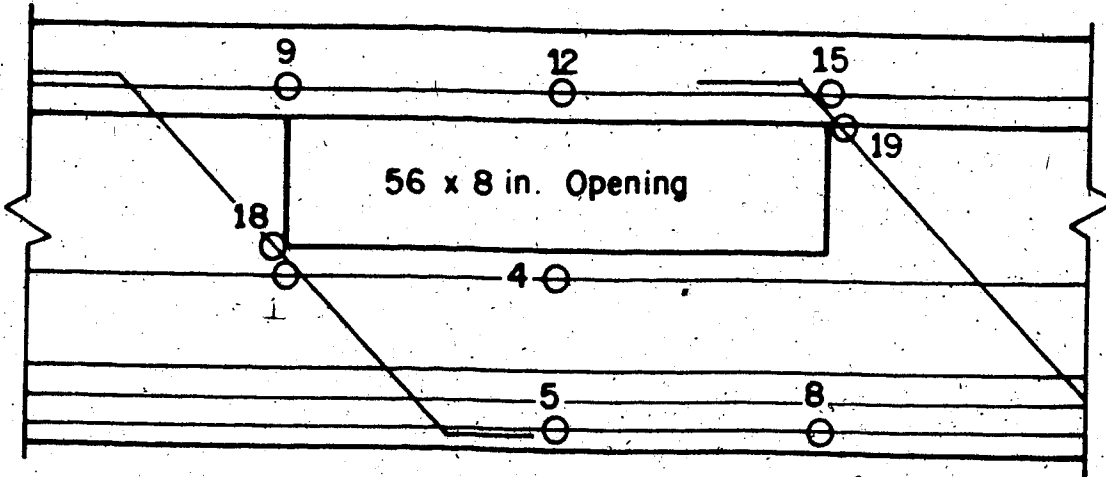
Support Side

Figure B6   Strain Gage Locations - BEAM D1

40 x 8 in. Opening

Support Side
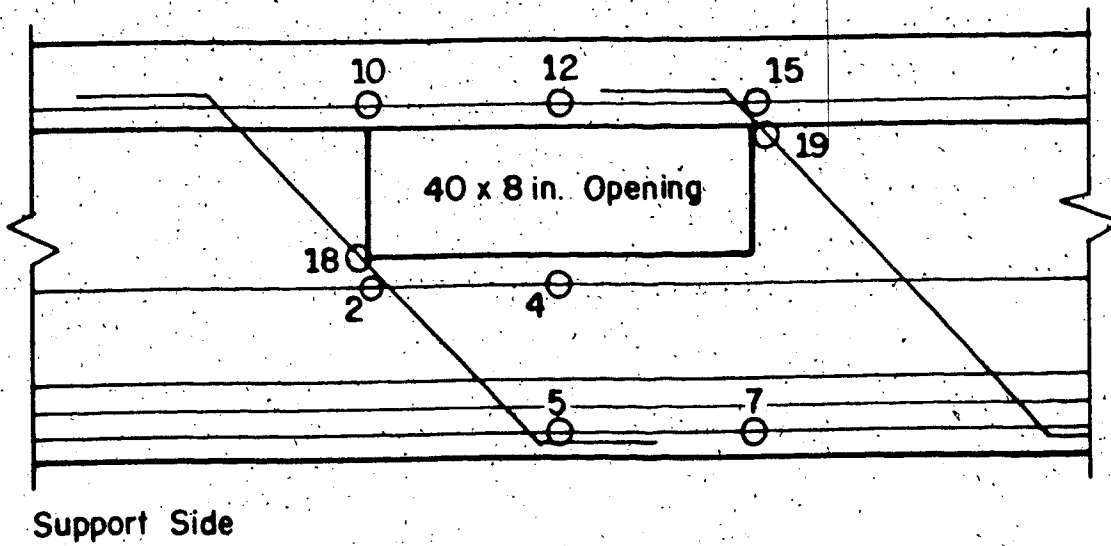
Figure B7   Strain Gage Locations – BEAM D2

24 x 8 in.
Opening

Support Side
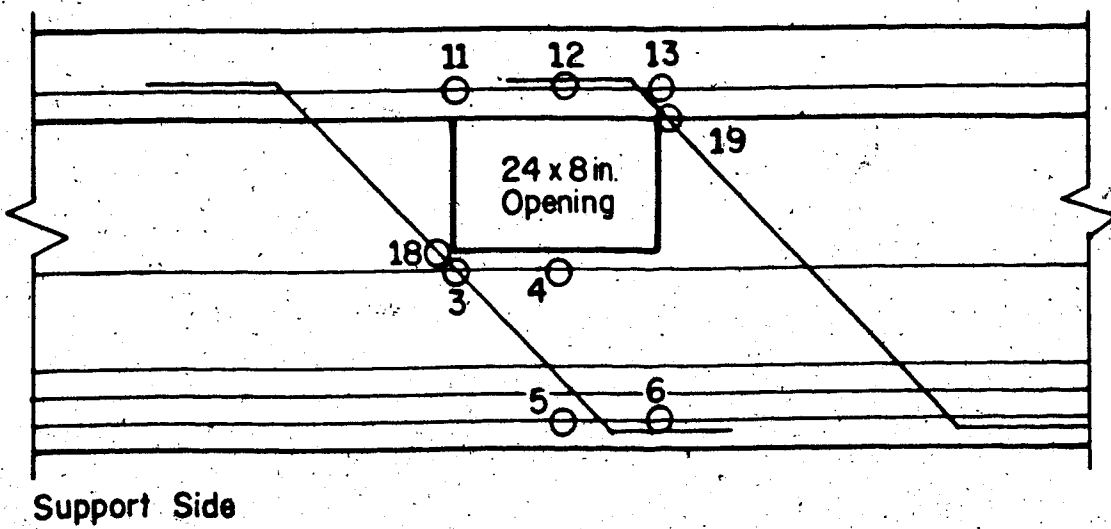
Figure B8   Strain Gage Locations – BEAM D3

Support Side
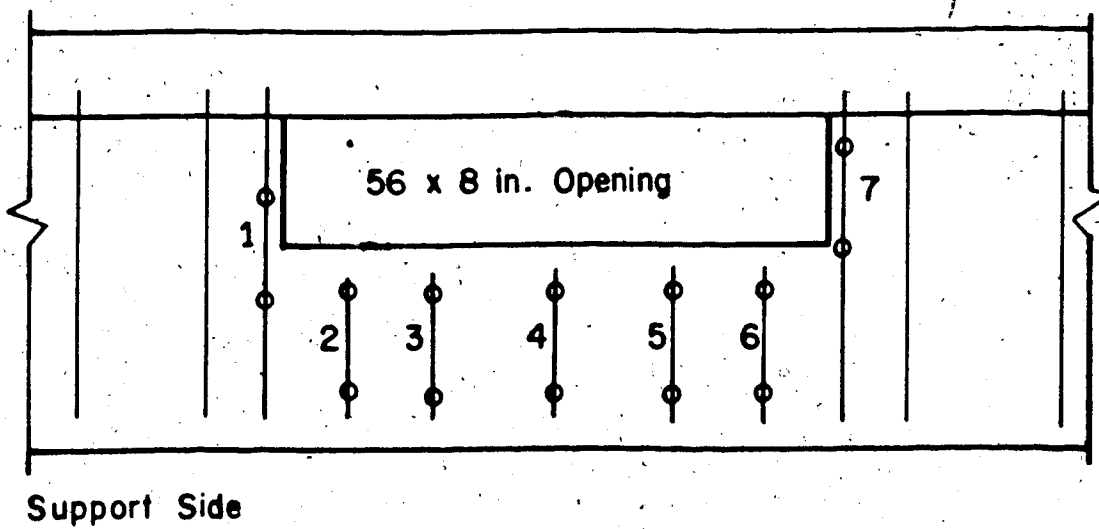
Figure B9   Demec Points on stirrups - BEAM B1 and BEAM D1.

Support Side
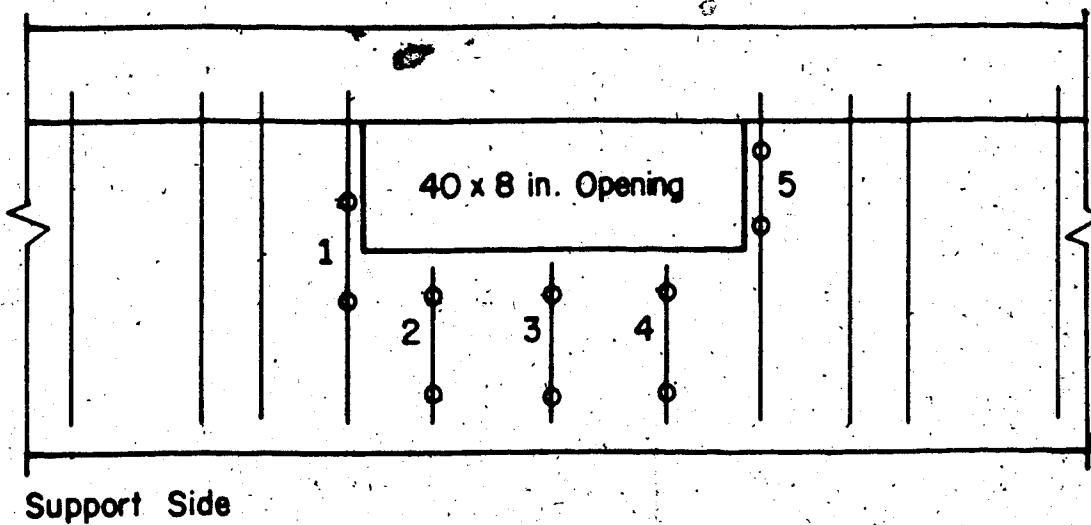
Figure B10   Demec Points on stirrups - BEAM B2 and BEAM D2.

24 x 8 in. Opening

Support Side
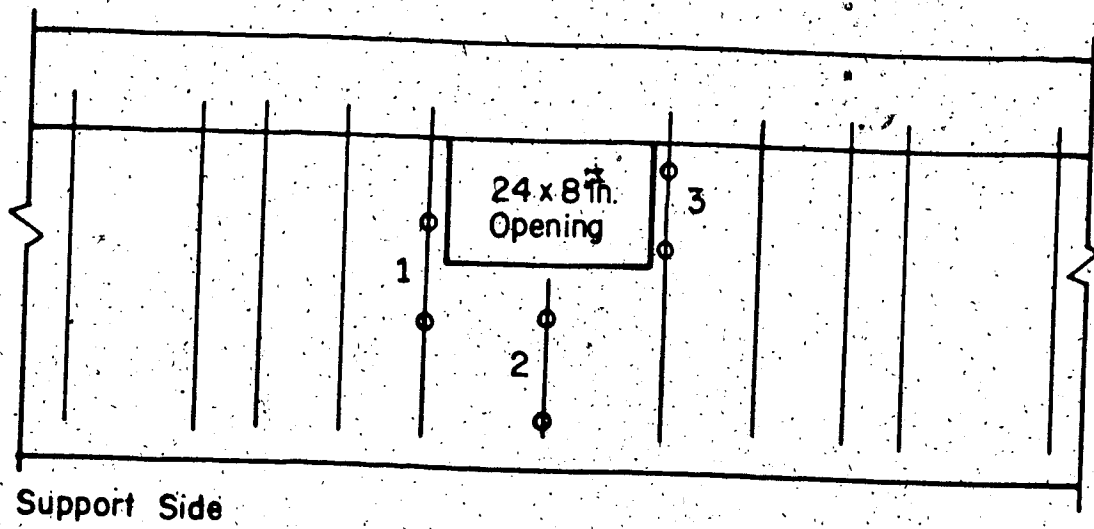
Figure B11   Demec Points on stirrups - BEAM B3 and BEAM D3.

56 x 8 in. Opening

Support Side
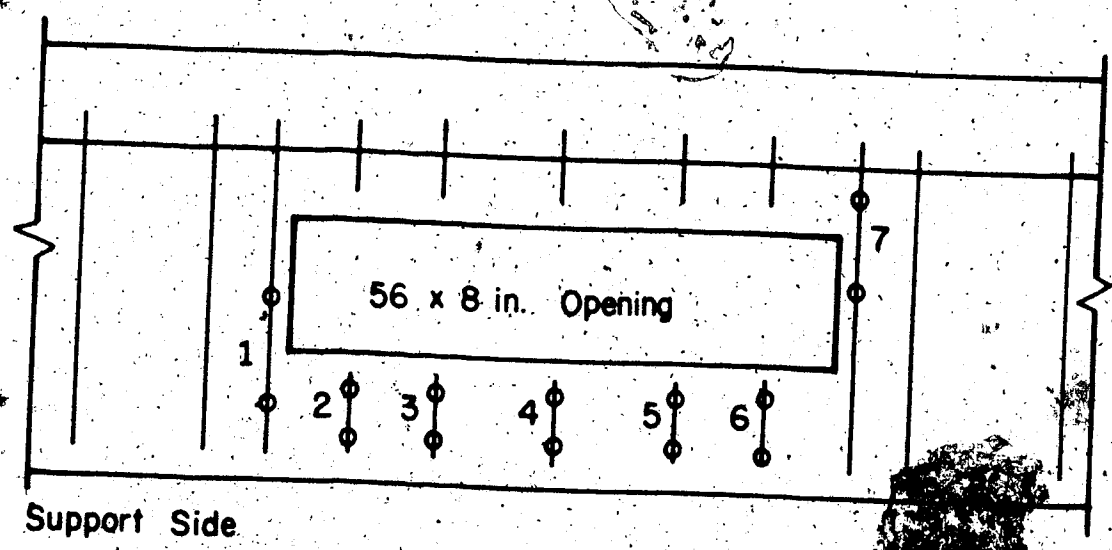
Figure B12   Demec Points on stirrups - BEAM C1.
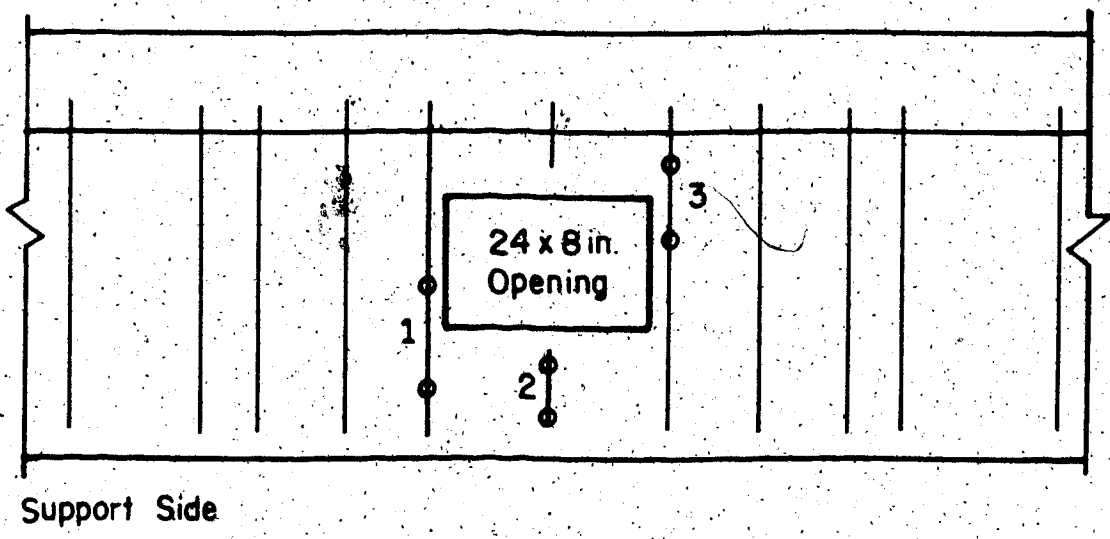
Figure B13   Demec Points on stirrups - BEAM C3.

4"

4"

5"   12"   5"   12"   5"   12"   5"

Plan view

56 x 8 in. Opening
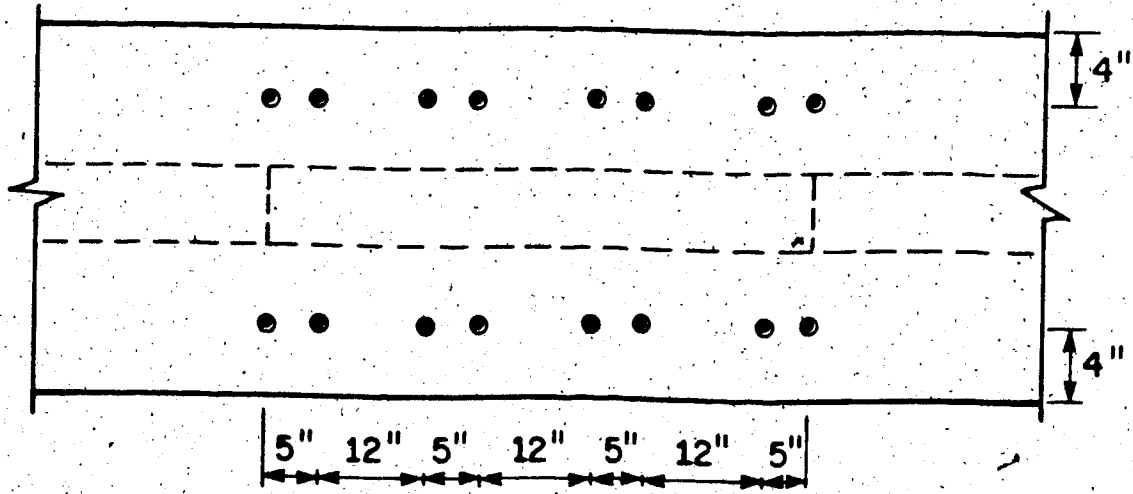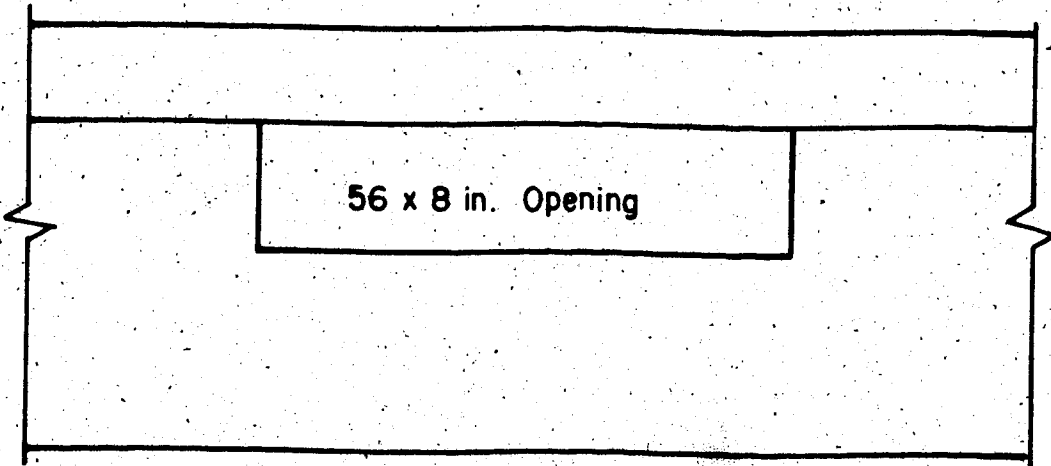
Beam elevation

Figure B14   Demec Points on top strut -BEAM B1 and
BEAM D1.

4"

4"

5" 14" 5"

Plan view

24 x 8 in.
Opening
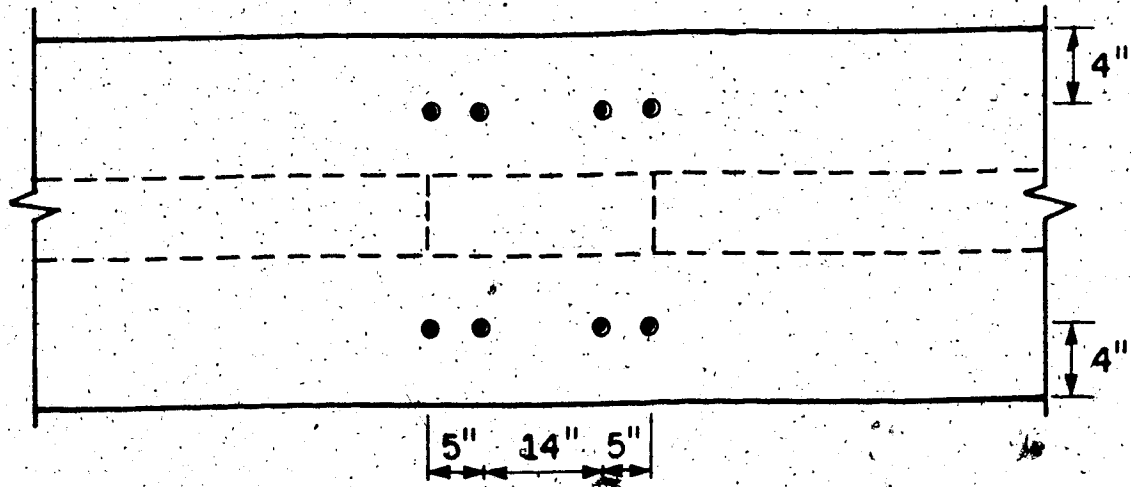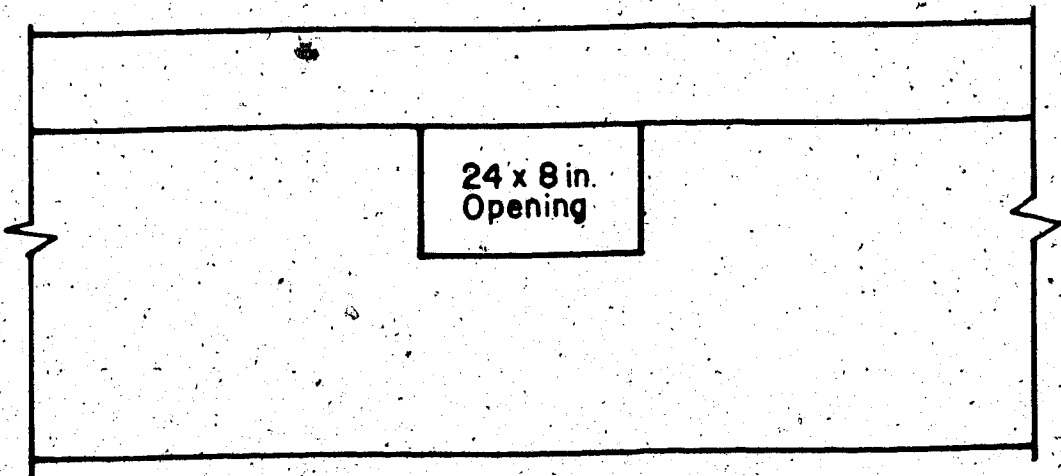
Beam elevation

Figure B15 Demec Points on top strut - BEAM B3 and
BEAM D3.

Plan view

56 x 8 in. Opening
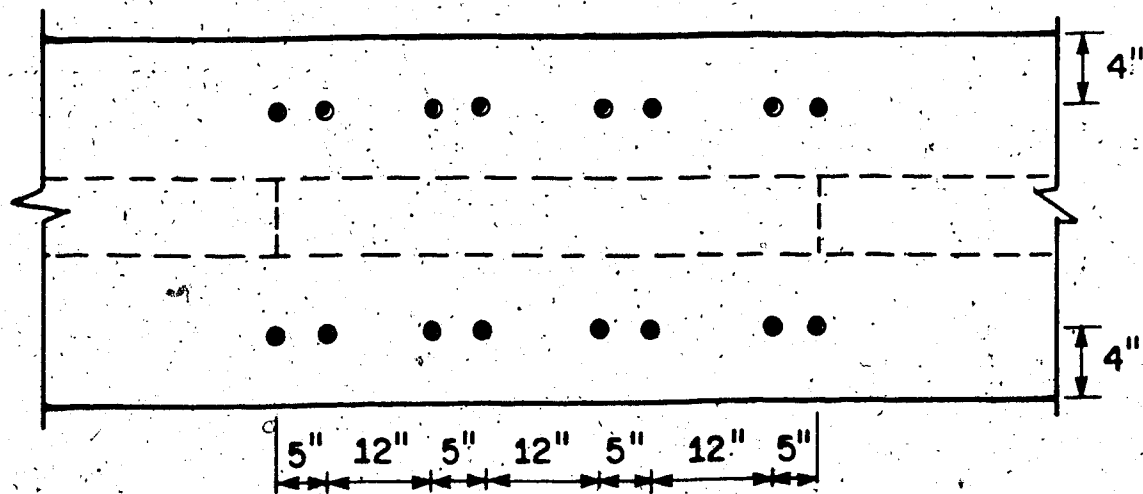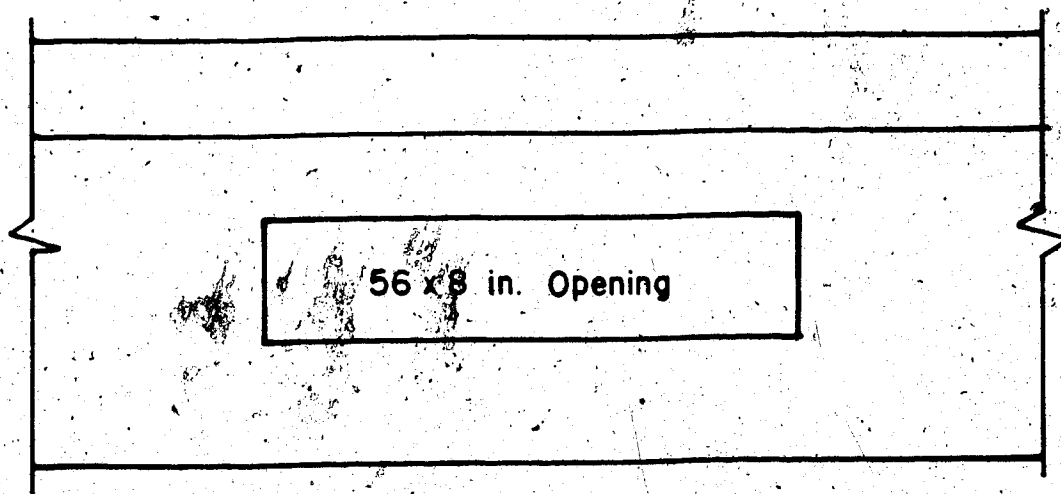
Beam elevation

Figure B16   Demec Points on top strut - BEAM C1.

5" 12 1/2" 5" 12 1/2" 5"

4"

4"

Plan view

40 x 8 in. Opening
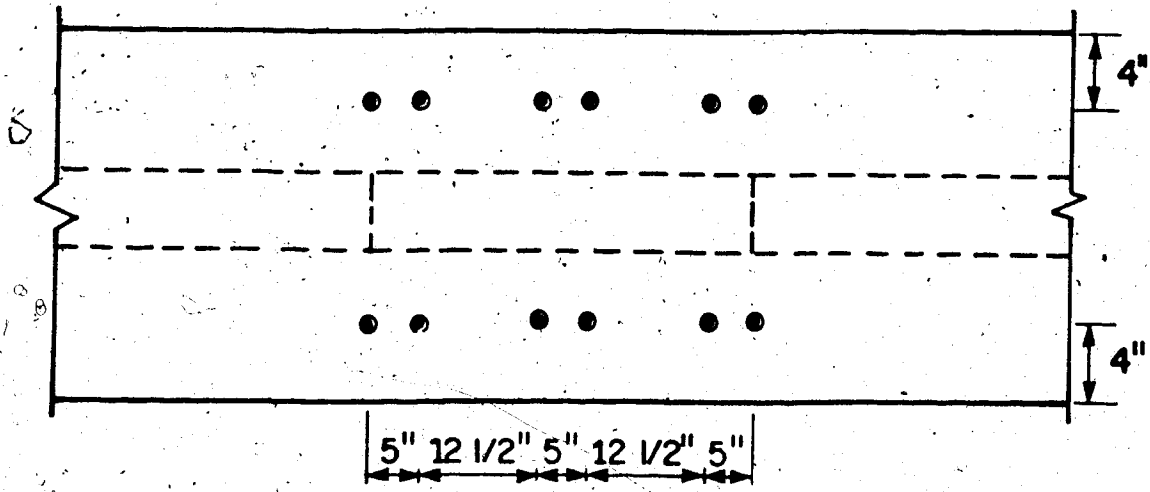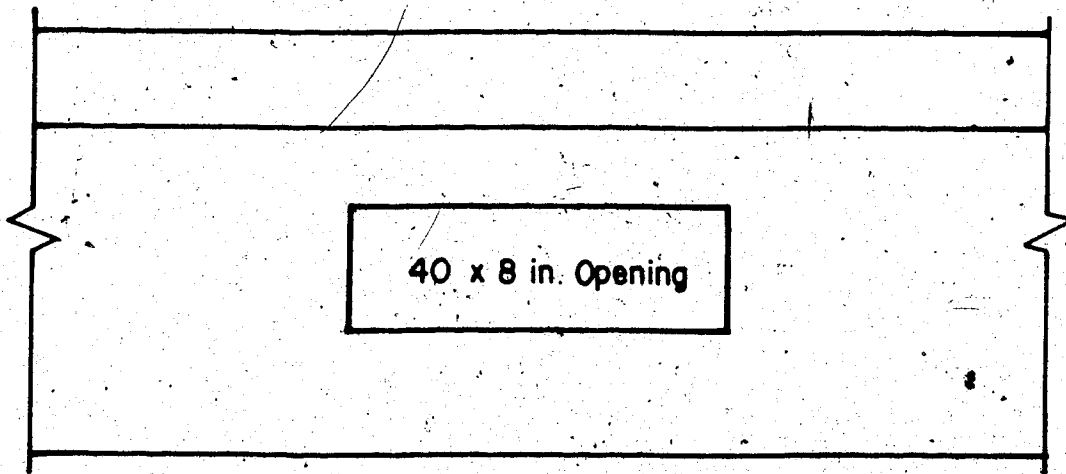
Beam elevation

Figure B17   Demec Points on top strut - BEAM C2.

Plan view

4"

4"

5" 14" 5"

24 x 8 in.
Opening
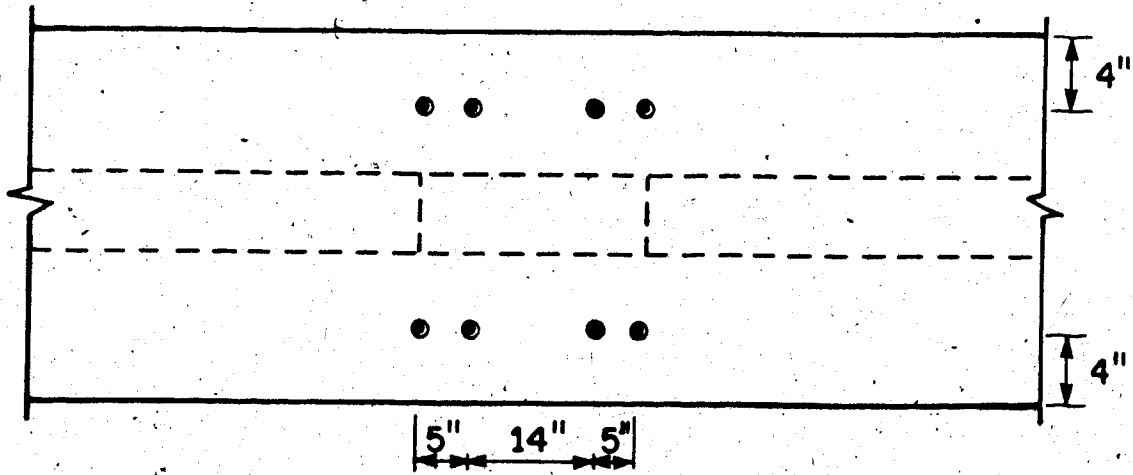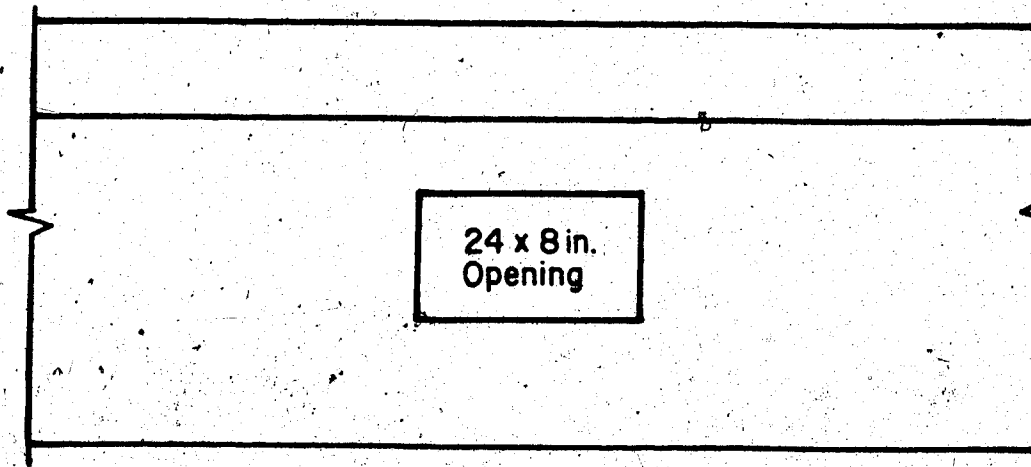
Beam elevation

Figure B18   Demec Points on top strut – BEAM C3

APPENDIX C

LOAD VS. FORCE FOR STIRRUPS AT THE OPENING

LOAD VS. STRAIN FOR LONGITUDINAL REINFORCEMENT

LOAD-DEFLECTION CURVE AT BOTH CORNERS OF THE OPENING

258
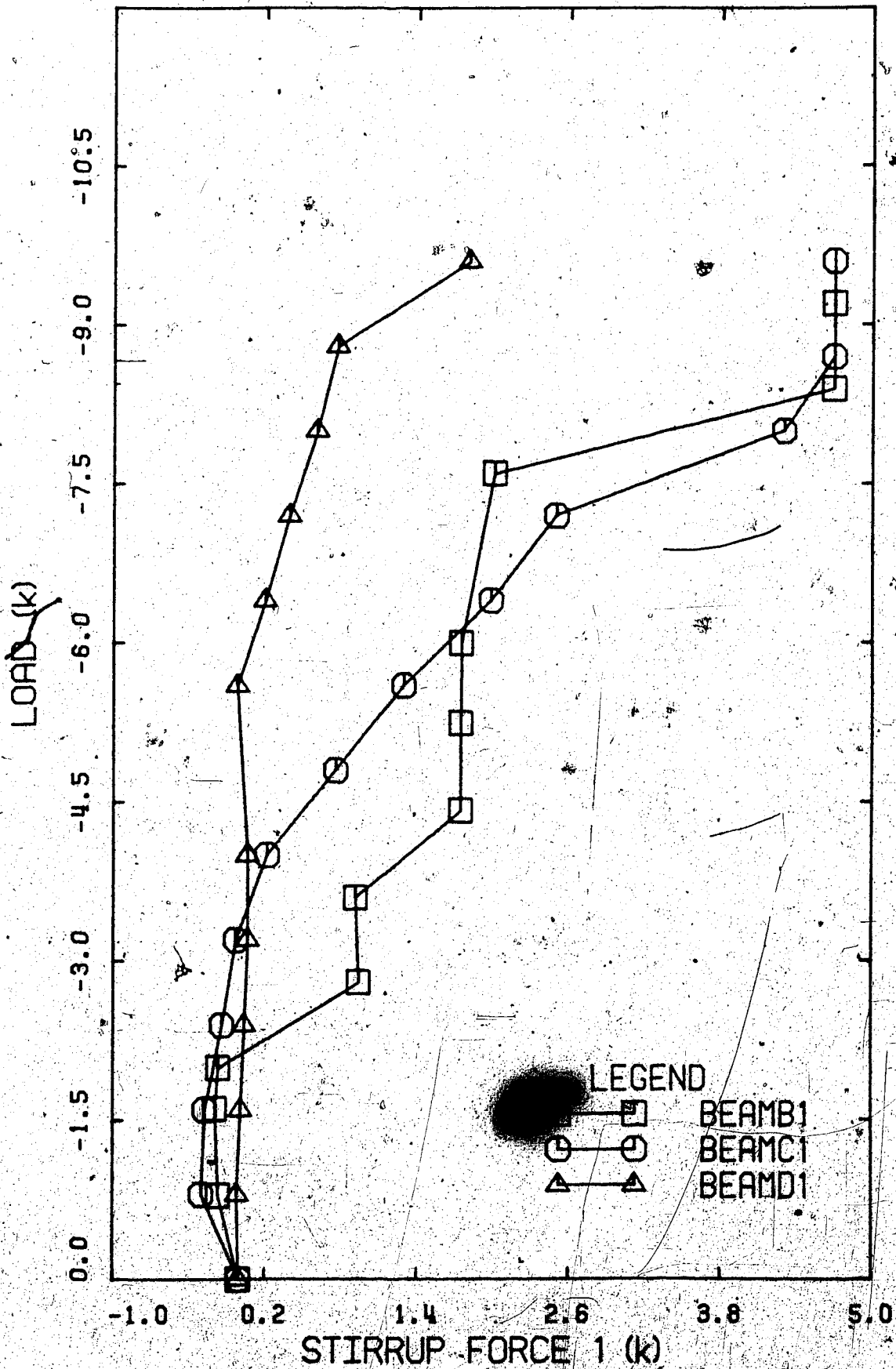
Figure C1 Force in Stirrup 1 – BEAM B1, BEAM C1 and
BEAM D1.
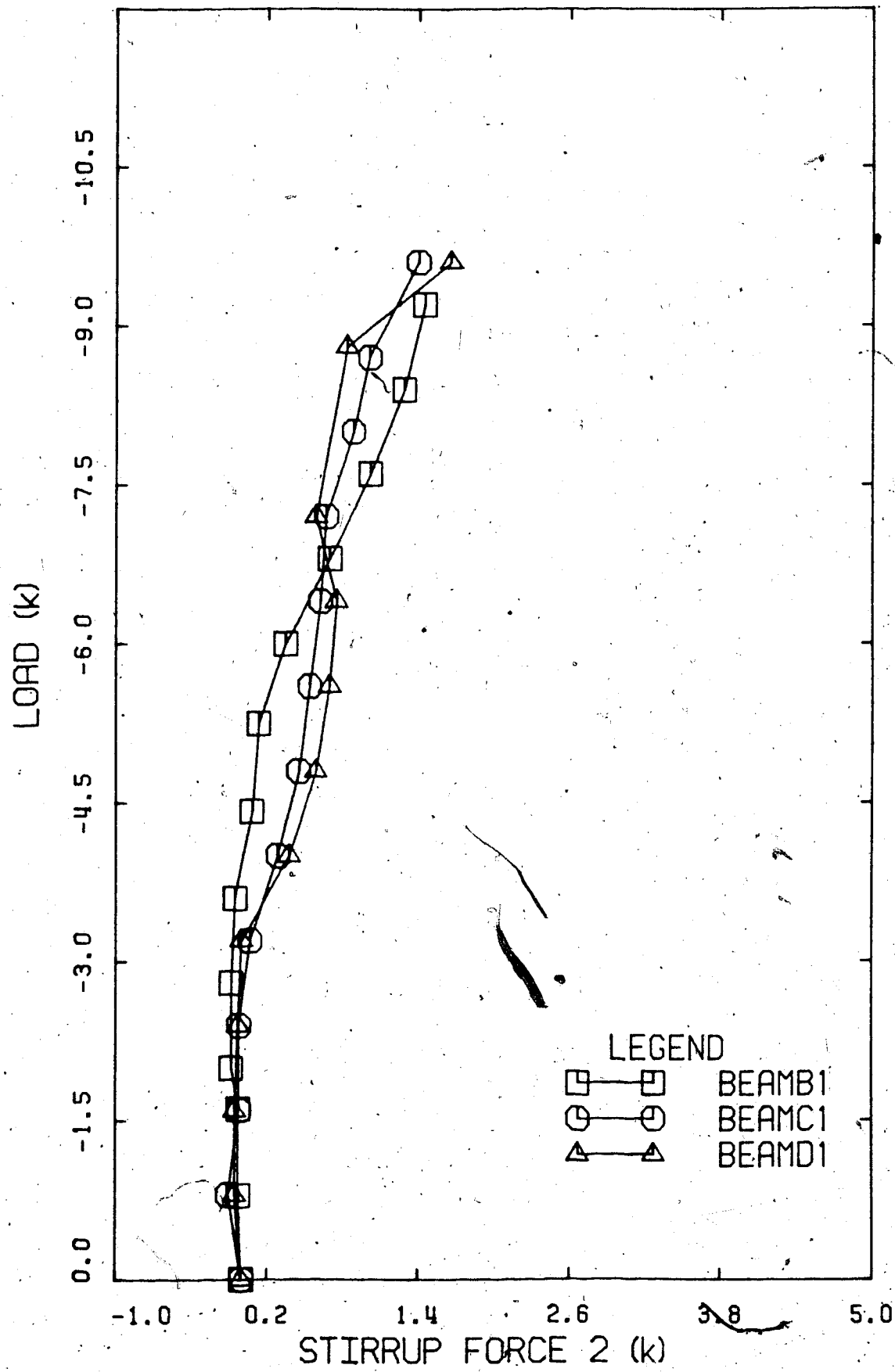
Figure C2   Force in Stirrup 2 - BEAM B2, BEAM C1 and
BEAM D1.
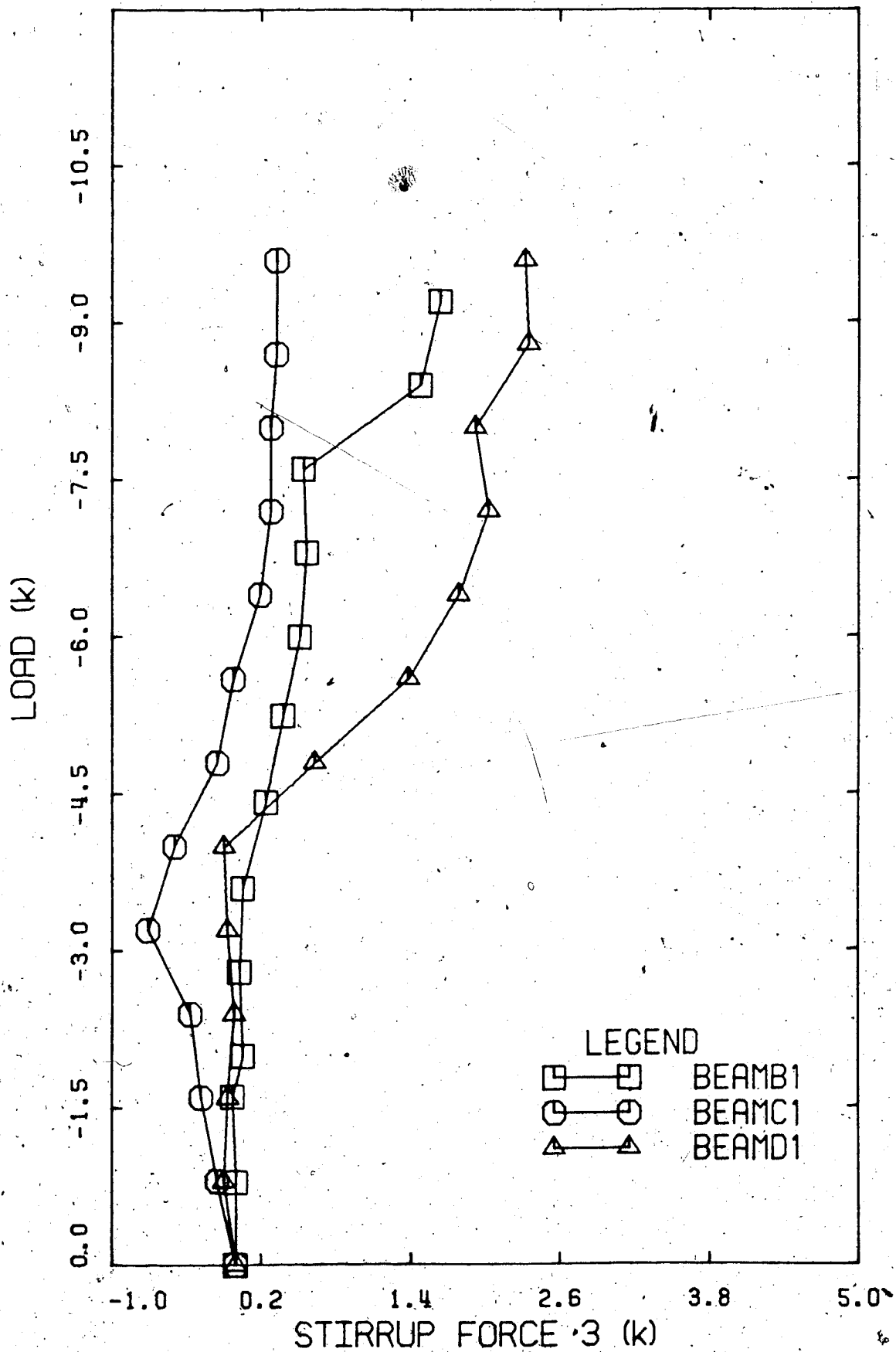
Figure C3   Force in Stirrup 3 - BEAM B1, BEAM C1 and
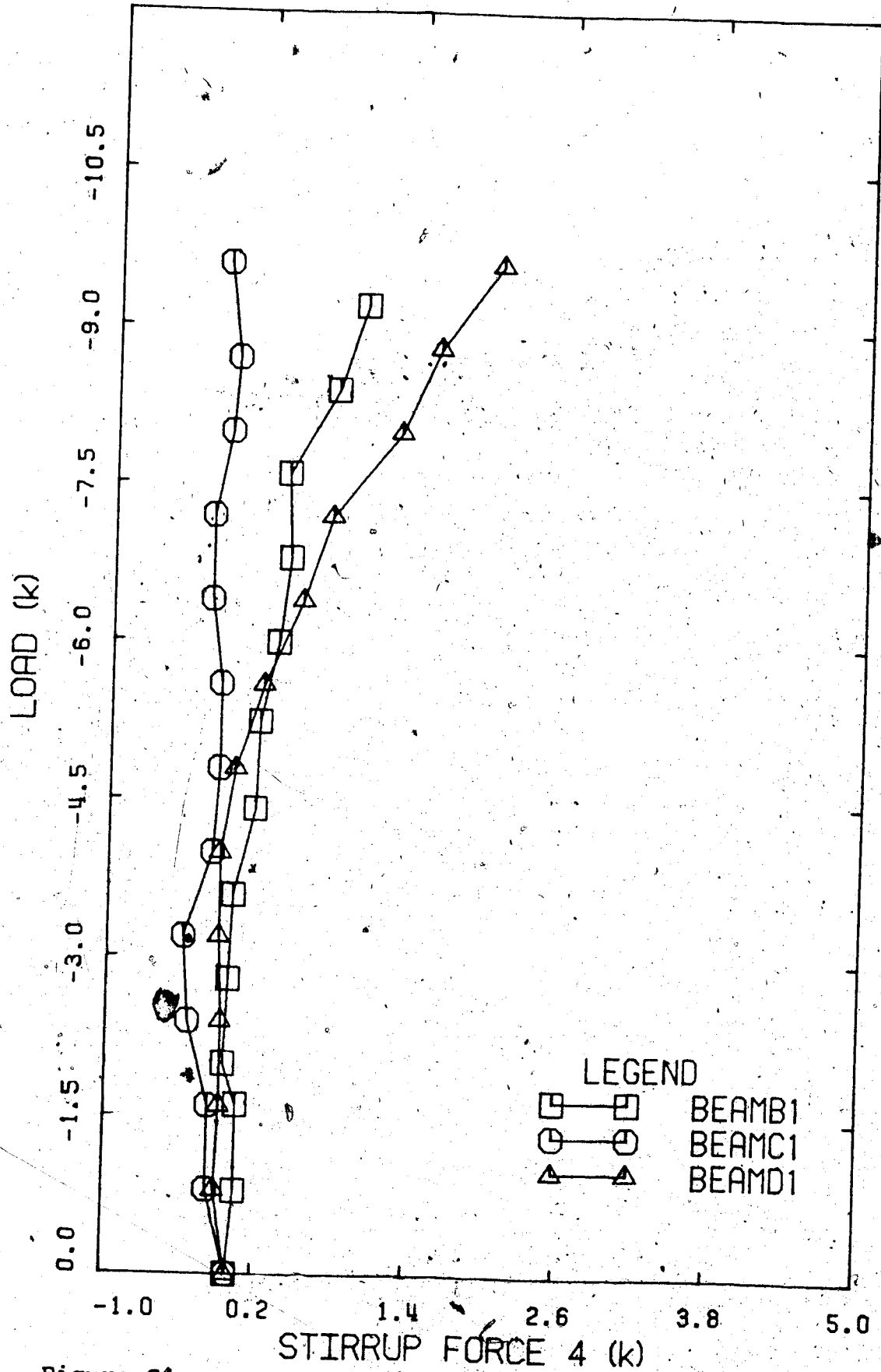
BEAM D1.

Figure C4   Force in Stirrup 4 - BEAM B1, BEAM C1 and
BEAM D1.
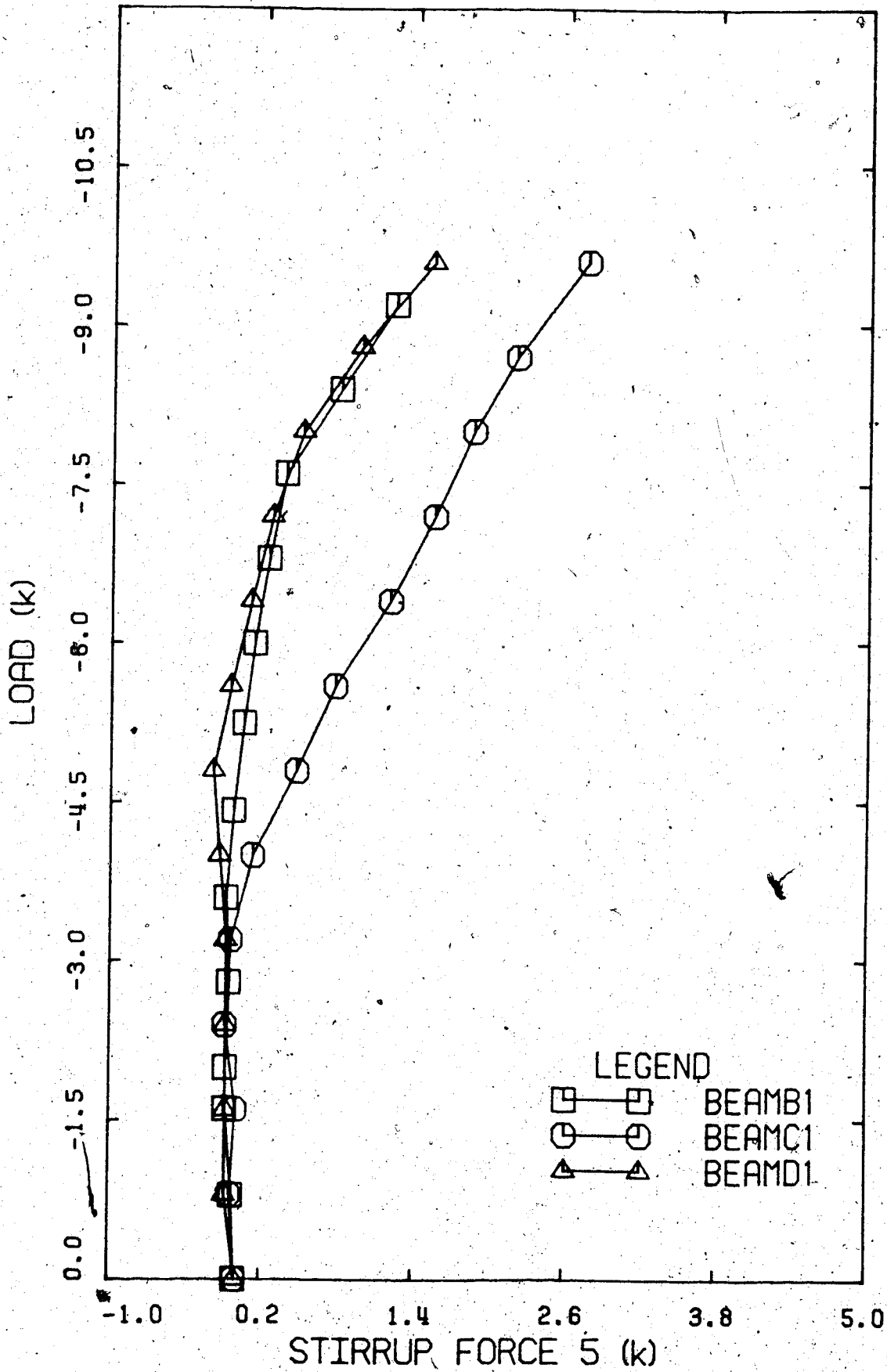
Figure C5   Force in Stirrup 5 - BEAM B1, BEAM C1 and
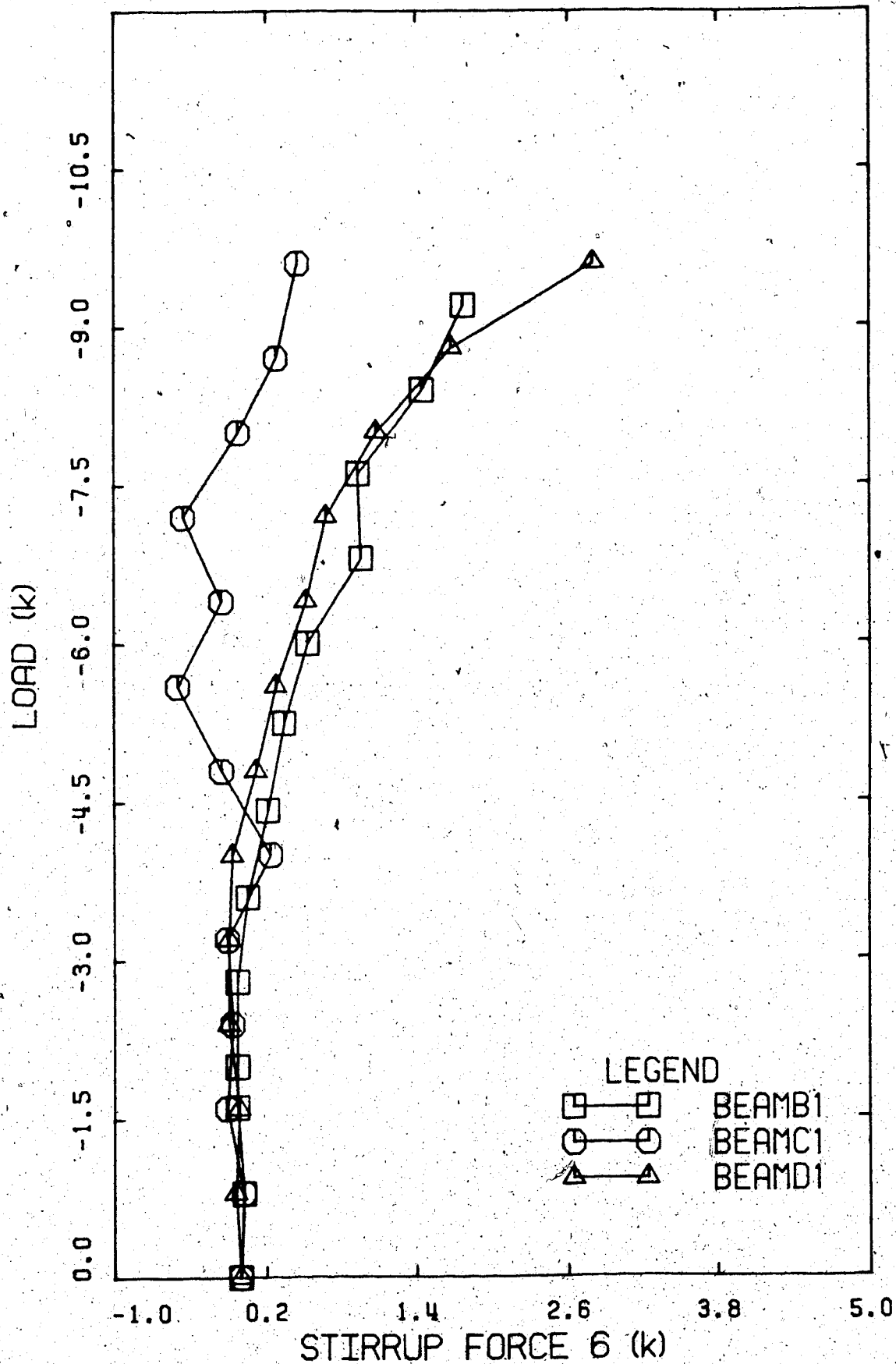
BEAM D1.

Figure C6.   Force in Stirrup 6 – BEAM B1, BEAM C1 and
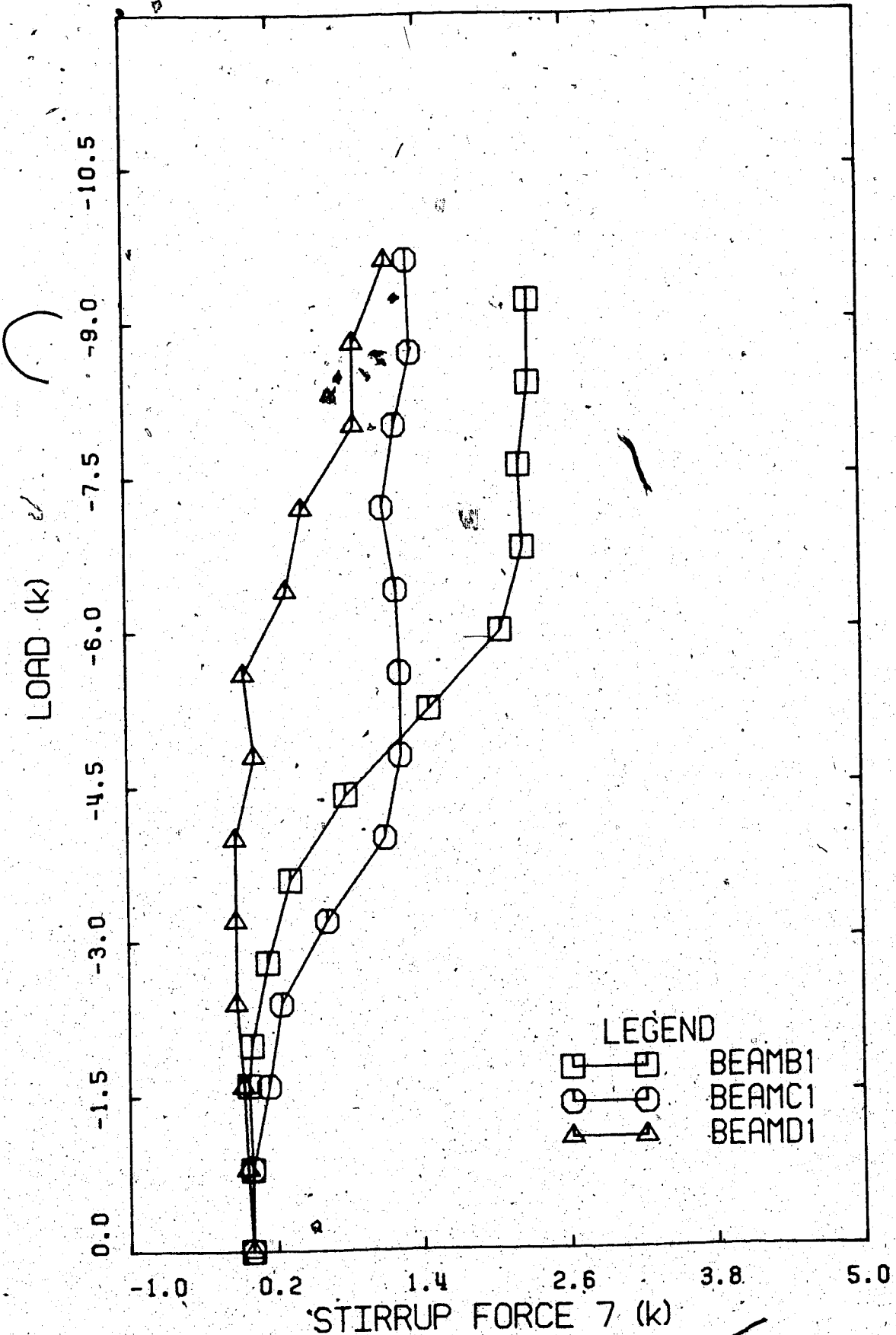
BEAM D1.

Figure C7   Force in Stirrup 7 - BEAM Bl, BEAM Cl and
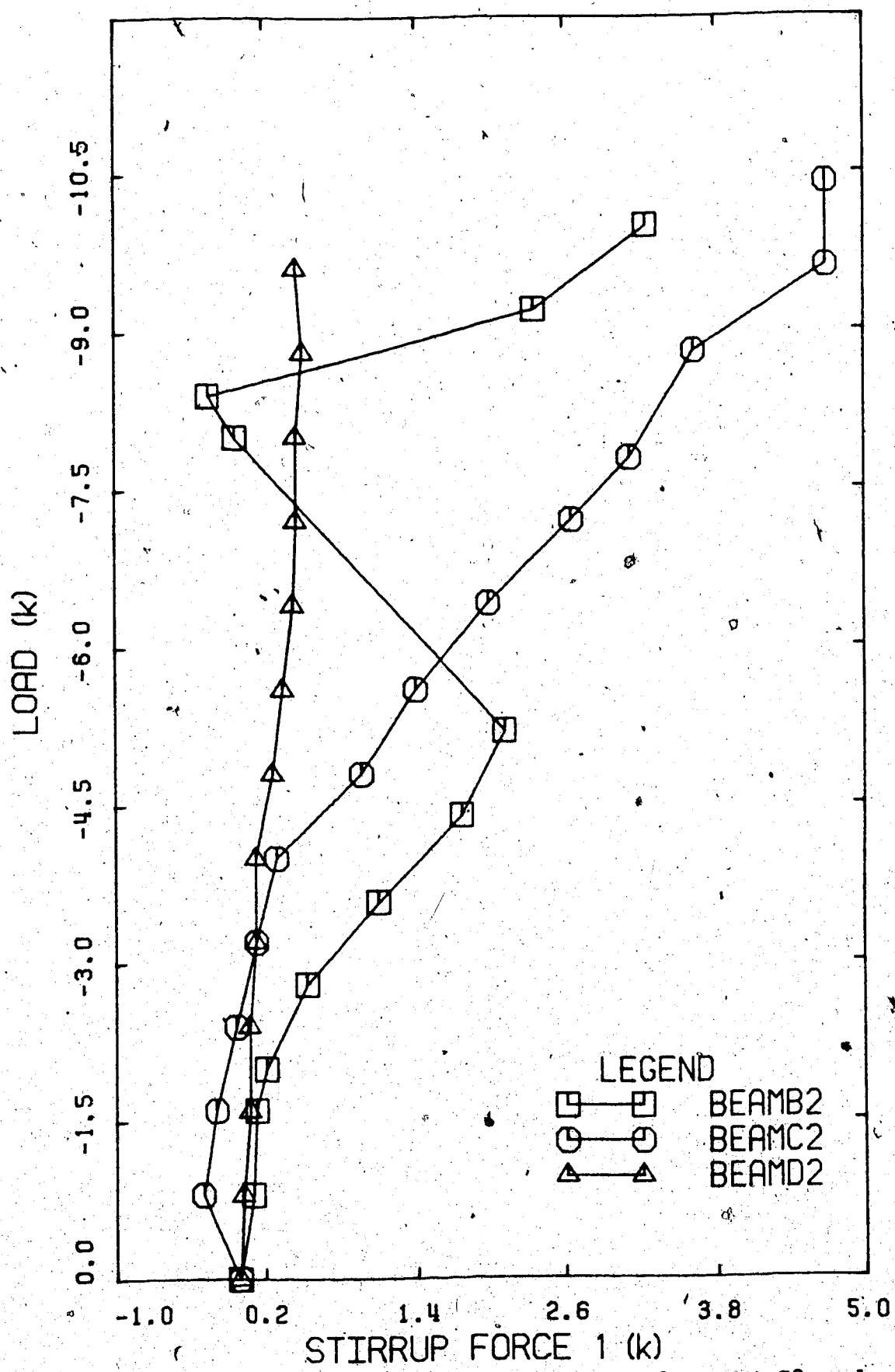
BEAM Dl.

Figure C8   Force in Stirrup 1 - BEAM B2, BEAM C2 and
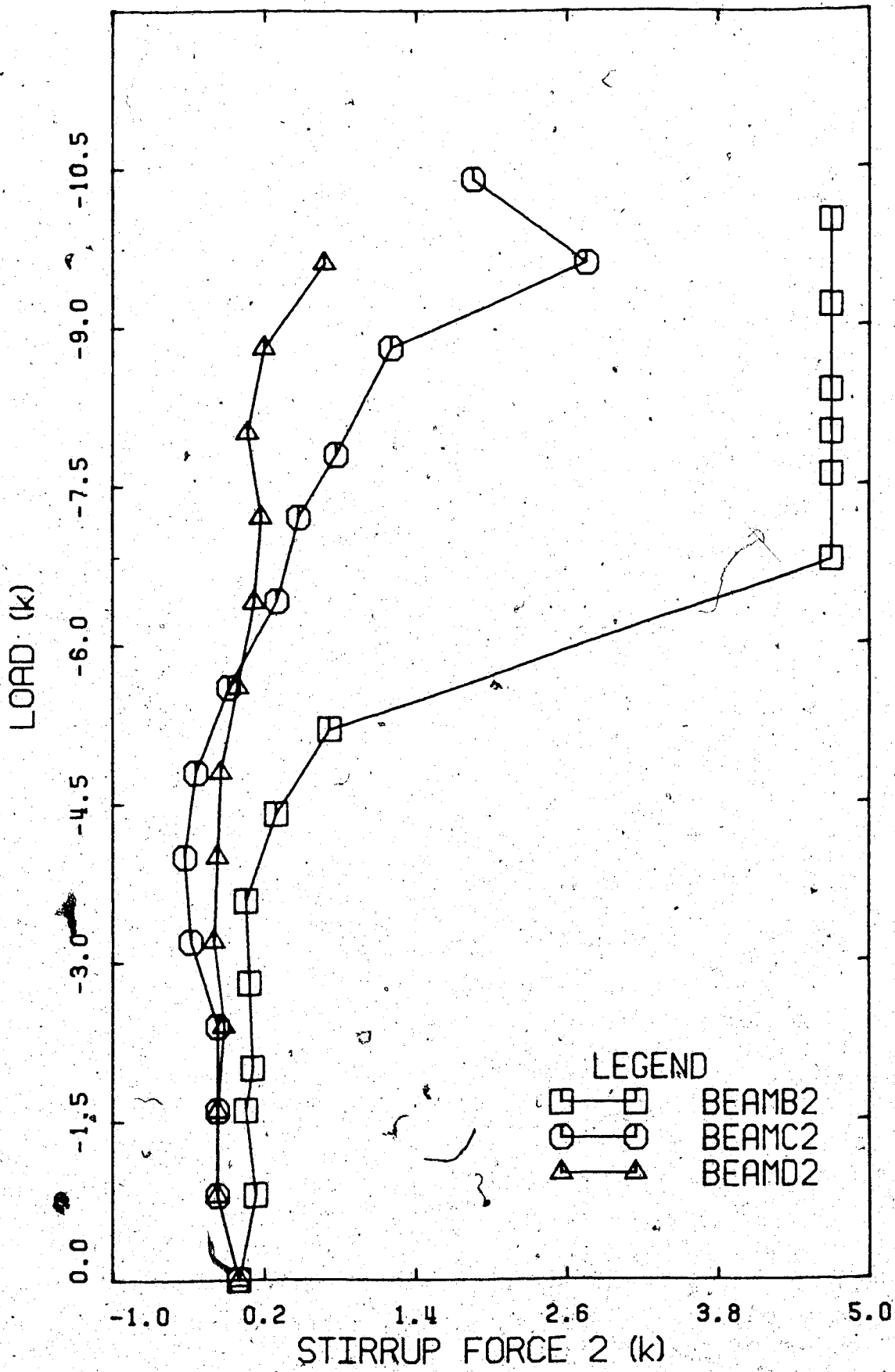
BEAM D2.

Figure C9   Force in Stirrup 2 - BEAM B2, BEAM C2 and
BEAM D2.
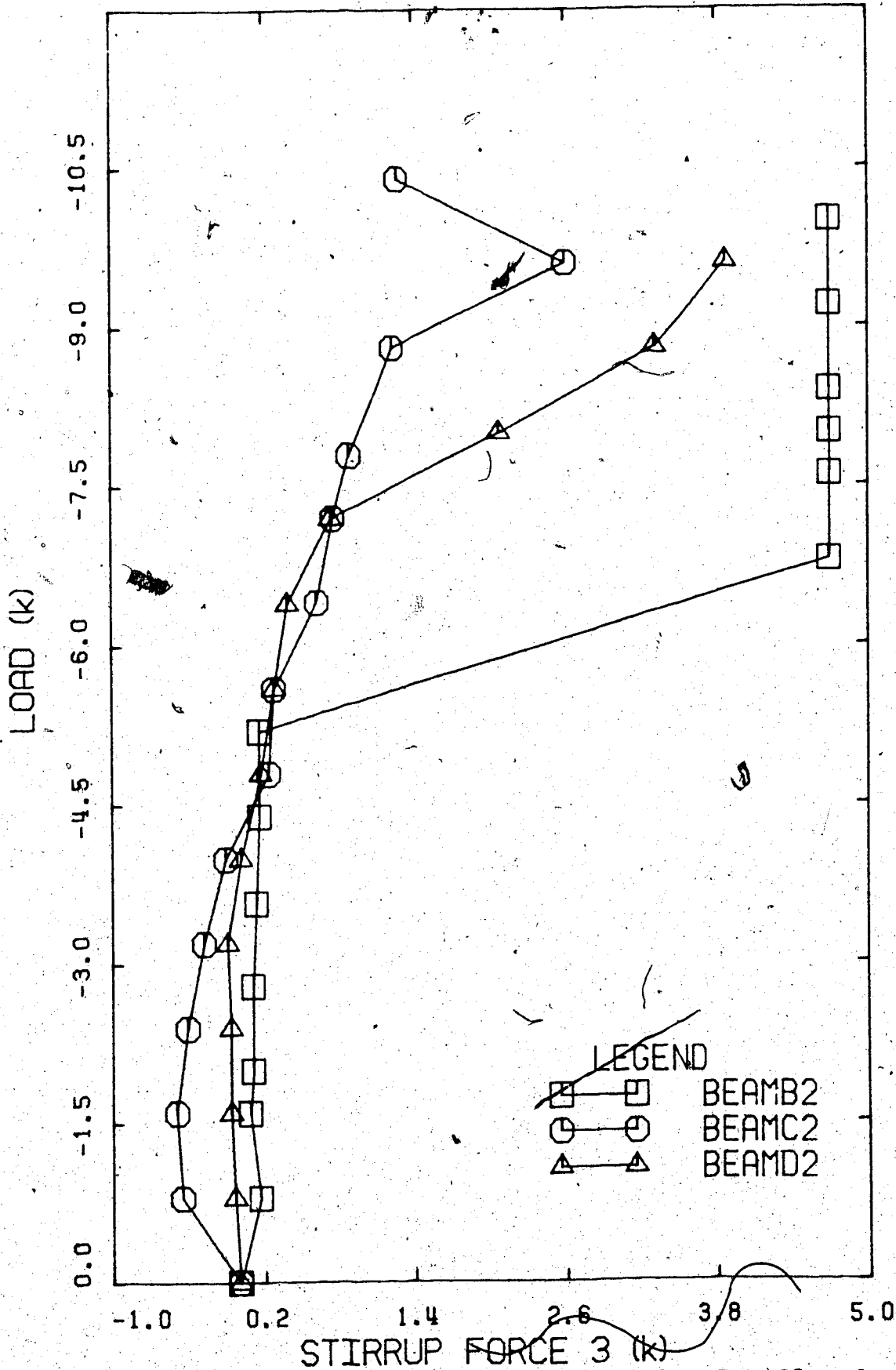
Figure C10   Force in Stirrup 3 - BEAM B2, BEAM C2 and
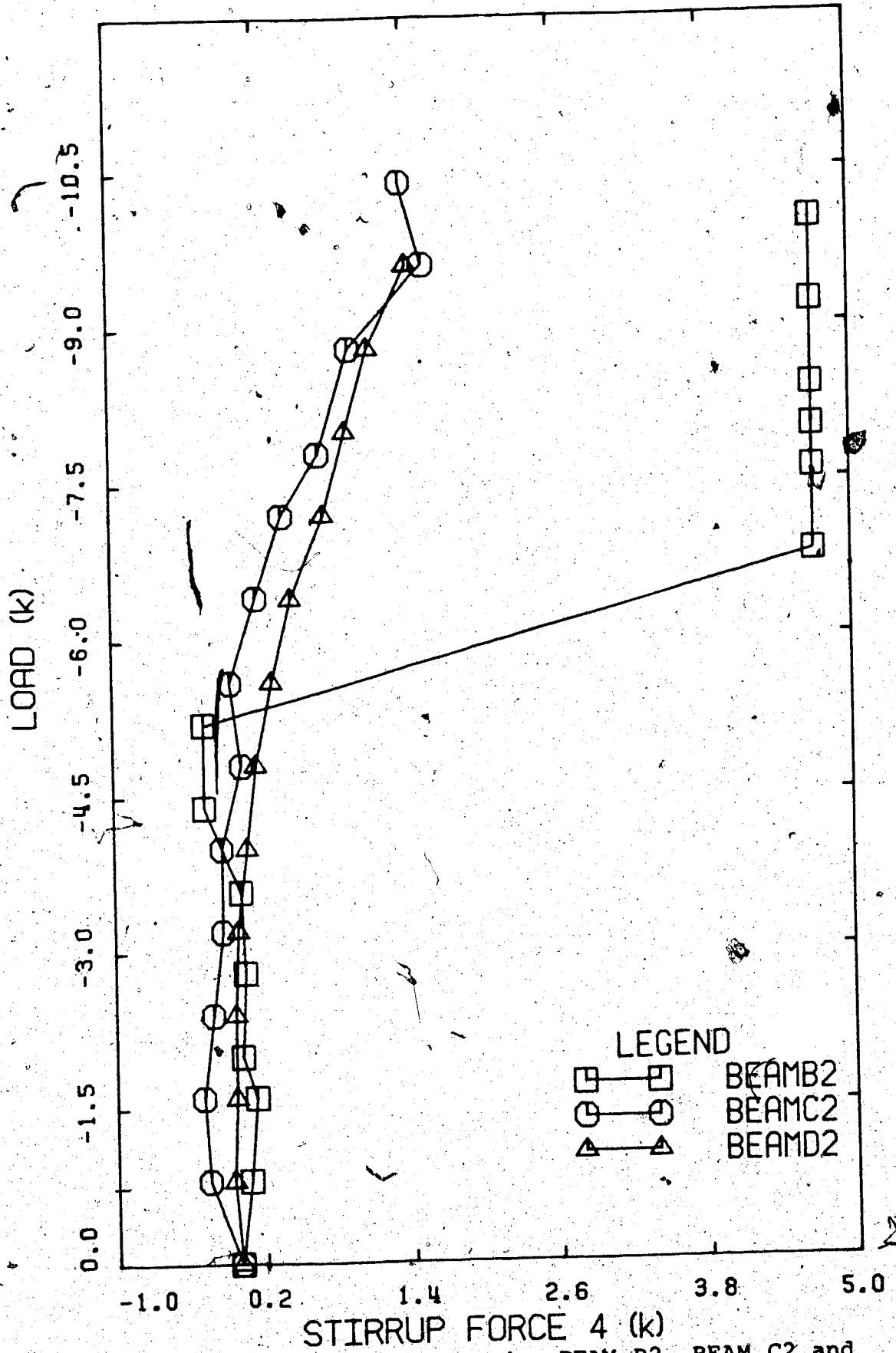
BEAM D2.

Figure C11   Force in Stirrup 4 - BEAM B2, BEAM C2 and
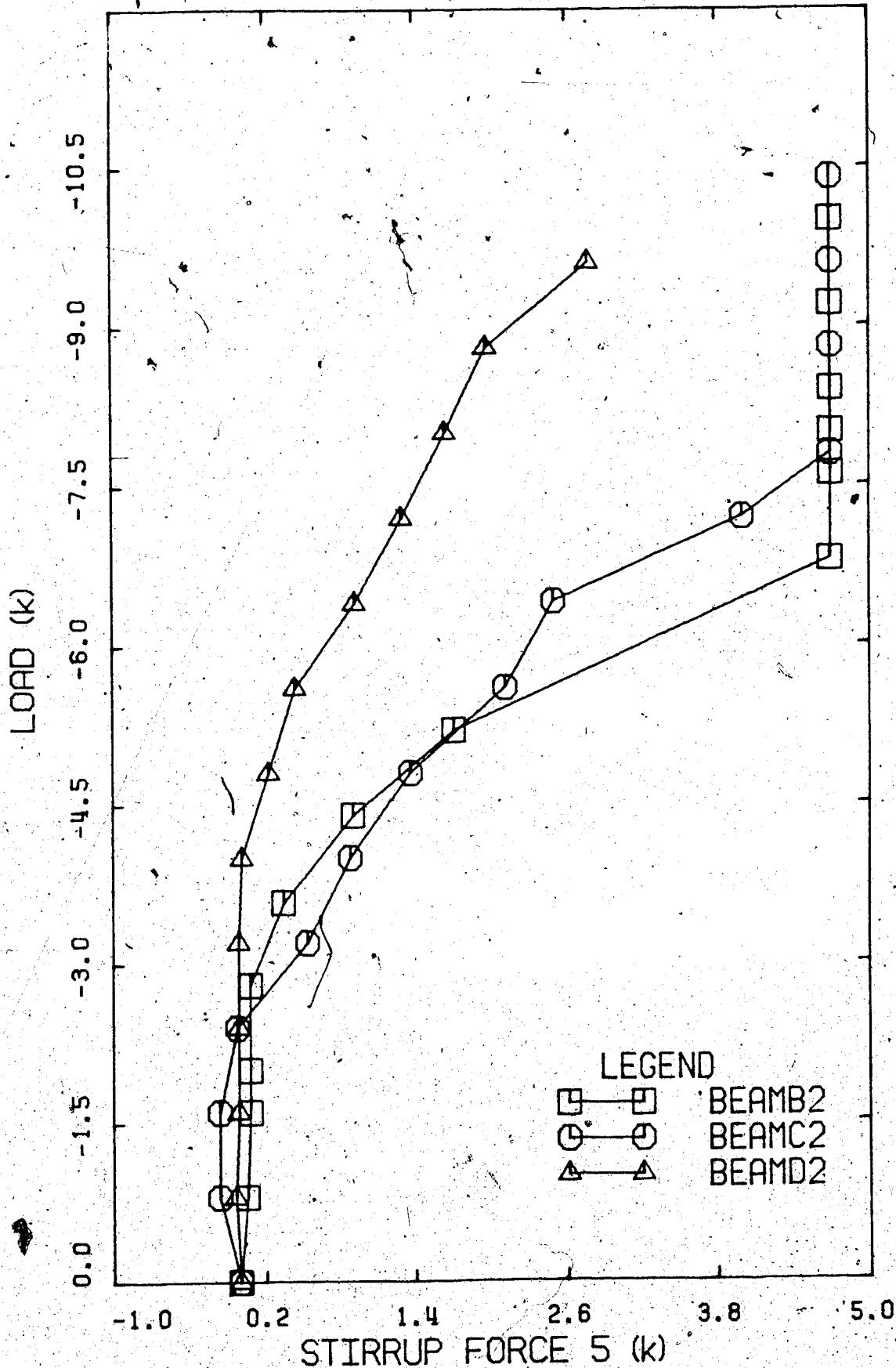
BEAM D2.

Figure C12   Force in Stirrup 5 – BEAM B2, BEAM C2 and
BEAM D2.
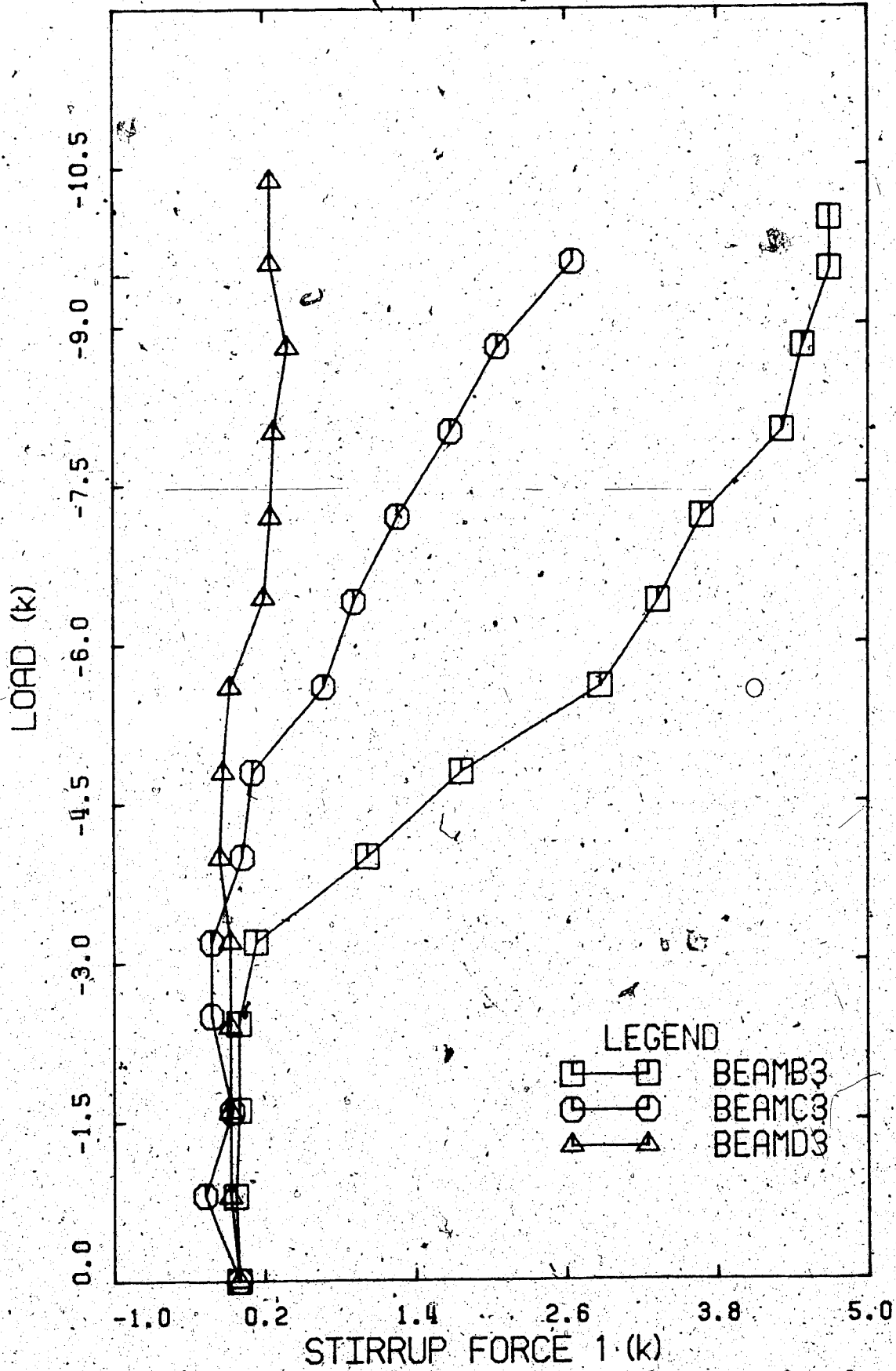
Figure C13   Force in Stirrup 1 - BEAM B3, BEAM C3 and
BEAM D3.
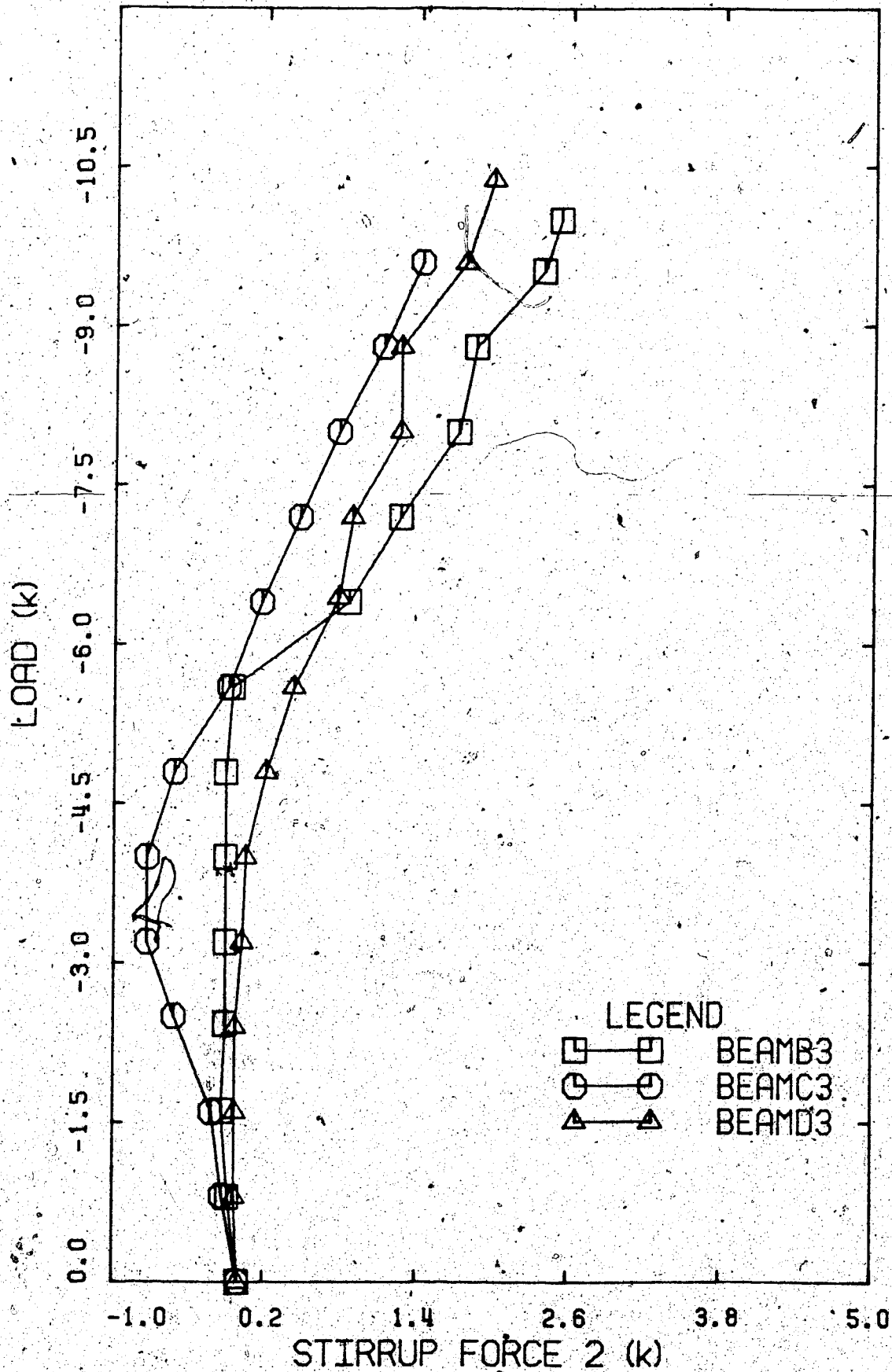
Figure C14   Force in Stirrup 2 - BEAM B3, BEAM C3 and
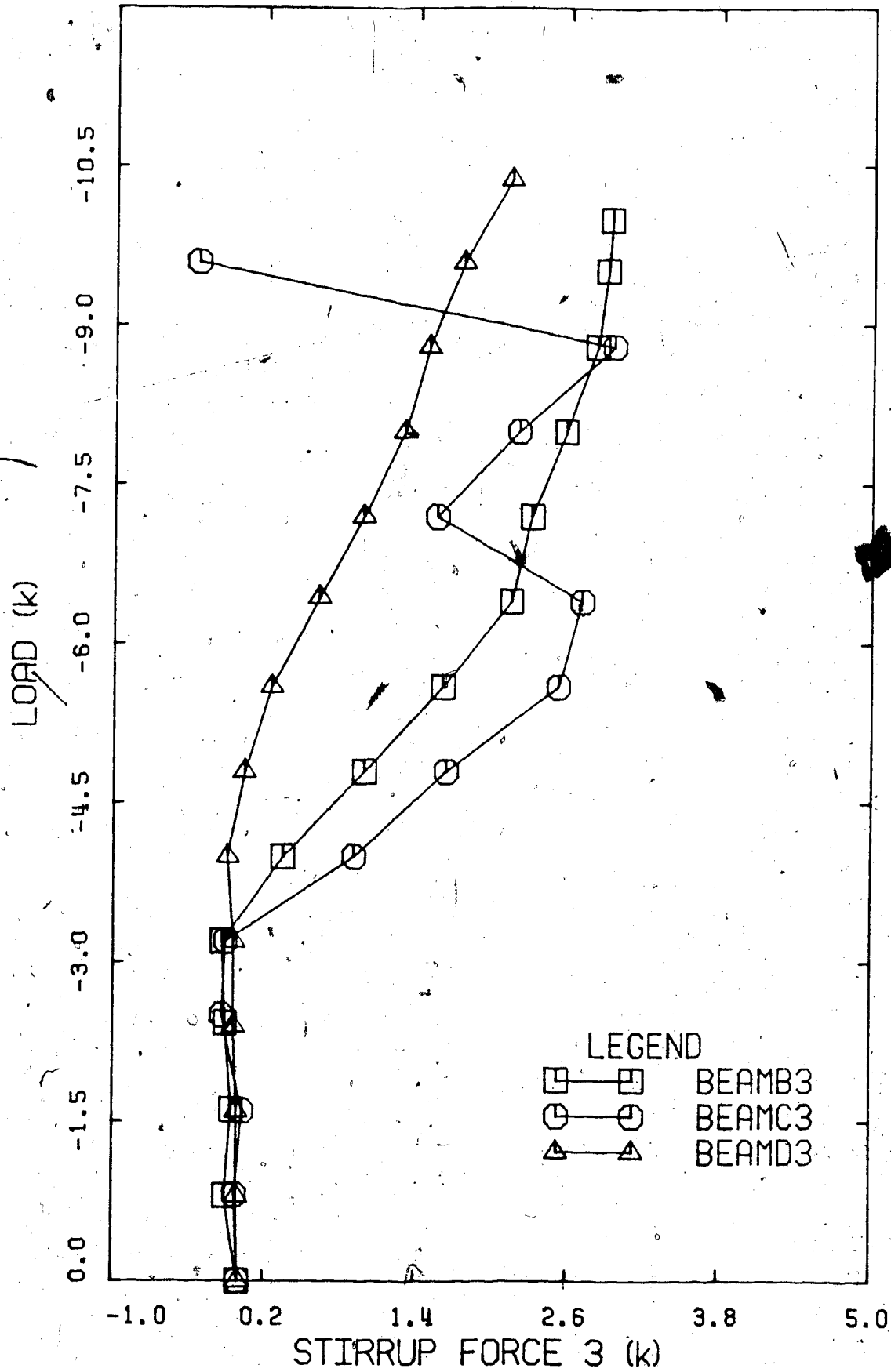
BEAM D3.

Figure C15   Force in Stirrup 3 - BEAM B3, BEAM C3 and
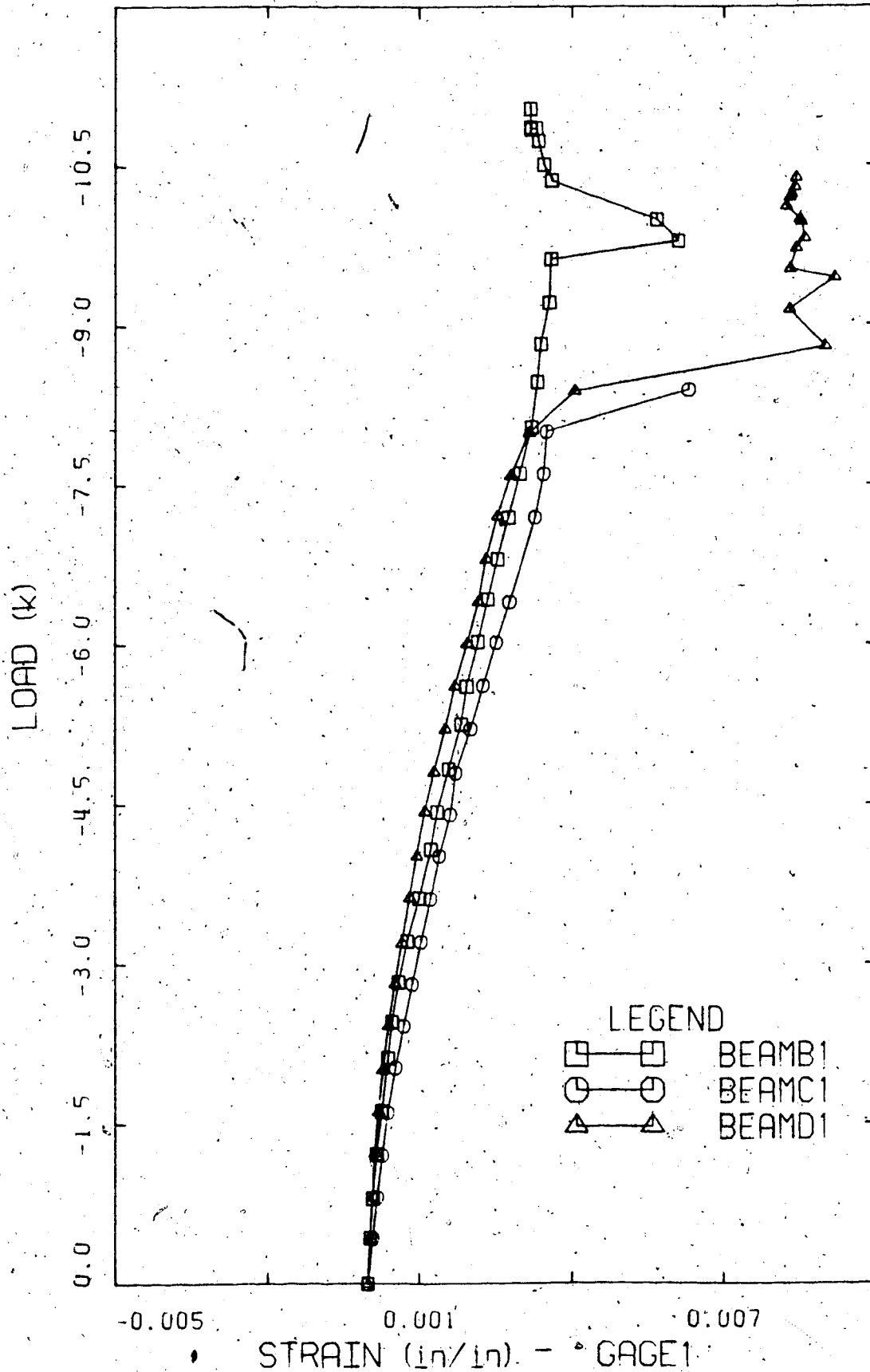
BEAM D3.

Figure C16   Strain in Gage 1 - BEAM B1, BEAM C1 and
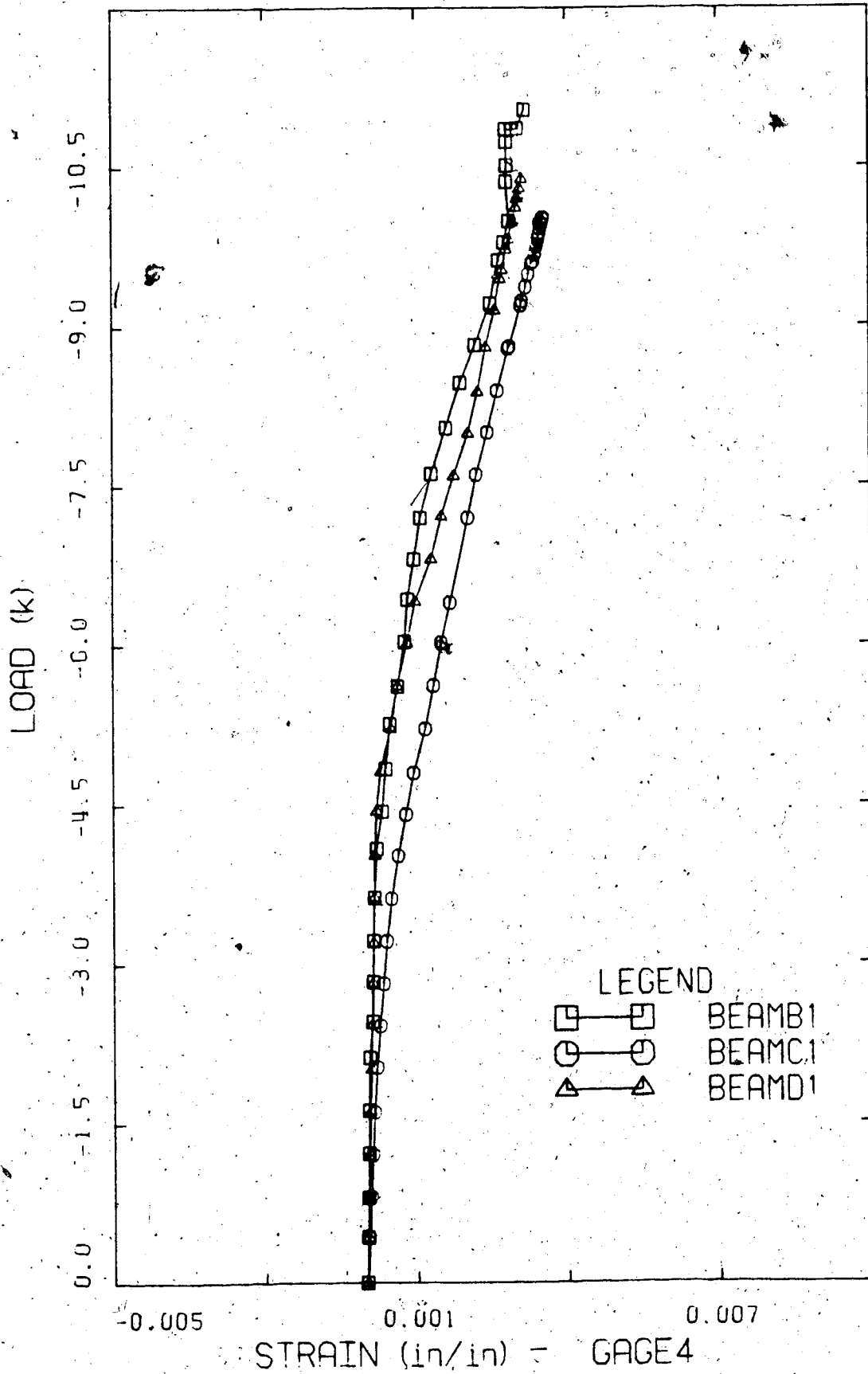
BEAM D1.

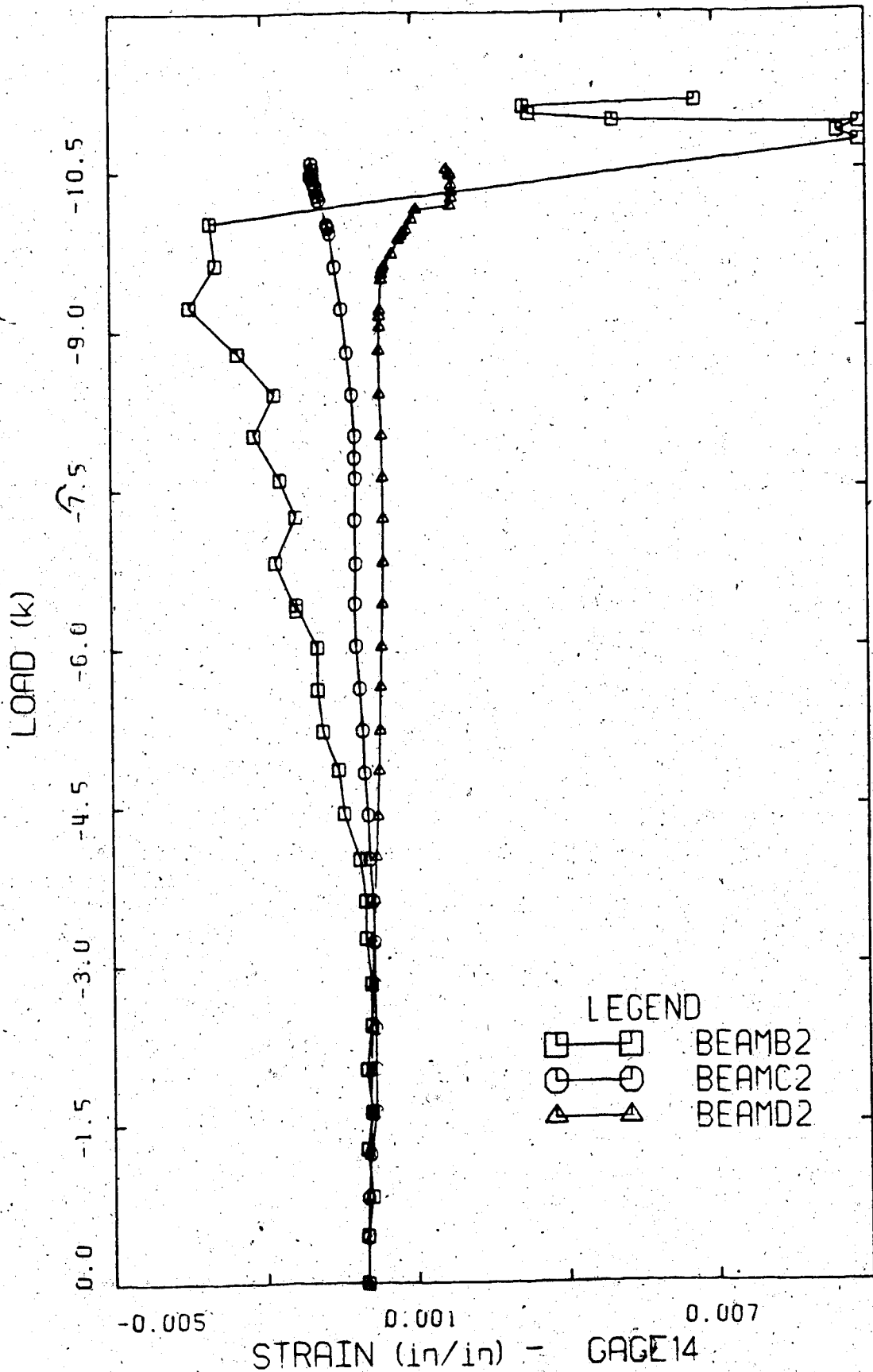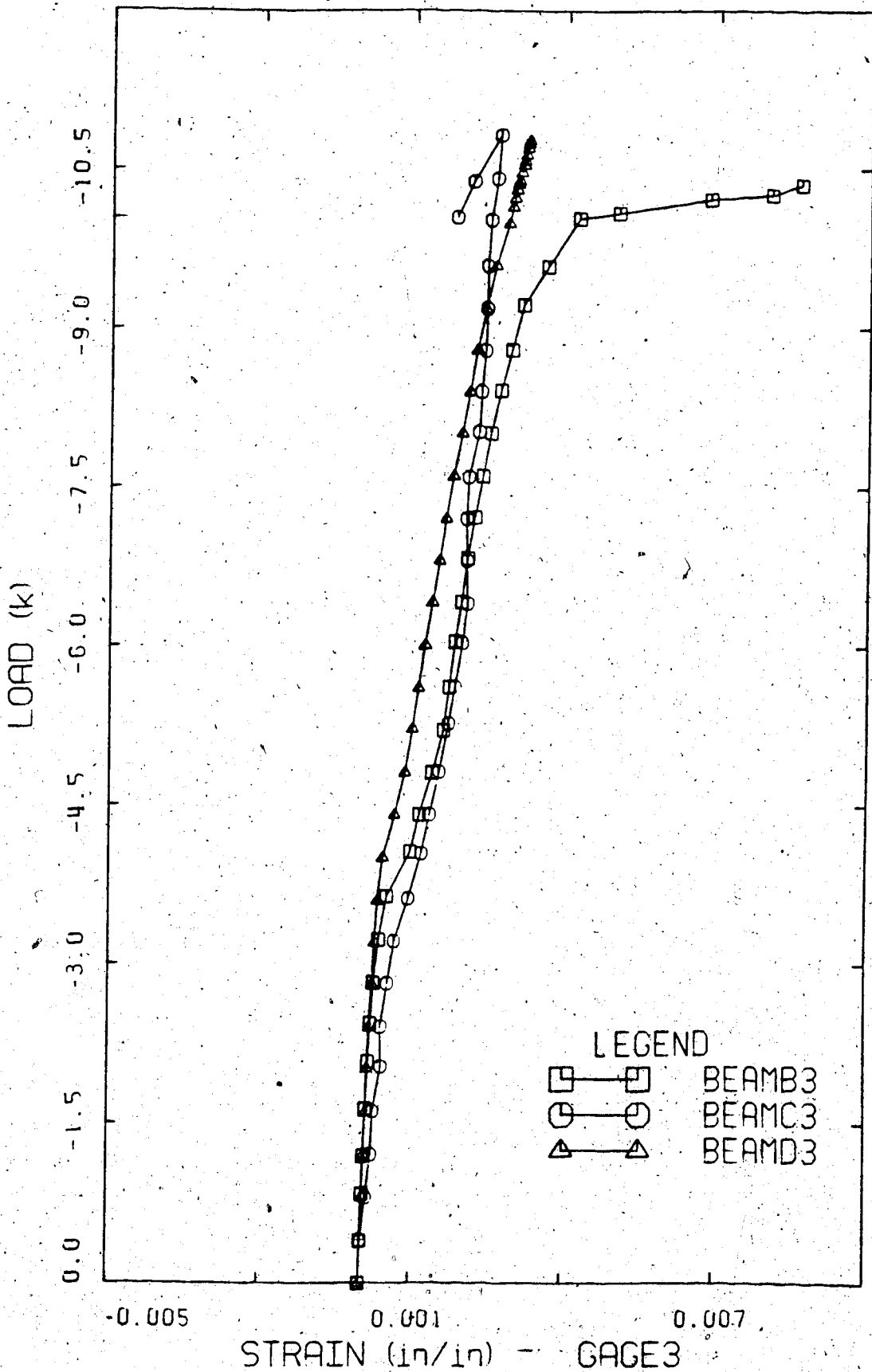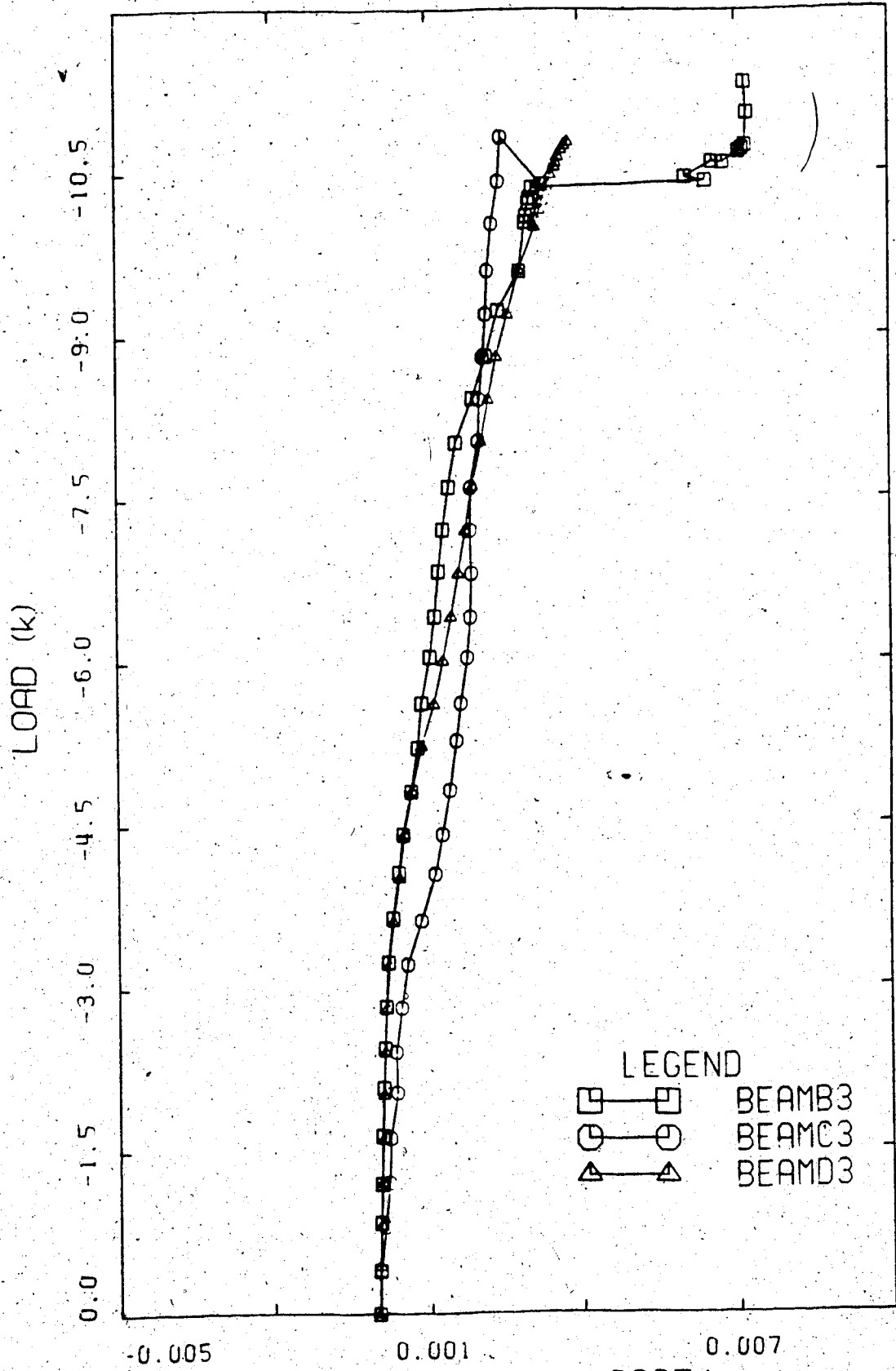Figure C17   Strain in Gage 4 - BEAM B1, BEAM C1 and
BEAM D1.
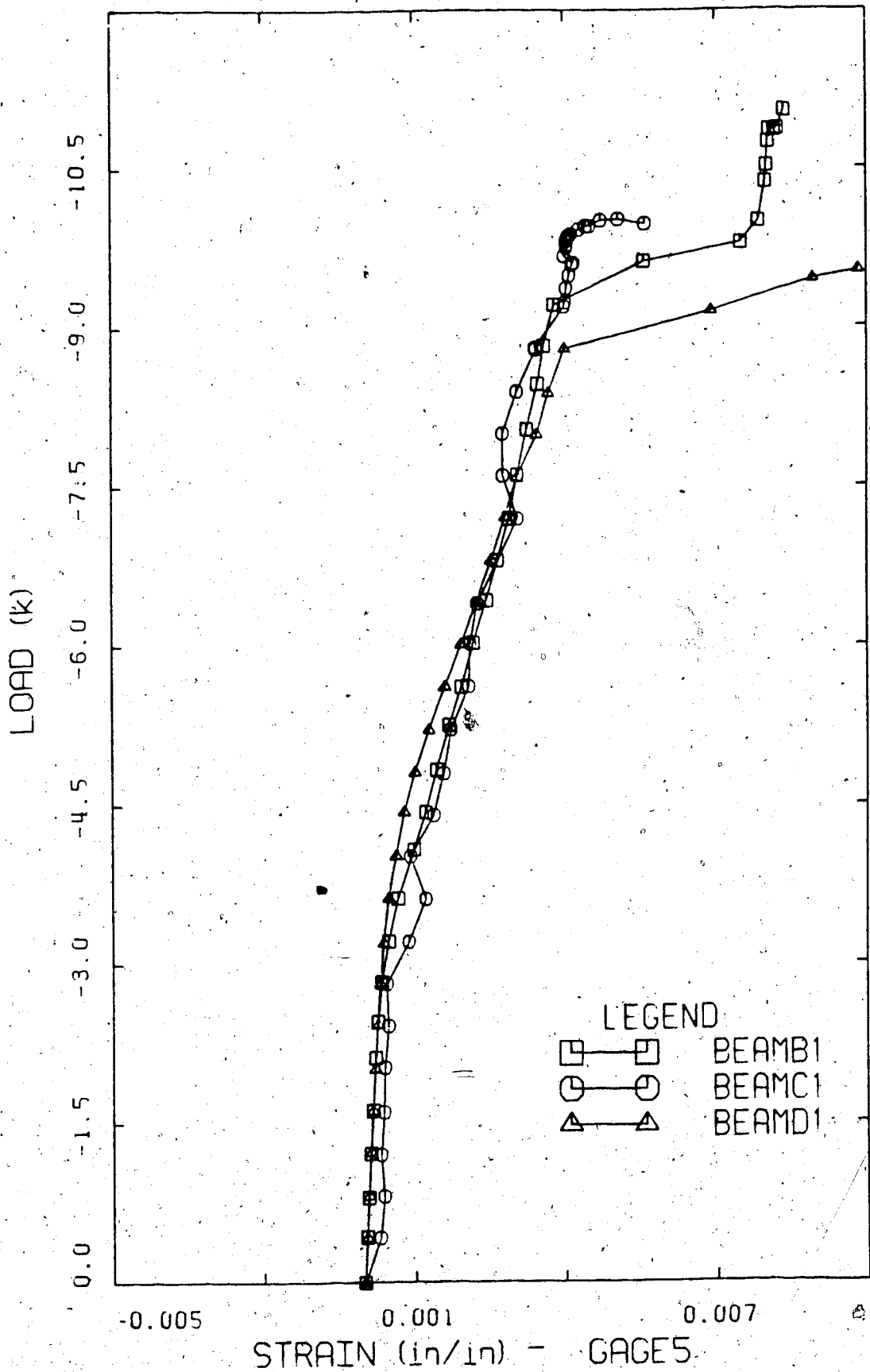
Figure C18   Strain in Gage 5 - BEAM B1, BEAM C1 and
BEAM D1.
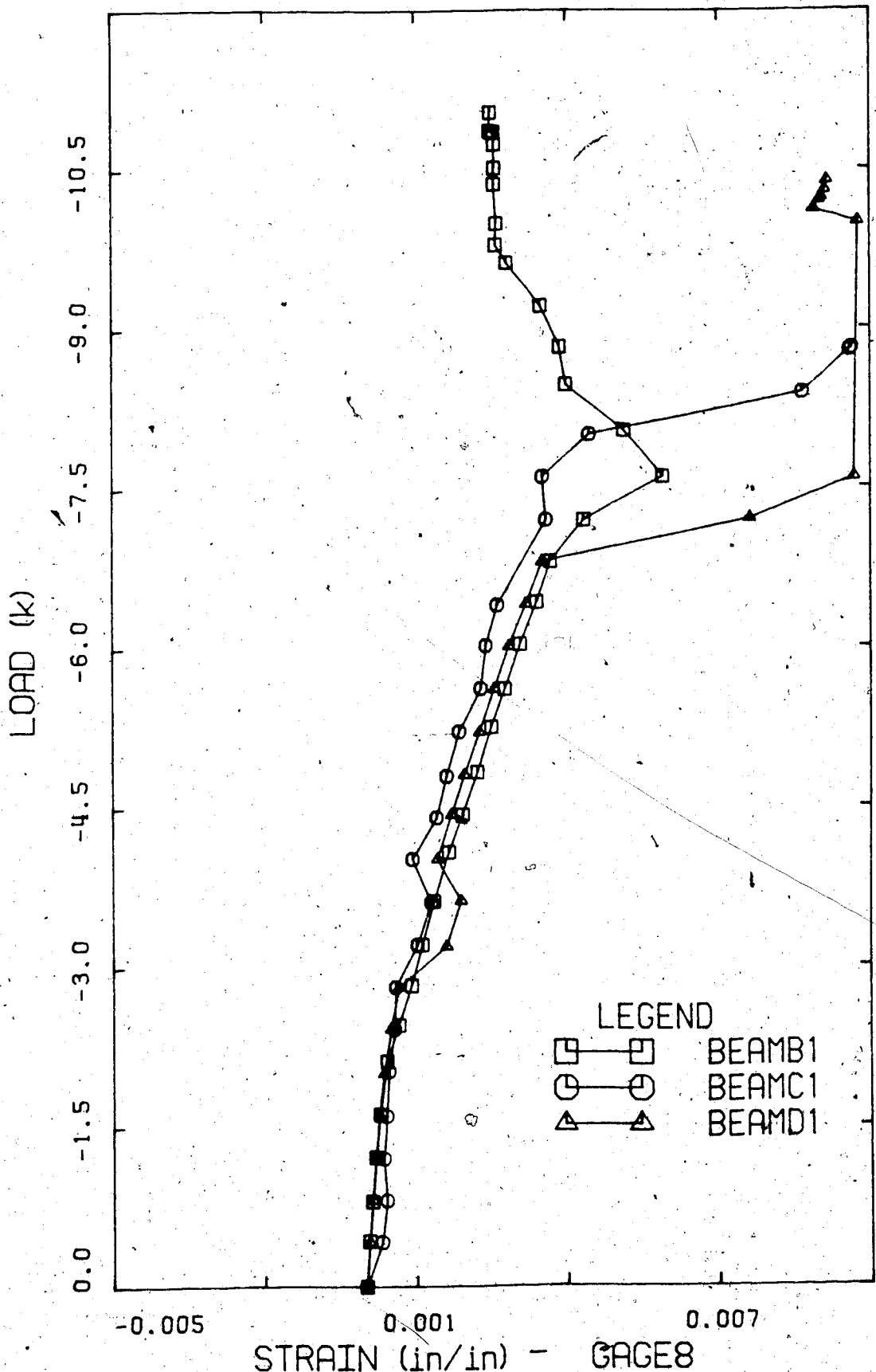
Figure C19   Strain in Gage 8 - BEAM B1, BEAM C1 and
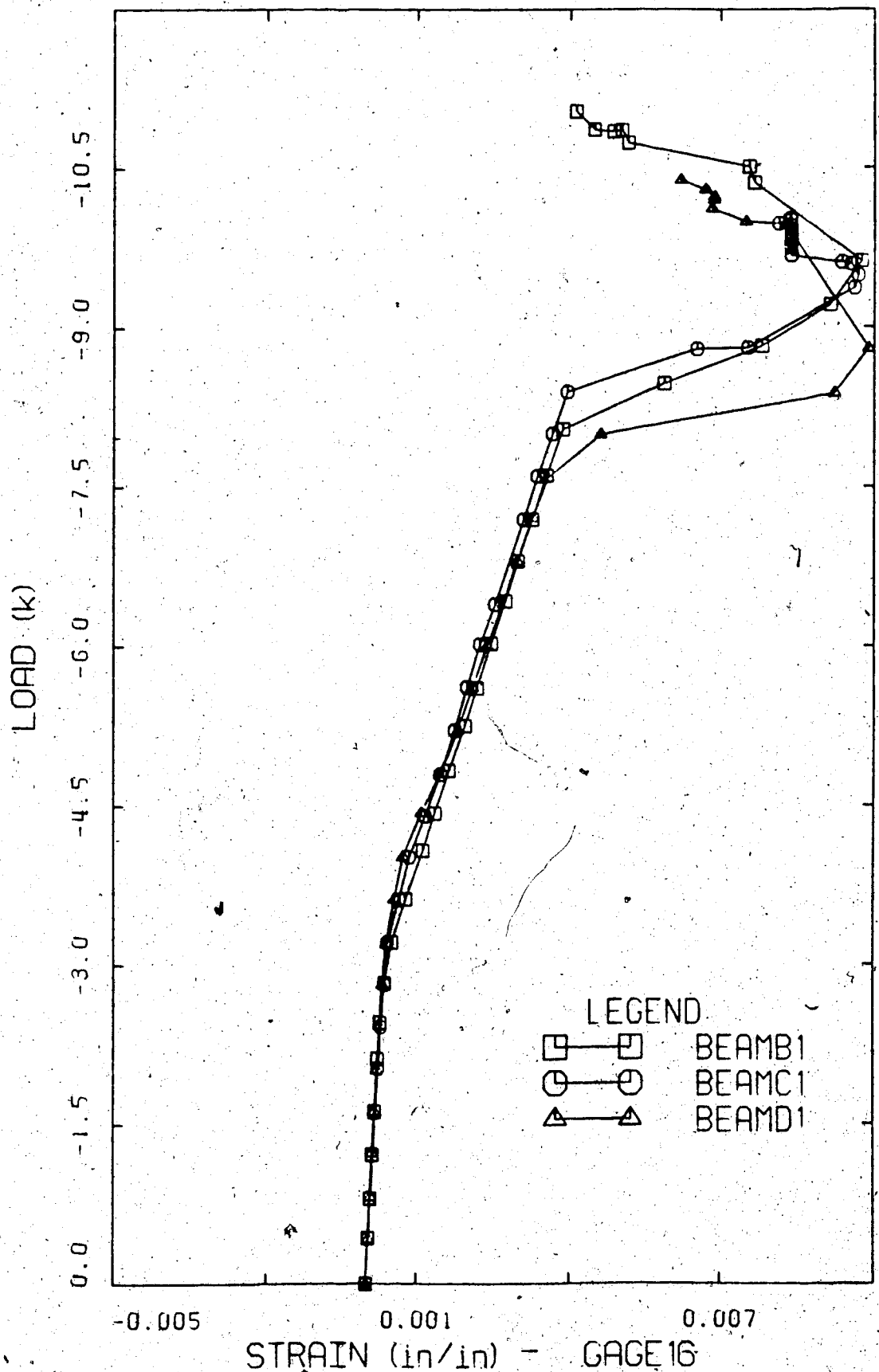
BEAM D1.

Figure C20   Strain in Gage 16 – BEAM B1, BEAM C1 and
BEAM D1.
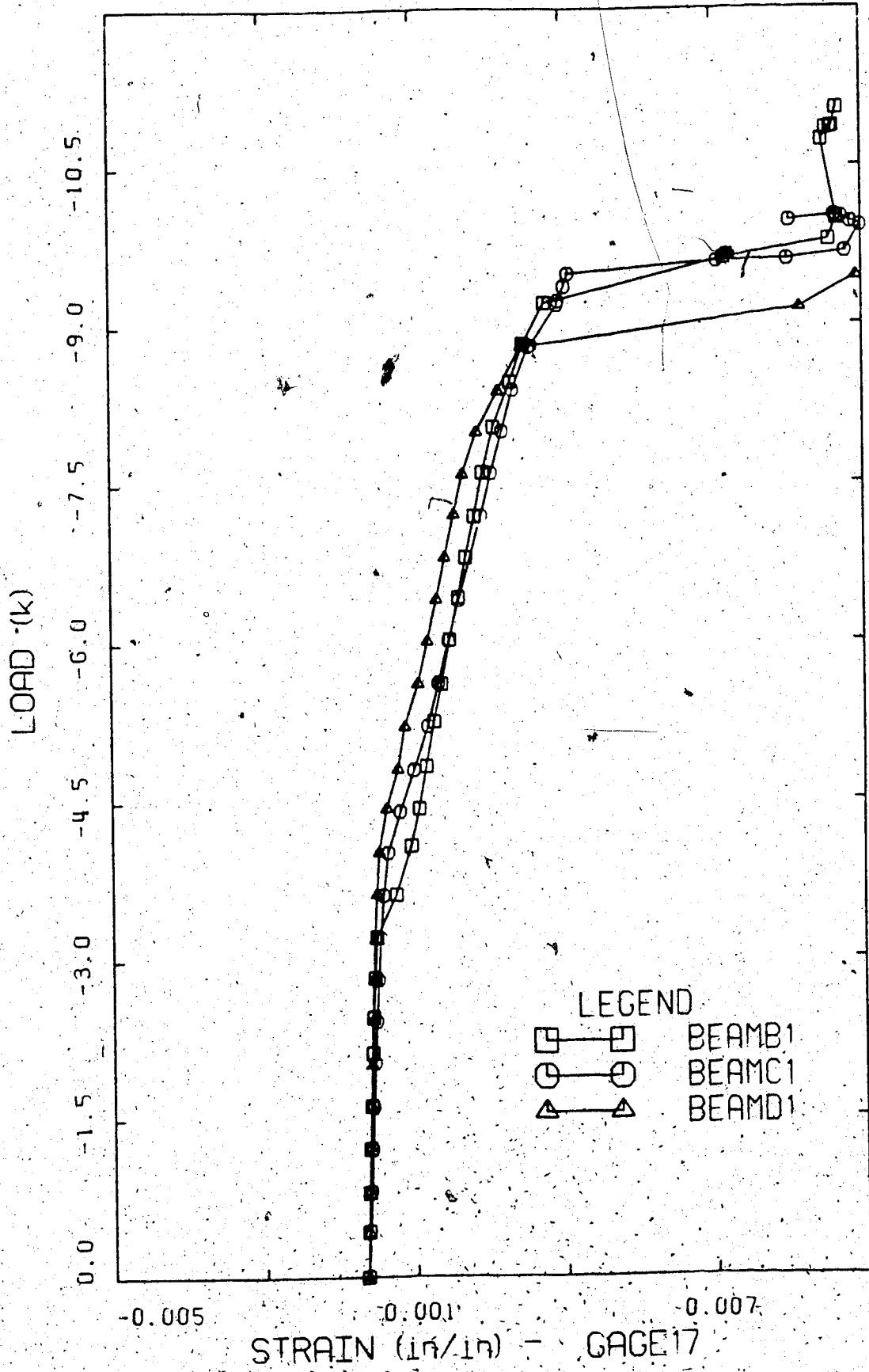
Figure C21   Strain in Gage 17 — BEAM B1, BEAM C1 and
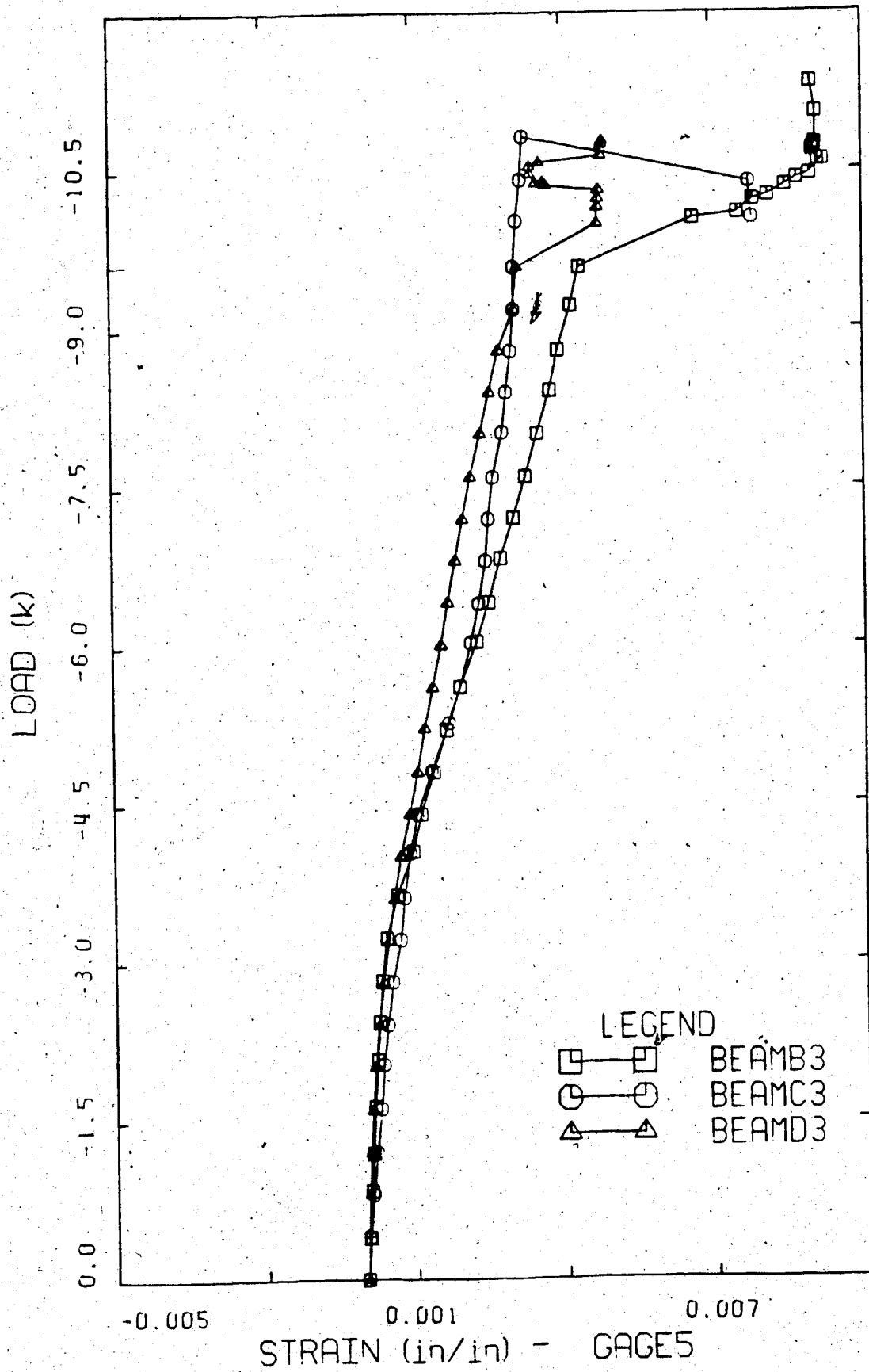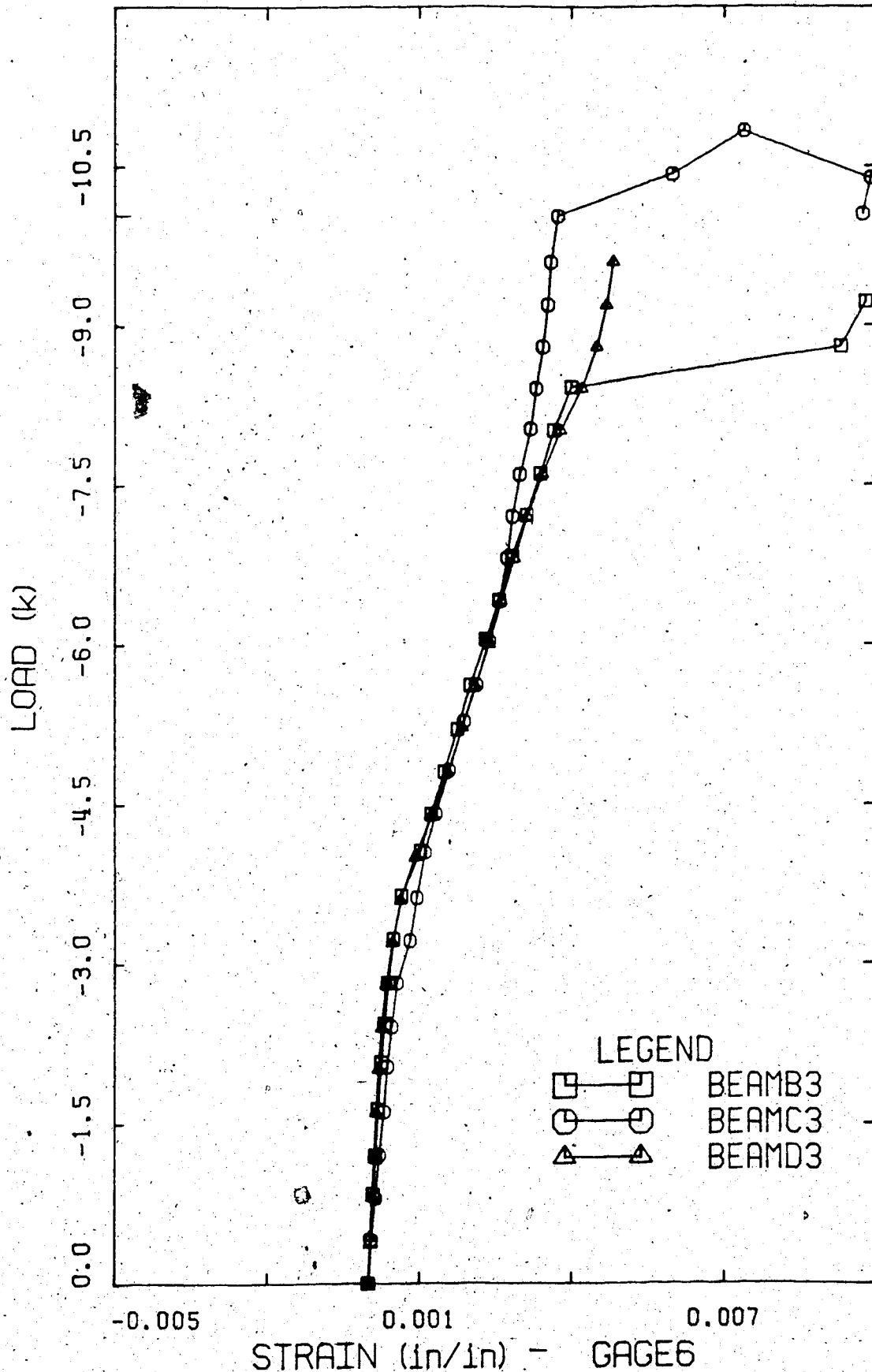BEAM D1.
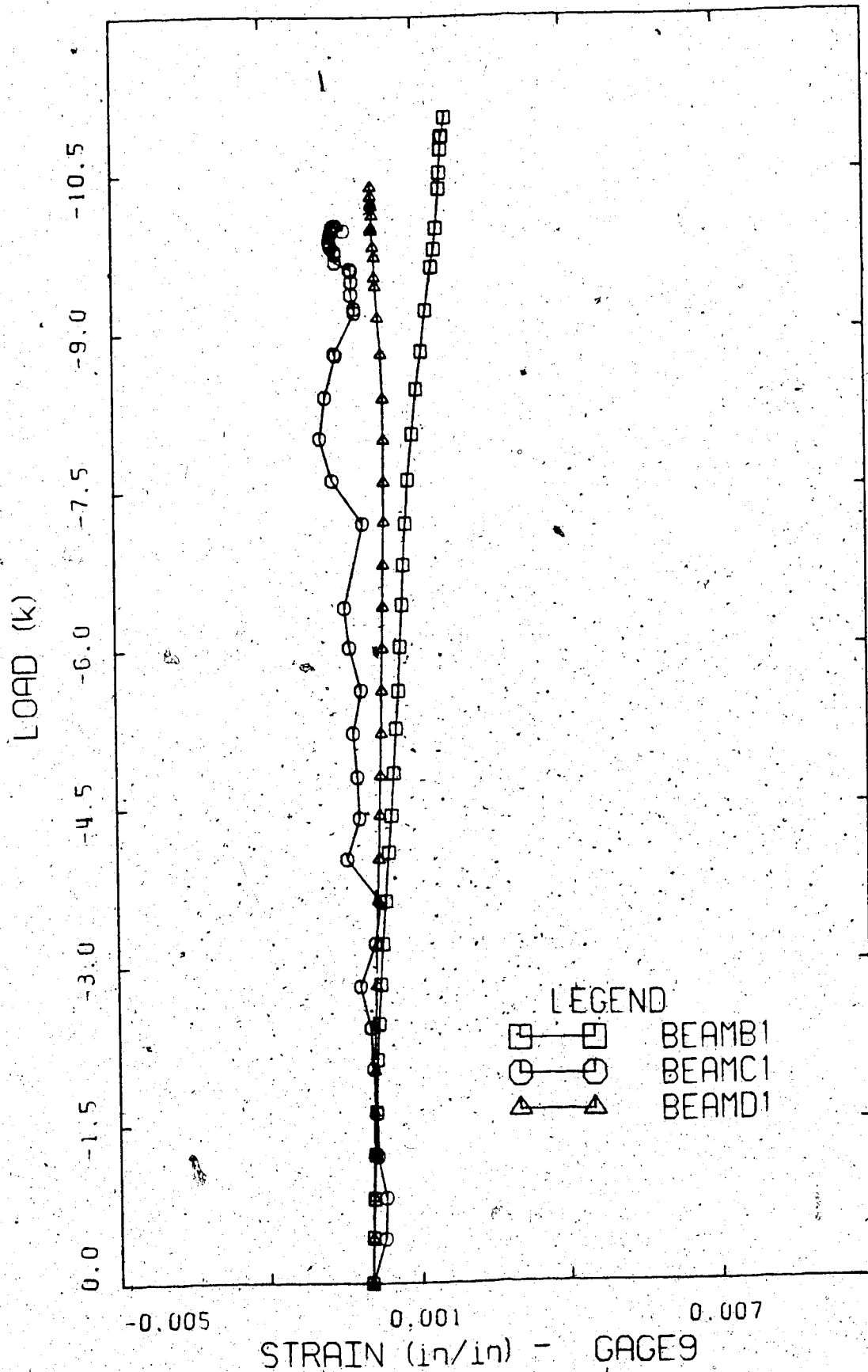
Figure C22   Strain in Gage 9 - BEAM B1, BEAM C1 and
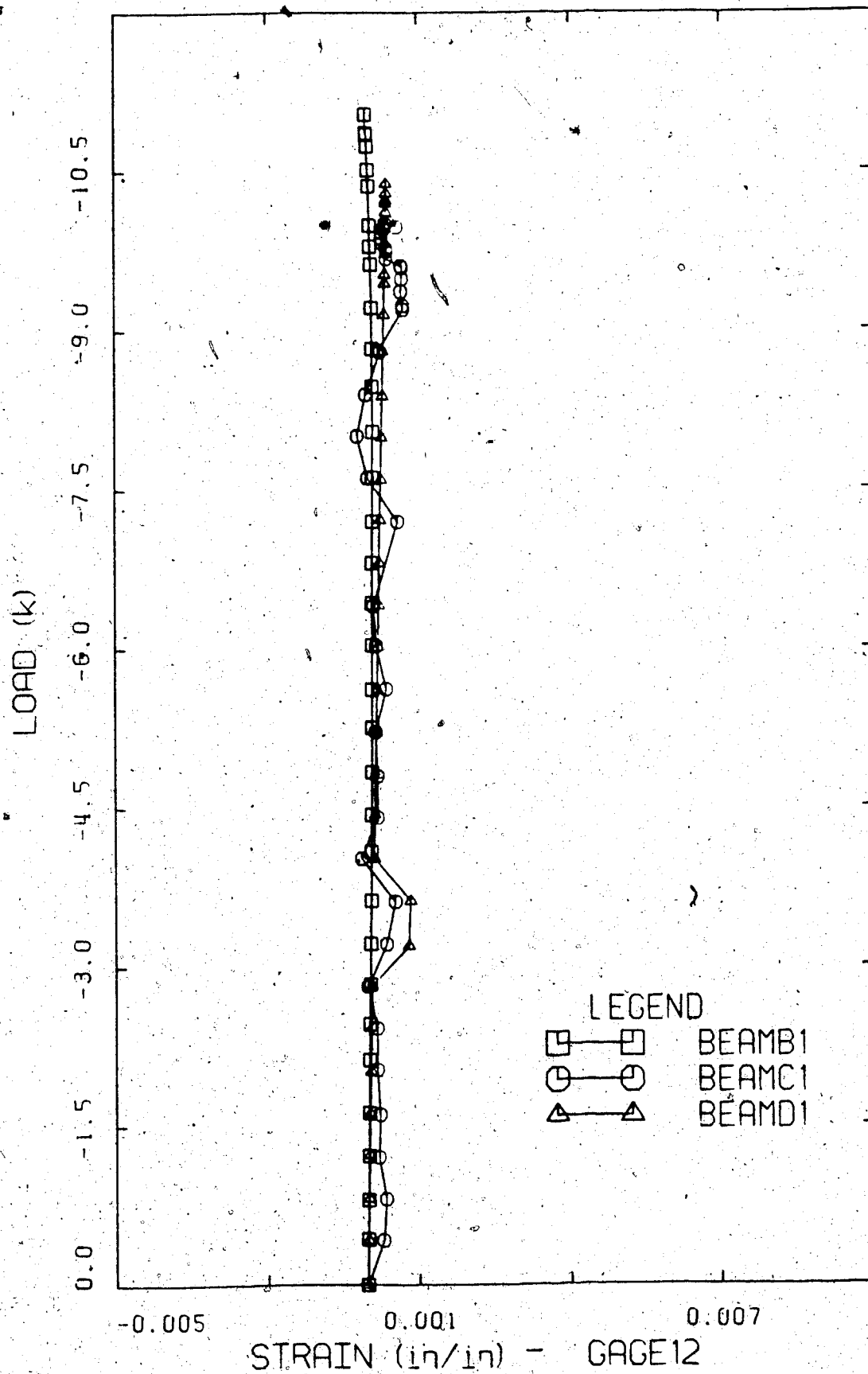
BEAM D1.
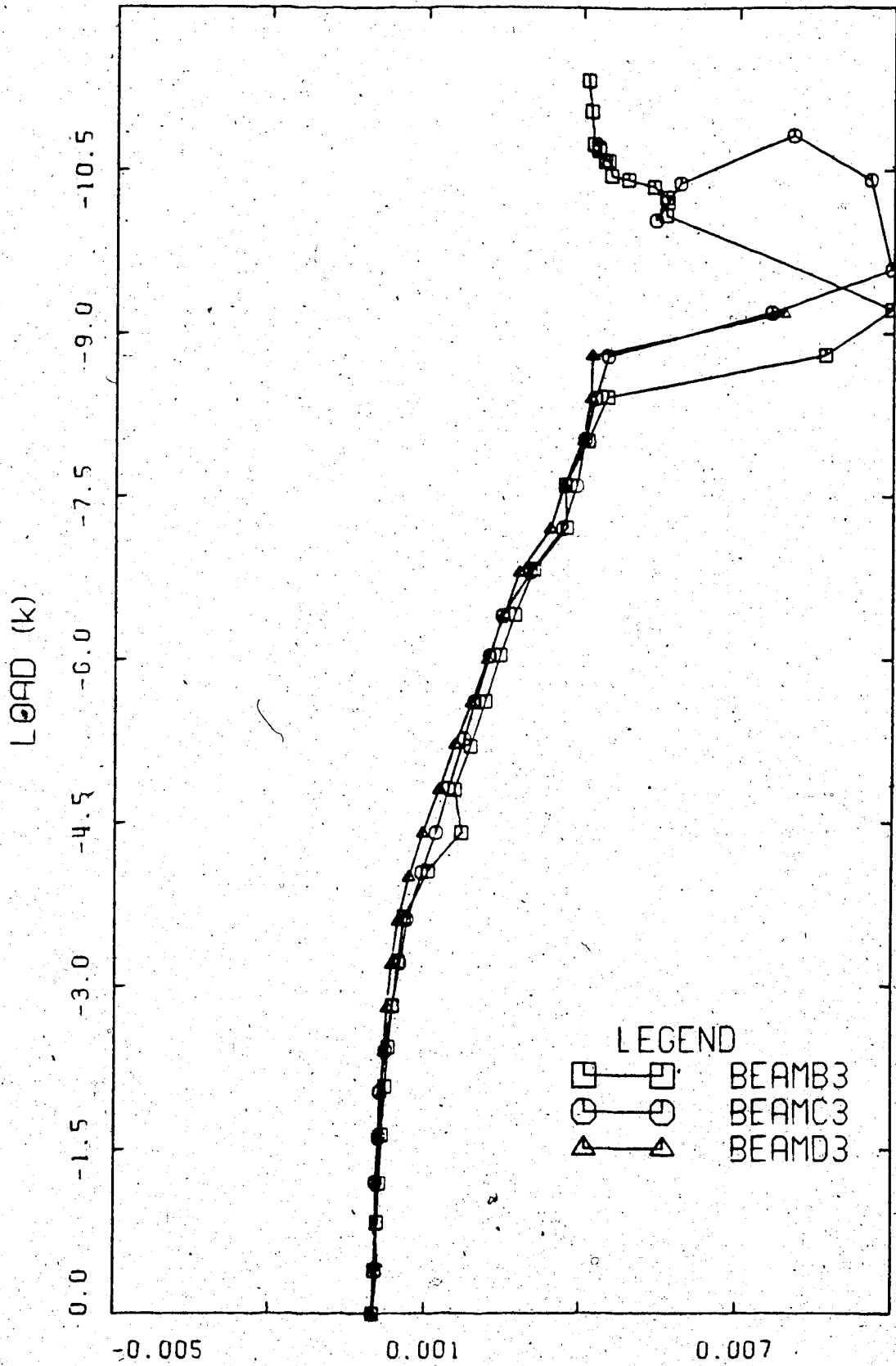
Figure C23   Strain in Gage 12 - BEAM B1, BEAM C1 and
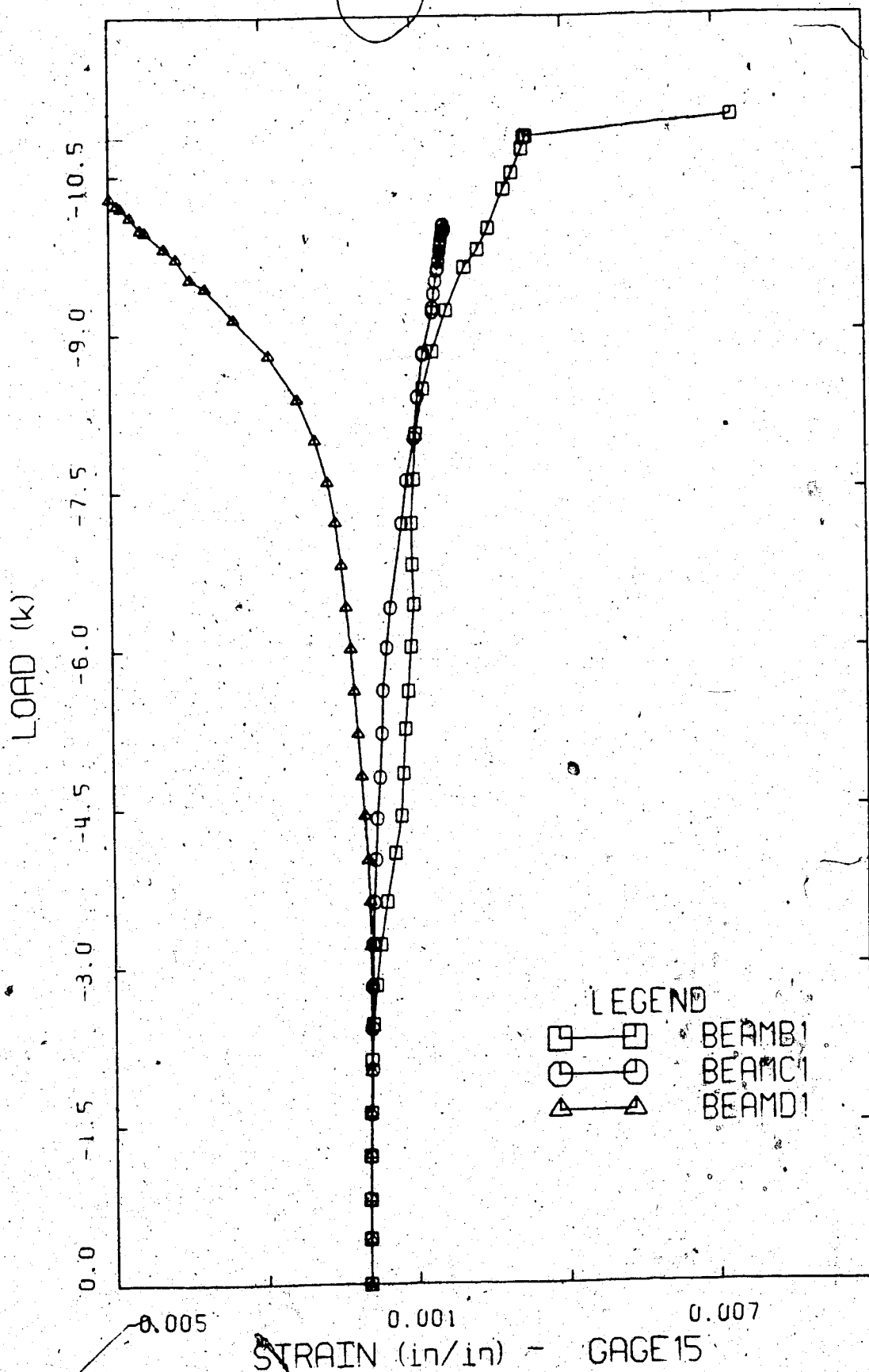
BEAM D1.

Figure C24   Strain in Gage 15 – BEAM B1, BEAM C1 and
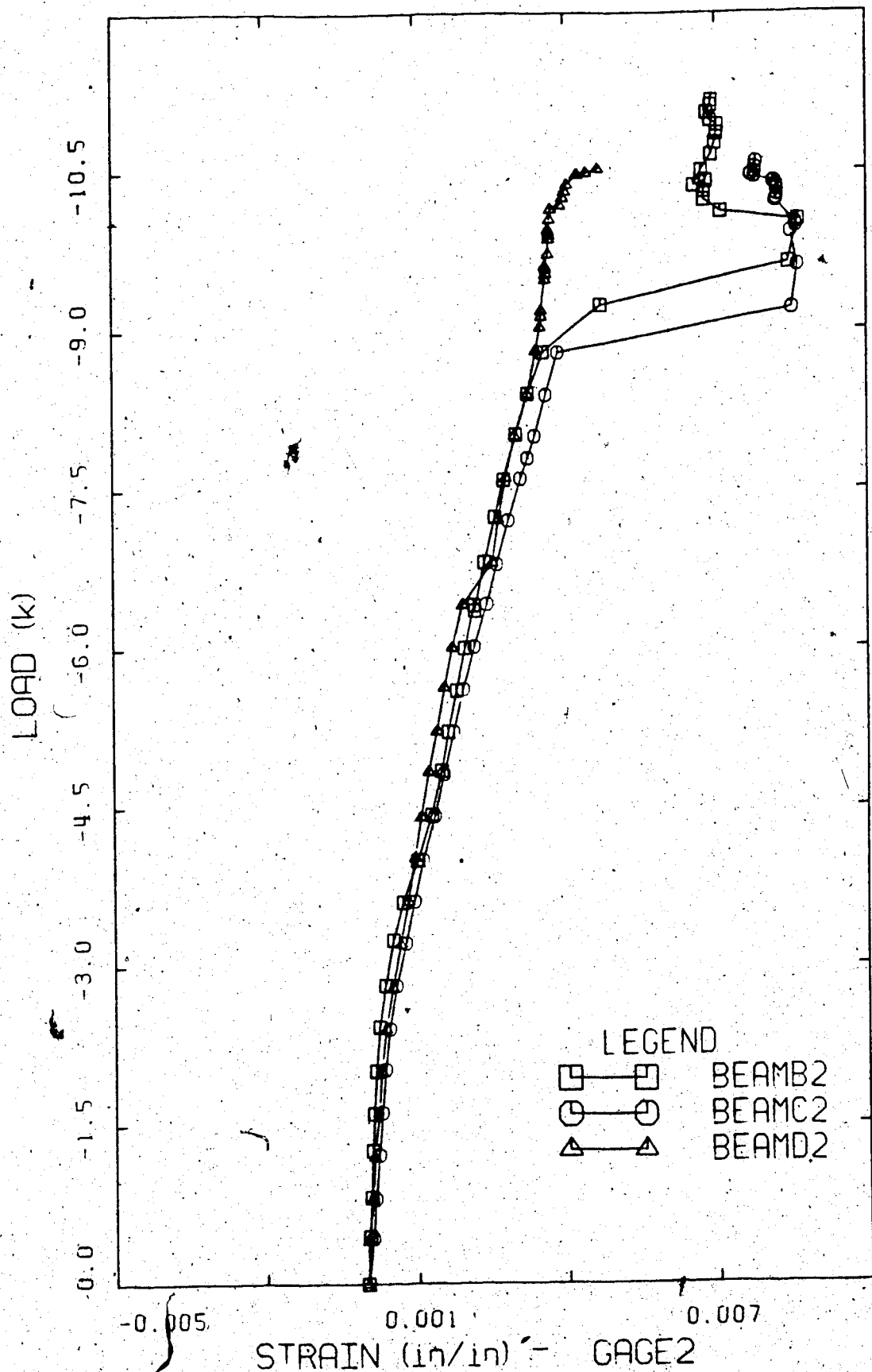
BEAM D1.

Figure C25   Strain in GAge 2 - BEAM B2, BEAM C2 and
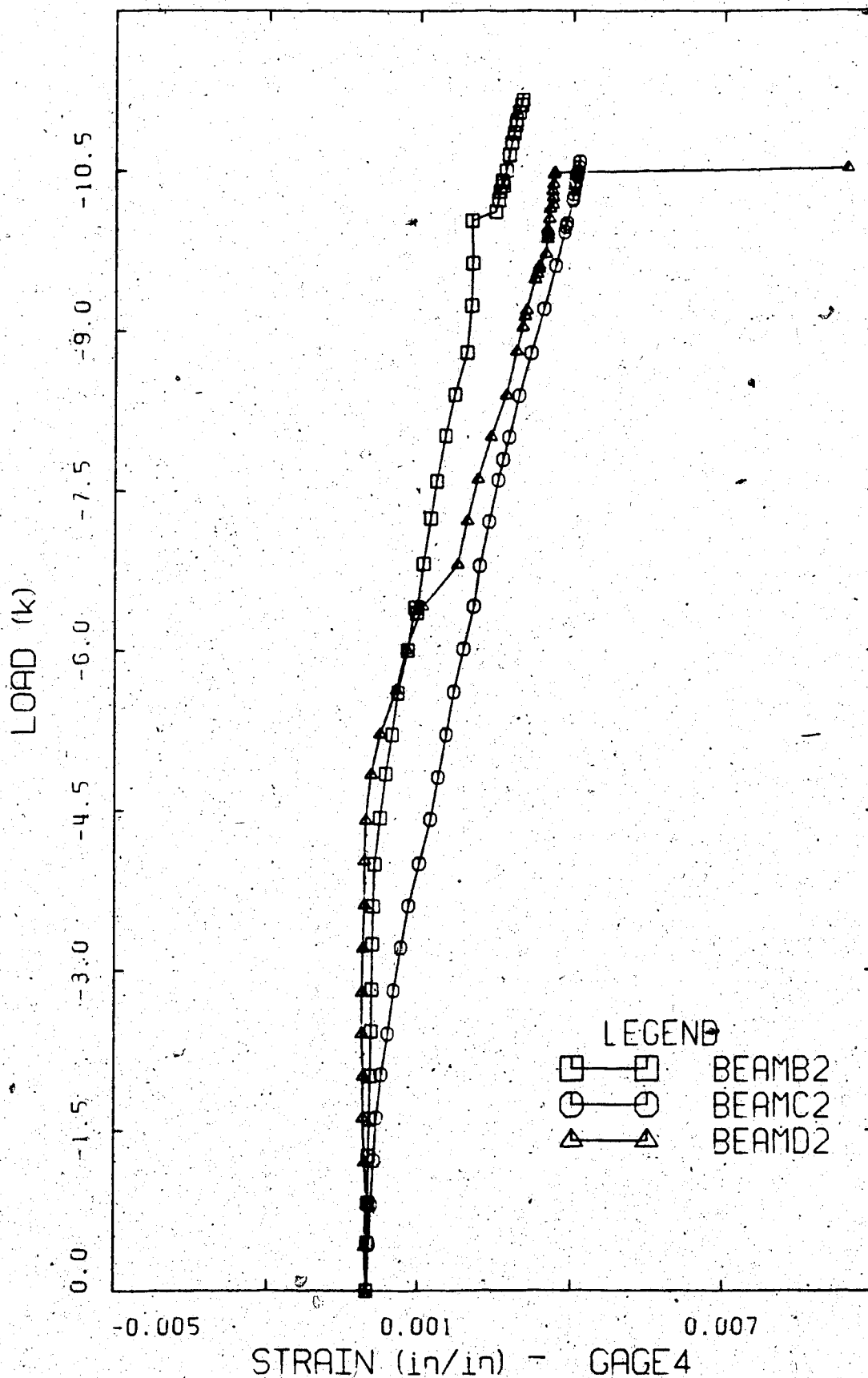
BEAM D2.

Figure C26   Strain in Gage 4 – BEAM B2, BEAM C2 and
BEAM D2.
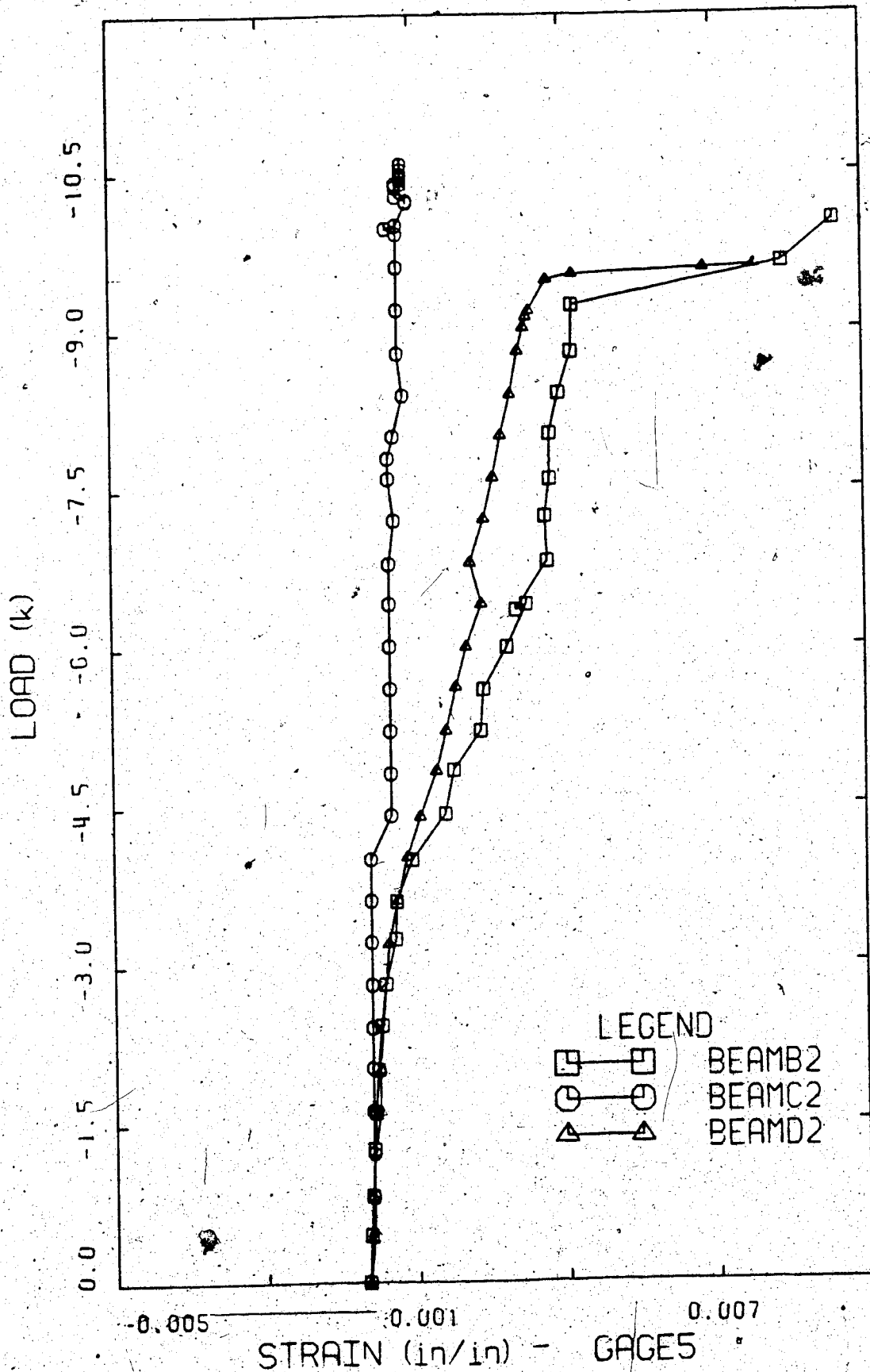
Figure C27   Strain in Gage 5 - BEAM B2, BEAM C2 and
BEAM D2.
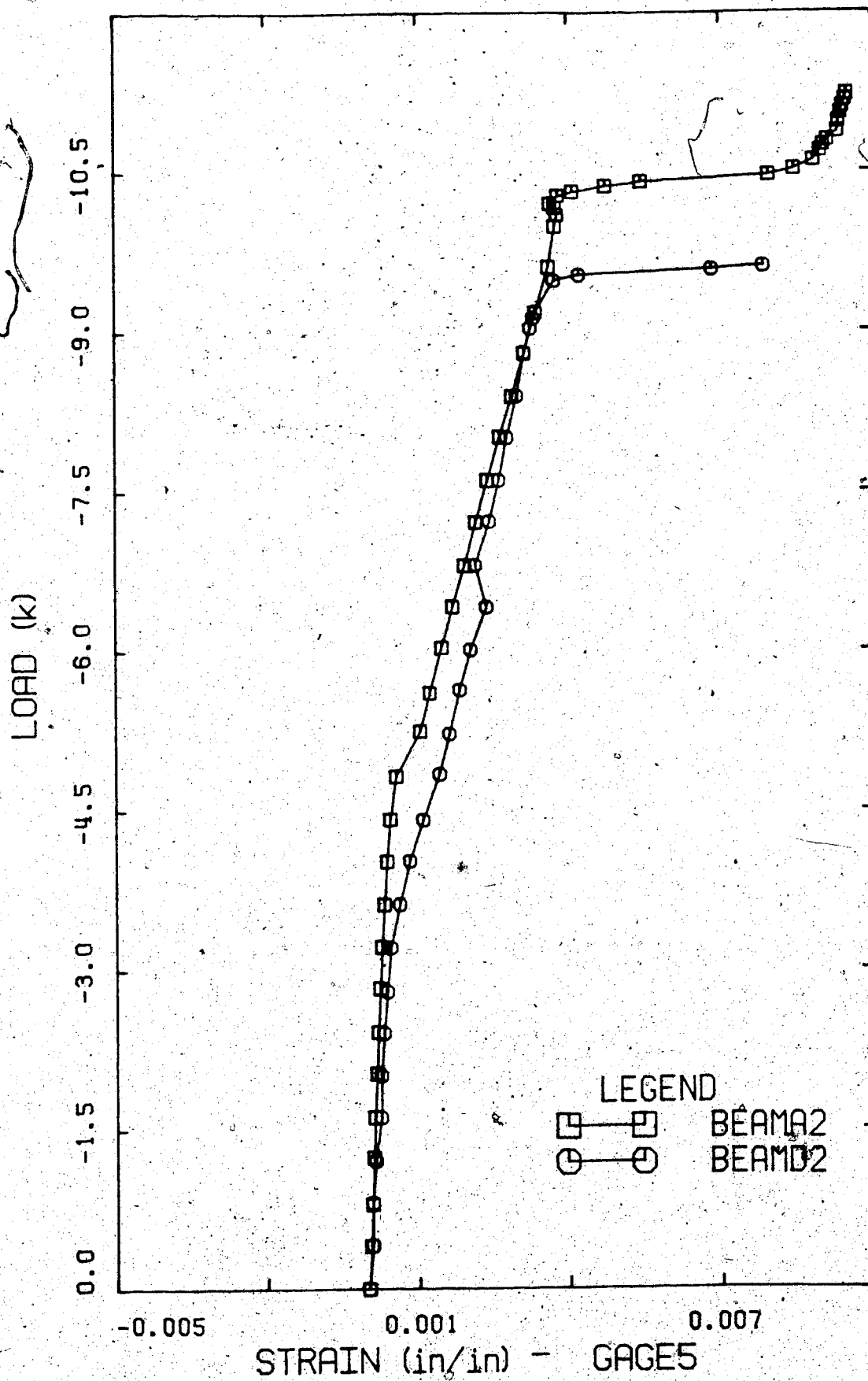
Figure C28 Strain in Gage 5 - BEAM A2 and BEAM D2.
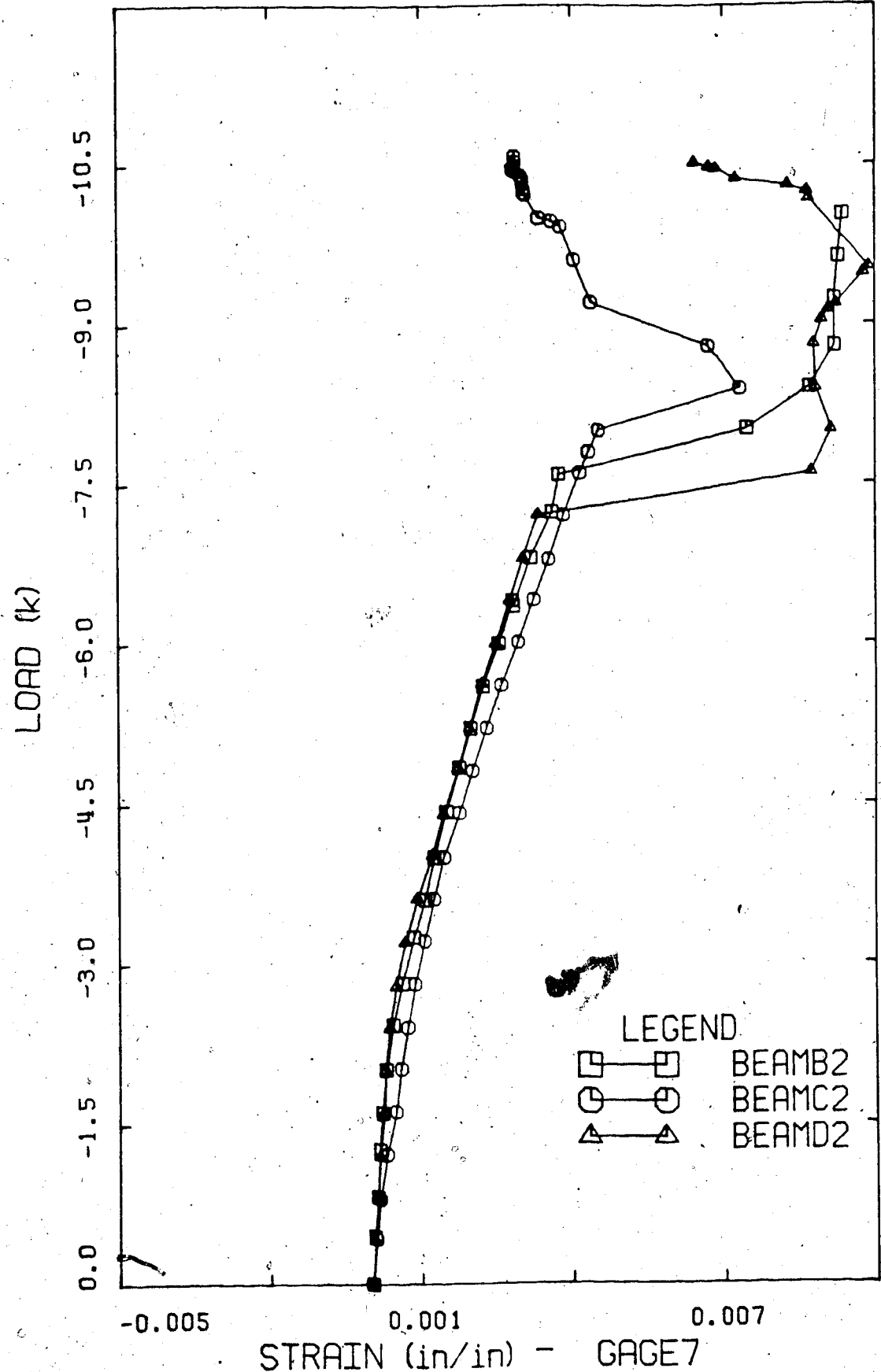
Figure C29   Strain in Gage 7 - BEAM B2, BEAM C2 and
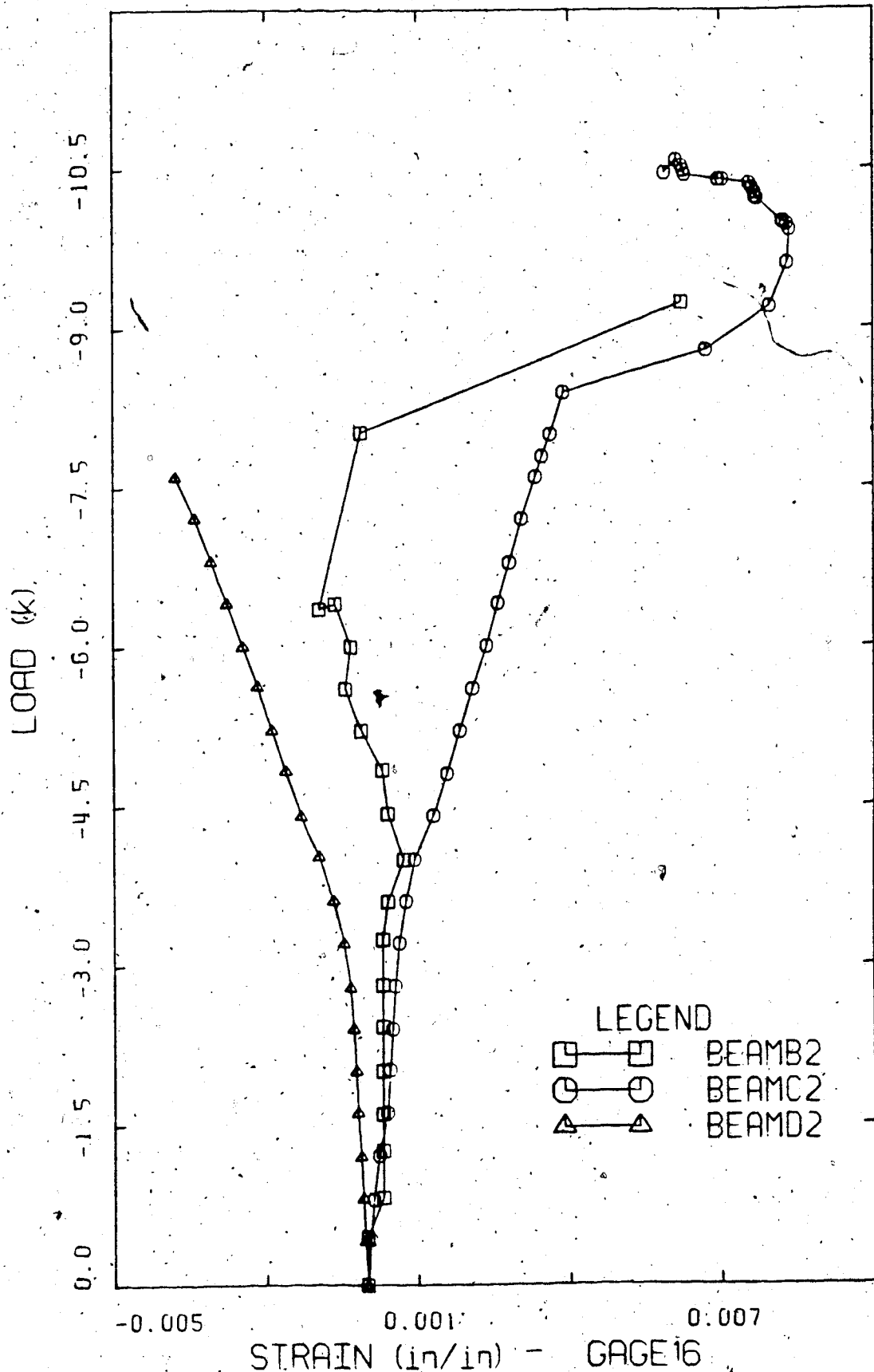
BEAM D2.

Figure C30   Strain in Gage 16 - BEAM B2, BEAM C2 and
BEAM D2.
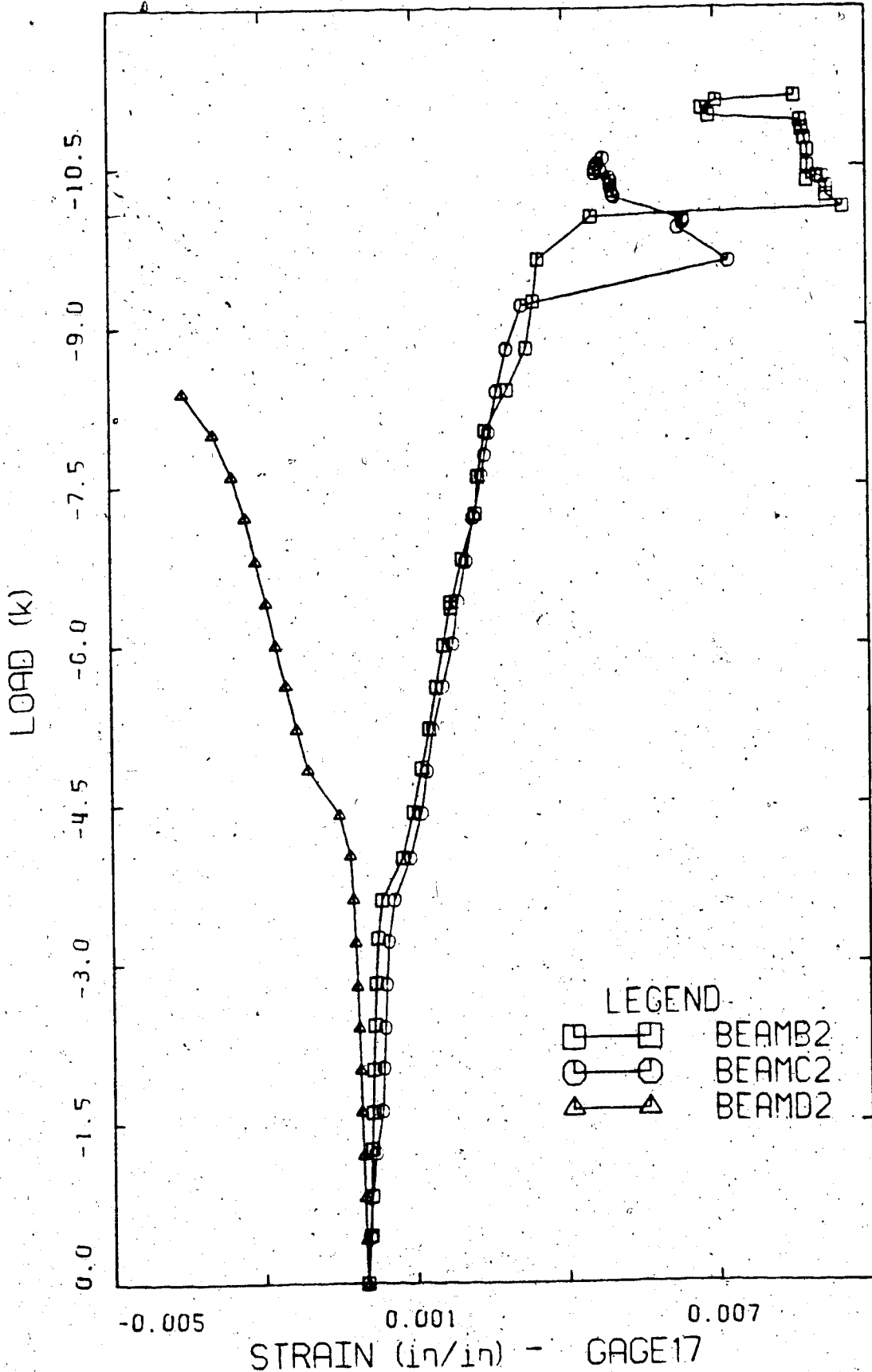
Figure C31   Strain in Gage 17 - BEAM B2, BEAM C2 and
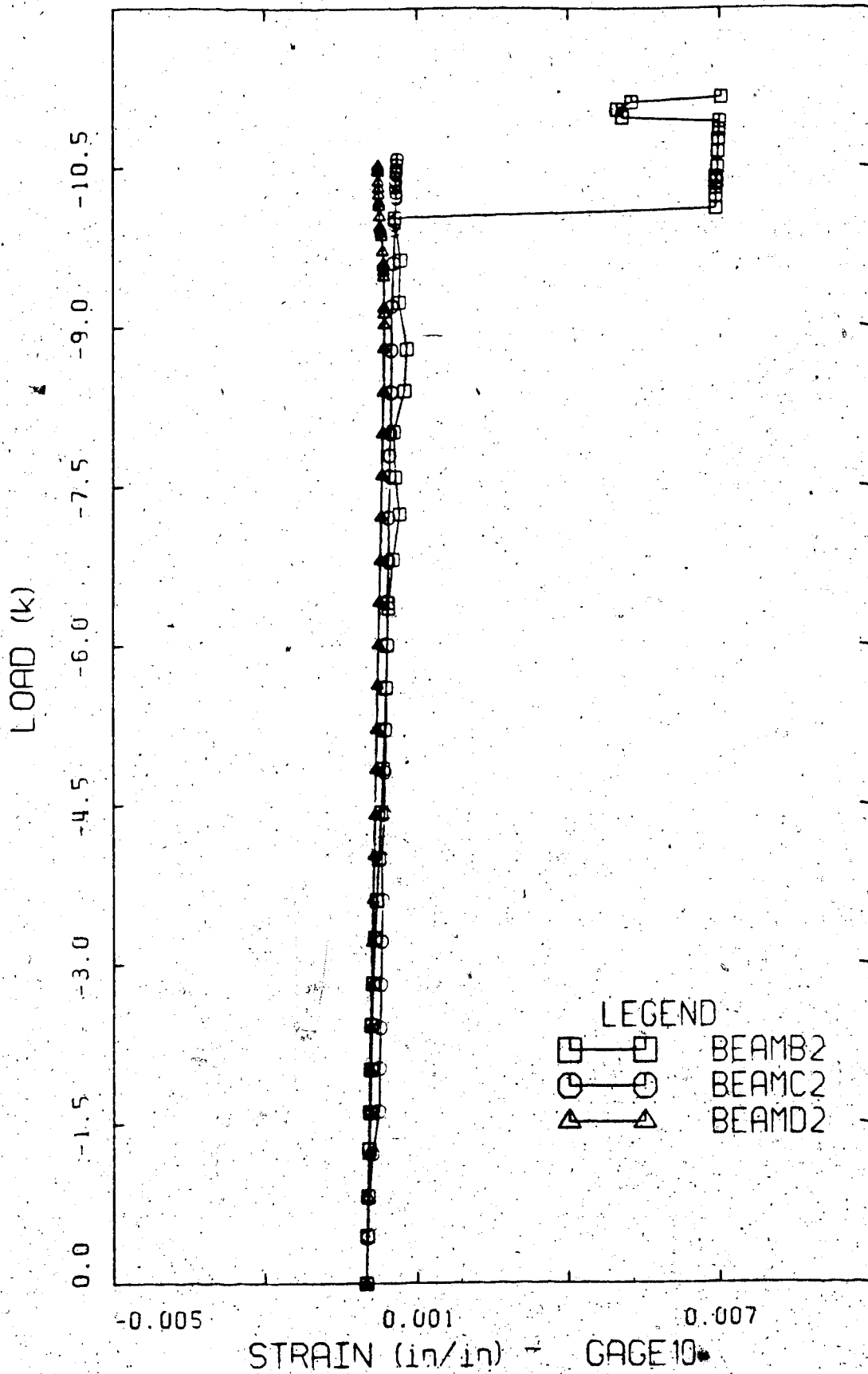
BEAM D2.

Figure C32   Strain in Gage 10 - BEAM B2, BEAM C2 and
BEAM D2.
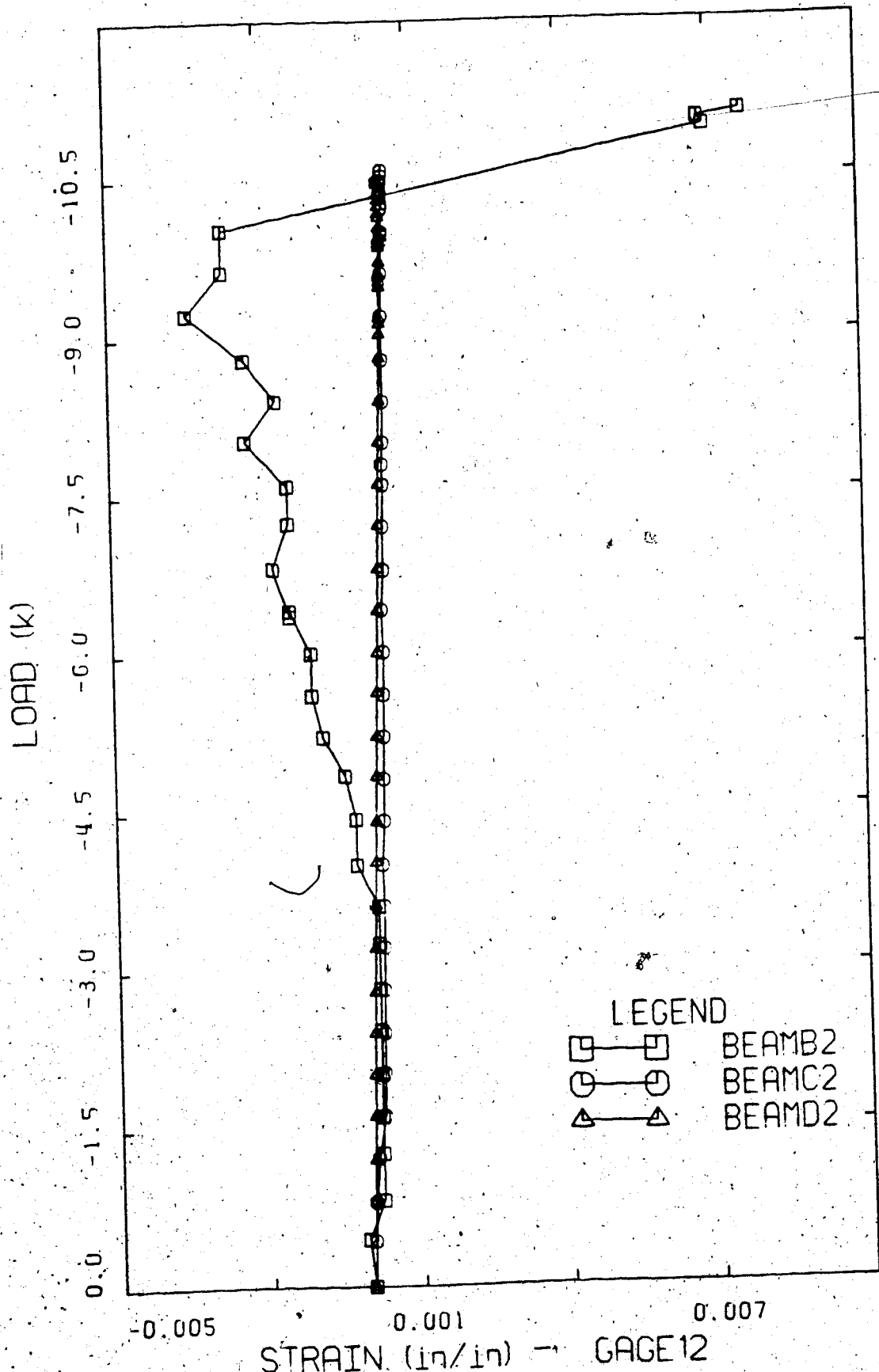
Figure C33   Strain in Gage 12 - BEAM B2, BEAM C2 and

BEAM D2.

Figure C34   Strain in Gage 14 - BEAM B2, BEAM C2 and

BEAM D2.

Figure C35   Strain in Gage 3 - BEAM B3, BEAM C3 and

BEAM D3.

Figure C36   Strain on Gage 4 - BEAM B3, BEAM C3 and
BEAM D3.

Figure C37   Strain in Gage 5 - BEAM B3, BEAM C3 and
BEAM D3.

Figure C38   Strain in Gage 6 - BEAM B3, BEAM C3 and

BEAM D3.

Figure C39   Strain in Gage 16 - BEAM B3, BEAM C3 and
BEAM D3.
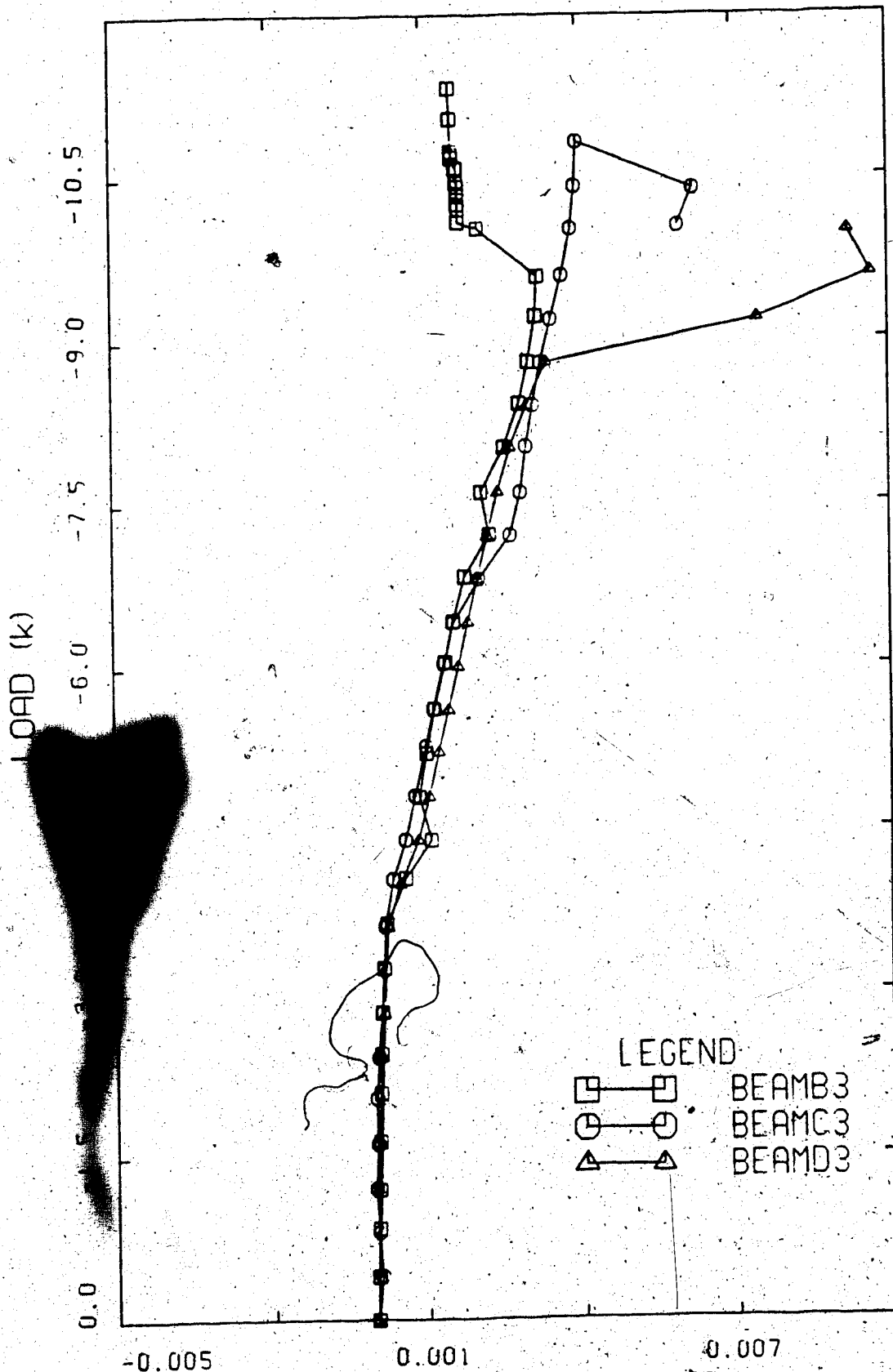
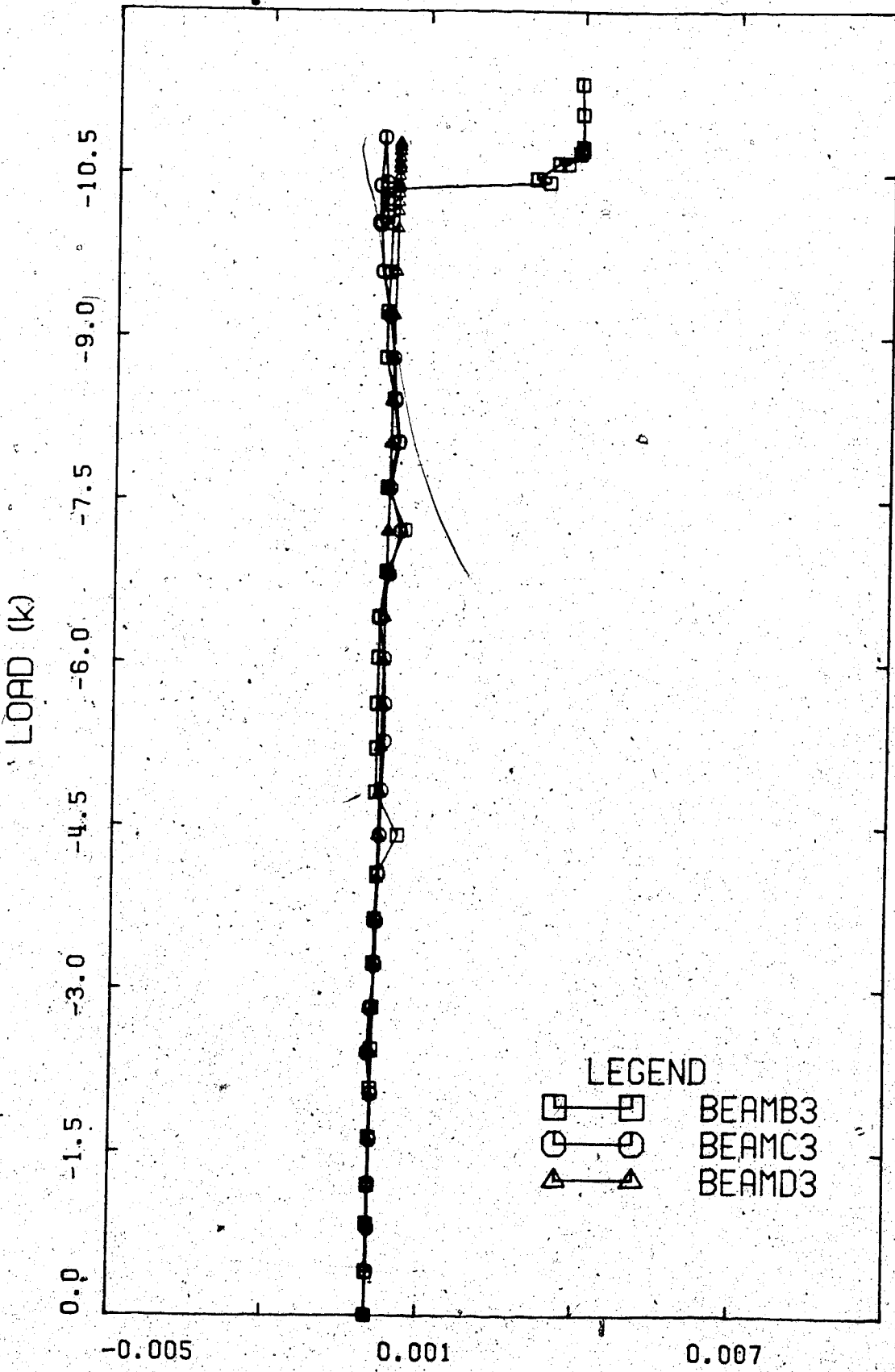Figure C40   Strain in Gage 17 - BEAM B3, BEAM C3 and
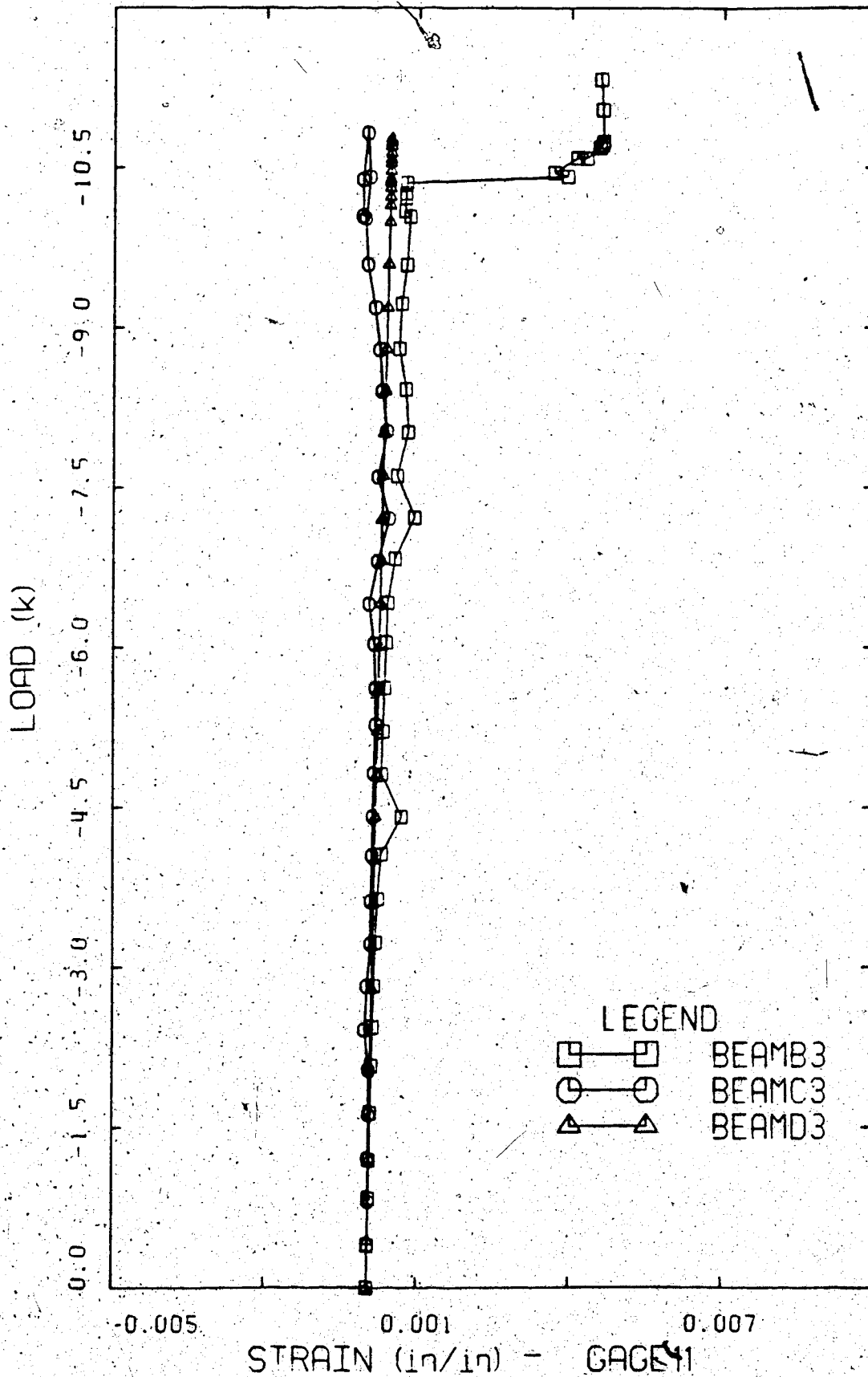
BEAM D3.

Figure C41   Strain in Gage 11 - BEAM B3, BEAM C3 and
BEAM D3.

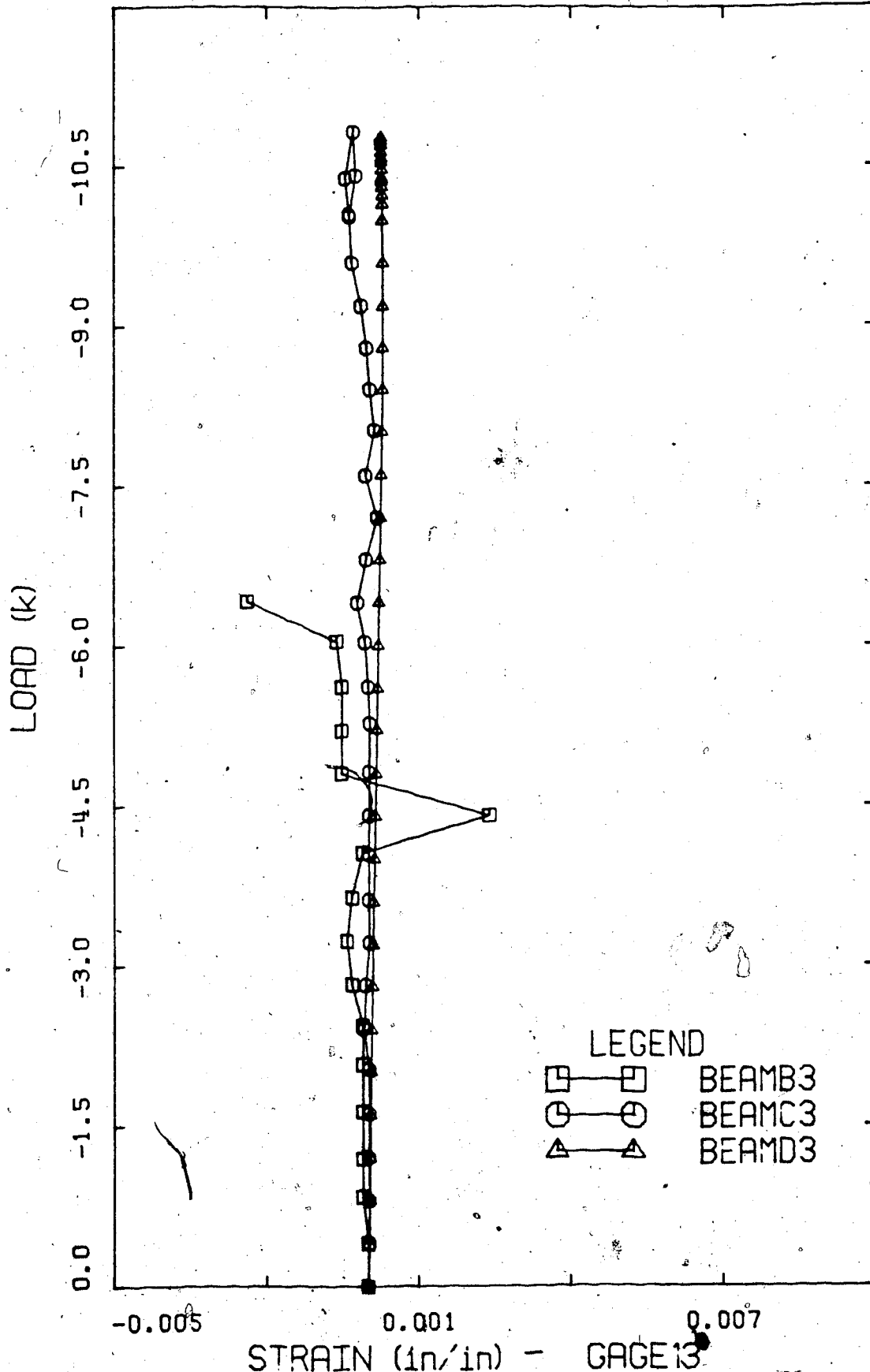Figure C42   Strain in Gage 12 - BEAM B3, BEAM C3 and

BEAM D3.

Figure C43   Strain in Gage 13 - BEAM B3, BEAM C3 and
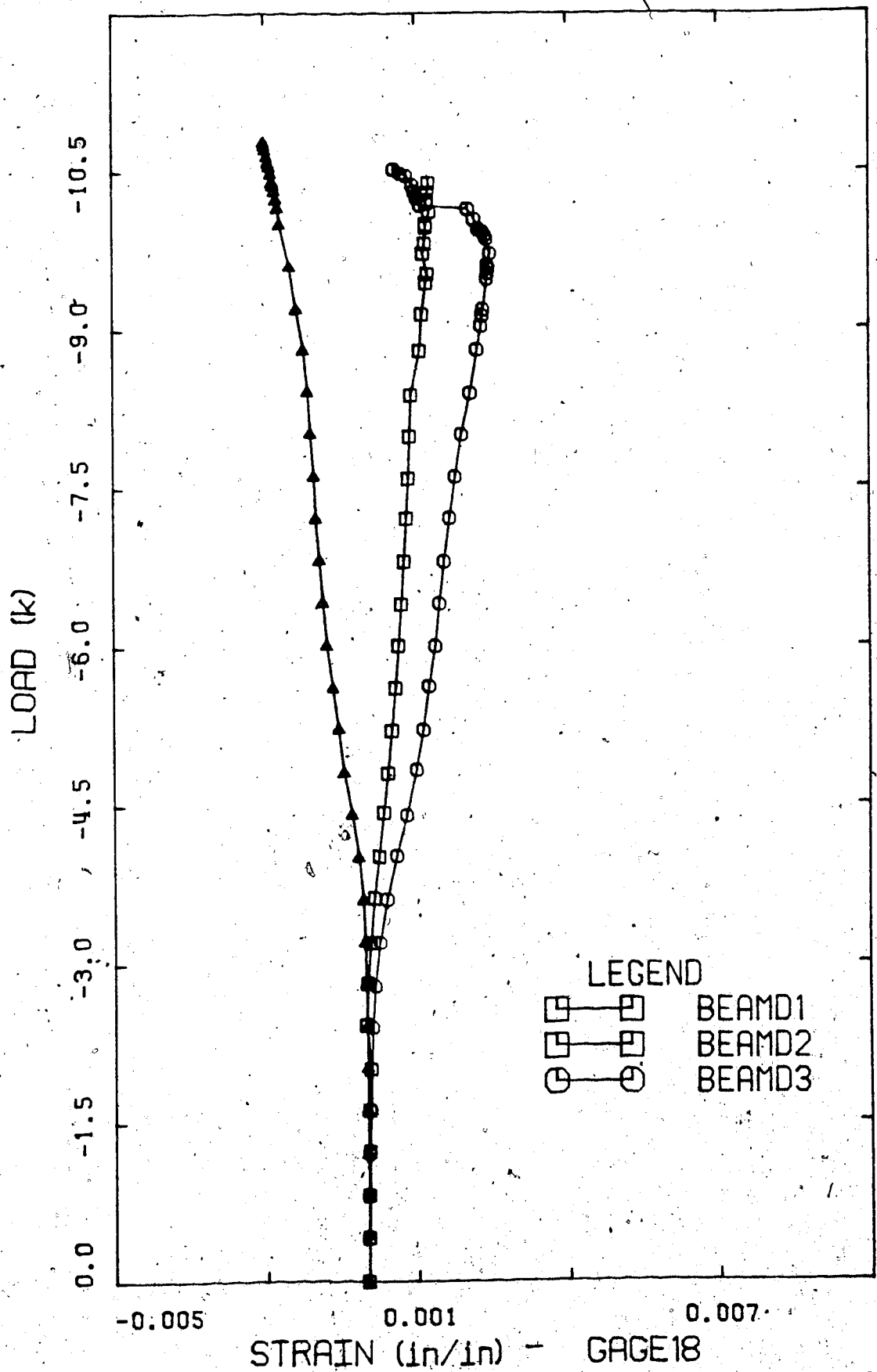
BEAM D3.

Figure C44   Strain in Gage 18 - BEAM D1, BEAM D2 and
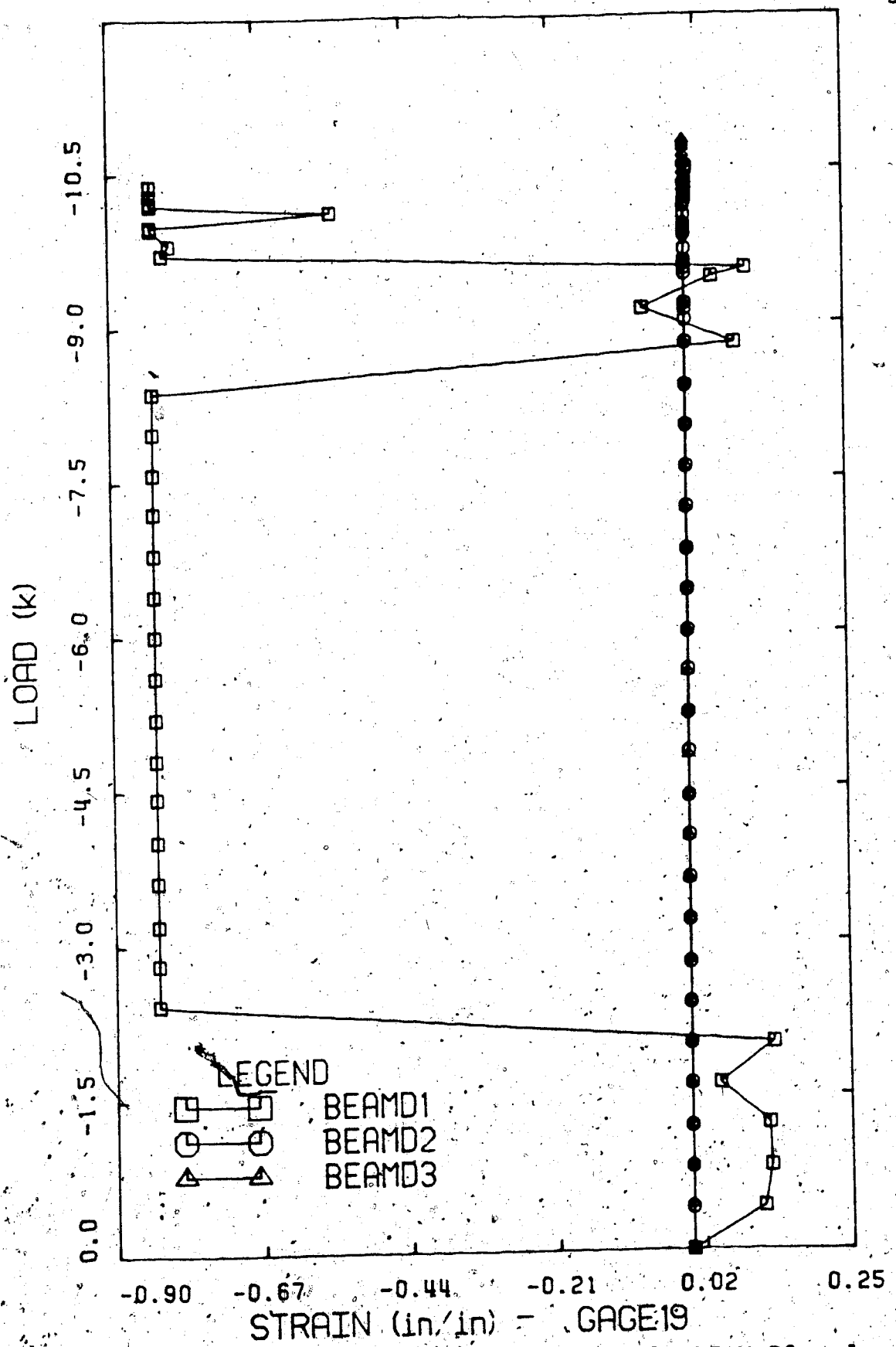
BEAM D3.

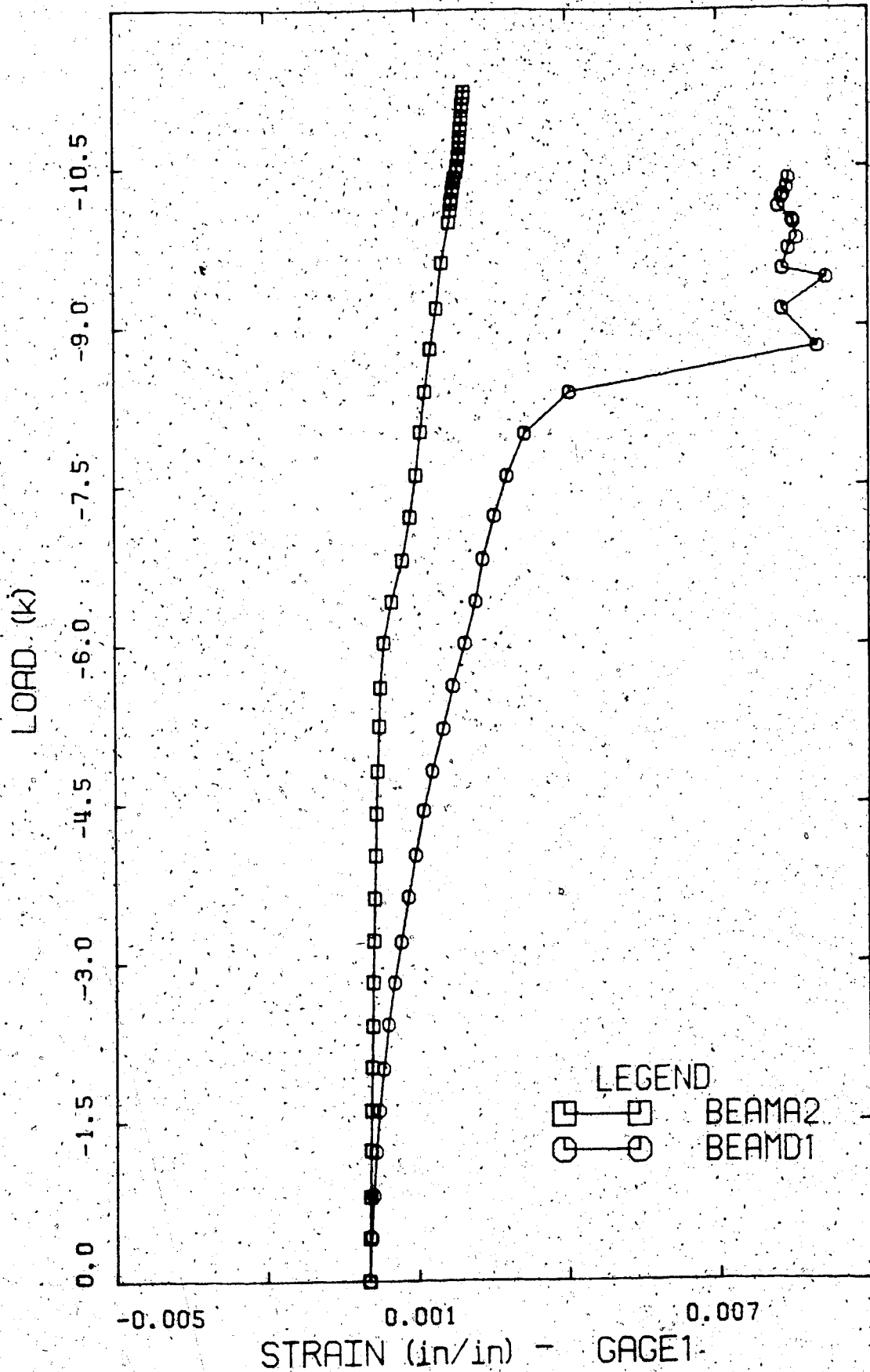Figure C45   Strain in Gage 19 - BEAM D1, BEAM D2 and

BEAM D3.

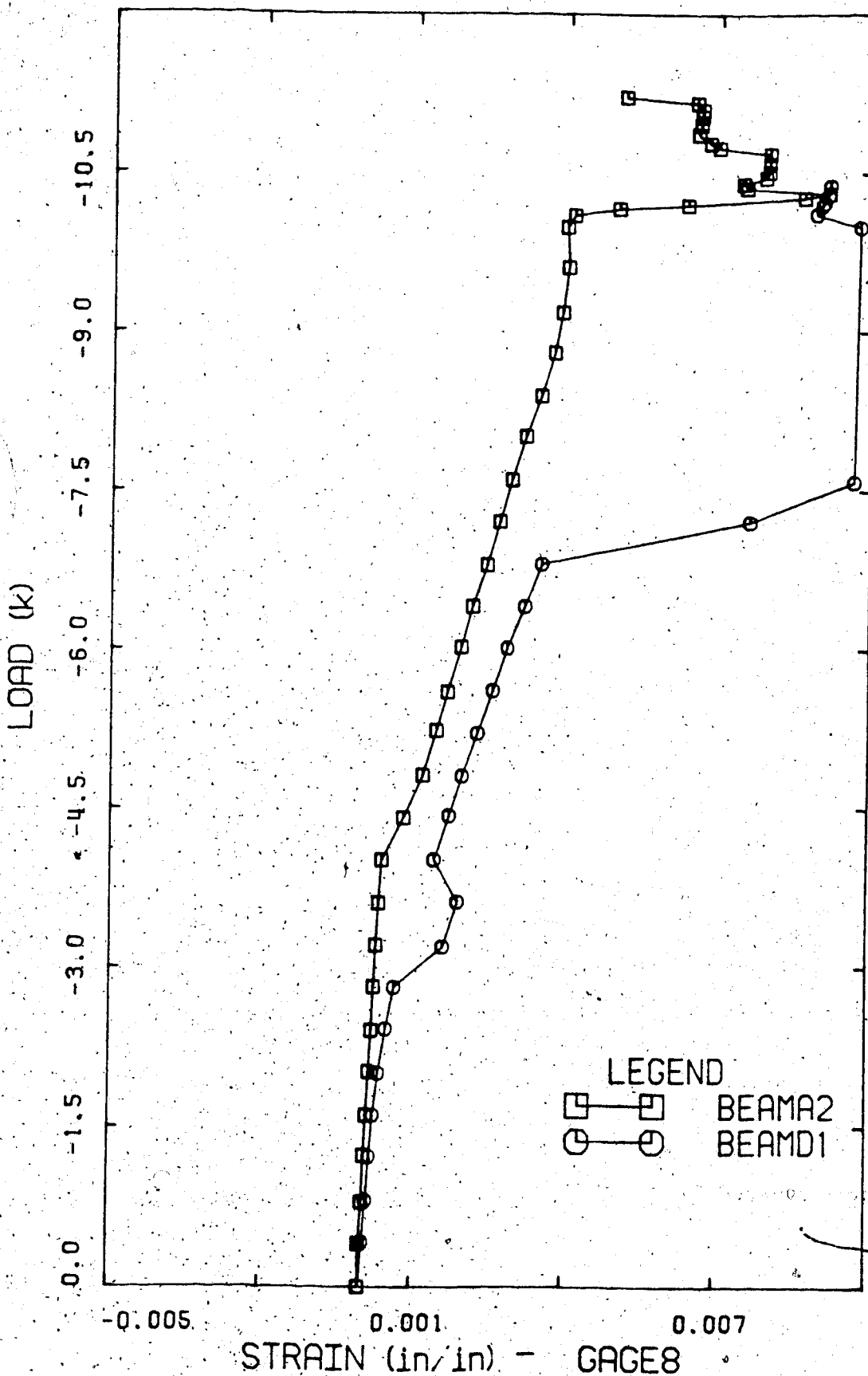Figure C46   Strain in Gage 1 - BEAM A2 and BEAM D1.

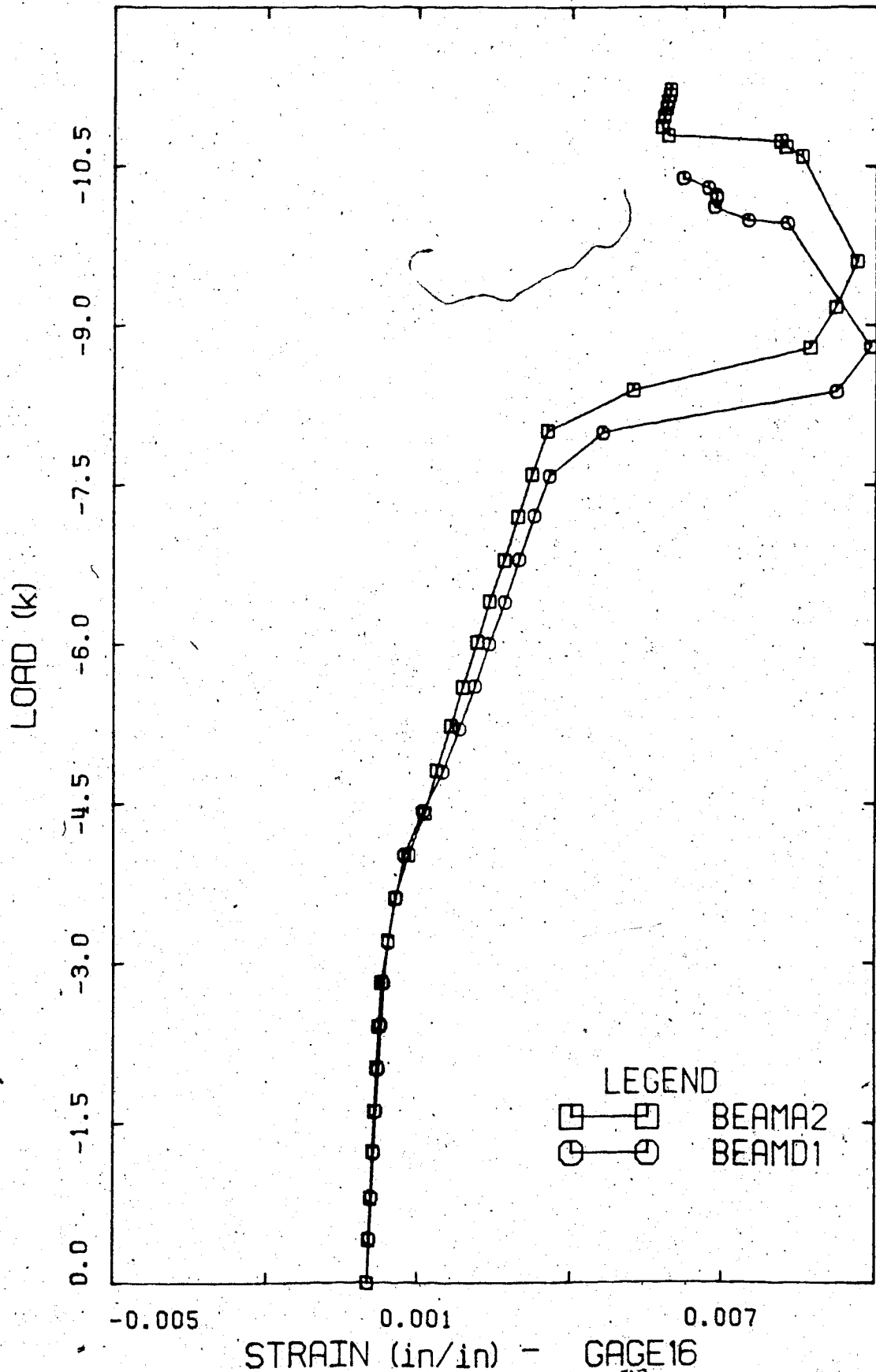Figure C47   Strain in Gage 8 - BEAM A2 and BEAM D1.

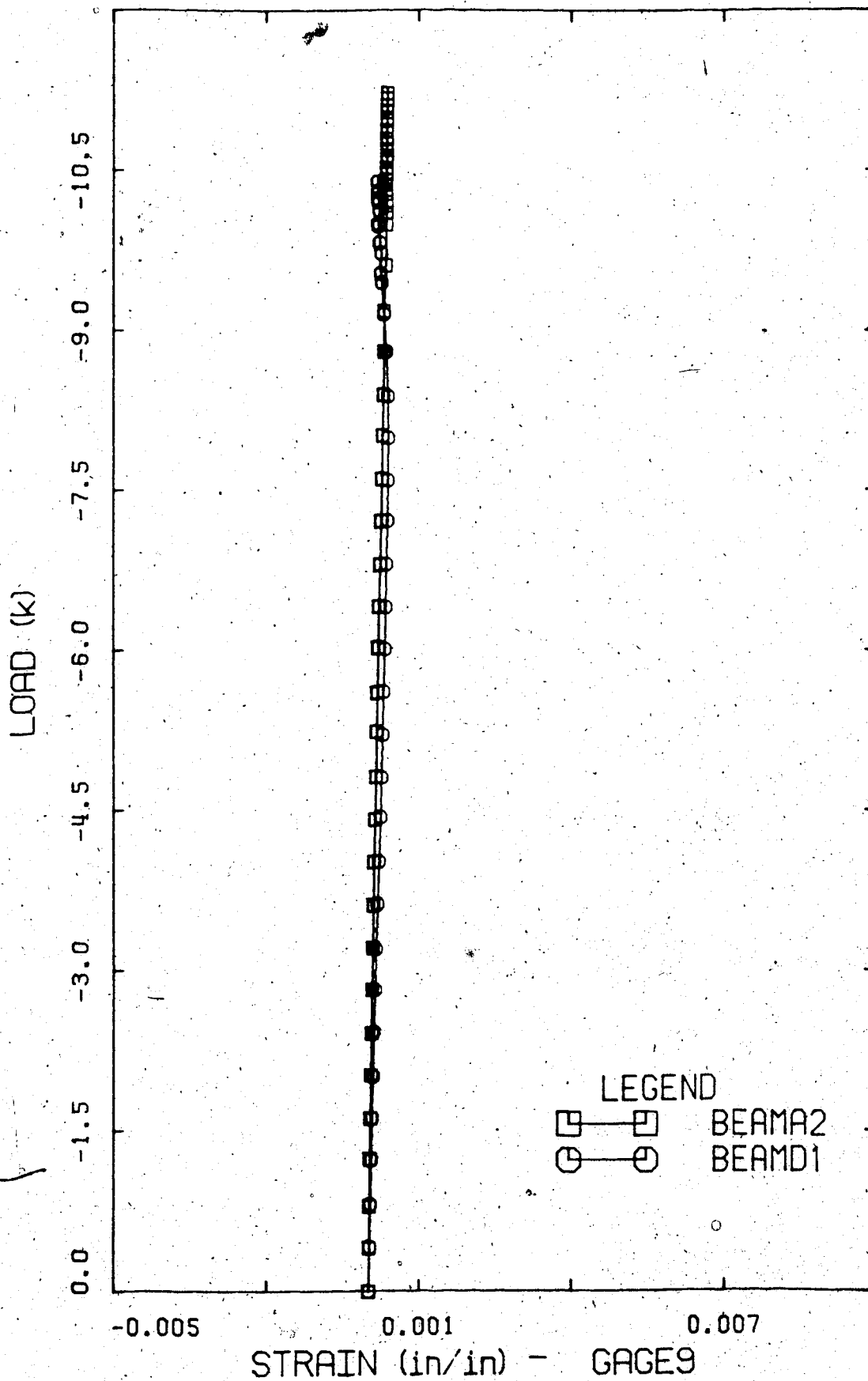Figure C48   Strain in Gage 16 – BEAM A2 and BEAM D1.

307

Figure C49   Strain in Gage 9 – BEAM A2 and BEAM D1.
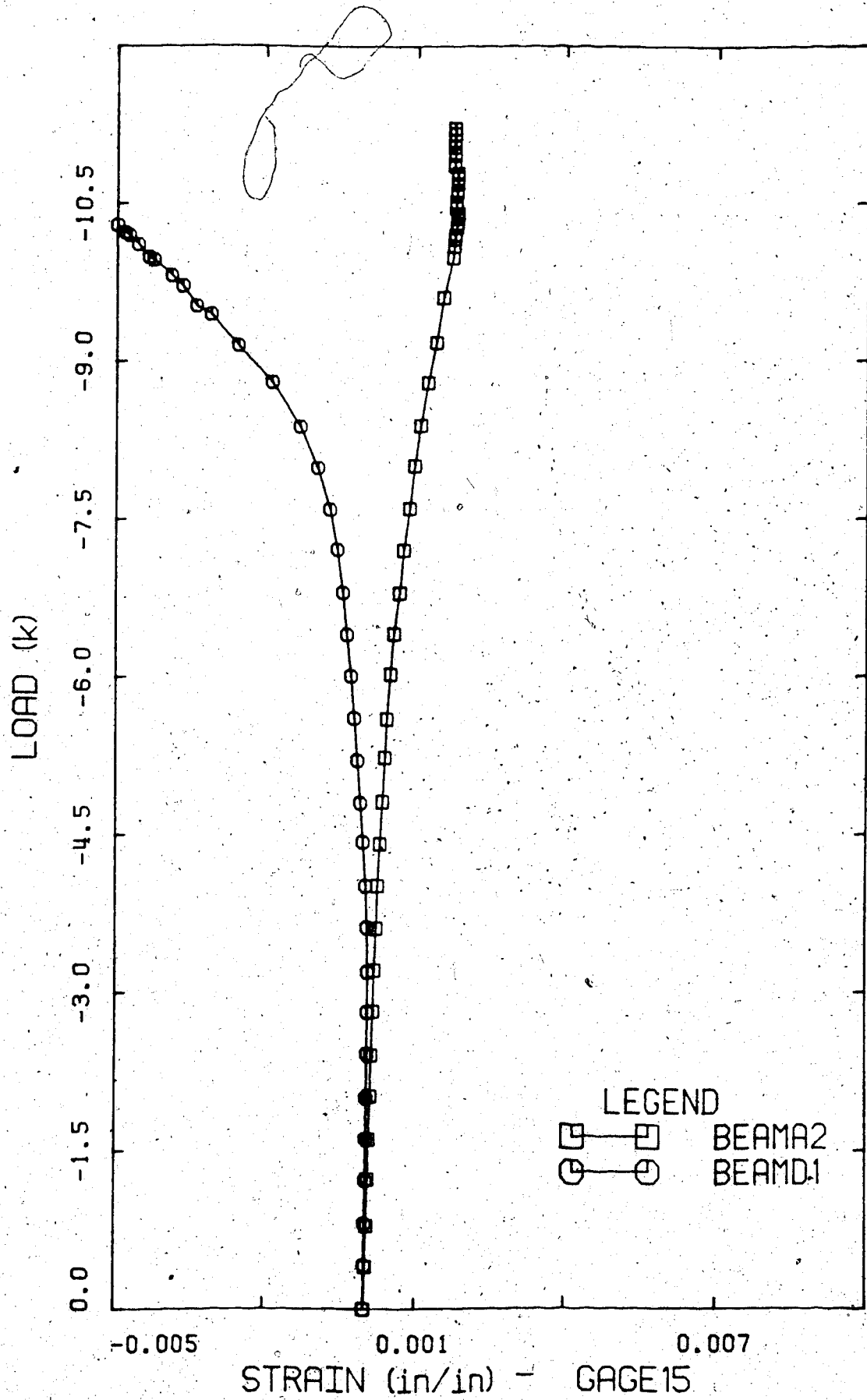
Figure C50   Strain in Gage 15 - BEAM A2 and BEAM D1.

Figure C51   Strain in Gage 2 - BEAM A2 and BEAM D2.

Figure C52   Strain in Gage 7 - BEAM A2 and BEAM D2.
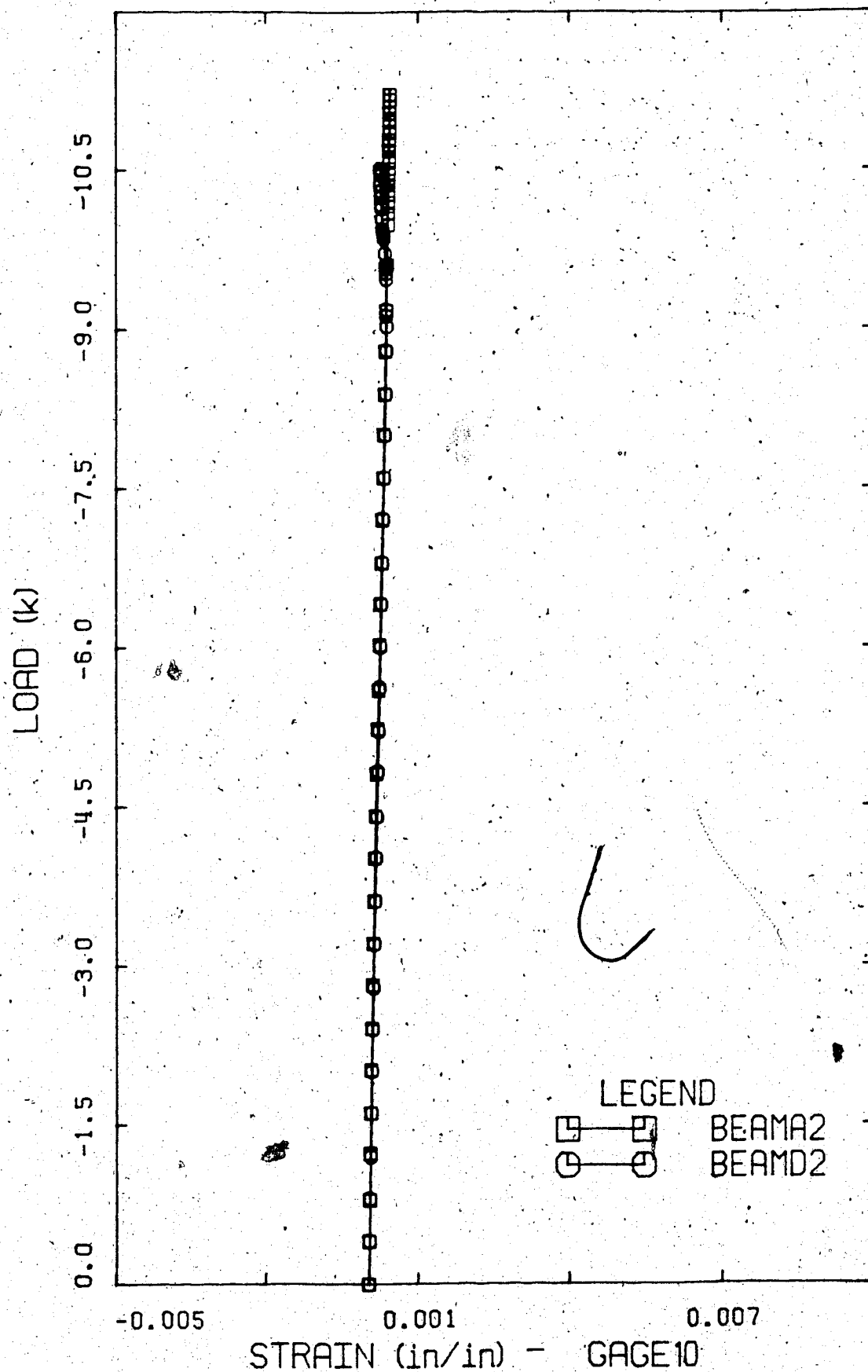
Figure C53   Strain in Gage 10 - BEAM A2 and BEAM D2.
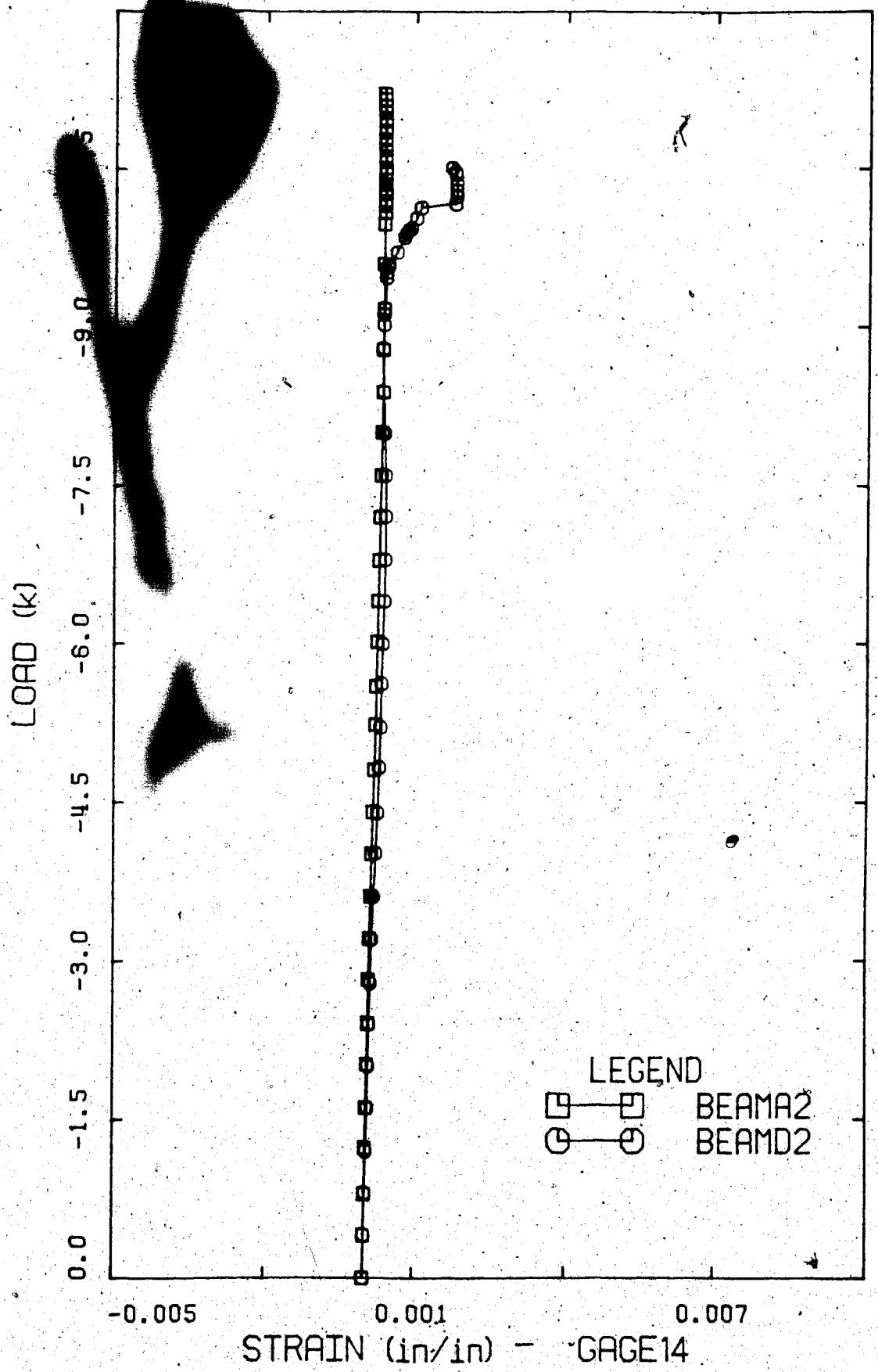
Figure C54   Strain in Gage 14 - BEAM A2 and BEAM D2.
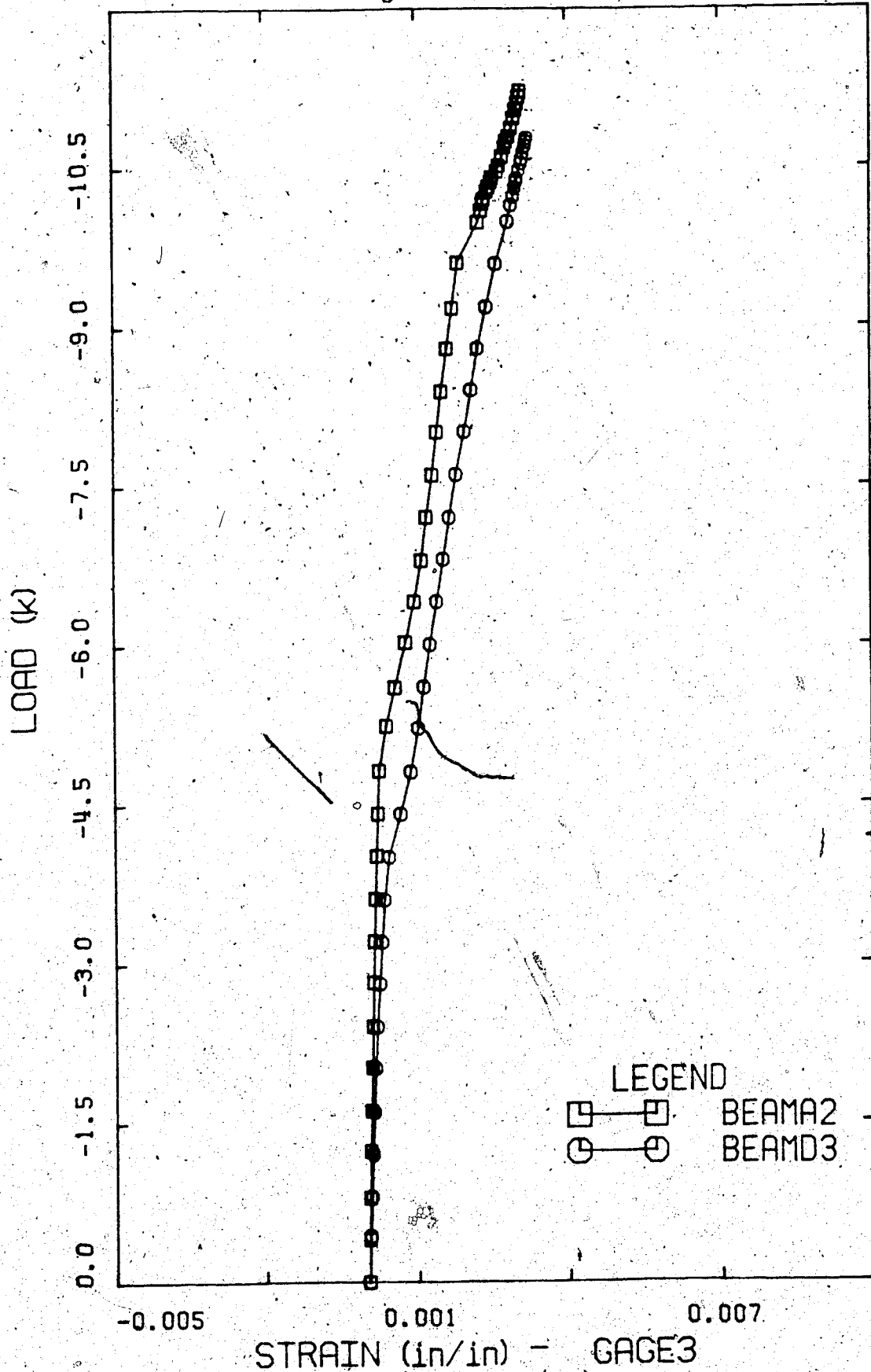
Figure C55   Strain in Gage 3 - BEAM A2 and BEAM D3.
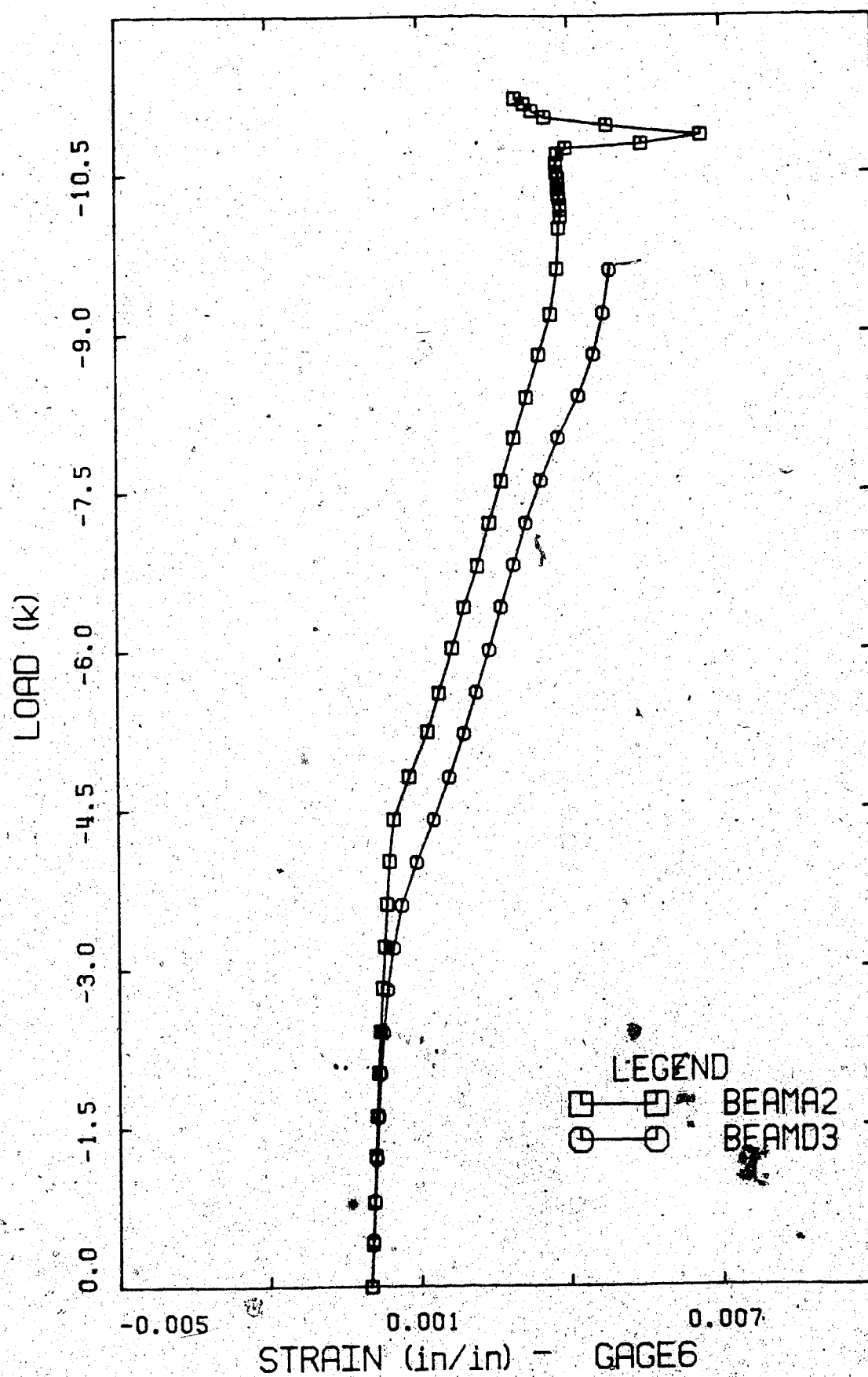
Figure C56   Strain in Gage 6 — BEAM A2 and BEAM D3.
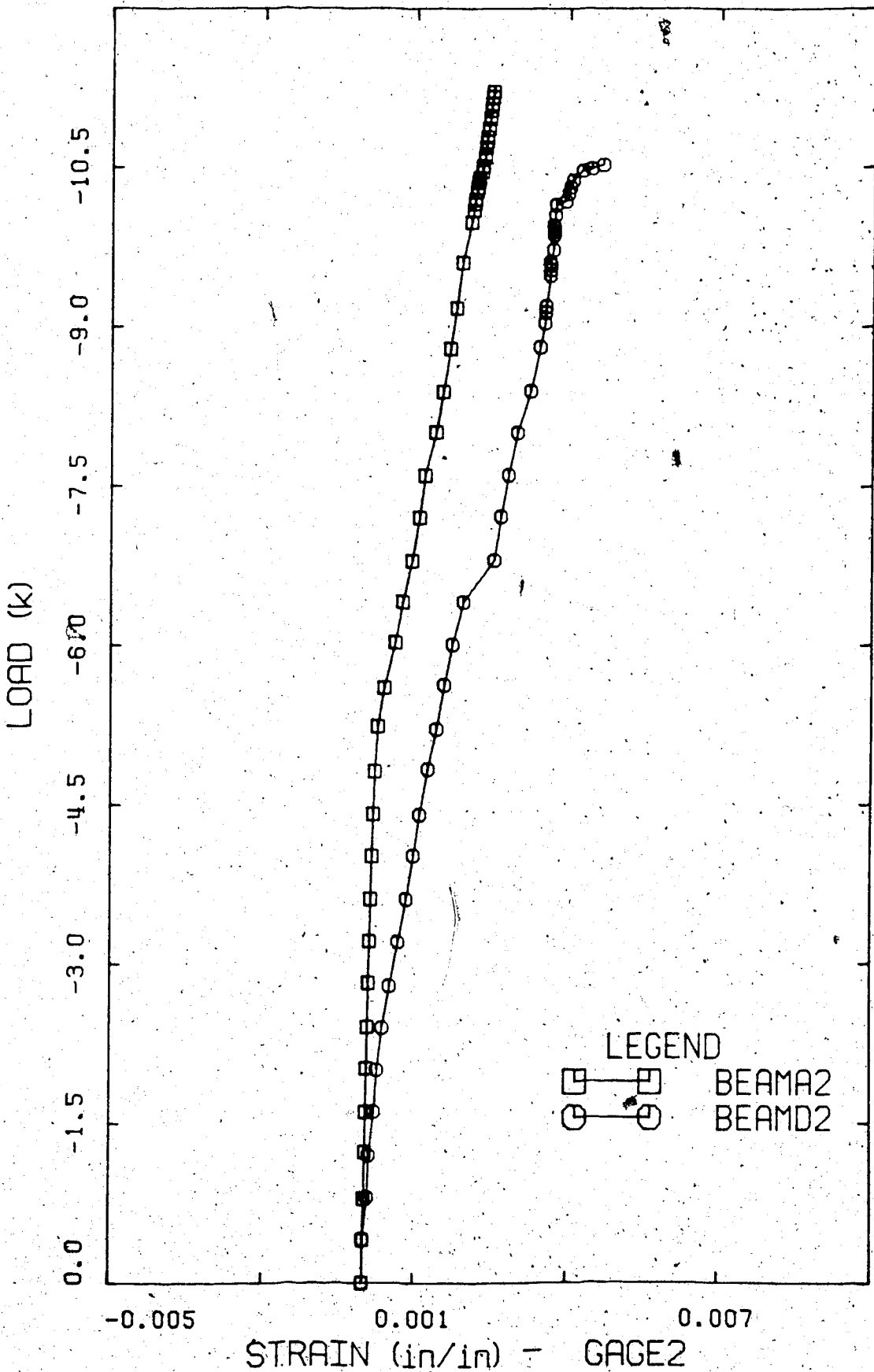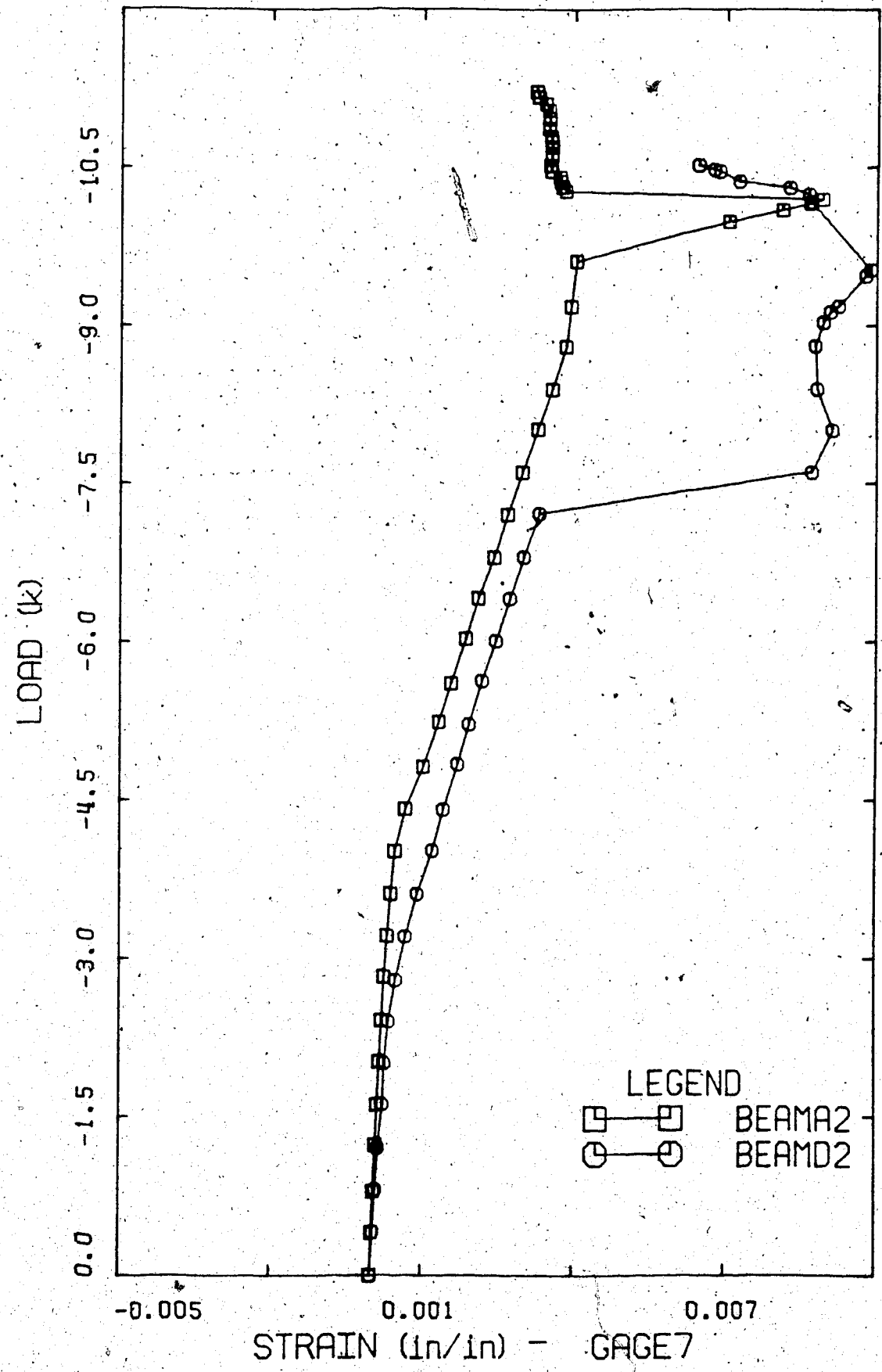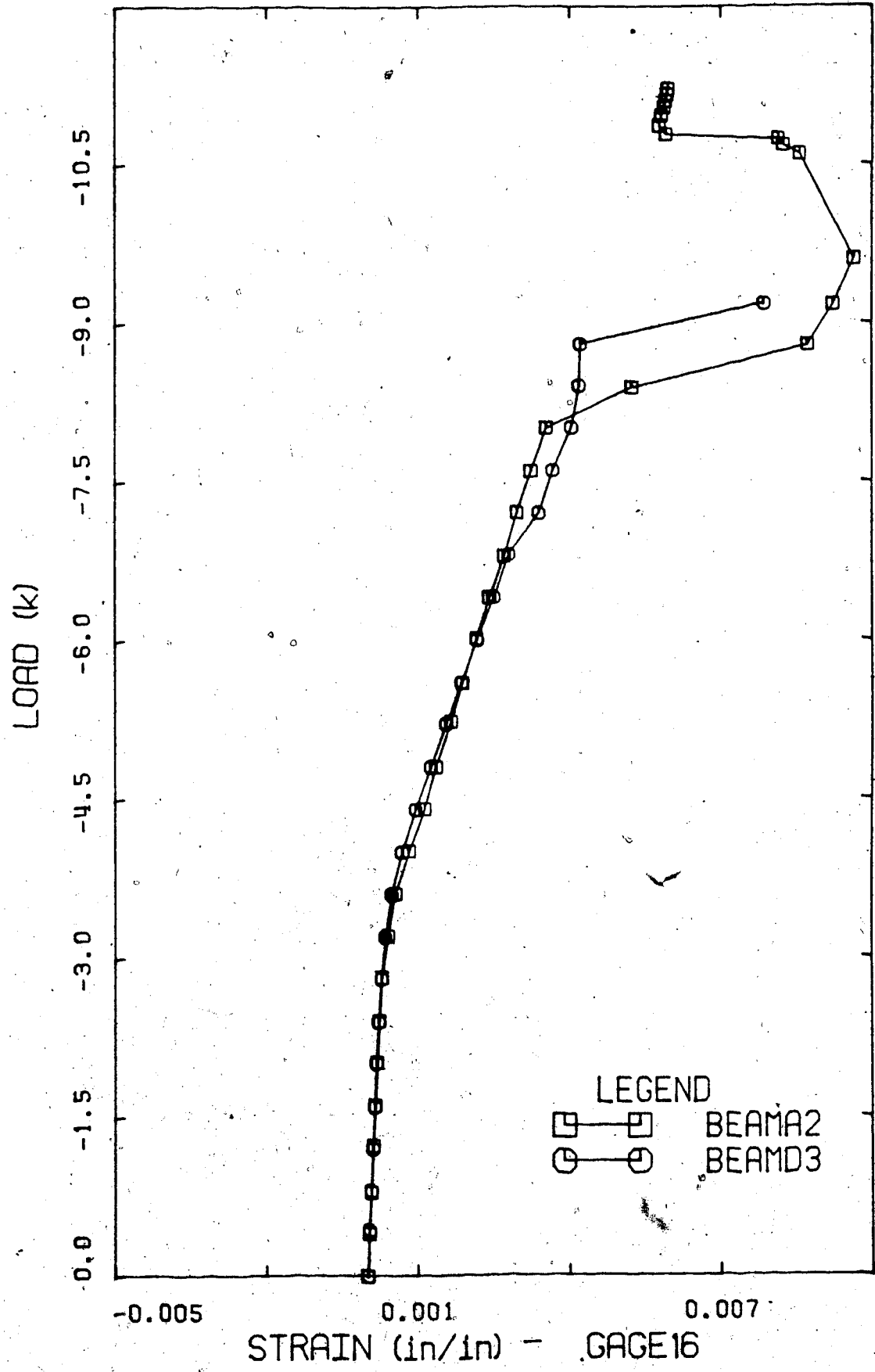
Figure C57   Strain in Gage 16 – BEAM A2 and BEAM D3.
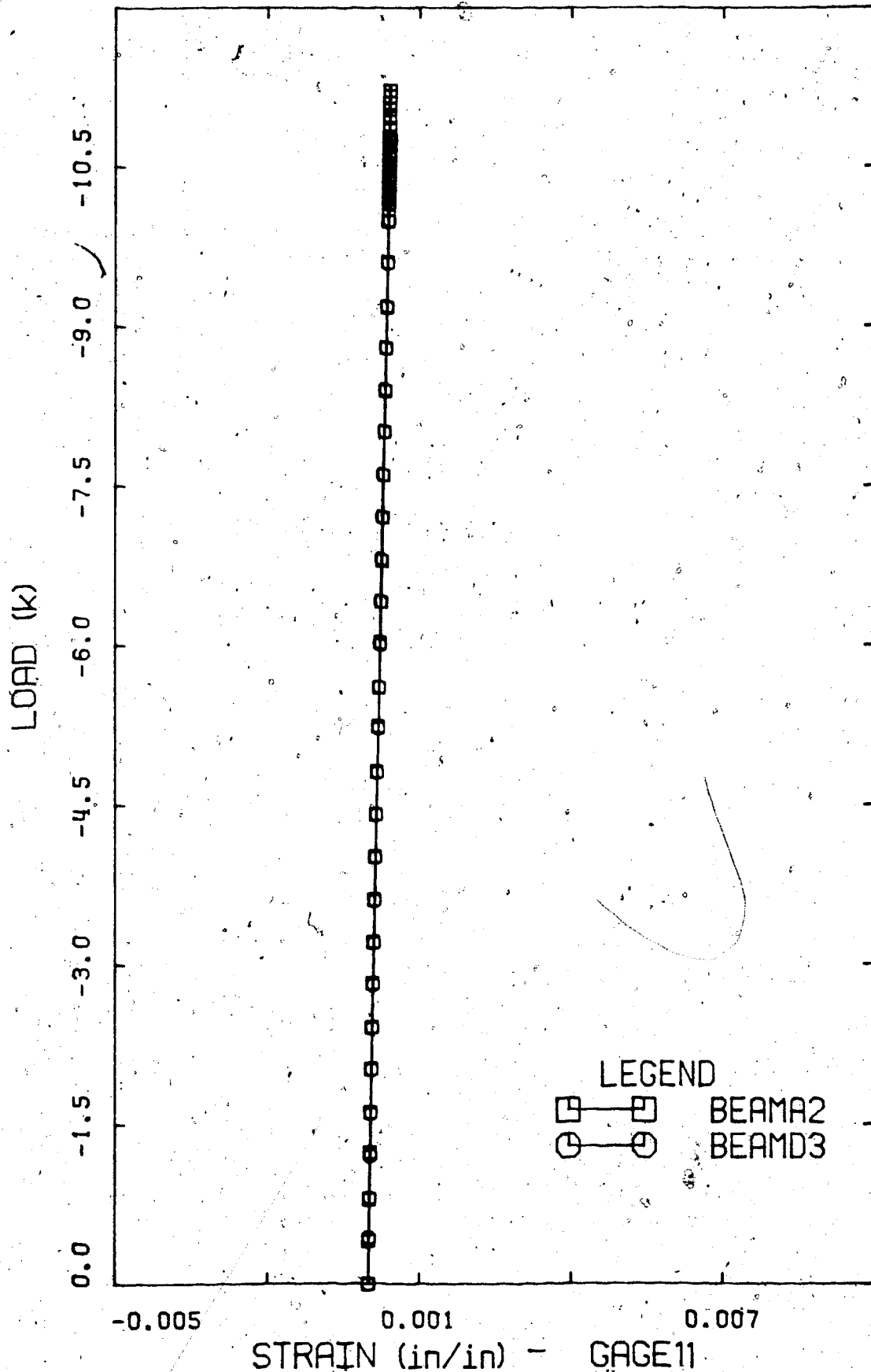
Figure C58   Strain in Gage 11 - BEAM A2 and BEAM D3.
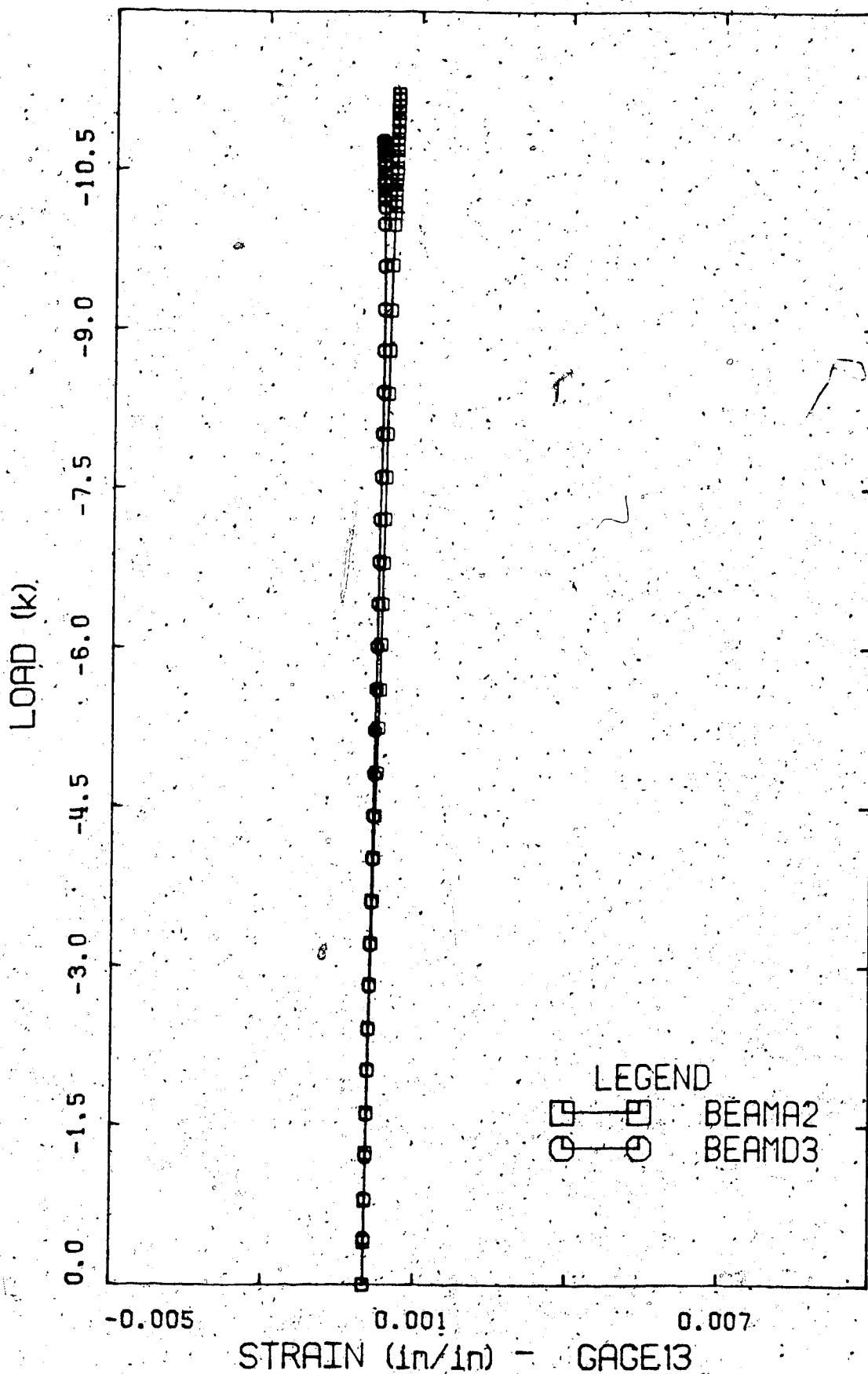
Figure C59   Strain in Gage 13 — BEAM A2 and BEAM D3:
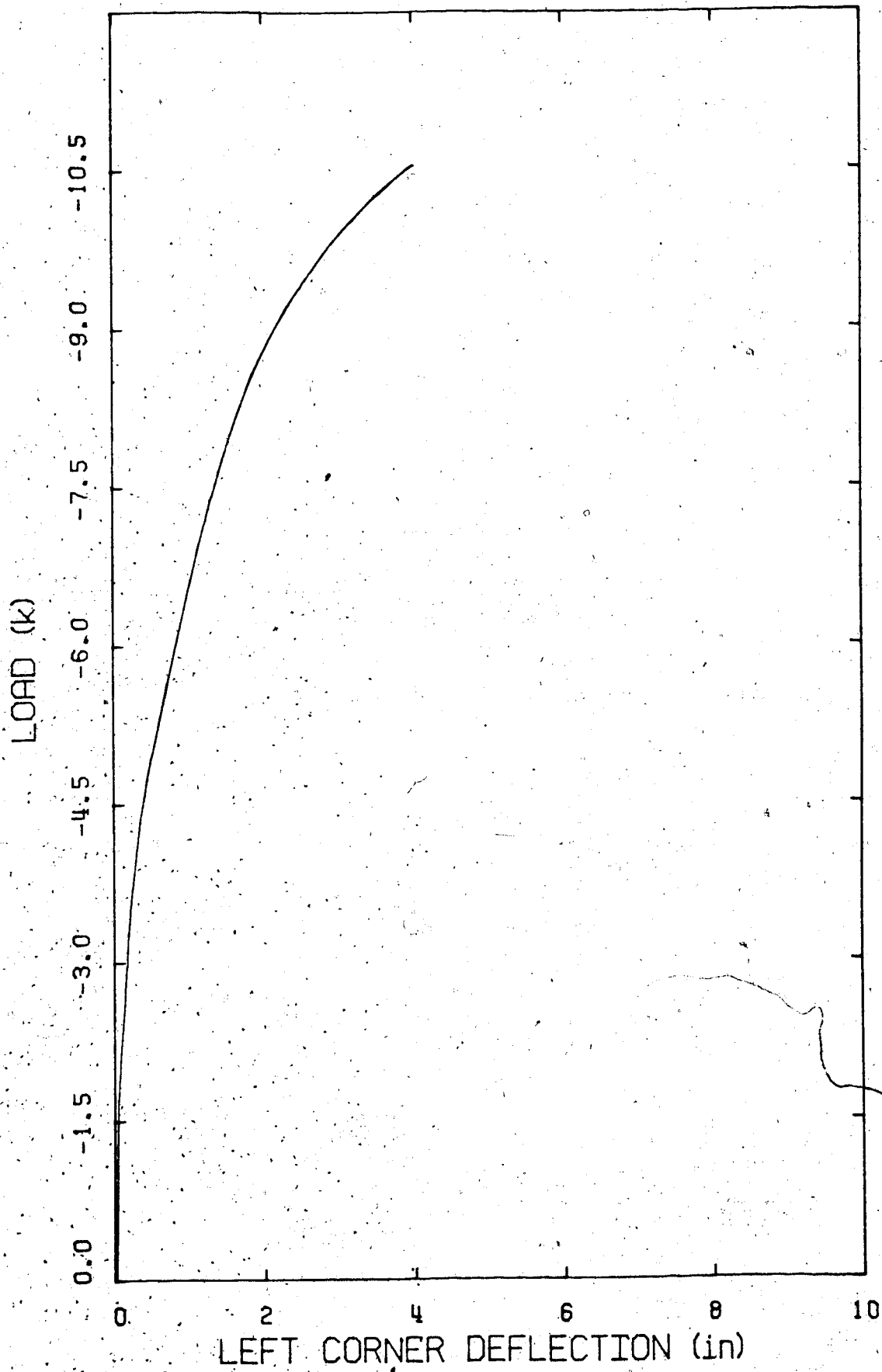
Figure C60   Load-Deflection Curve - BEAM B1.
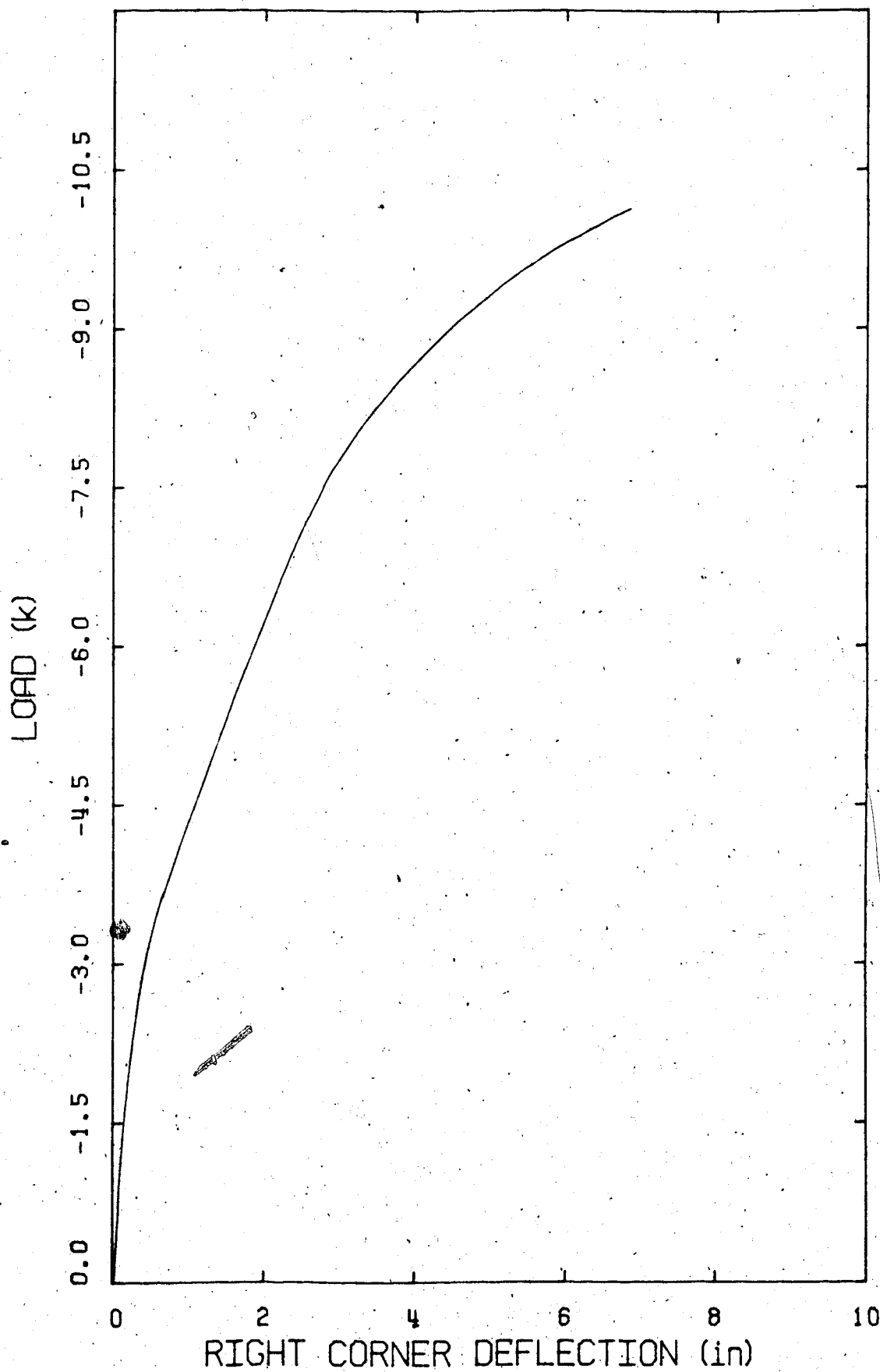
Figure C61   Load-Deflection Curve - BEAM B1.
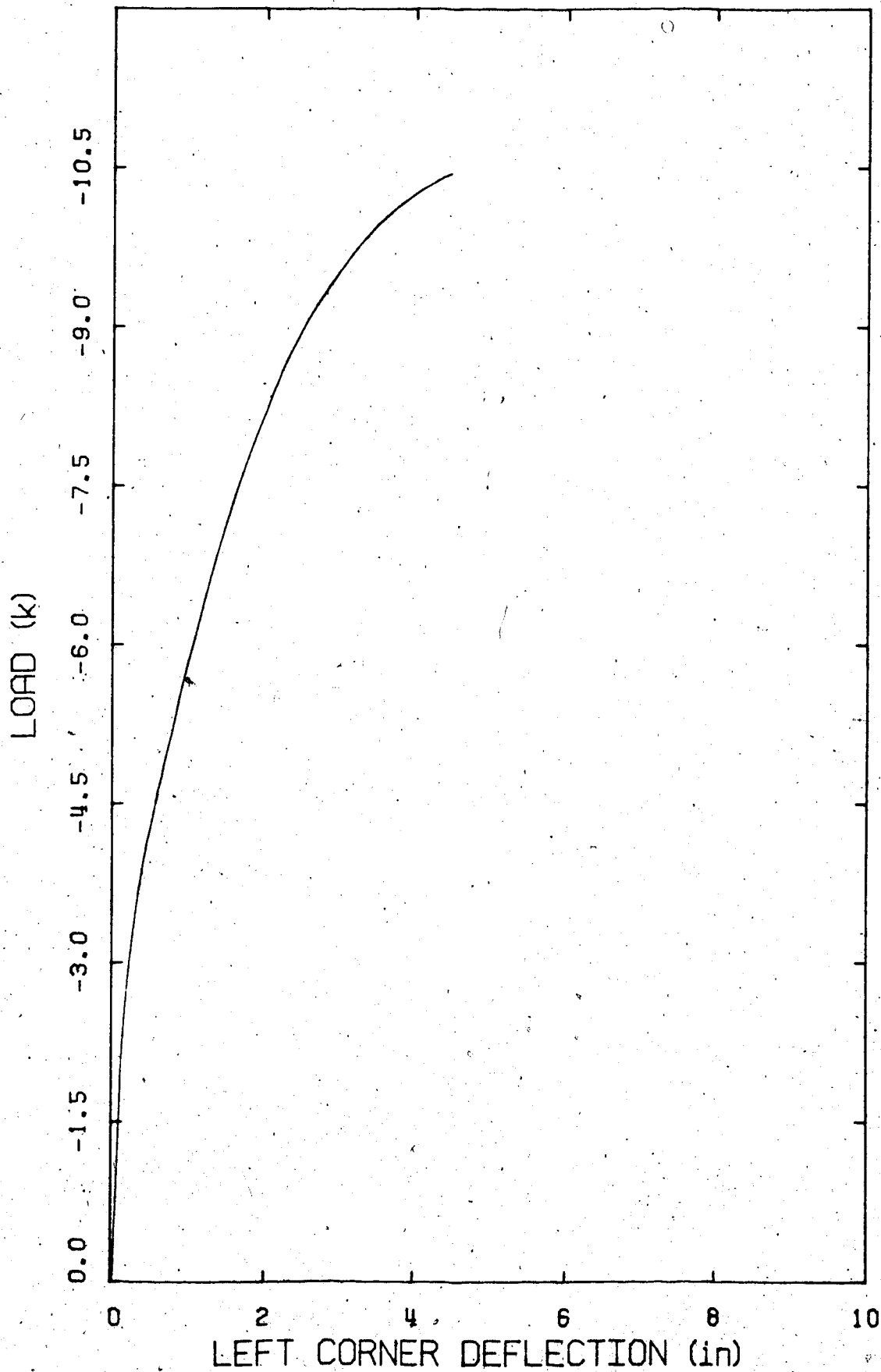
Figure C62   Load-Deflection Curve - BEAM B2.
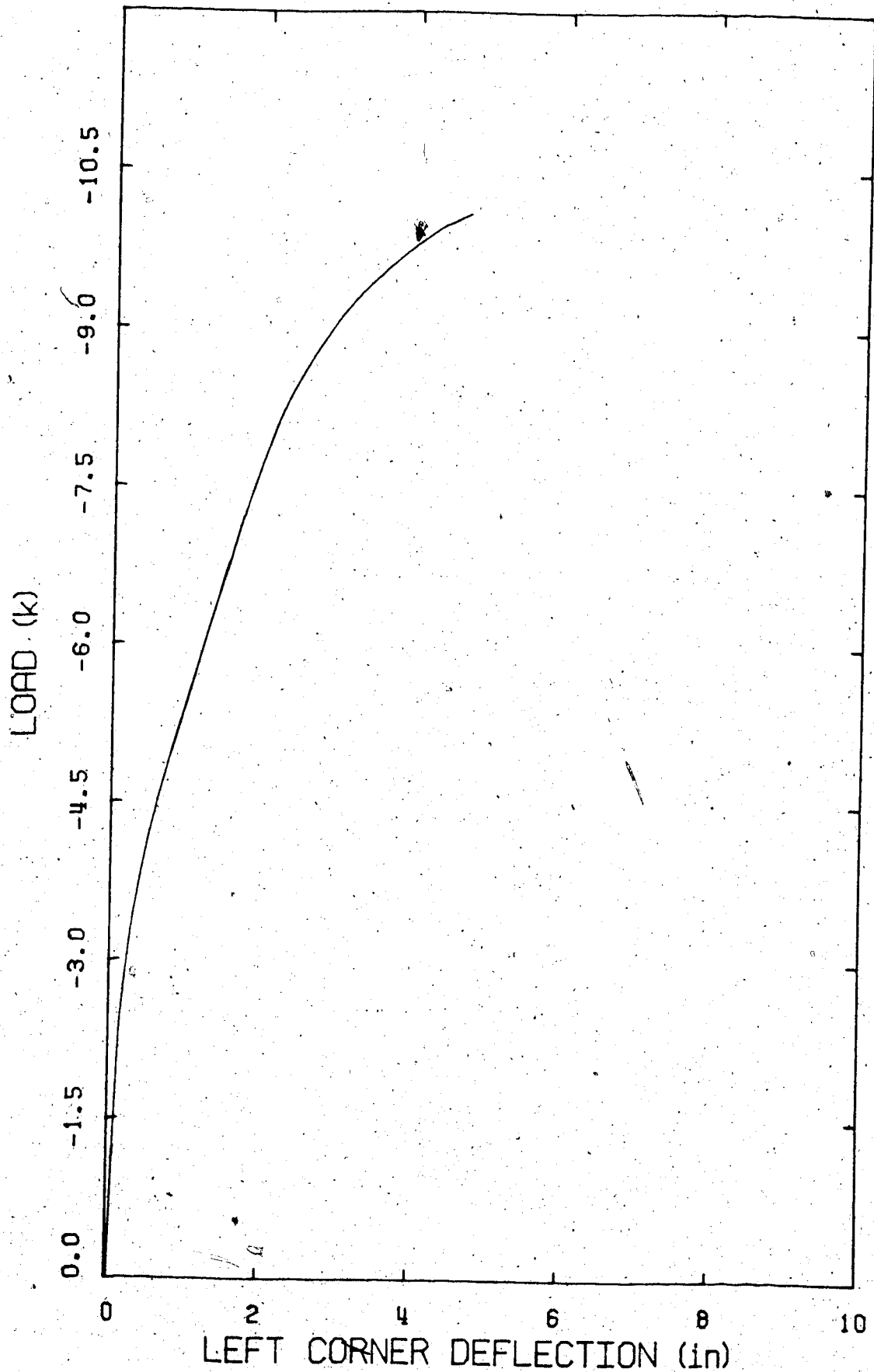
Figure C63   Load-Deflection Curve - BEAM B3.
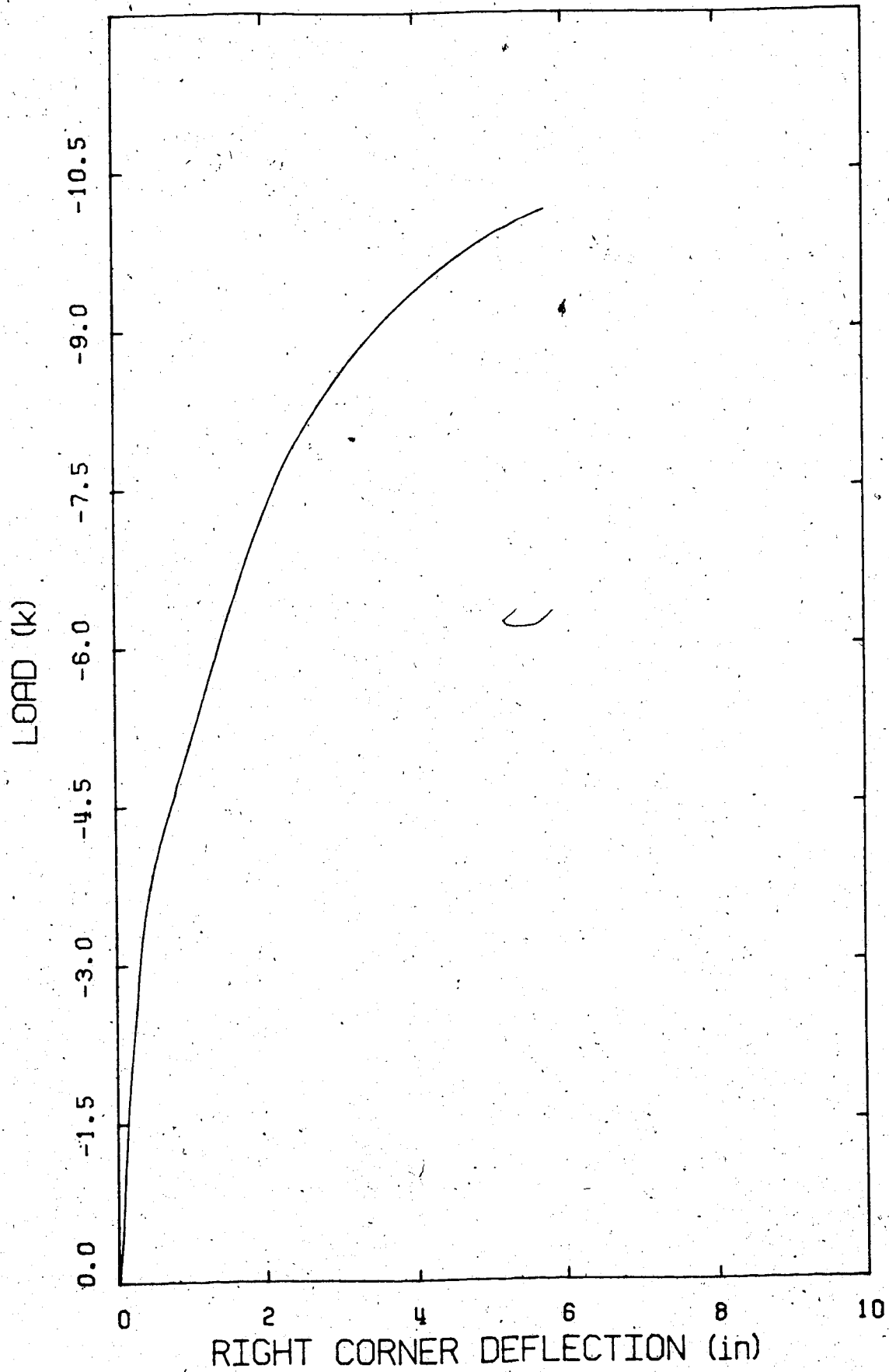
Figure C64   Load-Deflection Curve – BEAM B3.
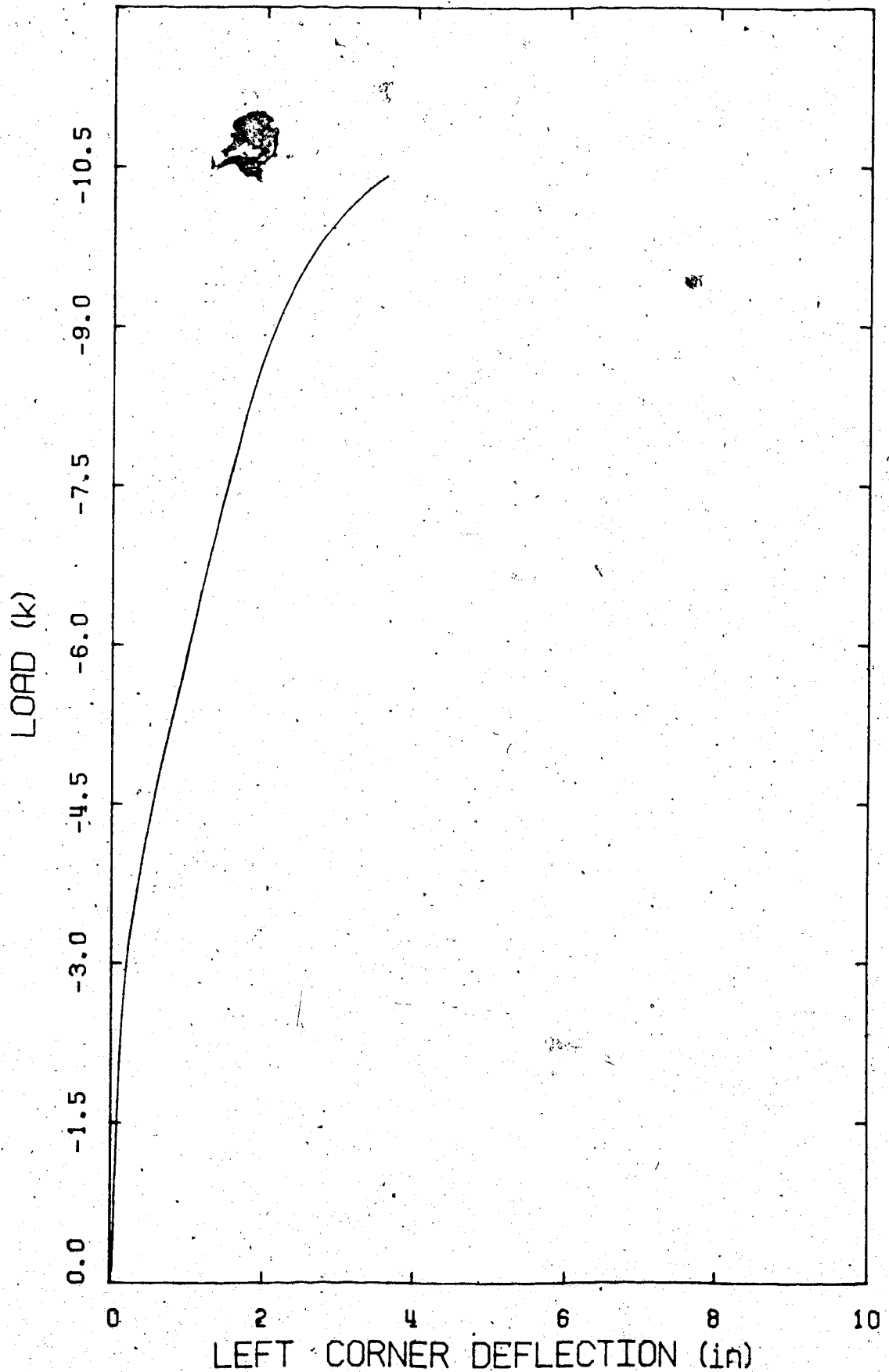
Figure C65   Load-Deflection Curve - BEAM Cl.
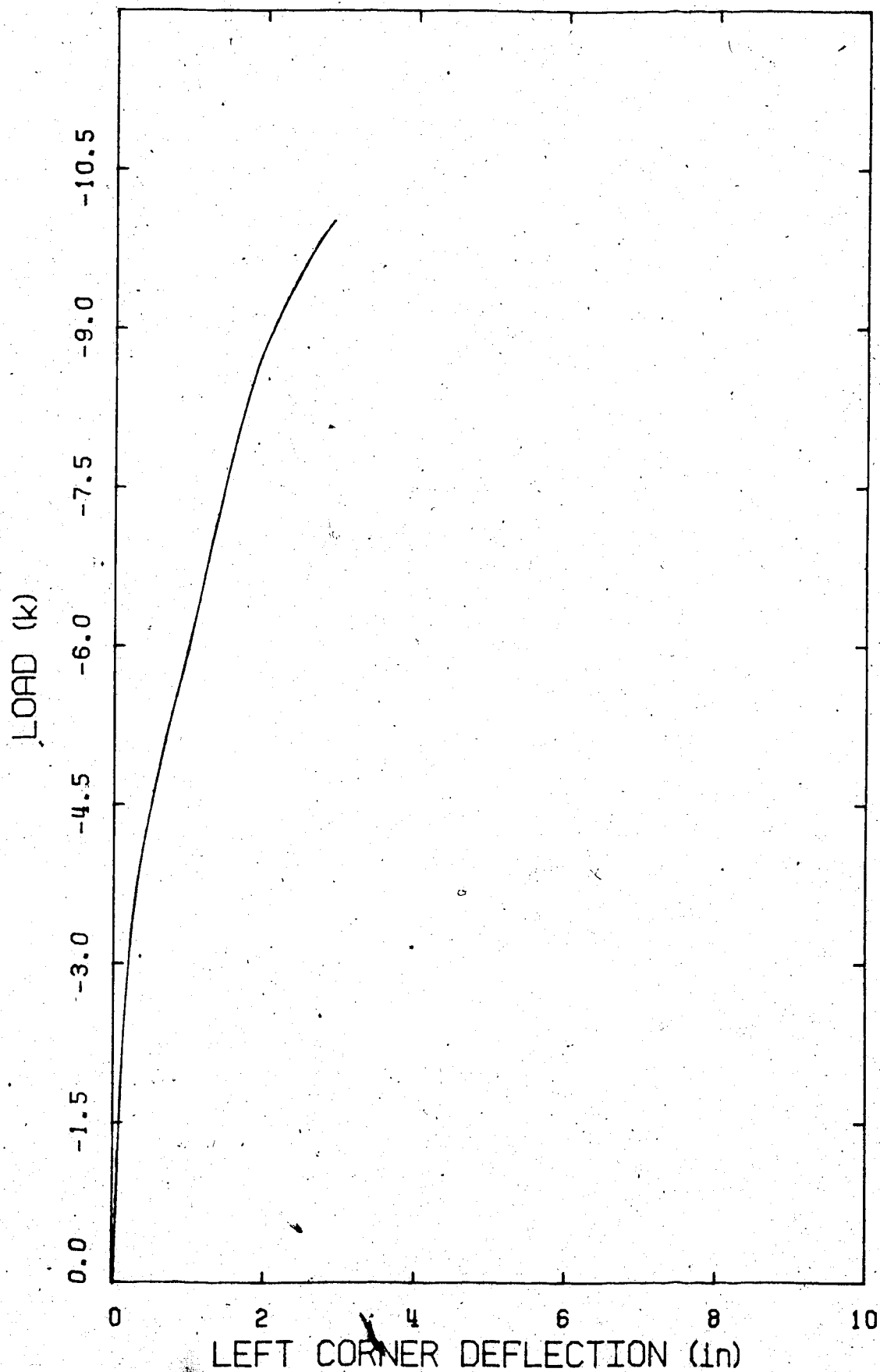
Figure C66   Load-Deflection Curve - BEAM C2.
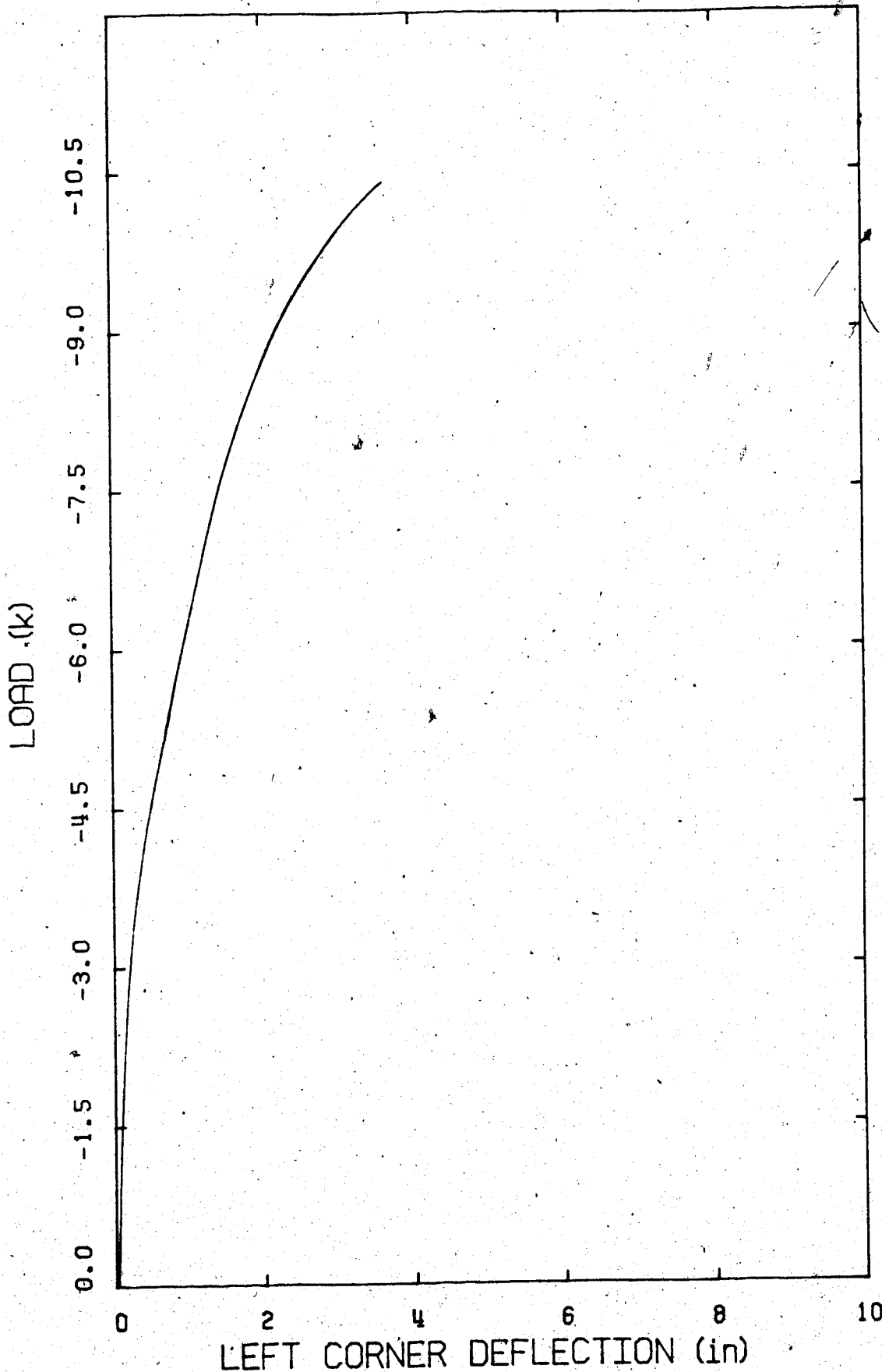
Figure C67   Load-Deflection Curve - BEAM C3.
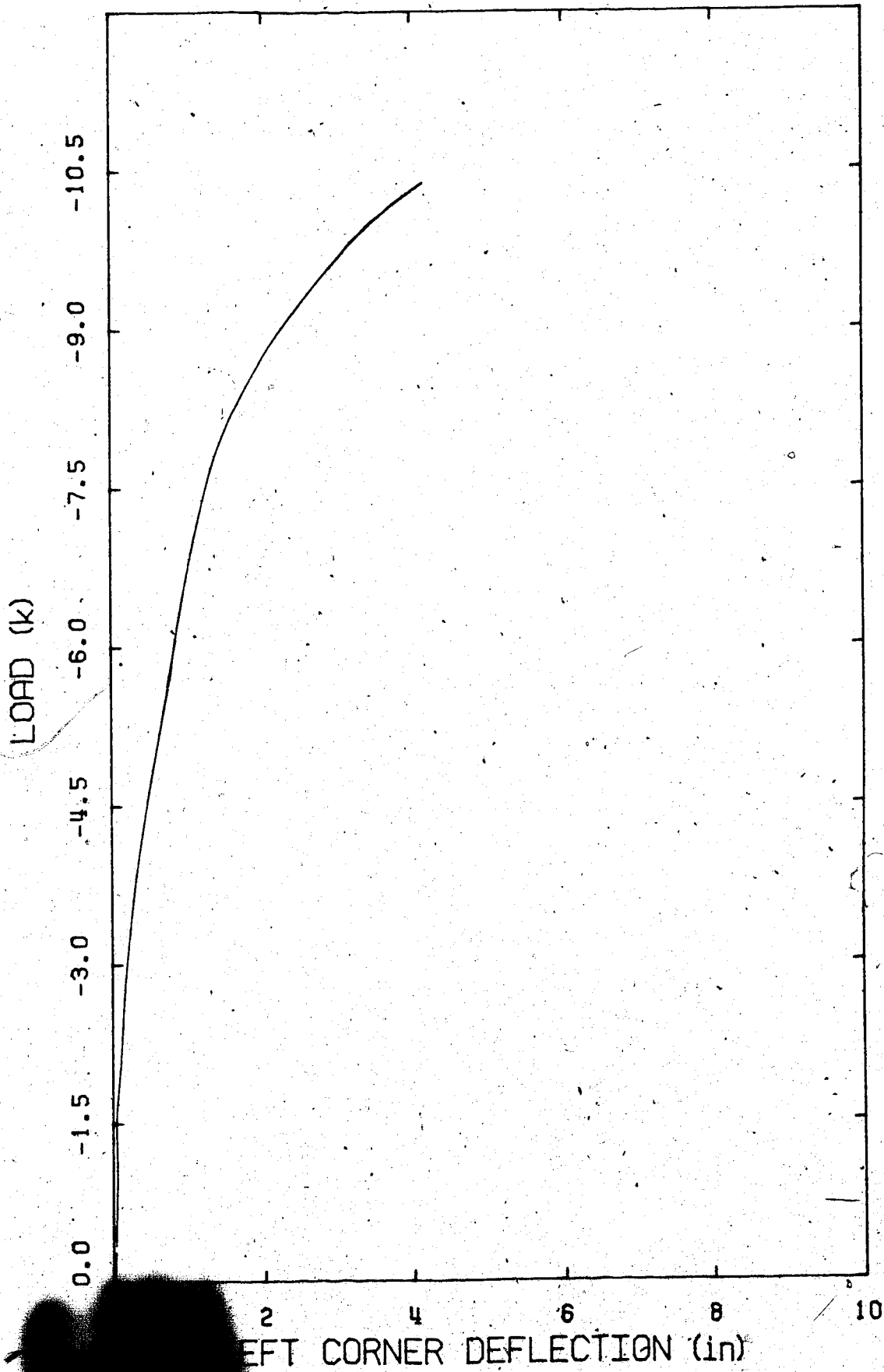
C68   Load-Deflection Curve - BEAM D1.
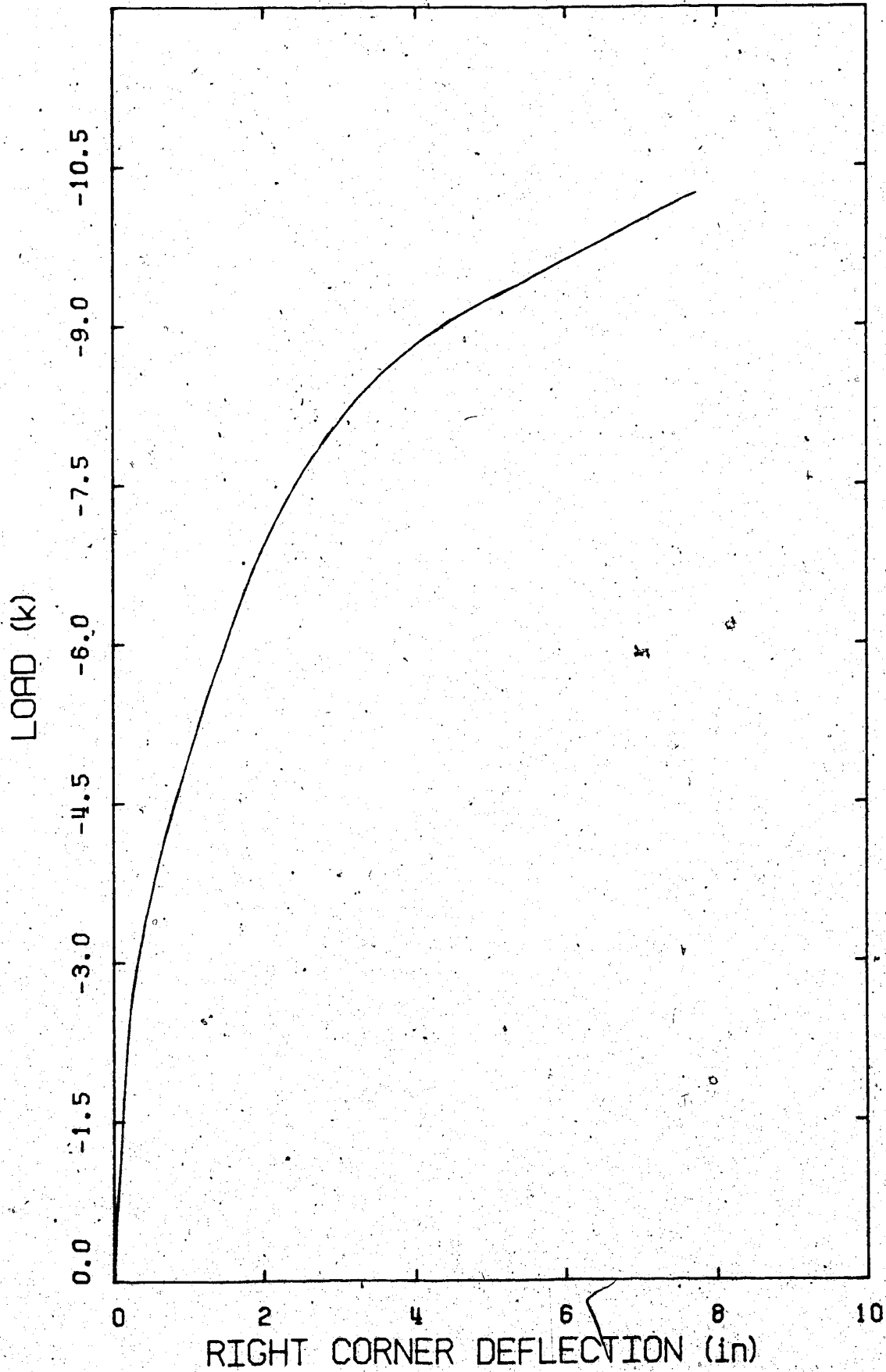
Figure C69   Load-Deflection Curve - BEAM D1.
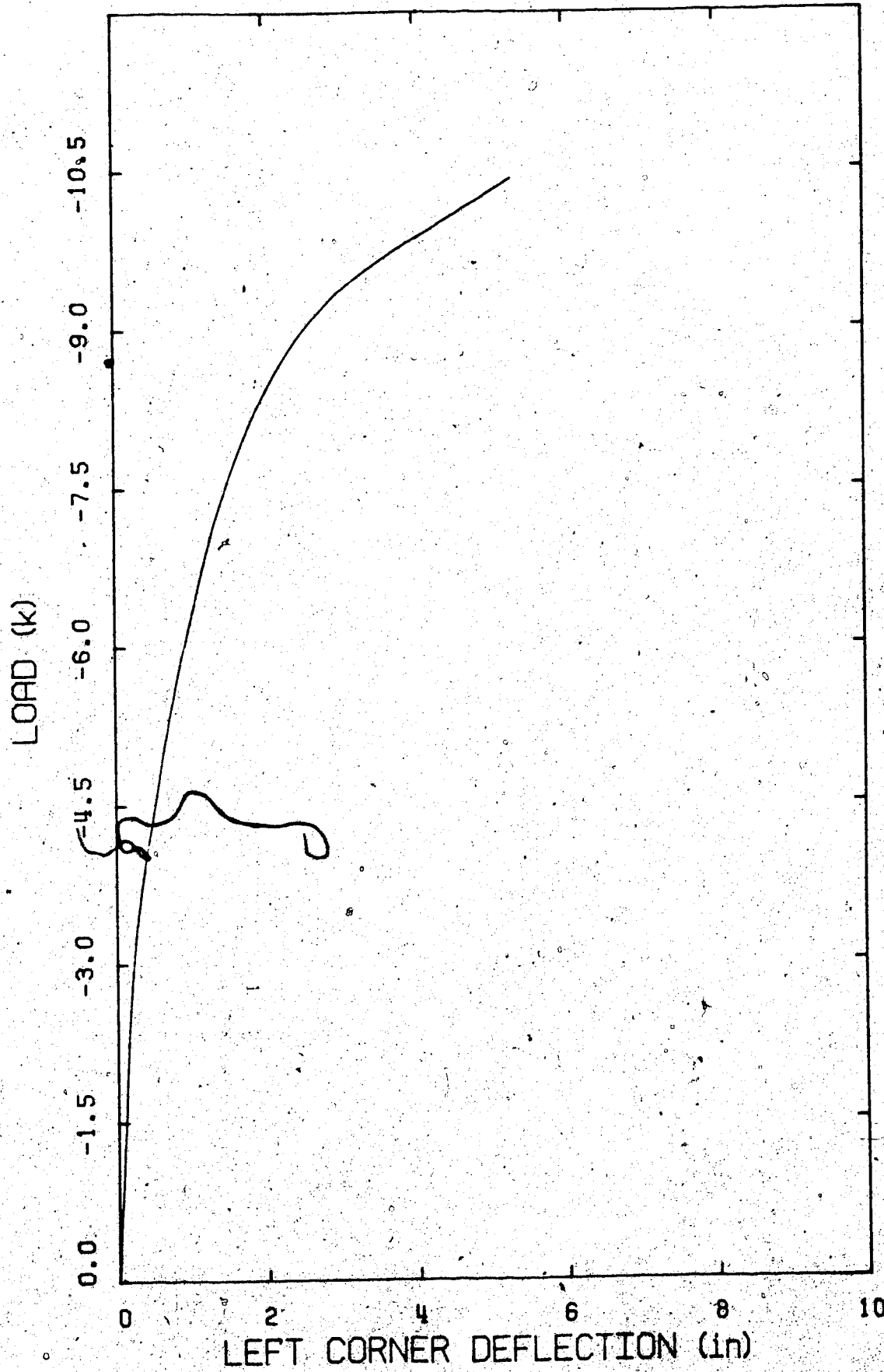
Figure C70   Load-Deflection Curve — BEAM D2.
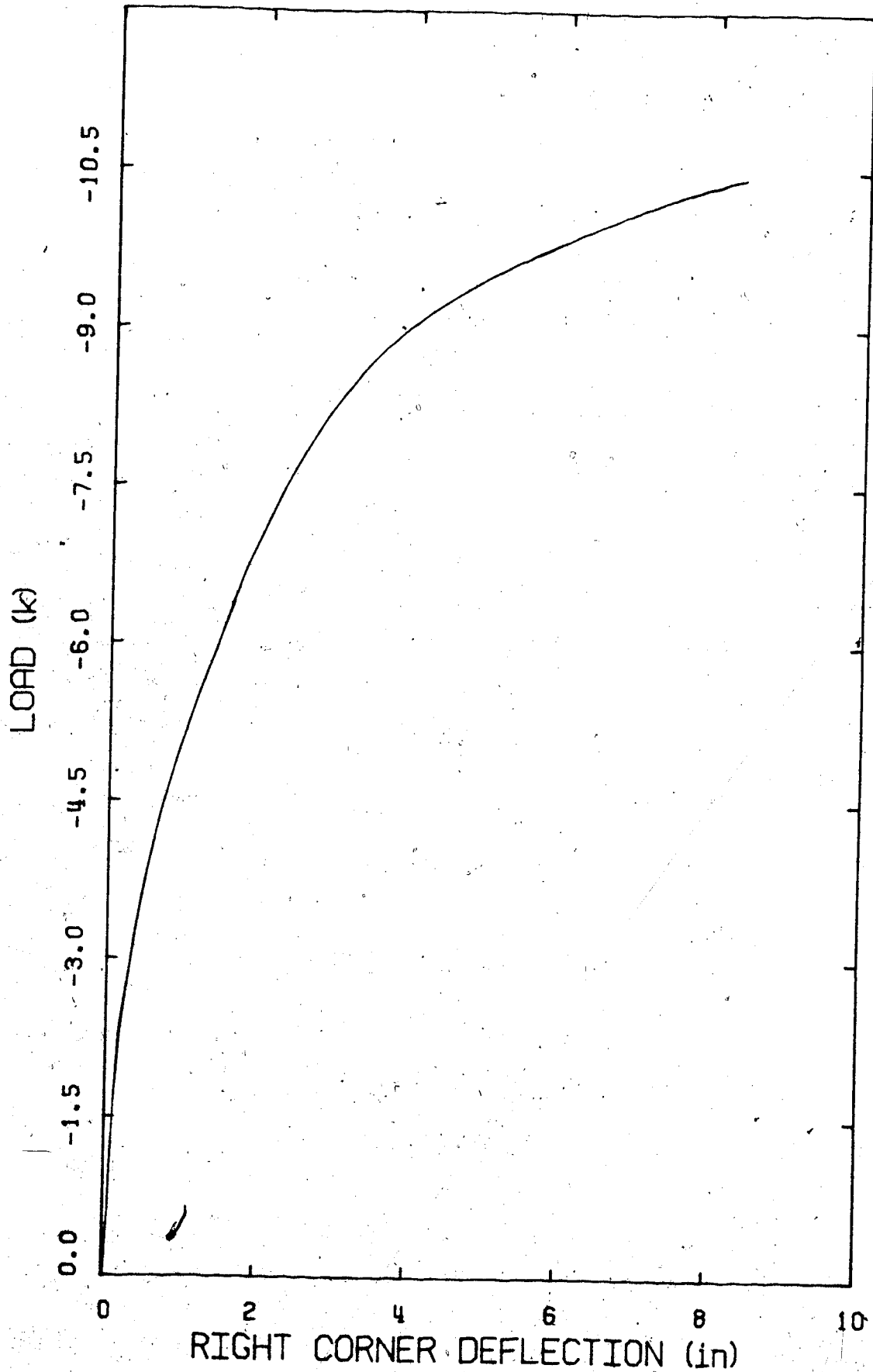
Figure C71   Load-Deflection Curve - BEAM D2.
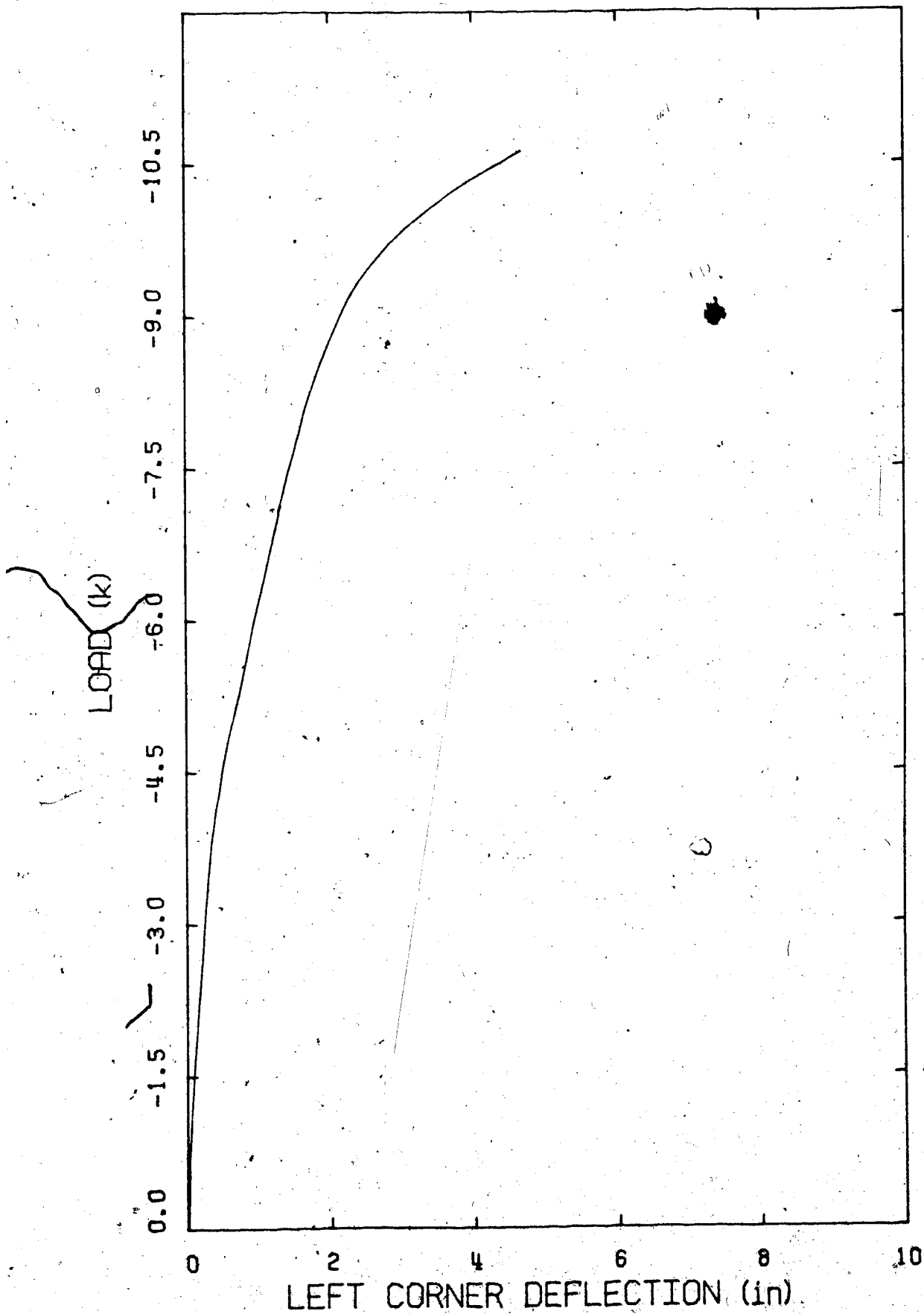
Figure C72   Load-Deflection Curve – BEAM D3.
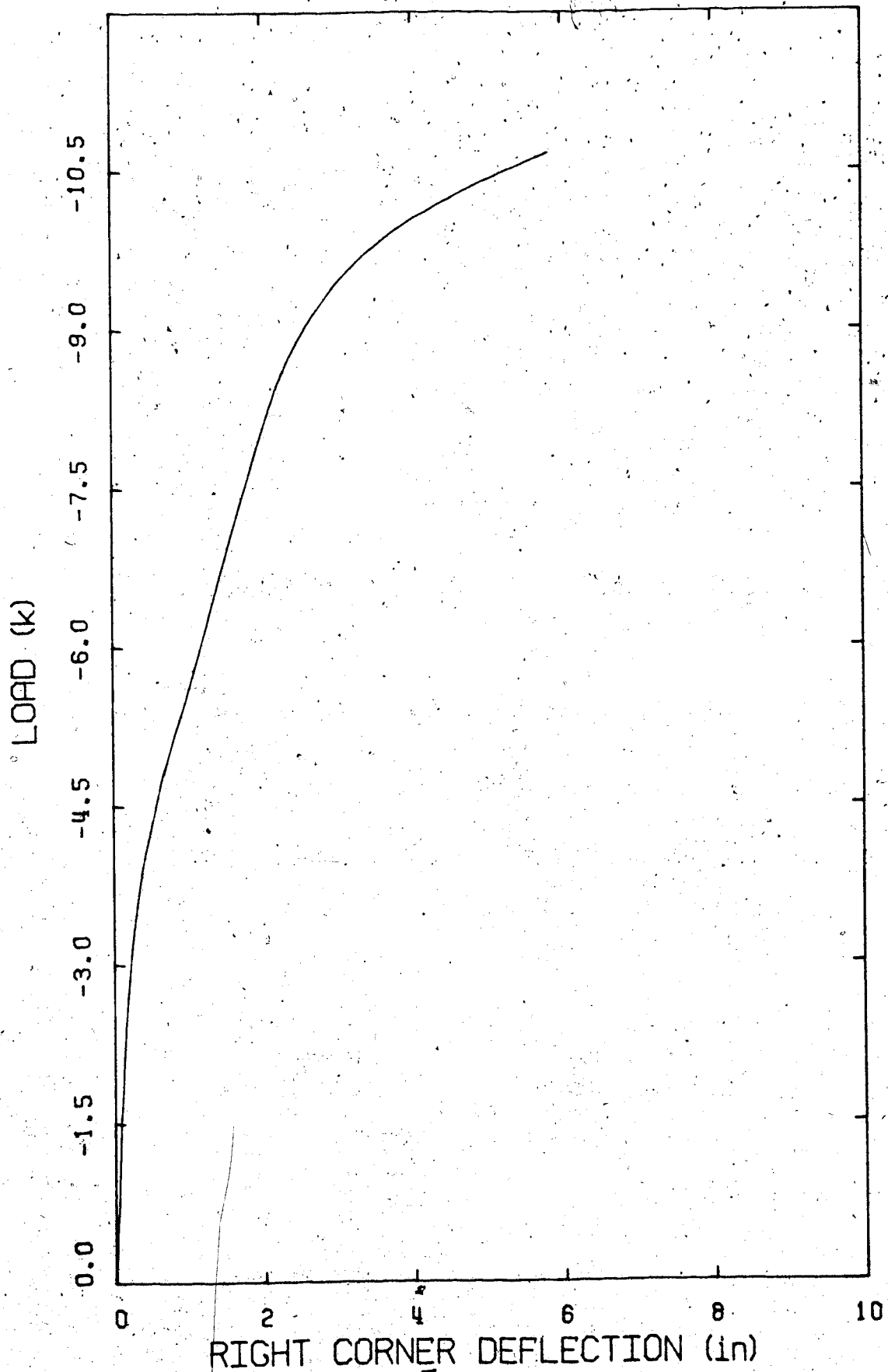
Figure C73   Load-Deflection Curve - BEAM D3.

APPENDIX D

ESTIMATION OF SHEAR CORRESPONDING TO FLEXURAL AND SHEAR CAPACITY OF THE STRUTS AND COMPARISON WITH TEST RESULTS

D.1 Introduction

In this appendix distribution of applied shear between the struts based on calculated flexural and shear capacities of the struts are estimated and compared with test results. First the ultimate moment and shear at the center of the opening are determined from applied loads. The axial tensile force T in the bottom strut and the axial compressive force C in the top strut are determined from equilibrium conditions at the center of the opening, as described in Chapter 6. The flexural capacities of top and bottom struts are determined from the computer program PREBEAM developed by Shushkewich[24], as mentioned in Chapter 6.

D.1.1 BEAM B1

Failure load - 11.03 kips

1. Ultimate moment at the center of the opening:

$M_u = 2(11.03)(104.4)-(11.03)(34.8)=1919.22$ in - kips.

2. Axial compressive force in the top strut:

$$C = \frac{1919.22 - 0.7(250)(0.32)(2)}{15} = 120.4 \text{ kips}$$

3. Axial tensile force in the bottom strut:

$$T = \frac{1919.22 - 0.7(250)(0.32)(17)}{15} = 64.4 \text{ kips}$$

4. Moment capacities at top and bottom struts obtained using the computer program PREBEAM and the known section properties are:

$M_1 = 126.17$ in - kips

$M_2 = 277.59$ in - kips

$M_3 = 233.15$ in - kips

$M_4 = 167.0$ in - kips

where the locations of these moments are indicated in Fig. D1.
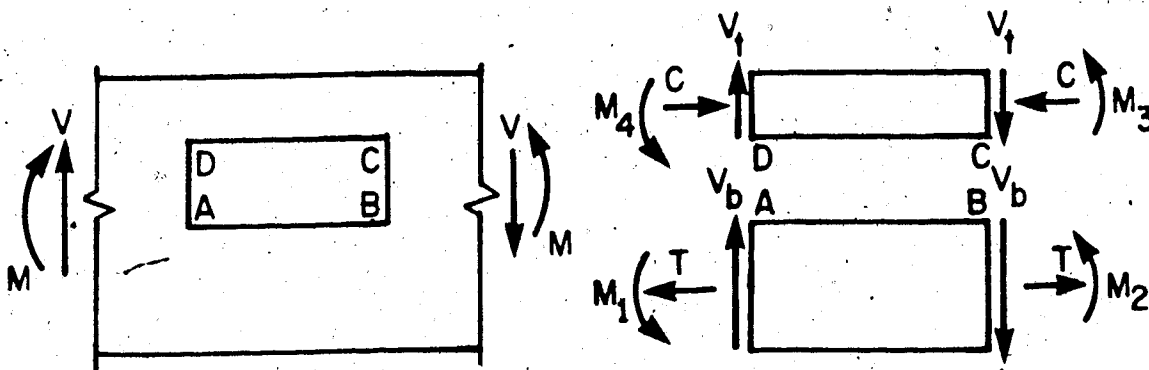
FIG. D1 - Moment Capacities at the Struts

5. Shear corresponding to the calculated flexural capacity of top strut:

$$V_{t_f} = \frac{M_3 + M_4}{\ell} = \frac{233.15 + 167.0}{56} = 7.15 \text{ kips}$$

6. Shear corresponding to the calculated shear capacity of top strut:

$$v_c = 2[1 + 0.0005 \,(\frac{120400}{80})]\sqrt{6900} = 290.73 \text{ psi}$$

$$V_{t_s} = 0.85(290.73)(20)(0.8)(4) = 15.8 \text{ kips}$$

7. Shear corresponding to the calculated flexural capacity of bottom strut:

$$V_{b_f} = \frac{M_1 + M_2}{\ell} = \frac{126.17 + 277.59}{56} = 7.21 \text{ kips}$$

8. Shear corresponding to the calculated shear capacity of bottom strut:

$$v_c = 2[1 + 0.002 \,(\frac{-64400}{40})] \sqrt{6900} = -368.81 \text{ psi}$$

$$V_{b_s} = \frac{2(0.02895)(81000)(0.8)(10)}{6.5} = 5.7 \text{ kips}$$

D.1.2 BEAM B2

Failure load - 11.40 kips

1. Ultimate moment at the center of the opening

$M_u = 2(11.4)(104.4) - (11.4)(34.8) = 1983.6$ in - kips

2. Axial compressive force in the top strut:

$$C = \frac{1983.6 - 0.7(250)(0.32)(2)}{15} = 124.7 \text{ kips}$$

3. Axial tensile force in the bottom strut:

$$T = \frac{1983.6 - 0.7(250)(0.32)(17)}{15} = 68.7 \text{ kips}$$

4. Moment capacities at top and bottom struts:

$M_1 = 110.97$ in - kips

$M_2 = 277.43$ in - kips

$M_3 = 228.38$ in - kips

$M_4 = 177.76$ in - kips

5. Shear corresponding to the calculated flexural capacity of top strut:

$$V_{t_f} = \frac{228.38 + 177.76}{40} = 10.15 \text{ kips}$$

6. Shear corresponding to the calculated shear capacity of top strut:

$$v_c = 2[1 + 0.0005(\frac{124700}{80})] \sqrt{6600} = 288.4 \text{ psi}$$

$$V_{t_s} = 0.85(288.4)(20)(0.8)(4) = 15.68 \text{ kips}$$

7. Shear corresponding to the calculated flexural capacity of bottom strut:

$$V_{b_f} = \frac{110.97 + 277.43}{40} = 9.71 \text{ kips}$$

8. Shear corresponding to the calculated shear capacity of bottom strut:

$$v_c = 2[1 + 0.002(\frac{-68700}{40})] \sqrt{6600} = -395.6 \text{ psi}$$

$$V_{b_s} = \frac{2(0.02895)(81000)(0.8)(10)}{8} = 4.69 \text{ kips}$$

D.1.3 BEAM B3

Failure load - 11.45 kips

1. Ultimate moment at the center of the opening:

$$M_u = 2(104.4)(11.45) - (11.45)(34.8) = 1992.3 \text{ in - kips.}$$

2. Axial compressive force in the top strut:

$$C = \frac{1992.3 - 0.7(250)(0.32)(2)}{15} = 125.3 \text{ kips}$$

3. Axial tensile force in the bottom strut:

$$T = \frac{1992.3 - 0.7(250)(0.32)(17)}{15} = 69.3 \text{ kips}$$

4. Moment capacities at top and bottom struts:

$M_1 = 138.51$ in - kips

$M_2 = 249.33$ in - kips

$M_3 = 217.96$ in - kips

$M_4 = 174.51$ in - kips

5. Shear corresponding to the calculated flexural capacity of top strut:

$$V_{t_f} = \frac{217.96 + 174.51}{24} = 16.35 \text{ kips}$$

6. Shear corresponding to the calculated shear capacity of top strut:

$$v_c = 2[1 + 0.005(\frac{125300}{80}) \sqrt{6100} = 278.04 \text{ psi}$$

$$V_{t_s} = 0.85(278.04)(20)(0.8)(4) = 15.12 \text{ kips}$$

7. Shear corresponding to the calculated flexural capacity of bottom strut:

$$V_{b_f} = \frac{138.51 + 249.33}{24} = 16.16 \text{ kips}$$

8. Shear corresponding to the calculated shear capacity of bottom strut:

$$v_c = 2[1 + 0.002 \ (\frac{-69300}{40}) \ \sqrt{6400} = -385.0 \ psi$$

$$V_{b_s} = \frac{2(0.02895)(81000)(0.8)(10)}{10.5} = 3.57 \ kips$$

D.1.4 BEAM C1

Failure load - 10.0 kips

1. Ultimate moment at the center of the opening:

$$M_u = 2(10.0)(104.4) - (10.0)(34.8) = 1740.0 \ in - kips$$

2. Axial compressive force in the top strut:

$$C = \frac{1740.0 - 0.7(250)(0.32)(0)}{16.33} = 106.55 \ kips$$

3. Axial tensile force in the bottom strut:

$$T = \frac{1740.0 - 0.7(250)(0.32)(16.33)}{16.33} = 50.55 \ kips$$

4. Moment capacities at top and bottom struts:

$$M_1 = 212.50 \ in - kips$$

$$M_2 = 212.50 \ in - kips$$

$$M_3 = 293.60 \ in - kips$$

$$M_4 = 231.42 \ in - kips$$

5. Shear corresponding to the calculated flexural capacity of top strut:

$$V_{t_f} = \frac{293.6 + 231.42}{56} = 9.37 \text{ kips}$$

6. Shear corresponding to the calculated shear capacity of top strut:

$$v_c = 2[1 + 0.0005\ (\frac{106550}{96})]\ \sqrt{6400} = 248.0 \text{ psi}$$

$$V_c = 0.85(248.0)(4)(0.8)(8) = 5.39 \text{ kips}$$

$$V_s = \frac{2(0.02895)(81000)(0.8)(8)}{6.5} = 4.61 \text{ kips}$$

$$V_{t_s} = 5.39 + 4.61 = 10.0 \text{ kips}$$

7. Shear corresponding to the calculated flexural capacity of bottom strut:

$$V_{b_f} = \frac{2 \times 212.50}{56} = 7.59 \text{ kips}$$

8. Shear corresponding to the calculated shear capacity of bottom strut:

$$v_c = 2[1 + 0.002(\frac{-50550}{24})]\ \sqrt{6400} = -513.6 \text{ psi}$$

$$V_{b_s} = \frac{2(0.02895)(81000)(0.8)(6)}{6.5} = 3.46 \text{ kips}$$

D.1.5 BEAM C2

Failure load – 10.57 kips

1. Ultimate moment at the center of the opening:

$$M_u = 2(10.57)(104.4)-(10.57)(34.8) = 1839.18 \text{ in} - \text{kips}$$

2. Axial compressive force in the top strut:

$$C = \frac{1839.18 - 0.7(250)(0.32)(0)}{16.33} = 112.6 \text{ kips}$$

3. Axial tensile force in the bottom strut:

$$T = \frac{1839.18 - 0.7(250)(0.32)(16.33)}{16.33} = 56.6 \text{ kips}$$

4. Moment capacities at top and bottom struts:

$$M_1 = 196.9 \text{ in} - \text{kips}$$

$$M_2 = 196.9 \text{ in} - \text{kips}$$

$$M_3 = 302.44 \text{ in} - \text{kips}$$

$$M_4 = 243.4 \text{ in} - \text{kips}$$

5. Shear corresponding to the calculated flexural capacity of top strut:

$$V_{t_f} = \frac{302.44 + 243.4}{40} = 13.64 \text{ kips}$$

6. Shear corresponding to the calculated shear capacity of top strut:

$$v_c = 2[1 + 0.0005(\frac{112600}{96})] \sqrt{6700} = 259.47 \text{ psi}$$

$$V_c = 0.85(259.47)(4)(0.8)(8) = 5.64 \text{ kips}$$

$$V_s = \frac{2(0.02895)(81000)(0.8)(8)}{8} = 3.75 \text{ kips}$$

$$V_{t_s} = 5.64 + 3.75 = 9.39 \text{ kips}$$

7. Shear corresponding to the calculated flexural capacity of bottom strut:

$$V_{b_f} = \frac{2 \times 196.9}{40} = 9.84 \text{ kips}$$

8. Shear corresponding to the calculated shear capacity of bottom strut:

$$v_c = 2[1 + 0.002(\frac{-56600}{24})] \sqrt{6700} = -605.71 \text{ psi}$$

$$V_s = \frac{2(0.02895)(81000)(0.8)(6)}{8} = 2.81 \text{ kips}$$

D.1.6 BEAM C3

Failure load - 10.50 kips

1. Ultimate moment at the center of the opening:

$$M_u = 2(10.5)(104.4) - (10.5)(34.8) = 1827.0 \text{ in - kips}$$

2. Axial compressive force in the top strut:

$$C = \frac{1827.0 - 0.7(250)(0.32)(0)}{16.33} = 111.8 \text{ kips}$$

3. Axial tensile force in the bottom strut:

$$T = \frac{1827.0 - 0.7(250)(0.32)(16.33)}{16.33} = 55.8 \text{ kips}$$

4. Moment capacities at top and bottom struts:

$M_1 = 197.94 \text{ in} - \text{kips}$

$M_2 = 197.94 \text{ in} - \text{kips}$

$M_3 = 301.85 \text{ in} - \text{kips}$

$M_4 = 167.04 \text{ in} - \text{kips}$

5. Shear corresponding to the calculated flexural capacity of top strut:

$$V_{t_f} = \frac{301.85 + 167.04}{24} = 19.53 \text{ kips}$$

6. Shear corresponding to the calculated shear capacity of top strut:

$$v_c = 2[1 + 0.0005(\frac{111800}{96})] \sqrt{6600} = 256.7 \text{ psi}$$

$$V_c = 0.85(256.7)(4)(0.8)(8) = 5.58 \text{ kips}$$

$$V_s = \frac{2(0.02895)(81000)(0.8)(8)}{10.5} = 2.85 \text{ kips}$$

$$V_{t_s} = 5.58 + 2.85 = 8.43 \text{ kips}$$

7. Shear corresponding to the calculated flexural capacity of bottom strut:

$$V_{b_f} = \frac{2 \times 197.94}{24} = 16.49 \text{ kips}$$

8. Shear corresponding to the calculated shear capacity of bottom strut:

$$v_c = 2[1 + 0.002(\frac{-55800}{24})] \sqrt{6600} = -593.05 \text{ psi}$$

$$V_{b_s} = \frac{2(0.02895)(81000)(0.8)(6)}{10.5} = 2.14 \text{ kips}$$

D.1.7 BEAM D1

Failure load - 10.40 kips

1. Ultimate moment at the center of the opening:

$$M_u = 2(10.4)(104.4) - (10.4)(34.8) = 1809.16 \text{ in - kips}$$

2. Axial compressive force in the top strut:

$$C = \frac{1809.16 - 0.7(250)(0.32)(2)}{15} = 113.14 \text{ kips}$$

3. Axial tensile force in the bottom strut:

$$T = \frac{1809.16 - 0.7(250)(0.32)(17)}{15} = 57.14 \text{ kips}$$

4. Moment capacities at top and bottom struts:

$M_1 = 147.33$ in - kips

$M_2 = 277.71$ in - kips

$M_3 = 231.17$ in - kips

$M_4 = 167.04$ in - kips

5. Shear corresponding to the calculated flexural capacity of top strut:

$$V_{t_f} = \frac{231.17 + 167.04}{56} = 7.11 \text{ kips}$$

6. Shear corresponding to the calculated shear capacity of top strut:

$$v_c = 2[1 + 0.0005(\frac{113140}{80})] \sqrt{6800} = 281.2 \text{ psi}$$

$$V_{t_s} = 0.85 (281.2)(20)(0.8)(4) = 15.3 \text{ kips}$$

7. Shear corresponding to the calculated flexural capacity of bottom strut:

$$V_{b_f} = \frac{147.33 + 277.71}{56} = 7.63 \text{ kips}$$

8. Shear corresponding to the calculated shear capacity of bottom strut:

$$v_c = 2[1 + 0.002(\frac{-57140}{40})] \sqrt{6800} = -305.1 \text{ psi}$$

$$V_{b_s} = \frac{2(0.02895)(81000)(0.8)(10)}{6.5} = 5.7 \text{ kips}$$

D.1.8 BEAM D2

Failure load - 10.50 kips

1. Ultimate moment at the center of the opening:

$$M_u = 2(10.5)(104.4) - (10.5)(34.8) = 1827.0 \text{ in - kips}$$

2. Axial compressive force in the top strut:

$$C = \frac{1827.0 - 0.7(250)(0.32)(2)}{15} = 114.3 \text{ kips}$$

3. Axial tensile force in the bottom strut:

$$T = \frac{1827.0 - 0.7(250)(0.32)(17)}{15} = 58.3 \text{ kips}$$

4. Moment capacities at top and bottom struts:

$$M_1 = 140.9 \text{ in - kips}$$

$$M_2 = 281.9 \text{ in - kips}$$

$$M_3 = 216.04 \text{ in - kips}$$

$$M_4 = 163.11 \text{ in - kips}$$

5. Shear corresponding to the calculated flexural capacity of top strut:

$$V_t = \frac{216.04 + 163.11}{40} = 9.48 \text{ kips}$$

6. Shear corresponding to the calculated shear capacity of top strut:

$$v_c = 2[1 + 0.0005(\frac{114300}{80})] \sqrt{6100} = 267.1 \text{ psi}$$

$$V_{t_s} = 0.85(267.1)(20)(0.8)(4) = 14.53 \text{ kips}$$

7. Shear corresponding to the calculated flexural capacity of bottom strut:

$$V_{b_f} = \frac{140.9 + 281.9}{40} = 10.57 \text{ kips}$$

8. Shear corresponding to the calculated shear capacity of bottom strut:

$$v_c = 2[1 + 0.002(\frac{-58300}{40})] \sqrt{6100} = -299.1 \text{ psi}$$

$$V_{b_s} = \frac{2(0.02895)(81000)(0.8)(10)}{8.0} = 4.69 \text{ kips}$$

D.1.9 BEAM D3

Failure load - 10.80 kips

1. Ultimate moment at the center of the opening:

$$M_u = 2(10.8)(104.4) - (10.8)(34.8) = 1879.2 \text{ in - kips}$$

2. Axial compressive force in the top strut:

$$C = \frac{1879.2 - 0.7(250)(0.32)(2)}{15} = 117.8 \text{ kips}$$

3. Axial tensile force in the bottom strut:

$$T = \frac{1879.2 - 0.7(250)(0.32)(17)}{15} = 61.8 \text{ kips}$$

4. Moment capacities at top and bottom struts:

$M_1 = 128.2$ in - kips

$M_2 = 282.1$ in - kips

$M_3 = 218.64$ in - kips

$M_4 = 167.37$ in - kips

5. Shear corresponding to the calculated flexural capacity of top strut:

$$V_{t_f} = \frac{218.64 + 167.37}{24} = 16.08 \text{ kips}$$

6. Shear corresponding to the calculated shear capacity of top strut:

$$v_c = 2[1 + 0.0005(\frac{117800}{80})] \sqrt{6200} = 273.2 \text{ psi}$$

$$V_{t_s} = 0.85(273.2)(20)(0.8)(4) = 14.86 \text{ kips}$$

7. Shear corresponding to the calculated flexural capacity of bottom strut:

$$V_{b_f} = \frac{128.2 + 282.1}{24} = 17.10 \text{ kips}$$

8. Shear corresponding to the calculated shear capacity of bottom strut:

$$v_c = 2[1 + 0.002(\frac{-61800}{40})] \sqrt{6200} = -329.1 \text{ psi}$$

$$V_{b_s} = \frac{2(0.02895)(81000)(0.8)(10)}{10.5} = 3.57 \text{ kips}$$

D.1.10 BEAM B4

Failure load - 8.61 kips

1. Ultimate moment at the center of the opening:

$M_u = 2.5(8.61)(108.0) - (8.61)(34.0) = 2031.96 \text{ in - kips}$

2. Axial compressive force in the top strut:

$$C = \frac{2031.96 - 0.7(270)(3)(0.153)(0)}{18} = 112.8 \text{ kips}$$

3. Axial tensile force in the bottom strut:

$$T = \frac{2031.96 - 0.7(270)(3)(0.153)(18)}{18} = 26.13 \text{ k}$$

4. Moment capacities in the top and bottom struts:

ϕM_1 = 389.2 in - kips

M_2 = 389.2 in - kips

M_3 = 244.75 in - kips

M_4 = 212.18 in - kips

5. Shear corresponding to the calculated flexural capacity of top strut:

$$V_{t_f} = \frac{244.75 + 212.18}{45} = 10.15 \text{ kips}$$

6. Shear corresponding to the calculated shear capacity of top strut:

$$v_c = 2[1 + 0.0005(\frac{112800}{192})] \sqrt{7820} = 228.15 \text{ psi}$$

$$V_{t_s} = 0.85(228.15)(48)(0.8)(4) = 29.78 \text{ kips}$$

7. Shear corresponding to the calculated flexural capacity of bottom strut:

$$V_{b_f} = \frac{2 \times 389.2}{45} = 17.2 \text{ kips}$$

8. Shear corresponding to the calculated shear capacity of bottom strut:

$$v_c = 2[1 + 0.002(\frac{-26130}{53.2})] \sqrt{7860} = 3.12 \text{ psi}$$

$$V_c = 0.85(3.12)(3.75)()(.8)(12) = 0.095 \text{ kips}$$

$$V_s = \frac{(0.021)(75000)(0.8)(12)}{6} = 2.52 \text{ kips}$$

$$V_{b_s} = 0.095 + 2.52 + 2.61 \text{ kips}$$

D.1.11 BEAM B5

Failure load - 7.62 kips

1. Ultimate moment at the center of the opening:

$$M_u = 2.5(7.62)(108.0) - (7.62)(34.0) = 1783.08 \text{ in - kips}$$

2. Axial compressive force in the top strut:

$$C = \frac{1783.08 - 0.7(270)(3)(0.153)(0)}{18} = 99.06 \text{ kips}$$

3. Axial tensile force in the bottom strut:

$$T = \frac{1783.08 - 0.7(270)(3)(0.153)(18)}{18} = 12.33 \text{ kips}$$

4. Moment capacities at top and bottom struts:

$$M_1 = 384.2 \text{ in - kips}$$

$$M_2 = 384.2 \text{ in - kips}$$

$$M_3 = 189.94 \text{ in - kips}$$

$$M_4 = 181.92 \text{ in - kips}$$

5. Shear corresponding to the calculated flexural capacity of top strut:

$$V_{t_f} = \frac{189.94 + 181.92}{60} = 6.19 \text{ kips}$$

6. Shear corresponding to the calculated shear capacity of top strut:

$$v_c = 2[1 + 0.0005(\frac{99060}{192}) \sqrt{7410} = 216.06 \text{ psi}$$

$$V_{t_s} = 0.85(216.06)(48)(0.8)(4) = 28.2 \text{ kips}$$

7. Shear corresponding to the calculated flexural capacity of bottom strut:

$$V_{b_f} = \frac{2 \times 384.2}{60} = 12.80 \text{ kips}$$

8. Shear corresponding to the calculated shear capacity of bottom strut:

$$v_c \ 2[1 + 0.002(\frac{-12330}{53.2})] \sqrt{7410} = 92.1 \text{ psi}$$

$$V_c = 0.85(92.10)(3.75)(0.8)(12) = 2.82 \text{ kips}$$

$$V_s = \frac{(0.021)(75000)(0.8)(12)}{6} = 2.52 \text{ kips}$$

$$V_{b_s} = 2.82 + 2.52 = 5.34 \text{ kips}$$

D.1.12 BEAM B7

Failure load - 8.55 kips

1. Ultimate moment at the center of the opening:

M_u = 2.5(8.55)(108.0) - (8.55)(34.0) = 2000.7 in - kips

2. Axial compressive force in the top strut:

$$C = \frac{2000.7 - 0.7(270)(3)(0.153)(0)}{18} = 111.15 \text{ kips}$$

3. Axial tensile force in the bottom strut:

$$T = \frac{2000.7 - 0.7(270)(3)(0.153)(18)}{18} = 24.4 \text{ kips}$$

4. Moment capacities at the top and bottom struts:

M_1 = 422.85 in - kips

M_2 = 422.85 in - kips

M_3 = 236.84 in - kips

M_4 = 194.48 in - kips

5. Shear corresponding to the calculated flexural capacity of top strut:

$$V_{t_f} = \frac{236.64 + 194.48}{60} = 7.18 \text{ kips}$$

6. Shear corresponding to the calculated shear capacity of top strut:

$$v_c = 2[1 + 0.0005(\frac{111150}{192})] \sqrt{8000} = 229.8 \text{ psi}$$

$$V_{t_s} = 0.85(229.8)(48)(0.8)(4) = 30.0 \text{ kips}$$

7. Shear corresponding to the calculated flexural capacity of bottom strut:

$$V_{b_f} = \frac{2 \times 422.85}{60} = 14.09 \text{ kips}$$

8. Shear corresponding to the calculated shear capacity of bottom strut:

$$v_c = 2[1 + 0.002(\frac{-24400}{53.2})] \sqrt{8000} = 14.79 \text{ psi}$$

$$V_c = 0.85(14.79)(3.75)(0.8)(12) = 0.452 \text{ kips}$$

$$V_s = \frac{(0.021)(75000)(0.8)(12)}{3} = 5.04 \text{ kips}$$

$$V_{b_s} = 0.452 + 5.04 = 5.5 \text{ kips}$$